UNIVERSITE SORBONNE PARIS CITE

Thèse préparée
À l'INSTITUT DE PHYSIQUE DU GLOBE DE PARIS
Ecole doctorale STEP'UP – ED N°560
IPGP – Equipe de Biogéochimie Environnementale

Mobilité du thallium et du radium dans l'environnement

par

Loïc Martin

présentée et soutenue publiquement le
20 Novembre 2017

Thèse de doctorat de Sciences de la Terre et de l'environnement
dirigée par Pr. Marc F. Benedetti

Devant un jury composé de :

Dr. Corinne Casiot Chargée de recherche CNRS (Université de Montpellier)	Rapporteur
Pr. Sébastien Rauch Professeur (Chalmers University of Technology)	Rapporteur
Pr. Bénédicte Ménez Professeure (Université Paris Diderot)	Examinateur
Dr. Andreas Voegelin Chercheur (EAWAG)	Examinateur
Dr. Caroline Simonucci Ingénieur-Chercheur (IRSN) I	Co-encadrant
Pr. Marc Benedetti Professeur (Université Paris Diderot)	Directeur de thèse

A mes parents,

REMERCIEMENTS

Je voudrais commencer par remercier toutes les personnes qui ont imaginé et proposé ce qui est devenu mon sujet de thèse en commençant par Caroline Simonucci, Christelle Courbet et Eric Viollier. Puis, les autres personnes impliquées dans mon recrutement et mon encadrement, Christelle Latrille, Setareh Rad, Alikiviadis Gourgiotis et Marc Benedetti. Lorsque vous m'avez recruté, j'étais en stage au Chili, dans une situation délicate, alors merci à tous de m'avoir offert une issue et surtout de m'avoir donné la chance de pouvoir faire cette thèse. Cette expérience dans la recherche fut pour moi réellement enrichissante et épanouissante.

Je voudrais également remercier les membres de mon jury pour avoir évalué mon travail et d'être venu jusqu'à Paris pour ma soutenance.

Il est temps maintenant de passer à des remerciements plus personnels. Je vais commencer par Christelle Courbet, qui malheureusement n'a pas pu rester dans l'encadrement de ma thèse jusqu'au bout. C'est avec grand plaisir que je retournerai faire des missions de terrain avec toi, mais en évitant de nous retrouver au milieu d'une rivière en plein orage avec le niveau d'eau qui monte dangereusement. Puisque j'en suis à remercier les personnes de l'IRSN, je vais enchainer avec Caroline. Je pense pouvoir écrire, sans exagérer, que si tu n'avais pas été là, ces 3 ans auraient été beaucoup plus compliquées et bien moins agréables. Je ne compte pas le nombre de repas que nous avons partagés, le nombre d'heures où tu as écouté mes idées farfelues ni le nombre de conseils que tu m'as donné. Tu m'as même supporté tout les jours la semaine avant mon rendu et surtout, tu as réussi à me faire améliorer (il y a encore du travail certes) mon orthographe, ce que personne n'avait réussi jusqu'ici. Un merci semble un peu cliché après ça mais quand même, merci d'avoir été ma co-encadrante de thèse ! Sur les documents seules Caroline est officiellement ma co-encadrante mais en réalité, il y en avait une deuxième, Christelle Latrille. De la même manière, je ne compte pas le nombre d'heures que tu as passé à écouter mes idées farfelues ou à répondre à mes questions à chaque fois que je débarquais dans ton bureau. Le travail qu'on a réalisé ensemble m'a beaucoup appris et je te suis vraiment reconnaissant d'avoir accepté de faire cela. Le chercheur que je suis aujourd'hui te doit beaucoup. Pour terminer, je tiens à remercier mon directeur de thèse, Marc. J'ai énormément appris à ton contact, grâce a ton exigence et tes conseils toujours très avisés. Merci d'avoir

toujours pris le temps de travailler avec moi, et surtout de m'avoir soutenu quand les différents partenaires de ma thèse posaient des problèmes et quand le projet n'allait pas dans la bonne direction.

J'ai eu la chance de pouvoir travailler dans plusieurs laboratoires pendant ma thèse. Je vais donc remercier toutes les personnes qui m'ont accueilli au L3MR et au LGE. L'ordre n'a aucune importance. Merci Nathalie M., Virginie et Virginie, Jacques, Nathalie, Delphine, Jean, Romain, Patrick, Serge, Catherine, Emilie, Yann, Alexandre, Rute, Didier, Alexis, Laure, Mickaël (merci de m'avoir aidé avec l'Element même quand je t'appelais les week-ends), Rémi, Maud, Emmanuelle et Andrea. Je n'oublie pas les doctorants (anciens et actuels) bien évidemment, Nicolas, Isabella, Yohann, Caroline, Yang, Jialan, Logan, Damien, Yasmine, Morgane, Claudia, Thaïs, Brice, Viviana, Sarah et Aubéry.

Je voudrais également remercier tout mes amis qui m'ont supporté durant de nombreuses soirées pendant ces trois ans. Je vais commencer par Izyan et Shafiq. Izyan a partagé le même bureau que moi pendant plus de 3 ans et a réussi à me supporter et même a devenir une amie proche. Ça méritait bien un paragraphe. Je n'oublie évidemment pas James, Thibaud, Benjamin, Anaïs, Tamara, Thomas C. Thomas G., Nicolas (mon frère de parents différents), David, Chloé et tous ceux que j'ai pu oublier.

Tout cela n'aurait pas été possible sans le soutient de ma famille, parmi eux ma sœur et surtout mes parents. Ils ont toujours été à mes cotés et m'ont toujours soutenu et je ne serais pas là ou j'en suis aujourd'hui sans eux. Merci, je vous aime !

Et le meilleur pour la fin. Assiya, ma charmante femme, ma moitiée. Que dire sinon que je t'aime. Sans toi à mes côtés, c'est certain que je ne pourrais être qui je suis aujourd'hui. Finalement on peut dire que ce travail t'appartient tout autant qu'à moi !

SOMMAIRE

Chapitre I : Introduction - Etat de l’art sur le comportement du thallium et du radium sur terre

PARTIE 1 : LE THALLIUM

Le thallium a été découvert en 1861 par le chimiste anglais William Crookes (Peter and Viraraghavan, 2005) lors d'une étude spectroscopique de résidus provenant d'une usine de production d'acide sulfurique (Nriagu 1998b). Sa forme métallique a ensuite été préparée pour la première fois par le français Claude-Auguste Lamy en 1862 (Peter and Viraraghavan, 2005 ; Nriagu 1998b). Les expériences qu'il réalise par la suite permettent de mettre en évidence la présence de thallium monovalent et trivalent (Nriagu, 1998b). La difficulté, à la fin du XIX^{ème} siècle de classer le thallium dans le tableau périodique suscite un intérêt important pour cet élément. En effet, comme le montre M. Doan dans son ouvrage « *Index to the Literature on Thallium, 1861-1896* » (Doan, 1899), une centaine de publications ont été écrites à cette époque sur ses propriétés physico-chimiques.

Sous sa forme pure, le thallium est un métal tendre, malléable et de couleur grise (Peter and Viraraghavan, 2005). Le thallium est classé dans la colonne 13 du tableau périodique des éléments, au même titre que le bore, l'aluminium, le gallium et l'indium. C'est un métal lourd comme le plomb ou le mercure. Son numéro atomique est 81. Il compte 37 isotopes et seuls les isotopes 203 et 205 (respectivement 30 % et 70 %) existent naturellement et sont stables. Parmi les isotopes radioactifs, le 201, utilisé en médecine comme produit de contraste (Bennett 2017), et le 204, utilisé comme radiotraceur (Liu *et al.*, 2011), peuvent être pris comme exemple avec une application. Sa masse atomique est 204.3833 ± 0.0002 (Lide 2009). L'intégralité des propriétés physico-chimiques de l'élément thallium sont récapitulées en annexe A.

1. LE THALLIUM DANS LES ENVIRONNEMENTS PROFONDS : du manteau à la croûte terrestre

1.1. Abondance du thallium dans la Terre

Dans l'une des premières études publiées sur le Thallium et sa géochimie, Denis M. Shaw (1952, 1957) a estimé l'abondance crustale de cet élément à 1.3 ppm (Shaw 1952). Par la suite d'autres études ont estimé cette abondance entre 0,0085 et 1,7 ppm (Sahl *et al.*, 1978). Ces chiffres permettent d'affirmer que le thallium est un élément trace dans la Terre silicatée. D'autres chiffres ont également été avancés, en faisant la distinction entre croûte continentale et

croûte océanique. Dans la première, la concentration est estimée entre 0,45 et 0,55 ppm (Sahl *et al.*, 1978; Wedepohl, 1995) et pour la seconde, elle est estimée à 0,013 ppm (Peter et Viraraghavan, 2005).

1.2. Comportement du thallium dans les processus magmatiques

Dans la Terre interne silicatée, les conditions sont plutôt réductrices et la seule espèce thermodynamiquement stable est Tl(I) (Rekhämper et Nielsen, 2004). De plus, Tl^+, l'espèce libre de Tl(I), a un rayon ionique de 1,50 Å (Shannon, 1976) proche des éléments alcalins comme le potassium (1,38 Å), le rubidium (1,52 Å) et le césium (1,67 Å) tous estimés par Shannon, (1976). Ces éléments ont donc des caractéristiques physico-chimiques très proches.

1.2.1. Comportement du thallium lors de la fusion

La fusion partielle de roches a pour effet de créer un fractionnement entre un liquide et une roche encaissante de composition différente (Jaujard, 2015). Les éléments aux rayons ioniques importants comme les alcalins (K^+ ou Na^+) quittent rapidement le solide pour se retrouver dans le liquide (Jaujard, 2015), ils sont dits « incompatibles » (Jaujard, 2015). Compte-tenu du rayon ionique du thallium (1,50 Å ; non hydraté, en coordinance VI), proche de celui du potassium, du césium et du rubidium (Shannon 1976), il est probable qu'il se retrouve lui aussi dans le liquide (Shaw, 1952 ; Heinrichs *et al.*, 1980). A cela s'ajoute le fait que plus le taux de fusion de la roche est important, plus le passage d'un grand nombre d'éléments chimiques du solide vers le liquide est favorisé (Jaujard, 2015).

Enfin, la nature de la roche qui va fondre a aussi un impact sur la composition des magmas (Jaujard, 2015). La combinaison de tous ces phénomènes a un impact sur la concentration en thallium dans le liquide magmatique initial (Heinrichs *et al.*, 1980).

1.2.2. Le thallium dans les minéraux issus de la cristallisation des magmas

Si l'on se base sur la suite réactionnelle de Bowen (Bowen, 1956), on peut avoir une idée du comportement du thallium en regardant sa concentration dans les différents minéraux. De manière simplifiée, dans la série des ferromagnésiens les minéraux cristallisent dans l'ordre suivant à températures décroissantes : olivines > pyroxènes > amphiboles > biotites > feldspaths potassiques, micas blanc et quartz. Nielsen *et al.* (2014) rapportent des concentrations en Tl

inférieures à une limite de détection de 1 ppb (LA-ICP-MS, Nielsen *et al*., 2014) dans des olivines, des pyroxènes (clino- et ortho-) et des spinelles contenus dans des lherzolithes. Des concentrations dans des amphiboles du complexe d'Ilimaussaq (Groenland) montrent des concentrations variant entre 33 et 180 ppb (Hettmann *et al.*, 2014). Les concentrations en thallium dans les micas et les feldspaths alcalins sont très diverses et varient de la centaine de ppb à la dizaine de ppm (Shaw, 1952 ; Shaw, 1957 ; Sahl *et al*. 1978). Cela semble confirmer que l'espèce Tl^+ peut se substituer au K^+ dans les réseaux cristallins (Shaw, 1952 ; Heinrichs *et al.*, 1980 par exemple) et traduit certainement un comportement lithophile et incompatible du thallium lors des processus de cristallisation. Les mêmes observations sont faites pour les feldspaths plagioclases (Sahl *et al*., 1978) où les minéraux de types anorthites (pôle Ca^{2+}) sont plutôt appauvris en Tl contrairement aux albites (pôle Na^+ ; Sahl *et al*., 1978).

Ces résultats sont appuyés par les références qui existent sur le partitionnement du thallium dans les roches ignées. Les coefficients de partages du thallium dans les pyroxènes, olivines et amphiboles (tableau 2) sont inférieurs à 1, signifiant que le thallium va préférentiellement rester dans le liquide (Adam et Green, 2006). Au contraire, ces valeurs sont très supérieures à 1 pour les micas et les feldspaths (tableau 1 ; Adam et Green, 2006; Bea *et al.*, 1994). Différentes études ont également montré une relation (non linéaire) entre le taux de MgO et l'abondance en thallium. En effet il semble que lorsque que la quantité de Mg diminue (MgO < 5 % environ) la concentration en thallium augmente dans les roches (Greaney *et al.*, 2017; Shu *et al.*, 2017). Cela confirmerait donc la faible abondance du thallium dans les minéraux férro-magnésiens.

Tableau 1 : Coefficients de partage pour le thallium pour différents minéraux et liquides. Pyr = pyroxène, Olv = olivine, Amp = amphibole, Grt = grenat.

Coefficient de partage (D)	Valeur	Référence	Remarques
Pyr/liq.	< 0,1	Adam et Green, 2006	Conditions expérimentales
Olv/lid.	< 0,15	Adam et Green, 2006	Conditions expérimentales
Amp/liq.	≤ 0,23 ± 0,04	Adam et Green, 2006	Conditions expérimentales
Grt/liq.	< LD	Adam et Green, 2006	Conditions expérimentales
Mica/liq.	Entre 3,0 ± 0,3 et 5,2 ± 0,3	Adam et Green, 2006	Conditions expérimentales
Biotite.	8,6 ± 0,3	Bea *et al.*, 1994	Calculé dans une migmatite (~gneiss)
Cordiérite	0,24 ± 0,08	Bea *et al.*, 1994	Calculé dans une migmatite (~gneiss)
Grenat	0,09 ± 0,05	Bea *et al.*, 1994	Calculé dans une migmatite (~gneiss)
K-feldspaths	3,7 ± 0,3	Bea *et al.*, 1994	Calculé dans une migmatite (~gneiss)
Plagioclase	0,06 ± 0,05	Bea *et al.*, 1994	Calculé dans une migmatite (~gneiss)
Sulfure/Silicate	Entre 4,1 et 18,8	Kiseeva et Wood, 2013	Expériences entre un liquide riche en FeS et un liquide basaltique anhydre
Sulfure/Silicate	1,1 ± 1,7	Greaney *et al.*, 2017	Calculé dans le lac de lave du Kilaeua Iki

Les concentrations en thallium dans les minéraux accessoires communs aux roches magmatiques sont très contrastées. Des micas riches en potassium comme le lépidolite ou la zinnwaldite peuvent être très enrichies en Tl avec des concentrations allant jusqu'à 300 ppm dans des pegmatites (Sahl *et al.*, 1978). Les tourmalines et magnétites (contrairement au reste du groupe des spinelles) ont des concentrations en thallium de l'ordre de la centaine de ppb (Sahl *et al.*, 1978), tandis que les grenats semblent contenir très peu de thallium (Adam et Green, 2006). Le thallium est donc un élément que l'on retrouve principalement dans les minéraux riches en potassium auquel il peut, à priori, se substituer. A l'opposé les minéraux férro-magnésiens en sont plutôt appauvris.

1.2.3. Le comportement du thallium lors de la formation des roches ignées

Il existe trois types de magmatismes issus de la fusion partielle du manteau qui sont plus ou moins reliés au contexte géodynamique (Jaujard 2015). La série tholéiitique (avec des magmas plus riches en ferromagnésiens) est reliée au volcanisme de dorsale, de point chaud et d'extension

continentale tandis que la série calco-alcaline est associée au magmatisme de subduction. Enfin la série alcaline, avec des magmas riches en Na et K est typique des débuts de l'extension continentale et de certains points chauds (Jaujard 2015). Un quatrième type de magma est lié à la fusion de la croûte continentale inférieure en contexte de collision et produit des magmas riche en aluminium (Jaujard, 2015). Aujourd'hui aucune donnée disponible dans la littérature ne permet d'associer un comportement particulier du thallium à une de ces séries magmatiques, mais la diversité des concentrations observées est bien réelle (Sahl *et al*., 1978 ; Heinrichs *et al*., 1980 ; Noll *et al*., 1996 ; Nielsen *et al*., 2017 ; Shu *et al*., 2017)

De nombreuses études ont montré un enrichissement en thallium lié au degré de différenciation croissant d'une série de roches (Shaw, 1952 ; Shaw, 1957 ; Sahl *et al.*, 1978 ; Nielsen *et al*., 2017; Prytulak *et al.*, 2017). Le volcanisme de l'arc des Tonga-Kermadec en est un exemple (Nielsen *et al.*, 2017). Les basaltes présentent une concentration moyenne de 9,9 ± 4,1 ppb tandis que les dacites (roches les plus différenciées) ont une concentration moyenne de 103,1 ± 24,2 ppb (Nielsen *et al.*, 2017). Cela est également observable sur des laves de l'Hekla (Islande) et de l'Anatahan dans les Iles Mariannes (Prytulak *et al.*, 2017). Des données plus anciennes (Shaw, 1952 ; Shaw, 1957 ; Sahl *et al.*, 1978) montrent également un enrichissement en thallium dans les roches les plus différenciées.

Cependant, la différenciation par la cristallisation fractionnée n'explique pas à elle seule la diversité des roches ignées. D'autre processus comme les sources du magma ou le contexte géodynamique entrent également en jeu (Pomerol *et al*., 2006 ; Prytulak *et al*. 2013 ; Jaujard, 2015). Le comportement du thallium est régulièrement corrélé avec d'autres éléments, soit pour expliquer son comportement, soit pour expliquer des phénomènes plus fondamentaux de la géochimie des magmas. Le rôle du soufre ou du dégazage lors de la cristallisation en sont des exemples (Shaw, 1952 ; De Albuquerque *et al*., 1971 ; Jochum et Verma, 1996 ; Noll *et al*., 1996 ; Prytulak *et al*., 2013 ; Nielsen *et al*., 2014 ; Nielsen *et al*., 2016 ; Nielsen *et al*., 2017 ; Prytulak *et al*., 2017 ; Shu *et al.*, 2017). Le thallium est ainsi souvent comparé au césium, au rubidium (Nielsen *et al*., 2006b ; Prytulak *et al*., 2013), au potassium (Barker *et al*., 2010), au cérium (Nielsen et al., 2014), au plomb ainsi qu'au lanthane (Noll *et al*., 1996 ; Prytulak *et al*., 2013 ; Prytulak *et al*., 2017).

1.2.4. Comportement lithophile vs. chalcophile

Le thallium est un élément au comportement lithophile et incompatible, qui a un comportement proche de celui du potassium, césium et rubidium. Pourtant, d'autres études ont également mis en avant un comportement chalcophile du thallium c'est-à-dire qu'il pourra se concentrer dans les phases riches en soufre (McGoldrick *et al*., 1979 ; Kiseeva et Wood, 2013 ; Nielsen *et al*., 2014).

En effet, les propriétés-physico-chimique du thallium montrent que compte tenu de sa configuration électronique polarisée (Nriagu, 1998 ; Lide 2009), le thallium est en principe plus apte à former des liaisons covalentes que les éléments alcalins et pourrait ainsi être incorporé dans les sulfures (Coggon *et al*., 2014). Le thallium est aussi considéré comme un « cation mou » (Pearson, 1968). On lui suppose donc un comportement chalcophile au même titre que le cuivre, le mercure ou l'argent (Pearson, 1968 ; Smith *et al*., 2002). Plus particulièrement, l'étude de McGoldrick et al., (1979) suggère que le thallium suivrait le soufre dans les magmas saturés en soufre. Nielsen *et al*. (2014) ont montré que le soufre interstitiel des lherzolites était bien plus enrichi en thallium que le reste des minéraux. Ils ont également montré que la concentration en thallium dans les basaltes de type MORB (*Mid-Ocean Ridge Basalts*) était contrôlée par ce soufre lors de la fusion partielle du manteau appauvri. Ils ont également ajouté que le thallium dans les liquides riches en soufre était incompatible et se retrouvait dans les sulfures de précipitation tardive (Nielsen *et al*., 2014). Des données expérimentales produites par Kiseeva et Wood (2013) semblent confirmer un comportement chalcophile du thallium. En effet, les coefficients de partage entre le liquide riche en sulfures et le liquide silicaté est très supérieur à 1, suggérant une concentration du thallium dans ces sulfures (Tableau 2 ; Kiseeva et Wood, 2013).

Cependant, d'autres données disponibles démontrent un comportement lithophile du thallium. Dans les laves de l'Hekla et de l'Antahan (Prytulak *et al*., 2017), le comportement du thallium est anti-corrélé à celui du soufre (Prytulak *et al*., 2017). De même que le coefficient de partage du thallium entre les sulfures et le liquides silicaté du lac de lave du Kilaeua Iki (1,1 ± 1,7) suggère un comportement modérément chalcophile (Greaney *et al*., 2017).

Les comportements chalcophile et lithophile du thallium semblent difficile à prévoir dans les processus magmatiques et fortement dépendant du contexte géologique. Cependant ces processus

vont induire un fractionnement important du thallium et contribuer à son inégale répartition dans les roches ignées et par conséquent dans les croutes terrestre et océanique.

1.3. Métamorphisme et altération hydrothermale

En dehors des zones de subduction, peu d'études présentent les impacts du métamorphisme sur le cycle du thallium dans la Terre interne. Le tableau 1 montre que les roches métamorphiques ont une concentration en thallium moyenne élevée, de l'ordre du ppm. Compte tenu de la variété des roches métamorphiques mais aussi de la diversité des roches mères, la question est de savoir quels mécanismes sont responsables de cette concentration moyenne importante.

1.3.1. Les transformations minéralogiques

L'une des modifications engendrées par le métamorphisme est liée au changement de conditions de pression et de température de la roche. Les minéraux qui la composent ne sont plus à l'équilibre et réagissent entre eux pour en former de nouveaux (Pomerol *et al*., 2006 ; Jaujard 2015). Il existe très peu d'étude à ce sujet pour le thallium. Cependant en se basant sur les données disponibles dans des contextes différents (magmatisme, par exemple), on peut déjà constater que de nombreux minéraux caractéristiques des faciès métamorphiques, comme les grenats, les amphiboles ou les pyroxènes, contiennent très peu de thallium. Il y a donc peu de chance que cela soit différent dans le cas des transformations minérales dans les phénomènes métamorphiques. D'autres minéraux typiques du métamorphisme comme les chlorites ou les épidotes n'ont *a priori* pas les réseaux cristallins nécessaires pour permettre l'incorporation d'un ion aussi gros que le Tl^+ (Baker *et al*., 2010).

Dans une étude publiée en 2009, Nielsen *et al*. (2009b) ont mesuré le thallium dans des xénolithes d'éclogites issus de kimberlites. Les concentrations de cet élément dans les grenats et les pyroxènes varient entre 0,2 et 1,8 ppb dans ce type d'échantillons. Cependant, les analyses de l'encaissant, constitué de la kimberlite et des produits d'altération, montrent des concentrations bien supérieures en thallium, allant de 12 à 464 ppb, suggérant l'importance du rôle des fluides dans la répartition du thallium (Nielsen *et al*., 2009b).

1.3.2. Métasomatose et circulation de fluides

Le thallium est connu pour être un élément chalcophile et lithophile dans les environnements magmatiques (Nielsen *et al*., 2014 ; Prytulak *et al*., 2017). Cela ne semble pas faire exception en contexte métamorphique. Lors de la métasomatose, le thallium est mobilisé par la circulation de fluides de la même manière que le potassium (Baker *et al*., 2010). Il va donc pouvoir se substituer à ce dernier et cristalliser dans les micas ou les feldspaths potassiques (Baker *et al*., 2010). Il a été observé également que le thallium pouvait être enrichi dans les liquides riches en soufre (McGoldrick *et al*., 1979 ; Heinrichs *et al*., 1980 ; Noll *et al*., 1996), ce qui explique que la plupart des minéraux de thallium soient des sulfures.

L'exemple du complexe de Collahuasi dans le nord des Andes chiliennes met en avant un comportement lithophile du thallium (Baker *et al*., 2010). Dans ce cas, les concentrations en thallium observées ne sont pas dues aux processus magmatiques, mais plutôt à la circulation de fluides de hautes températures (Baker *et al*., 2010). En effet ces fluides ont dans un premier temps précipité des feldspaths potassiques et des biotites qui ont été enrichis en thallium. Ensuite, ces phases ont été altérées et appauvries en thallium (Baker *et al*., 2010).

Lors de la précipitation de liquide riche en soufre, il est fréquent de retrouver des minéraux riches en thallium, voire des minéraux de thallium (Biagioni *et al*., 2013 ; Hettmann *et al*., 2014). L'étude de Biagioni *et al*. (2013) montre même que le thallium est mobile avec des fluides de basse température du faciès des schistes verts. Les minéraux sulfurés contenant du thallium sont la pyrite, la galène ou la sphalérite dans lesquels les teneurs en Tl peuvent dépasser la centaine de ppm (Zhang et al., 1998 ; Zhou et al., 2008 ; Biagioni *et al*., 2013 ; Hettmann *et al*., 2014 ; Barkov *et al*., 2015 ; D'Orazio *et al*., 2017). Les circulations hydrothermales entrainent aussi parfois, la précipitation de minéraux rares tels que l'astrophyllite et la djerfisherite enrichis en Tl, lequel se substitue probablement au potassium (Hettmann *et al*., 2014 ; Barkov *et al*., 2015).

1.4. Le thallium dans le manteau

Les roches du manteau lithosphériques sont des roches ultramafiques constituées de péridotites et de pyroxènites (Pomerol *et al*., 2006). La concentration moyenne en thallium

estimée dans ces roches est de 72 ± 71 ppb (n = 14 ; De Albuquerque *et al.*, 1971 ; Sahl *et al.*, 1978 ; Heinrichs *et al.*, 1980 ; Nielsen *et al.*, 2015).

Au niveau des dorsales, les péridotites sont appauvries et si l'on se base sur l'ensemble des données disponibles dans la littérature, la concentration moyenne de ces roches en thallium est de 90,5 ± 49,6 ppb (fig. 1). Cependant, les récentes estimations calculées pour le manteau, dont la fusion génère les MORB sont de 0,5 ± 0,1 ppb (fig. 1 , Nielsen *et al*., 2014). Les mesures sur une harzburgite de référence, non altérée donnent une concentration en thallium de 1,05 ppb (Nielsen *et al*., 2015). Cet écart d'un ordre de grandeur peut s'expliquer de la manière suivante. Les études plus anciennes (Shaw, 1952 ; Shaw 1957 ; De Albuquerque *et al*., 1971 ; Shal *et al*., 1978 ; Heinrichs *et al*., 1980) avaient la contrainte d'analyser des roches « riches » en thallium pour dépasser les limites de détection imposées par leurs techniques de mesure de l'époque et les échantillons analysés proviennent tous de massifs anciens appartenant au domaine continental. Tous sont donc susceptibles d'avoir subi une forme d'altération or le thallium peut être très mobile dans ce genre de contexte. Il est donc possible que les valeurs mesurées soient le reflet d'une redistribution des composants de la roche due à la circulation d'un fluide entrainant ainsi une surestimation de la concentration en Tl (Nielsen *et al*., 2014). D'une manière générale, les roches ultra mafiques de par leur composition minérale (riches en ferro-magnésiens) sont relativement pauvres et cela même en cas d'altération hydrothermale. Elles ne constituent pas un réservoir de thallium important.

1.5. Le thallium dans la croûte océanique

1.5.1. Description

La répartition du thallium dans la lithosphère océanique est très variable comme le montre la figure 1. Cette variabilité s'observe également pour chaque type de lithologie où les écarts types sur la concentration moyenne sont importants (fig. 1).

Les sédiments des fonds océaniques sont hétérogènes et sont représentés de manière schématique, par des sédiments riches en carbonates et/ou en silice, des argiles pélagiques et des sédiments (nodules ou encroutements) ferromagnésiens (fig. 1). Ces derniers sont extrêmement riches en thallium et peuvent en contenir jusqu'à 200 ppm (Rekhämper *et al.*, 2002). Sans faire

une moyenne globale pour l'ensemble des sédiments, il apparaît que la couche supérieure de la croûte océanique concentre le plus de thallium (fig. 1).

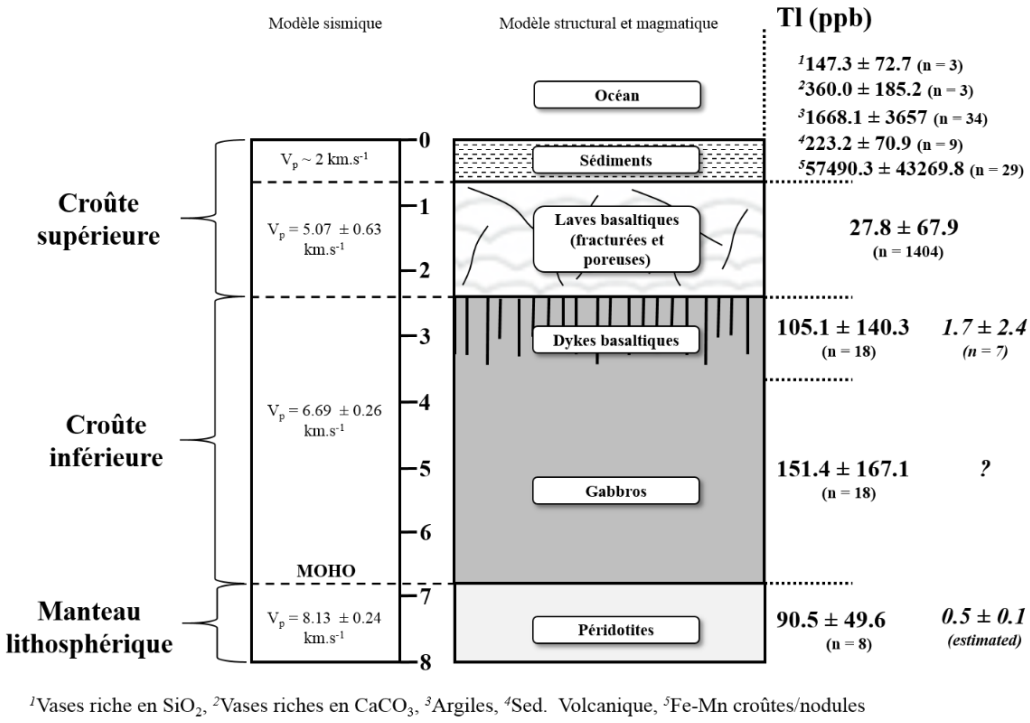

Figure 1 : Abondance relative du thallium dans les différents compartiments de la lithosphère océaniques. Les données présentées ici montrent une estimation de la composition de la lithosphère océanique au niveau des dorsales. Les phénomènes de zone de subduction n'apparaissent pas. Les données en gras proviennent de : De Albuquerque *et al*. (1971), Heinrichs *et al*. (1980), Sahl *et al*. (1978), Rekhämper *et al*. (2002), Nielsen *et al*. (2006a, 2014, 2016, 2017), Jenner *et al*. (2012) et Kelley *et al*. (2013). Les données en italiques sont issues de la compilation des données des articles de Nielsen *et al*. (2006a, 2014, 2016, 2017). Le schéma est adapté de Juteau et Maury (2008).

Les roches volcaniques de la croûte océanique sont principalement des MORB dont la concentration moyenne est de 27,8 ± 67,9 ppb. L'écart type important s'explique principalement par les phénomènes d'altération liés aux interactions avec l'eau de mer et les fluides hydrothermaux. Les laves de points chauds appartenant elles aussi au domaine océanique ont des concentrations moyennes similaires pour les OIB (*Ocean Island Basalts*), estimées à 28,7 ± 29,4 ppb (n = 19) pour les Açores, tandis que celle des picrites est estimée à 7,0 ± 6,8 (n = 26 ; Nielsen *et al.*, 2006b ; Nielsen *et al.*, 2007). Des concentrations plus importantes peuvent être observées dans les arcs insulaires liés à des zones de subduction où certaines séries de roches volcaniques

sont différenciées (Noll *et al*., 1996 ; Prytulak *et al*., 2013 ; Nielsen *et al*., 2016 ; Nielsen *et al*., 2017 ; Shu *et al*., 2017). Les roches plutoniques de la croûte océanique qui sont représentées par les gabbros, ont une concentration moyenne de 150 ppb mais présentent une très grande variabilité (fig. 1). Cependant, pour les mêmes raisons que les roches du manteau (§1.4), il est difficile de savoir si les données disponibles, toutes issues de gabbros potentiellement altérés, représentent des gabbros à l'équilibre avec leurs conditions de formation initiale.

En partant du principe que le soufre contrôle la quantité de thallium dans le liquide de fusion d'une lherzolite (Nielsen *et al*., 2014) et que dans tous les cas le thallium est un élément incompatible, il est possible d'émettre l'hypothèse que le produit de fusion soit enrichi en thallium. Cette concentration est similaire à celle analysée sur les verres de MORB, c'est-à-dire autour de 15 ppb (Jenner *et al*., 2012 ; Nielsen *et al*., 2014). Les dégazages et la cristallisation fractionnée vont induire des variations dans la concentration en Tl du liquide car le Tl est un élément volatile (Gauthier et Le Cloarec, 1998 ; Baker *et al.*, 2009), Le premier phénomène (les dégazages), va entraîner une perte en thallium, appauvrissant le liquide et les minéraux qui se forment. Le deuxième phénomène (la cristallisation fractionnée) va entraîner un enrichissement du liquide en thallium, ce dernier étant incompatible (que ce soit pour les silicates ou les sulfures). Il est donc envisageable que la concentration en thallium dans les gabbros qui cristallisent lentement soit similaire à celle observée dans les verres de MORB et donc en équilibre avec le produit de fusion (Nielsen *et al*., 2014). Cependant, les circulations de fluides dans cette partie de la croûte océanique sont mal connues (Nielsen *et al*., 2006a) et cela pourrait tout à fait produire une redistribution du thallium et expliquer des concentrations plus élevées et variables comme celles calculées pour la figure 1. Plus de données sont donc nécessaires pour comprendre la dynamique du thallium dans la coûté océanique inférieure et donc sa répartition.

1.5.2. Altération hydrothermal de la croûte océanique

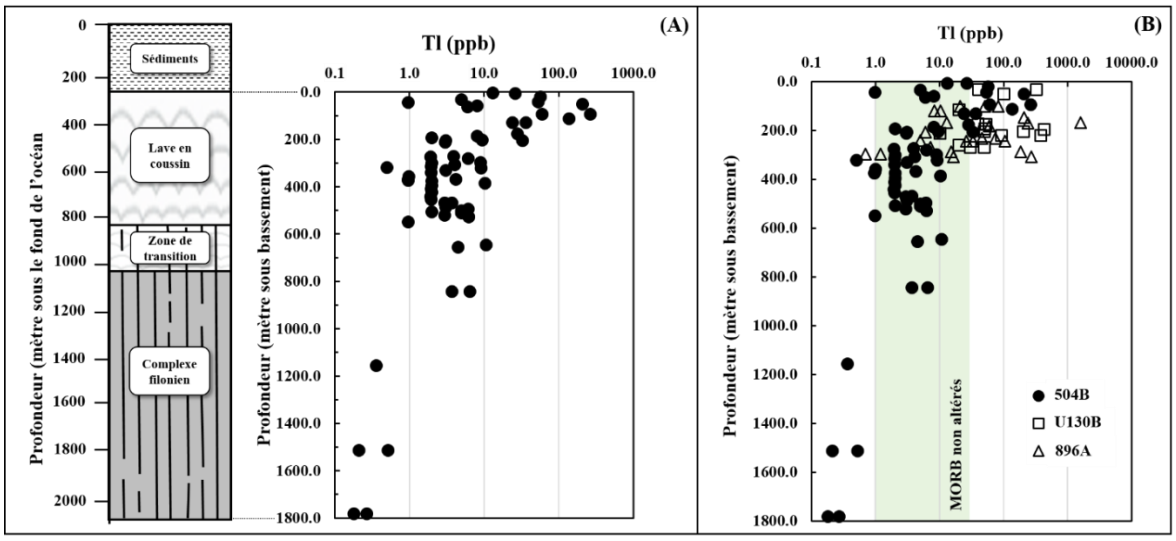

Figure 2 : Evolution de la concentration en thallium dans les basaltes de la croûte océaniques. (A) ces évolutions sont fonction de la profondeur et de la lithologie (adapté de Juteau et Maury, 2008) au niveau du forage 504B (Hubberten *et al*., 1983). (B) la tendance générale en fonction de la profondeur, en comparaison des MORB non altérés issus de Coggon *et al*. (2014). Les concentrations en Tl sont représentées en échelle logarithmique.

La croûte océanique est soumise à la circulation de deux types de fluides. Des fluides hydrothermaux de hautes températures (> 200°C) parallèles à l'axe des dorsales qui vont circuler en profondeur jusqu'au niveau des complexes filoniens (fig. 2A ; Juteau et Maury, 2008 ; Nielsen *et al*., 2006a). Ces fluides seront à l'origine des fumeurs des dorsales (Juteau et Maury, 2008). Le second type concerne des fluides de basses températures (< 100°C) qui circulent perpendiculairement à l'axe des dorsales, sur les flancs et qui affectent les 600 premiers mètres de la croûte océanique (sédiments + roches volcaniques ; Nielsen *et al*., 2006a).

Tableau 3 : Concentrations moyennes en Tl des fluides hydrothermaux altérant la croûte océanique (d'après Nielsen *et al*., 2006a).

	[Tl] ($.10^{-11}$ mol.kg^{-1})	T_{moy} (°C)
Fluides haute-T	2047,00 ± 1461,54 (n = 11)	344 ± 42
Fluides basse-T	8,95 ± 8,84 (n = 4)	27 ± 24
Eau de mer	6,5	

Les figures 2A et 2B montrent que les concentrations en thallium dans les 400 premiers mètres sous le plancher océanique affichent des concentrations en thallium pouvant dépasser

1000 ppb (figure 2B). Si l'on compare ces valeurs aux basaltes non altérés (fig. 2B) calculées à partir des données de Jenner et O'Neil (2012) et Nielsen *et al*., (2014), on constate un enrichissement en thallium dans les premières centaines de mètres sous le plancher océanique. Ce phénomène s'explique par la circulation de fluides à basse température (proche de l'eau de mer) dans cette zone. Ces fluides vont s'enrichir en thallium au contact des sédiments marins puis circuler dans les fractures du plancher océanique. Ensuite, au contact des bactéries sulfato-réductrices, le thallium sera piégé dans les pyrites néoformées (Coggon *et al*., 2014). Coggon *et al*. (2014) affirment que ce serait le mécanisme dominant dans le piégeage du thallium dans la croûte océanique altérée. Nielsen *et al*. (2006a) ajoutent qu'une fraction du thallium pourrait être adsorbée sur les argiles qui se forment dans ces conditions d'altération.

A l'opposé, les roches plus profondes, au niveau des complexes filoniens, ont des concentrations similaires sinon plus faibles que les MORB non altérés (fig. 2A et 2B). Nielsen *et al*. (2006a) ont expliqué ce résultat par un lessivage du thallium par les fluides hydrothermaux de hautes températures qui se retrouvent enrichis en thallium (tableau 3). Ces circulations de fluides sont sources de thallium pour les océans.

1.6. Le thallium dans la lithosphère continentale

L'abondance du thallium dans la lithosphère continentale est très hétérogène de par l'extrême diversité des roches qui la compose (tableau 1). Certaines études en ont estimé les concentrations en éléments traces (Wedepohl, 1995 ; Rudnik et Gao, 2003 par exemple). Wedepohl (1995) donne une concentration moyenne pour le thallium de 750 ppb pour la croûte supérieure et de 260 ppb pour la croûte inférieure, tandis que Rudnik et Gao (2003) calculent une concentration moyenne de 900 ppb pour la première et n'en calculent pas pour la seconde. La première constatation est donc que la croûte continentale est plus enrichie en thallium que la croûte océanique.

Tableau 2 : Concentrations moyennes en thallium des principaux types de roches formant la croûte continentale. Données compilées d'après Shaw (1952 et 1957), Sighinofli et Santos (1974), Sahl *et al*. (1978), Heinrichs *et al*. (1980), Ikramuddin *et al*. (1983), Kaplan et Mattigod (1998), Nielsen *et al*. (2005), Zhou *et al*. (2008) Baker *et al*. (2010), Belzile et Chen (2017), D'Orazio *et al*. (2017) et Nielsen *et al*. (2017).

Type de roche	Tl ($\mu g.kg^{-1}$)
Sédiments/alluvions	1623 ± 2496 (n = 38)
Roches sédimentaires détritiques	892 ± 956 (n = 66)
Roches sédimentaires carbonatées	541 ± 552 (n = 18)
Charbons	12 904 ± 38552 (n = 12)
Gisements (sulfures)	419 097 ± 1 120 058 (n = 112)
Latérites	100 (n = 2)
Roches volcaniques	713 ± 1198 (n = 146)
Roches plutoniques	1822 ± 2537 (n = 271)
Roches métamorphiques	1861 ± 3924 (n = 107)

Les sédiments actuels ont des concentrations en thallium de l'ordre du ppb, du même ordre de grandeur que les roches plutoniques et métamorphiques mais supérieures aux roches volcaniques et sédimentaires. Il semble donc que les phénomènes d'altération de surface soient source d'enrichissement en thallium. Cela a déjà été suggéré pour l'érosion des roches volcaniques (Calderoni *et al*., 1985). Au contraire, les roches sédimentaires qu'elles soient détritiques ou carbonatées présentent une concentration en Tl, inférieure de 50 % par rapport aux sédiments (actuels). Une des hypothèses pour expliquer ceci serait une remobilisation du thallium par les fluides au moment de la diagénèse.

Les charbons et les gisements de sulfures, bien qu'ils représentent une faible fraction de la croûte continentale, peuvent être très enrichis en thallium (tableau 1). Dans le cas des charbons, ce sont ceux riches en soufre qui sont les plus riches en thallium (Sahl *et al.*, 1978 ; Peter et Viraraghavan, 2005). Les roches magmatiques de la croûte continentales sont également plus concentrées en thallium que les roches magmatiques de la croûte océanique (fig. 1 et tableau 2). Les lithologies volcaniques sont plus appauvries en thallium que les plutoniques, probablement dû au fait que le thallium est un élément très volatil (Gauthier et Le Cloarec, 1998 ; Baker *et al.*, 2009).

2. LE THALLIUM DANS LES ENVIRONNEMENTS DE SURFACE : de la roche mère à l'atmosphère

Les multiples processus intervenant dans les environnements de surface, aux interfaces entre la Terre solide, l'hydrosphère, la biosphère et l'atmosphère vont engendrer une diversité importante de concentration en thallium. L'objectif de cette sous-partie est de présenter un aperçu de la répartition du thallium à la surface de la Terre. Le comportement géochimique du thallium et sa spéciation seront abordés pleinement dans une autre partie.

2.1. Les sources de thallium

Les sources de thallium pour l'environnement sont multiples et sont divisées entre sources d'origines naturelles et sources d'origines anthropiques. A l'échelle de la planète le thallium est un élément faiblement concentré mais les activités humaines ont perturbé son cycle et ont conduit à changer sa répartition (Peter et Viraraghavan, 2005 ; Karbowska, 2016 ; Belzile et Chen, 2017).

Le thallium naturel provient de l'activité volcanique (Baker *et al*., 2009 ; Kellerhals *et al*., 2010), de l'hydrothermalisme des dorsales océaniques (Rehkämper et Nielsen, 2004) et de l'altérations de minéraux riches en thallium (Xiao *et al*., 2004b ; Zhou et *al*., 2008 ; Voegelin *et al*., 2015).

L'une des principales sources de thallium anthropogénique est l'industrie minière, principalement par les processus d'altération des déchets miniers (Cheam, 2001 ; Lis *et al*., 2003 ; Casiot *et al*., 2011 ; Campanella *et al*., 2017 par exemple). Cela concerne les industries extractives liées à l'exploitation de gisements de sulfures (Pb, Zn, Cu pour les principaux) et de charbon. Les fonderies, les cimenteries et les centrales thermiques au charbon sont également des sources importantes de thallium (Dolgner *et al*., 1983 ; Cheam, 2001 ; Lis *et al*, 2003 ; Vaněk *et al*., 2011 ; Vaněk *et al*., 2013 ; Liu *et al*., 2016 ; Belzile et Chen, 2017). Le thallium provient également des rejets non contrôlés des effluents d'industrie l'utilisant comme matière première (Bennett 2017), mais aussi de lixiviat de décharges notamment celles où sont entreposées des objets contenants des composants électroniques (Law et Turner, 2011).

2.2. Le thallium dans les environnements continentaux

2.2.1. Les sols

Ces compartiments font probablement partie avec les rivières (paragraphe suivant) des environnements continentaux les plus décrits (en termes de concentration) en ce qui concerne le thallium. Les contenus en sont très dépendants de la roche mère sur laquelle le sol se développe. L'étude de Voegelin *et al*. (2015) rapporte des concentrations très élevées en thallium (de l'ordre du millier de ppm) dans des sols d'une région Suisse résultant de la pédogénèse d'amas hydrothermaux riches en thallium, arsenic et fer. D'autre études ont également rapporté des concentrations élevées de thallium, variant du ppm à la dizaine de ppm, dans des sols se développant sur des minéralisations riches en sulfures (Xiao *et al.* 2004a ; Vaněk, *et al*. 2015).

Les sources anthropiques de thallium pour les sols sont liées aux activité minières, soit par le rejet de thallium atmosphérique par les fonderies (Lis et al. 2003 ; Álvarez-Ayuso *et al*., 2013 ; Vaněk, *et al*. 2013 ; Vaněk, *et al*. 2017), soit en se développant sur des déchets miniers (Yang *et al*., 2005 ; Gomez-Gonzalez *et al*., 2015) avec des concentrations pouvant dépasser les 200 ppm.

Tremel *et al*. (1997) ont calculé une concentration médiane pour les horizons supérieurs de 244 sols français à 0,29 ppm avec 90 % des valeurs inférieures à 1,54 ppm. Dans la péninsule de Kola, la médiane des concentrations en Tl dans les horizons O a été calculée à 0,10 ppm avec 98 % des valeurs inférieures à 0,22 ppm (de Caritat et Reimann, 2017). Des enrichissements en thallium (entre 0,22 et 0, 35 ppm) ont été observés à proximité de mines ou de fonderies ainsi qu'au voisinage de la roche mère (de Caritat et Reimann, 2017). Ces données montrent que la concentration en thallium dans les sols varie énormément en fonction du type de roche mère et que les contaminations d'origine anthropique ne sont pas nécessairement celles qui génèrent les concentrations les plus élevées.

2.2.2. Les rivières et fleuves

La quantité de thallium dans les systèmes de rivières va d'abord se répartir entre le sédiment et la colonne d'eau, puis dans cette dernière, entre les fractions particulaires, colloïdales et dissoutes (fig. 3). La concentration moyenne en thallium dans les sédiments de rivière se situe à

4,03 ± 6.39 ppm[1] (n = 28 ; médiane = 1.70 ppm; 90ème centile = 10,07 ppm ; données tirées Belzile et Chen, 2017), les valeurs les plus élevées provenant de sites pollués par des activités minières (Belzile et Chen, 2017). Le fractionnement du thallium dans la colonne d'eau entre les différentes fractions dépend de la lithologie et du mode d'occupation du bassin versant, ainsi que de la nature des matières en suspension. Dans la grande majorité des rivières étudiées, 80 % du thallium se concentre dans la phase inférieure à 0,45 µm (Nielsen *et al*., 2005 ; Law et Turner, 2011 ; Casiot *et al*., 2011).

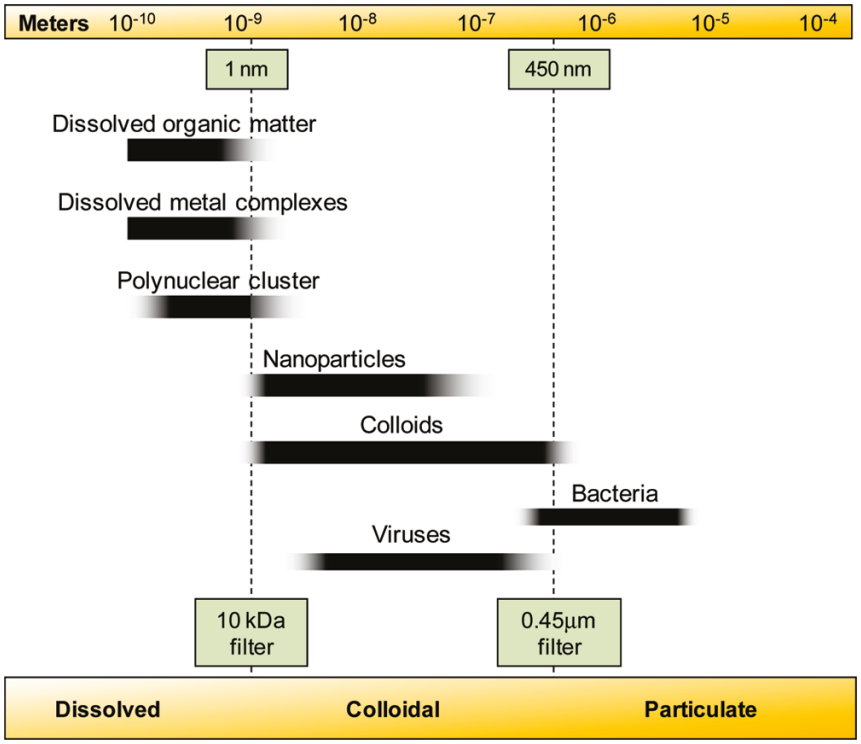

Figure 3 : Echelle des tailles des différents composés présents dans un échantillon d'eau brute (d'après Aiken *et al*., 2011).

Les concentrations en thallium dans la fraction inférieure à 0,45 µm sont très variées. Elles sont dépendantes des caractéristiques du bassin versant du cours d'eau (taille, mode d'occupation, lithologie). Nielsen *et al*. (2015) ont estimé sur 16 grands fleuves mondiaux que la fraction dissoute (inférieure à 0,45 µm) du thallium naturel (excluant les apports anthropiques) est relativement faible et de l'ordre de 2,93 ± 1,95 .10^{-11} mol.L^{-1}. Cette valeur est proche de la

[1]Les concentrations moyennes calculées pour les sédiments de rivières et de lacs (Belzile et Chen, 2017) ne tiennent pas compte des méthodes de digestions utilisées par les différents auteurs. Cependant ces méthodes semblent avoir un impact sur les concentrations mesurées (de Caritat et Reimann, 2017) et ainsi induire une erreur supplémentaire dans les moyennes.

celle rapportée par Kaplan et Mattigod (1998) et reportée dans le tableau 3. Des concentrations plus élevées ont pu être mesurées dans des rejets miniers avec des valeurs atteignant plus de 10^{-6} mol.L^{-1} (Casiot *et al*., 2011 ; Campanella *et al*., 2017).

Tableau 3 : Concentrations moyennes en thallium pour les eaux naturelles rapportées par Kaplan et Mattigod (1998).

	[Tl] en mol.L^{-1}
Eaux souterraines	$3.55\ 10^{-8}$
Rivières	$9.8\ .10^{-11}$
Lacs	$9.8\ .10^{-11}$
Tourbières	$9.8\ .10^{-11}$
Eau de mer	$6.4\ .10^{-11}$

Des échantillons du bassin Amazonien, provenant de diverses campagnes effectuées par des chercheurs de l'IPGP, ont été analysés pour mesurer les concentrations en thallium. Ces résultats sont présentés dans l'annexe C.

2.2.3. Les lacs et réservoirs

Le cycle du thallium dans les lacs est similaire à celui des rivières. Les sources sont également les mêmes que pour les rivières, mais le thallium dans les lacs et les réservoirs reste moins étudié (Karbowska, 2016 ; Belzile et Chen, 2017). La concentration moyenne en thallium (fraction < 0.45 µm), d'après les données réunies dans l'étude de Belzile et Chen (2017) est de $2{,}90 \pm 5{,}73\ .10^{-10}$ mol.L^{-1} (n = 21 ; médiane = $5{,}72\ .10^{-11}$ mol.L^{-1} ; $90^{ème}$ centile = $9{,}79\ .10^{-10}$ mol.L^{-1}). Cette valeur est 3 fois supérieure à la valeur reportée dans le tableau 3. Cette différence s'explique par l'influence de lacs contaminés au thallium dans la base de données utilisée par Belzile et Chen (2017). Les sédiments lacustres ont une concentration moyenne en thallium (estimée avec la base de données de Belzile et Chen, 2017) de 1168,8 ± 2530,3 ppb[12] (n = 25 ; médiane = 560,0 ppb ; $90^{ème}$ centile = 1518,0 ppb).

2.2.4. Les eaux de sources et les eaux souterraines

Le thallium dans les eaux souterraines et les eaux de sources est assez peu mesuré. Les concentrations en Tl sont principalement le reflet des interactions entre l'eau et les roches. Dans le cas des eaux souterraines, si celles-ci ont une connexion avec la surface (recharge dans le cas

[2]Voir note 1 page 19

des nappes), la concentration en Tl peut être influencée par l'impact des activités anthropiques. Ces eaux (sources et souterraines) peuvent également être des sources de thallium pour les rivières ou les lacs. Les concentrations moyennes calculées pour ces les eaux souterraines et les eaux de sources l'ont été à partir de la base de données de Belzile et Chen (2017). Elle est de 1,63 ± 4,15 $.10^{-9}$ mol.L^{-1} (n = 8 ; médiane = 1,66 $.10^{-10}$ mol.L^{-1} ; 90ème centile = 3,88 $.10^{-9}$ mol.L^{-1}) pour les eaux souterraines, ce qui est inférieure à la valeur du tableau 3. Dans les eaux de sources, la concentration moyenne en thallium est estimée à 2,25 ± 5,26 $.10^{-8}$ mol.L^{-1} (n = 8 ; médiane = 1,30 $.10^{-9}$ mol.L^{-1} ; 90ème centile = 5,95 $.10^{-8}$ mol.L^{-1}).

2.3. Le thallium dans les environnements océaniques et côtiers

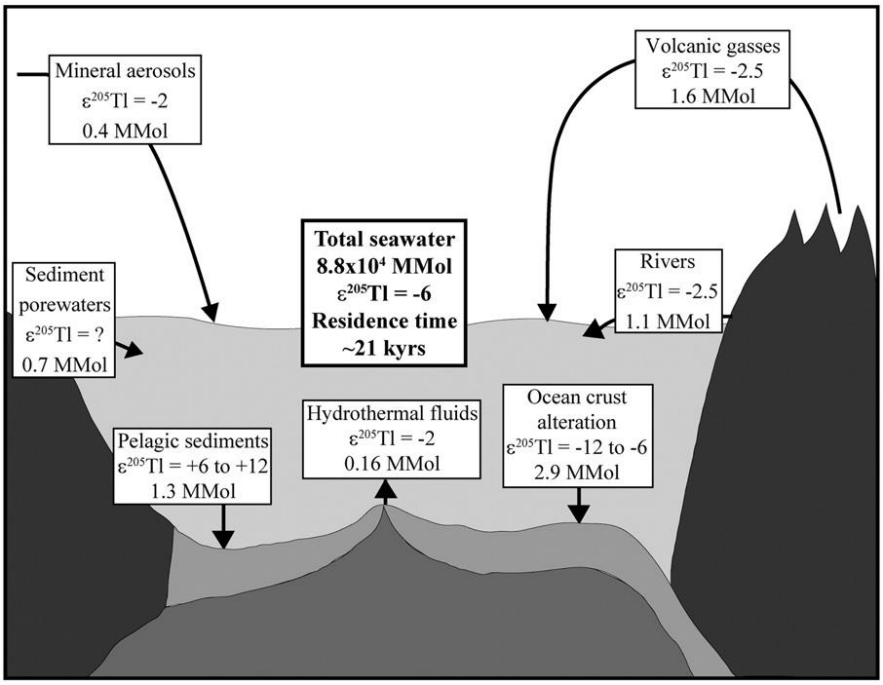

Figure 4 : Les cycles naturels du thallium dissous dans les océans (Nielsen *et al.*, 2009a). Les valeurs en 10^6 mol correspondent aux quantités de thallium dans chaque réservoir. Les ε correspondent au fractionnement isotopique du thallium.

Rehkämper et Nielsen (2004) ont estimé la concentration moyenne de l'eau de mer en Tl dissous à 6.5 ± 0.5 $.10^{-11}$ mol.L^{-1} similaire à la valeur de 6,4 $.10^{-11}$ mol.L^{-1} déterminée par Kaplan et Mattigod (1998). Les variations de concentrations avec la profondeur sont faibles et sont comprises entre 5,5 et 10,0 $.10^{-11}$ mol.L^{-1} dans l'océan Pacifique par exemple (Rehkämper et Nielsen, 2004).

Les sources de thallium pour les océans sont les rivières, les particules atmosphériques, le volcanisme de surface et les fluides hydrothermaux (fig. 4 ; Rehkämper et Nielsen 2004 ; Nielsen *et al*., 2005 ; Nielsen *et al*., 2009a). La figure 4 ne décrit que le cycle naturel du thallium. Les apports des rivières et des aérosols seraient certainement supérieurs si l'on y incluait les apports anthropiques (Nielsen *et al*., 2005). On pourrait également imaginer que les pollutions liées aux industries extractives offshores (pétrole, gaz ou autres), les activités côtières (raffinage, activités portuaires et autres industries lourdes), ainsi que l'altération des déchets au fond des océans puissent constituer aussi des sources de thallium. Néanmoins, ces quantités demeurent inconnues.

Les fleuves et rivières vont contribuer de plusieurs façons au cycle du thallium dans les océans. Dans un premier temps par la charge dissoute (discutée en section 2.2.) et ensuite par la charge particulaire qui va se déposer dans les marges continentales. Cependant, peu d'études traitent de ce sujet. Hu *et al*. (2016) ont montré que le thallium des cinq premiers centimètres des sédiments de la mer de Bohai (Chine du Nord) était principalement d'origine naturelle malgré la pression anthropique de la zone. Ils ajoutent également que le thallium est principalement sur la phase résiduelle, donc certainement peu biodisponible (Hu *et al.*, 2016). Des données provenant de la Mer Noire montrent des concentrations de l'ordre de 4,0 $.10^{-10}$ $mol.L^{-1}$ dans la colonne d'eau (Belzile et Chen 2017). Des concentrations relevées sur la côte proche de Kaoshiung (Taiwan) varient entre 4,9 ± 0,5 $.10^{-10}$ et 1,0 ± 0,1 $.10^{-9}$ $mol.L^{-1}$ (Belzile et Chen 2017) suggérant un impact des activités côtières. Au contraire, dans les eaux de la Mer de Ross (Antarctique) peu impactées par les activités humaines, les concentrations sont plus faibles et proches de 2,5 $.10^{-11}$ $mol.L^{-1}$ (Karbowska 2016).

Les estuaires vont également contrôler les apports de thallium aux environnements côtiers. Les études montrent qu'une quantité importante de thallium est sur la charge particulaire (Turner *et al*., 2010 ; Law et Turner, 2011) mais que celle-ci diminue avec la salinité au profit du thallium dissous (Nielsen *et al*., 2005 ; Turner *et al*., 2010). Les sédiments pélagiques des fonds océaniques ont des concentrations très variables, comme montré sur la figure 1 (section 1.5). Les phases les plus enrichies en thallium sont les argiles pélagiques et les croûtes d'oxyde de fer et de manganèse (Rehkämper *et al*., 2002 ; Rehkämper et Nielsen, 2004 ; Nielsen *et al*., 2016 ; Nielsen *et al*., 2017).

2.4. Le thallium dans l'atmosphère

Le thallium est un éléments très volatil (Baker *et al*., 2009) ce qui le rend très sensible à une dispersion atmosphérique. Les émissions de thallium liées aux activités volcaniques (source naturelle) sont de l'ordre du $pg.m^{-3}$ (Kellerhalls *et al*., 2010), tandis que celles provenant des activités anthropiques sont de l'ordre du $ng.m^{-3}$ (Belzile et Chen, 2017). Dans de nombreuses villes les concentrations en thallium dans les particules atmosphériques sont également de l'ordre du $ng.m^{-3}$ (Belzile et Chen, 2017).

Une étude menée en Suisse sur une tourbière, datant de l'Holocène, a montré une augmentation importante de la concentration en thallium dans les dépôts depuis le début de l'ère industrielle (Shotyk et Krachler, 2004). Avant cette époque, les variations de la quantité de thallium provenaient uniquement des alternances climatiques et des changements de flux provenant du volcanisme de surface (Shotyk et Krachler, 2004 ; Baker *et al*., 2009). La spéciation du thallium et son comportement dans l'atmosphère restent néanmoins très mal connus et relativement peu étudiés (Belzile et Chen, 2017).

3. GEOCHIMIE DU THALLIUM DANS LES ENVIRONNEMENTS DE SURFACE

Les concentrations en thallium dans les environnements de surface sont donc très variées et dépendent fortement du contexte géologique, du climat et de l'occupation de la zone (anthropisation, végétation, occupation et utilisation des sols, aménagement des cours d'eau, …). Cependant comme pour les autres éléments traces, les propriétés de transport du thallium, sa mobilité, sa biodisponibilité et sa toxicité potentielle ne dépendent pas seulement de sa concentration, mais aussi de se son comportement géochimique (par rapport aux phases porteuses ou aux minéraux), de sa distribution dans les différents compartiments de la zone critique et enfin, de sa spéciation dans l'environnement.

3.1. Les espèces de thallium

3.1.1. Le couple Tl(III)/Tl(I)

Le thallium présente deux état d'oxydation, thallium (I), la forme réduite et thallium (III) la forme oxydée. Le couple Tl(III)/Tl(I) ($Tl^{3+} + 2e^- \rightarrow Tl^+$) a un potentiel d'oxydoréduction élevé avec Eh = 1,28 V (Lin et Nriagu, 1998a). Dans la terre interne, Tl(I) est la forme

thermodynamiquement stable de thallium (Rehkämper et Nielsen, 2004 ; Prytulak *et al*., 2017). Le constat est le même pour les environnements de surface où Tl(III) n'existe en principe que dans les environnements très oxydant (Vink, 1993 ; Lin et Nriagu, 1998a).

3.1.2. Hydrolyse du thallium

Le Thallium(I) ne forme qu'un seul complexe hydroxylé, $Tl^{I}OH$, qui se forme de manière significative qu'à des pH supérieurs à 10 (Lin et Nriagu, 1998a ; Lin et Nriagu, 1998b). De plus ce complexe ne précipite pas dans les conditions environnementales (Lin et Nriagu, 1998b). Au contraire, thallium(III) forme plusieurs complexes avec les ions OH^-: $TlOH^{2+}$, $Tl(OH)_2^+$, $Tl(OH)_3$ et $Tl(OH)_4^-$ (Lin et Nriagu, 1998a). Ces espèces ne sont pas présentes en solution au même gamme de pH et par ordre d'apparition croissant, elles s'organisent dans cette ordre, $TlOH^{2+}$ < $Tl(OH)_2^+$ < $Tl(OH)_3$ < $Tl(OH)_4^-$ (Lin et Nriagu, 1998a ; Lin et Nriagu, 1998b). L'espèce $Tl(OH)_3$, susceptible d'être la plus stable dans les eaux naturelles, est très insoluble ($Ks = 10^{-45,2}$; Lin et Nriagu, 1998b). Plusieurs auteurs ont publié des constantes d'hydrolyse pour le thallium qui sont récapitulées dans l'annexe B.

3.1.3. Les complexes de thallium

L'ensemble des constantes de stabilité des complexes existant dans la littérature pour Tl(I) et Tl(III) est récapitulé en annexe B. Le thallium (I) forme peu de complexe avec les différents anions majeurs inorganiques des eaux naturelles et reste principalement sous sa forme libre Tl^+ (Lin et Nriagu, 1998 a; Xiong, 2007 ; Xiong, 2009). Cependant à températures plus élevées (supérieures à 100°C), les complexes $TlCO_3^-$ et $TlSO_4^-$ vont dominer aux pH supérieurs à 5 (Xiong, 2007). De même, en milieu réducteur où le soufre domine, le complexe TlHS sera l'espèce dominante pour des pH supérieurs à 6 (Xiong, 2007). Le constat est similaire avec les molécules organiques, hormis EDTA (acide éthylène diamine tétraacétique), dont le complexe avec Tl^+ devient l'espèce principale de Tl(I) à pH > 6 (Xiong, 2009). Le thallium (I) complexe également très peu avec les acides fulviques d'après Kaplan et Mattigod (1998). Une étude a également montré peu de complexation entre des acides humiques et Tl^+ (Liu *et al*., 2011).

Au contraire, Thallium (III) forme en principe beaucoup plus de complexes avec les anions (Kaplan et Mattigod, 1998; Lin et Nriagu, 1998a; annexe B). Les complexes les plus stables sont *a priori* ceux formés avec les chlorures, $Tl^{III}Cl^{2+}$, $Tl^{III}Cl_2^+$ et $Tl^{III}Cl_4^-$ (Kaplan et Mattigod, 1998).

Le thallium (III) a également une forte affinité pour le DTPA (acide diéthylène triamine penta acétique) ce qui a permis de mettre au point des protocoles de mesure de cette espèce dans les eaux naturelles (Casiot *et al*., 2011 ; Campanella *et al*., 2017).

3.1.4. Les phases minérales de thallium

Les minéraux de thallium sont rares et cristallisent en présence de quantités de thallium qui sont rarement atteintes sur terre (Xiong, 2007 ; Biagioni *et al*., 2013 ; Hettmann *et al*., 2014 ; Barkov *et al*., 2015). La majorité de ces minéraux sont des sulfures et ne seront stables que dans des conditions réductrices rarement atteintes dans les environnements de surfaces (Vink, 1998 ; Xiong, 2007). En revanche, leur altération deviendra une source de thallium pour ces environnements. A l'opposé, les oxydes de thallium, Tl^{I}_2O et $Tl^{III}_2O_3$ sont stables sous conditions oxydantes (Vink, 1993).

L'avicennite ($Tl^{III}_2O_3$) et la dorallcharite ($Tl^{I}_{0,8}K_{0,2}Fe_3(SO_4)_2(OH)_6$) sont deux minéraux que l'on retrouve dans les fronts d'altération (zones oxydées) des sulfures et sont donc susceptibles de contrôler la solubilité du thallium quand ils sont présents (Radtke *et al*., 1978; Balič Žunic *et al*., 1994). Les composés solides de Tl(I) sont d'ailleurs pour la majorité très solubles, notamment TlCl(s), Tl_2CO_3(s), TlOH(s), Tl_2SO_4(s) et Tl_2O(s) et précipitent rarement en solution (Kaplan et Mattigod, 1998 ; Xiong 2009). Dans des conditions d'eaux de mines très acides il est possible d'arriver à la saturation de lanmuchangite ($TlAl(SO_4)_2.12H_2O$) mais dans la très majeure partie des cas, le thallium reste en solution dans les environnements de surface (Vink, 1993 ; Xiong, 2009). Dans le cas des minéraux de Tl(III) les plus importants sont $Tl(OH)_3$ et l'avicennite. Ces derniers vont contrôler la solubilité du thallium(III) (Lin et Nriagu, 1998 ; Xiong, 2009).

3.2. Spéciation du thallium dans les environnements de surface

3.2.1. Spéciation du thallium dans les eaux naturelles

Dans les systèmes aquatiques, le thallium est présent sous ses deux états d'oxydations, Tl(I) et Tl(III) (Lin et Nriagu, 1999 ; Belzile et Chen, 2017). Thallium(I) est en théorie l'espèce thermodynamiquement la plus stable dans les environnements de surface (Vink, 1993 ; Xiong, 2009) et a été spécifiquement identifié comme l'espèce majoritaire dans certaines rivières (Casiot et al., 2011) ainsi que dans les océans (Rehkämper et Nielsen, 2004). Tl(III) a lui été mesuré

comme l'espèce majoritaire dans la colonne d'eau de certains systèmes lacustres comme ceux des Grand Lacs américains (Lin et Nriagu, 1999 ; Karlsson *et al*., 2006) ainsi que dans des eaux de consommation (Campanella *et al*., 2017). Thallium(III) n'est théoriquement stable que dans des environnements très oxydants (Vink, 1993) mais des photo-réactions ou des processus microbiens peuvent oxyder Tl(I) (Twining *et al*., 2003 ; Karlsson *et al*., 2006). La précipitaiton de $Tl(OH)_3$, la complexation sur du Fe(III) colloïdale (Karlsson *et al*., 2006) ou sur d'autres colloïdes non identifiés (Lin et Nriagu, 1999) seraient responsables de la stabilisation du thallium(III). En effet, cette forme de thallium a un fort potentiel réducteur et sans stabilisation, elle se réduit rapidement en Tl(I) (Karlsson *et al*., 2006).

Tableau 4 : Distribution modélisée des espèces de Tl(I) (% du total) dans différents système aquatique (Kaplan et Mattigod, 1998). TlOH, TlF, $TlNOPO_4$- et $TlPO_4^{2-}$ sont négligeables.

Espèce de Tl(I)	Eau souterraine	Eau de rivière	Lac eutrophique	Eau de tourbière	Eau de mer
Tl^+	90.4	82.7	76.8	32.4	51.9
$TlHCO_3$	4.4	1.2	2.0	-	0.5
$TlCO_3^-$	-	-	-	-	0.1
$TlSO_4^-$	3.6	0.4	0.8	-	11.2
TlCl	0.1	0.1	0.1	-	30.7
$TlCl_2$	-	-	-	-	5.4
Tl-fulvate	1.4	15.6	20.3	67.6	0.2

Thallium(I) reste la forme la plus étudiée du thallium. Kaplan et Mattigod (1998) ont modélisé la spéciation du thallium dissous dans les différents systèmes aquatiques (tableau 4). En dehors des eaux de mer, la majorité du thallium est sous sa forme libre Tl^+ et forme peu d'autre complexe (Kaplan et Mattigod, 1998). Dans les eaux douces (lacs et rivières), une part non-négligeable de thallium est complexée aux acides fulviques (Kaplan et Mattigod, 1998). Cependant ces constantes n'ont jamais été vérifiées par des données expérimentales, ce qui laisse un doute sur l'affinité du thallium pour la matière organique. En définitive les interactions entre le thallium et la matière organique dissoute restent très peu étudiées.

Casiot *et al*., (2011) ont mis en évidence que la majorité du thallium qu'ils avaient mesuré dans leur système (colonne d'eau de ruisseaux situés en sortie de mine) se trouvait dans la phase inférieure à 1nm (10 kD), traduisant une faible affinité pour la fraction particulaire en l'occurrence des particules d'oxyhydroxyde de fer. Ces observations, associées avec celles montrant que la majorité du thallium se trouvait dans la fraction inférieure à 450 nm (Nielsen *et*

al., 2005 ; Law et Turner, 2011) suggère que la spéciation thallium dans les eaux naturelles se résume principalement à sa forme libre et des complexes dissous. Le rôle des colloïdes semble donc limité comme le montre la faible affinité du thallium(I) pour les oxyhydroxyde de fer (Casiot *et al*., 2011 ; Liu *et al*., 2011 ; Peacock et Moon, 2012 ; Coup *et al*., 2015) et d'aluminium (Bidoglio *et al*., 1993) récapitulés dans les figures 5A et 5B. Cela est particulièrement évident aux pH acides (fig. 5A et 5B).

3.2.2. Spéciation du thallium aux interfaces

L'étude des phénomènes de sorption sur les croûtes ferromagnésiennes des fonds océaniques, très enrichie en thallium a montré une préférence du thallium pour les oxydes de manganèse (Peacock et Moon, 2012). Les oxydes de type birnessite (δ-MnO_2) sont réputés pour adsorber le Tl(I) à leur surface et l'oxyder en Tl(III) (Bidoglio *et al*., 1993 ; Peacock et Moon, 2012). Bidoglio *et al*. (1993) avancent l'hypothèse que thallium(III) précipite en avicennite ($Tl^{III}_2O_3$) à la surface des oxydes de manganèse. Peacock et Moon (2012), ont mis en évidence que thallium(I) en présence de birnessite hexagonale ($Na_{0,3}Ca_{0,1}K_{0,1}(Mn^{IV},Mn^{III})_2O_4$ .1,5H_2O[3]) allait être oxydé en thallium(III) et former des complexes tridentates avec les feuillets du minéral. Les mêmes auteurs ont montré que la sorption avec une birnessite triclinique[4] ou de la todorokite ($(Na,Ca,K,Ba,Sr)_{1-x}(Mn,Mg,Al)_6O_{12}$ .3-4H_2O) ne menait pas à l'oxydation du thallium et que ce dernier se contentait de former des complexes de sphère externe avec les sites réactifs de ces minéraux (Peacock et Moon, 2012).

Les interactions entre les minéraux les biofilms bactériens ont également un rôle important dans la dynamique des éléments traces aux interfaces. Malheureusement, peu d'étude existe à ce sujet sur le thallium. Smeaton *et al*. (2012), ont cependant montré que la dégradation biotique de la jarosite conduisait à un relarguage du thallium dans l'environnement au même titre que les dégradations abiotiques. Enfin la spéciation du thallium aux interfaces avec les surfaces biologiques est tout aussi peu étudiée. Une étude a montré que certaine espèce d'algue verte pouvait servir de technologie de bioremédiation du thallium (Birungi *et al*., 2015). Smeaton *et al*.

[3]La formule indiquée entre parenthèse est une formule générique de la birnessite. Pour plus de détails sur les différents minéraux mentionner, se rapporter à l'étude de Peacock et Moon (2012).
[4]Voir note ci-dessus

(2012) dans la seule étude sur les interactions entre des biofilms et du thallium, ont montré qu'aucune accumulation de Tl(I) par la bactérie *Shewanella putrefaciens* n'était observée.

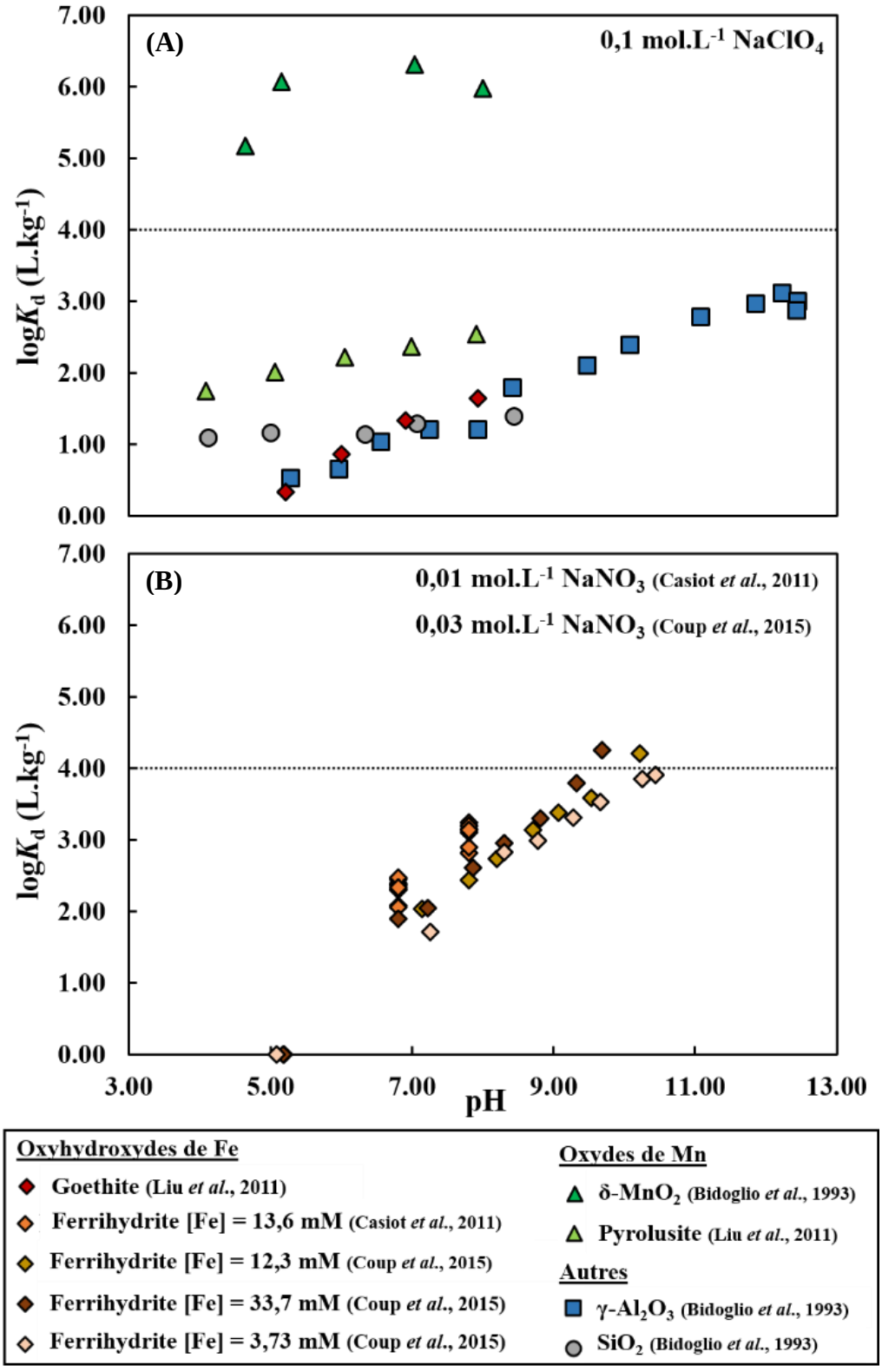

Figure 5 : (A) Comparaison des logK_d pour les oxyhydroxydes en présence de thallium(I). (B) Comparaison des logK_d acquis par différents auteurs pour la ferrihydrite en présence de thallium(I)

3.2.3. Spéciation dans les sols

La spéciation et la répartition du thallium dans les sols vont principalement dépendre de la roche mère et de la source de thallium (Yang *et al*., 2005 ; Vaněk *et al*., 2009 ; Vaněk *et al*., 2013 ; Gomez-Gonzalez *et al*., 2015 ; Voegelin *et al*., 2015). En effet, dans un sol où la roche mère est la source en thallium, sa répartition entre les différents horizons va dépendre de la dissémination des minéraux de cette roche mère (Yang *et al*., 2005 ; Vaněk *et al*., 2009 ; Gomez-Gonzalez *et al*., 2015). Si le thallium est dans les minéraux résiduels, comme le quartz ou les alumino-silicates, le thallium ne sera pas facilement mobilisable par les processus de pédogenèse (Yang *et al*., 2005 ; Vaněk *et al*., 2009 ; Gomez-Gonzalez *et al*., 2015). Cependant certains minéraux de la roche mère vont être altérés et des minéraux secondaires contenant du thallium comme la jarosite ($KFe_3(OH)_6(SO_4)_2$ où le thallium peut se substituer au potassium) ou l'avicennite ($Tl^{III}_2O_3$) vont alors se former et être observés (Voegelin *et al*., 2015). Lorsqu'ils sont à leur tour dégradés, ils deviennent une source de thallium labile pour le sol. Dans les sols impactés par des apports anthropogéniques, le thallium va s'accumuler dans les horizons supérieurs du sol et ainsi être plus échangeables et biodisponibles (Yang *et al*., 2005 ; Vaněk *et al*., 2013).

Voegelin *et al*. (2015) ont montré que les oxydes de manganèse et l'illite était les phases minérales les plus associés au thallium pendant la pédogénèse. Dans d'autre étude, une part importante du thallium est située dans la fraction réductible et donc associée aux oxydes de manganèse et oxyhydroxides de fer (Vaněk *et al*., 2009 ; Vaněk *et al*., 2012 ; Vaněk *et al*., 2013). Les argiles sont également considérées comme associées au thallium en se basant sur les propriétés similaires entre Tl^+ et K^+ mais sans réelles observations (Tremel *et al*., 1997; Vaněk *et al*., 2009; Vaněk *et al*., 2012). Cependant, les processus de sorption dans les sols demandent plus d'études, en particulier en ce qui concerne les interactions avec les argiles (Voegelin *et al*., 2015).

Le rôle de la matière organique des sols (SOM) semble limité (Vaněk *et al*., 2009 ; Vaněk *et al*., 2012 ; Vaněk *et al*., 2013 ; Voegelin *et al*., 2015) même si comme le résume très bien Vaněk *et al*. (2011), l'association du thallium avec les acides humiques des SOM ne peut pas être

négligée puisqu'elle n'a jamais été étudiée. Vaněk *et al*. (2013) ont également montré que la matière organique des sols et son impact sur le pH du sol pouvait avoir un rôle sur la mobilité du thallium et sur la dégradation de minéraux porteurs de thallium. De même, dans la rhizosphère, les acides organiques présents ont un impact similaire d'autant plus que le thallium à une faible affinité pour ces derniers (Vaněk *et al*., 2012).

4. TOXICITE, PRODUCTION ET UTILISATION DU THALLIUM

4.1. Toxicité et utilisations du thallium

Rapidement après sa découverte, la toxicité du thallium fut avérée et de nombreux cas d'empoisonnements (aigües ou chroniques) furent rapportés (Nriagu, 1998b). Le thallium est en réalité un élément non essentiel pour les organismes (Rodríguez-Mercado and Altamirano-Lozano, 2013). Certaines études montrent qu'il est plus toxique que le cadmium, l'arsenic, le plomb, le mercure, le zinc ou le cuivre pour les mammifères (Cheam, 2001 ; Rodríguez-Mercado and Altamirano-Lozano, 2013). Preuves des inquiétudes liées à sa toxicité, le thallium est classé « polluant prioritaire » par l'Agence Américaine de Protection de l'Environnement (EPA[5]). Plus récemment, le thallium a été classé comme un TCE (*Technological Critical Elements*, *TCEs*), un élément stratégique pour les nouvelles technologies ayant une menace potentielle pour la santé (Cobelo-García *et al.*, 2015).

Le thallium pénètre dans l'organisme via la peau, la paroi gastro-intestinale et les poumons (Peter and Viraraghavan, 2005). Cependant, les mécanismes menant à la toxicité du thallium restent mal connus notamment dans le cas d'exposition chronique (Peter et Viraraghavan, 2005 ; Rodríguez-Mercado et Altamirano-Lozano, 2013).

Une des hypothèses pour expliquer la toxicité du thallium serait sa complexation avec les groupes sulfhydriles des protéines ou des membranes mitochondriales ayant pour conséquence l'inhibition de l'activité enzymatique (Peter et Viraraghavan, 2005). Quelques études se sont intéressées à cette complexation (Montes *et al.*, 2007 ; Gharib et Shamel 2009 ; Gharib 2010) sans toutefois lever le flou sur ces hypothèses. Un autre phénomène, plus connu, viendrait de la compétition entre K^+ et Tl^+ qui bloquerait l'activation enzymatique (Peter et Viraraghavan, 2005 ;

[5] https://www.epa.gov/sites/production/files/2015-09/documents/priority-pollutant-list-epa.pdf

Rodríguez-Mercado et Altamirano-Lozano, 2013). Il semblerait également que Tl^{+} soit plus toxique que Tl^{3+} pour les humains et les mammifères en général (Rodríguez-Mercado et Altamirano-Lozano, 2013). D'autres études ont montré, que Tl^{3+} était plus toxique pour certaines espèces d'algues et d'invertébrés aquatiques (Rodríguez-Mercado et Altamirano-Lozano, 2013). Enfin, beaucoup de questions restent sans réponses, quant aux effets génétiques d'un empoisonnement au thallium (Rodríguez-Mercado et Altamirano-Lozano, 2013).

Les symptômes d'un empoisonnement aigüe au thallium sont des vomissements, des diarrhées et une perte de cheveux, mais aussi des effets et des dommages irréversibles sur le système nerveux, les poumons, le cœur, le foie et les reins (Peter et Viraraghavan, 2005 ; Rodríguez-Mercado et Altamirano-Lozano, 2013). Les effets chroniques sont plus difficiles à évaluer. L'étude de Zhang *et al.* (1998) dans le district de Lanmuchang a révélé des symptômes d'anorexie, des maux de tête, et des douleurs dans l'abdomen ainsi que dans tout le corps.

Les modes de contamination au thallium sont multiples, allant de l'exposition naturelle (Peter et Viraraghavan, 2005 ; Xiao *et al*., 2004b) à une exposition liée aux activités humaines (Dolgner *et al*., 1983 ; Zhang *et al*., 1998 ; Xiao *et al*., 2004 a; Peter et Viraraghavan, 2005). Voici quelques exemples de problème de santé publique liée à une exposition au thallium. Le premier se déroule en Chine, où l'érosion d'un amas sulfuré très riche en thallium a pollué les sols et contaminé l'environnement proche, sans générer de pollution au-delà de la localité concernée (Zhou *et al*., 2008). Une autre étude a révélé la contamination de l'eau de consommation par du thallium dans une ancienne région minière de Toscane en Italie, ce qui a exposé les habitants à une contamination chronique (Campanella *et al.*, 2016). Cependant, les personnes les plus exposées à un empoisonnement au thallium restent les mineurs et les travailleurs des industries qui l'utilisent comme composé ou matière première (Peter et Viraraghavan, 2005 ; Rodríguez-Mercado et Altamirano-Lozano, 2013).

Les utilisations du thallium sont variées et ont évolué au cours du temps. Au début du XX^{ème} siècle, le thallium était utilisé dans des produits de consommation comme les crèmes dépilatoires, dans la mort aux rats, les pesticides et dans le traitement de la syphilis, la tuberculose et les suées nocturnes (Nriagu 1998b). Il fut heureusement rapidement retiré de ces produits et interdit suite à de nombreux empoisonnements (Nriagu 1998b). Aujourd'hui, le thallium est principalement utilisé dans les industries de hautes technologies. Il entre dans la composition de lentilles, prismes

et fenêtres de détection des infrarouges, ainsi que dans des équipements de transmission (Bennett 2017). On le retrouve également dans des filtres cristallins de mesures acoustiques et optiques, et comme charges dans des verres et cristaux d'appareils de détections des rayons gamma (Bennett 2017). Enfin, le thallium entre dans la composition de superconducteurs Tl-Ba-Ca-Cu (Bennet 2017), ainsi que dans les alliages avec du mercure et dans les liquides de hautes densités pour la séparation des minéraux (Bennett 2017). Le thallium a toujours des applications dans le domaine de la santé. Sous forme de chlorures de thallium 201, isotope radioactif, il sert de produit de contraste dans l'imagerie cardiovasculaire (Nriagu 1998 b; Bennett 2017). Cependant, cette utilisation décline au profit du technétium 99 (Bennett 2017).

Les risques de pollution au thallium à grande échelle sont faibles et sont en réalité, limités à quelques régions comme le montre les exemples cités précédemment. Cependant le thallium est un élément très toxique et le principe de précaution a conduit les autorités de nombreux pays à réguler et contrôler les niveaux de thallium dans l'environnement (Peter et Viraraghavan, 2005). Quelques exemples de normes de régulations du thallium dans l'environnement sont présentés dans le tableau 5.

Tableau 5 : Seuils de concentrations en thallium accepté en Chine et aux Etats-Unis

Pays/Organisation	Eau potable	Air	Référence
Etats-Unis (USEPA)	2 µg.L^{-1}		Peter et Viraraghavan, 2005
Chine	0,1 µg.L^{-1}		Xiao *et al*., 2012
OMS		0,1 mg.m^{-3}	Peter et Viraraghavan, 2005

4.2. Production du thallium

Les gisements de thallium sont rares et ne sont pas les principales sources (Nriagu, 1998b). Il provient essentiellement de gisements de zinc, plomb et/ou cuivre auxquels il est associé aux sulfures. En effet, lors des processus de raffinage des minerais, le thallium est concentré dans les résidus et devient un produit de valorisation secondaire (Nriagu, 1998b ; Bennett, 2017). La production annuelle de thallium se situe autour de 10 tonnes (pour l'année 2016 ; Bennett 2017) et se concentre en Chine, au Kazakhstan et en Russie (Bennett, 2017). Les réserves en thallium sont difficilement estimables et sont principalement associées aux ressources en zinc, cuivre ou plomb (Bennett, 2017). Une certaine quantité de thallium serait également disponible dans les

résidus de combustion de charbon (Nriagu, 1998b). A ce jour, aucun processus de recyclage du thallium n'existe. Cependant, la demande en thallium étant faible et ayant même tendance à diminuer (Bennett, 2017), il semble peu probable que les ressources en thallium deviennent un enjeu stratégique particulier, contrairement à d'autre métaux tels que les terres rares, le tantale, ou les platinoïdes.

REFERENCES

Adam, J., & Green, Æ. T. (2006). Trace element partitioning between mica- and amphibole-bearing garnet lherzolite and hydrous basanitic melt : 1. Experimental results and the investigation of controls on partitioning behaviour, Contrib. Mineral. Petrol., 152, 1–17. http://doi.org/10.1007/s00410-006-0085-4

Aiken, G. R., Hsu-Kim, H., & Ryan, J. N.(2011). Influence of Dissolved Organic Matter on the Environmental Fate of Metals, Nanoparticles, and Colloids. . *Environmental Science and Technology*, *45*, 3196–3201. http://doi.org/10.1021/es103992s

Álvarez-Ayuso, E., Otones, V., Murciego, A., García-Sánchez, A., & Santa Regina, I. (2013). Zinc, cadmium and thallium distribution in soils and plants of an area impacted by sphalerite-bearing mine wastes. *Geoderma*, *207-208*, 25–34. http://doi.org/10.1016/j.geoderma.2013.04.033

Baker, R. G. a., Rehkämper, M., Hinkley, T. K., Nielsen, S. G., & Toutain, J. P. (2009). Investigation of thallium fluxes from subaerial volcanism—Implications for the present and past mass balance of thallium in the oceans. *Geochimica et Cosmochimica Acta*, *73*(20), 6340–6359. http://doi.org/10.1016/j.gca.2009.07.014

Baker, R. G. A., Rekhämper M., Ihlenfeld, C., Oates, C. J. & Coggon, R. (2010). Thallium isotope variations in an ore-bearing continental igneous setting: Collahuasi Formation, northern Chile. *Geochimica et Cosmochimica Acta*, *74*, 4405–4416. http://doi.org/10.1016/j.gca.2010.04.068

Balič Žunic, T., Moëlo, Y., Lončar, Z. & Micheelsen, H. (1994). Dorallcharite, $Tl^{I}_{0,8}K_{0,2}Fe_3(SO_4)_2(OH)_6$, a new member of the jarosite family. *Eur. J. Mineral*., *6*, 255–263

Barkov, A. Y., Martin, R. F. & Cabri L. J. (2015). Rare sulfides enriched in K, Tl and Pb from the Noril'sk and Salmagorsky complexes, Russia : new data and implications. *Mineralogical Magazine*, *79*, 799–808. http://doi.org/10.1180/minmag.2015.079.3.20

Bea, F., Pereira, M. D. & Stroh, A. (1994). Mineral/leucosome trace-element partitioning in a peraluminous migmatite (a laser ablation-ICP-MS study). *Chemical Geology*, *117*, 291–312.

Belzile, N., & Chen, Y. (2017). Applied Geochemistry Thallium in the environment : A critical review focused on natural waters , soils , sediments and airborne particles. *Applied Geochemistry*, *84*, 218–243. http://doi.org/10.1016/j.apgeochem.2017.06.013

Bennett, S. M. (2017). Thallium. US Geological Survey, *Mineral Commodity Summaries*, 170–171. https://minerals.usgs.gov/minerals/pubs/commodity/thallium/mcs-2017-thall.pdf

Biagioni, C., D'Orazio, M., Vezzoni, S., Dini, A., & Orlandi, P. (2013). Mobilization of TI-Hg-As-Sb-(Ag,Cu)-Pb sulfosalt melts during low-grade metamorphism in the Alpi Apuane (Tuscany, Italy). *Geology*, *41*(7), 747–750. http://doi.org/10.1130/G34211.1

Birungi, Z. S., & Chirwa, E. M. N. (2015). The adsorption potential and recovery of thallium using green micro-algae from eutrophic water sources. *Journal of Hazardous Materials*, *299*, 67–77. http://doi.org/10.1016/j.jhazmat.2015.06.011

Bowen, N. L. (1956). The evolution of the igneous rocks. Dover Publications

Calderoni, G., Ferri, T., Giannetti, B. & Masi, U. (1985). The behavior of thallium during alteration of the K-alkaline rocks from the Roccamonfina volcano (Campania, southern Italy), *Geochimica et Cosmochimica Acta*, *48*, 103–113.

Campanella, B., Onor, M., D'Ulivo, A., Giannecchini, R., D'Orazio, M., Petrini, R., & Bramanti, E. (2016). Human exposure to thallium through tap water: A study from Valdicastello Carducci and Pietrasanta (northern Tuscany, Italy). *Science of the Total Environment*, *548-549*, 33–42. http://doi.org/10.1016/j.scitotenv.2016.01.010

Campanella, B., Casiot, C., Onor, M., Perotti, M., Petrini, R., & Bramanti, E. (2017). Talanta Thallium release from acid mine drainages : Speciation in river and tap water from Valdicastello mining district (northwest Tuscany). *Talanta*, *171*(May), 255–261. http://doi.org/10.1016/j.talanta.2017.05.009

Casiot, C., Egal, M., Bruneel, O., Verma, N., Parmentier, M. & Elbaz-Poulichet F. (2011). Predominance of Aqueous Tl(I) Species in the River System Downstream from the Abandoned Carnoulès Mine (Southern France). *Environ. Sci. Technol.*, *45*, 2056–2064.

Cheam, V. (2001). Thallium Contamination of Water in Canada, *Water Qual. Res. J. Canada*, *36*(4), 851–877.

Cobelo-García, A., Filella, M., Croot, P., Frazzoli, C., Du Laing, G., Ospina-Alvarez., N., Rauch, S., Salaun, P., Schäfer, J., Zimmermann, S. (2015). COST action TD1407 : network on technology-critical elements (NOTICE) - from environmental processes to human health threats. *Environ. Sci. Pollut. Res*, *22*, 15188–15194. http://doi.org/10.1007/s11356-015-5221-0

Coggon, R. M., Rehka, M., Atteck, C., Teagle, D. A. H., Alt, J. C., & Cooper, M. J. (2014). Controls on thallium uptake during hydrothermal alteration of the upper ocean crust, *Geochimica et Cosmochimica Acta*, *144*, 25–42. http://doi.org/10.1016/j.gca.2014.09.001

Coup, K. M., & Swedlund, P. J. (2015). Demystifying the interfacial aquatic geochemistry of thallium (I): New and old data reveal just a regular cation. *Chemical Geology*, *398*, 97–103. http://doi.org/10.1016/j.chemgeo.2015.02.003

De Albuquerque, C. A. R., Muysson, J. R., & Shaw, D. M. (1971). Thallium in basalts and related rocks. *Chemical Geology*, *10*, 41–58.

Doan, M. (1899). Index to the Literature on Thallium, 1861-1896. Smithsonian Institution, Washington DC.

Dolgner, R., Brockhaus, A., Ewers, U., Wiegand, H., Majewsky, F., & Soddemann, H. (1983). Repeated surveillance of exposure to thallium in a population living in the vicinity of a cement plant emitting dust containing thallium. *Int Arch Occup Environ Health*, *52*, 79–94

de Caritat, P., & Reimann, C. (2017). Publicly available datasets on thallium (Tl) in the environment—a comment on "Presence of thallium in the environment: sources of contaminations, distribution and monitoring methods" by Bozena Karbowska, Environ Monit Assess (2016) 188:640 (DOI 10.1007/s1. *Environmental Monitoring and Assessment*, *189*(5), 232. http://doi.org/10.1007/s10661-017-5945-z

D'Orazio, M., Biagioni, C., Dini, A., & Vezzoni, S. (2017). Thallium-rich pyrite ores from the Apuan Alps , Tuscany , Italy : constraints for their origin and environmental concerns, 687–707. http://doi.org/10.1007/s00126-016-0697-1

Gauthier, P. J., & Le Cloarec, M. F. (1998). Variability of alkali and heavy metal fluxes released by Mt. Etna volcano, Sicily, between 1991 and 1995. *Journal of Volcanology and Geothermal Research*, *81*(3-4), 311–326. http://doi.org/10.1016/S0377-0273(98)00002-X

Gharib, F., & Shamel, A. (2009). Solvent Effects on Protonation and Complexation of Cysteine and Thallium (I) in Different Aqueous Solutions of Methanol. *J. Chem. Eng. Data.*, *54*, 933–939.

Gharib, F. (2010). Solvent Effects on Protonation and Complexation of Penicillamine and Thallium (I) in Different Aqueous Solutions of Methanol. *J. Chem. Eng. Data.*, *55*, 1547–1553.

Gomez-Gonzalez, M. A., Garcia-Guinea, J., Laborda, F., & Garrido, F. (2015). Thallium occurrence and partitioning in soils and sediments affected by mining activities in Madrid province (Spain). *Science of the Total Environment*, *536*, 268–278. http://doi.org/10.1016/j.scitotenv.2015.07.033

Greaney, A. T., Rudnick, R. L., Helz, R. T., Gaschnig, R. M., Piccoli, P. M., & Ash, R. D. (2017). The behavior of chalcophile elements during magmatic differentiation as observed in Kilauea Iki lava lake Hawaii. *Geochimica et Cosmochimica Acta*, *210*, 71–96. http://doi.org/10.1016/j.gca.2017.04.033

Heinrichs, H., Schulz-Dobrick, B. & Wedepohl, K. H. (1980). Terrestrial geochemistry of Cd, Bi, Tl, Pb, Zn and Rb. *Geochimica et Cosmochimica Acta*, *44*, 1519–1533.

Hettmann, K., Kreissig, K., Rehkämper, M., Wenzel, T., Mertz-Kraus, R. & Markl, G. (2014). Thallium geochemistry in the metamorphic Lengenbach sulfide deposit, Switzerland : Thallium-isotope fractionation in a sulfide melt. *American Mineralogist*, *99*, 793–803. http://doi.org/10.2138/am.2014.4591

Hubberten, H.-W., Emmermann, R. & Puchelt, H. (1983) Geochemistry of basalts from Costa Rica Rift Sites 504 and 505. *Init. Repts. DSDP*, pp. 791–803.

Ikramuddin, M., Asmeron, Y., Nordstrom, P. M., Kinart, K. P., Martin, W. M., Digby, S. J. M., Elder, D. D., Nijak, W. F. & Afemari, A. A. (1983). Thallium: a potential guide to mineral deposit, *Journal of Geochemical Exploration*, *19*, 465–490.

Jaujard, D. (2015). Géologie, Géodynamique – Pétrologie – Etude de terrains. *Sciences fondamentales*, Ed. Maloine, 336p. ISBN 978-2-224-03375-0

Jenner, F. E., & O'Neill, H. S. C. (2012). Analysis of 60 elements in 616 ocean floor basaltic glasses. Geochemistry, Geophysics, Geosystems, 13(1), 1–11. http://doi.org/10.1029/2011GC004009

Jochum, K. P., & Verma, S. P. (1996). Extreme enrichment of Sb, Tl and other trace elements in altered MORB. *Chemical Geology*, *130*, 289–299.

Juteau, T. & Maury, R. (2008). La croûte océanique – Pétrologie et dynamique endogène. Société géologique de France & Vuibert, 470p. ISBN 978-2-7117-4069-7

Kaplan, D. I., & Mattigod S. V. (1998). Aqueous geochemistry of thallium. In *Thallium in the Environment*, 15–29. Edited by J. O. Nriagu. John Wiley & Sons, Inc. New York

Karlsson, U., Karlsson, S., & Düker, A. (2006). The effect of light and iron(ii)/iron(iii) on the distribution of Tl(i)/Tl(iii) in fresh water systems. *Journal of Environmental Monitoring*, *8*(6), 634. http://doi.org/10.1039/b516445a

Karbowska, B. (2016). Presence of thallium in the environment : sources of contaminations, distribution and monitoring methods. *Environmental Monitoring and Assessment*, *188*, 640–659. http://doi.org/10.1007/s10661-016-5647-y

Kellerhalls, T., Tobler, L., Brütsch, S., Sigl, M., Wacker, L., Gäggeler, H. W. & Schwikowski, M. (2010). Thallium as a Tracer for Preindustrial Volcanic Eruptions in Ice Core Record from Illimani, Bolivia. *Environmental Science & Technology*, *44*, 888–89. http://doi.org/10.1021/es902492n

Kelley, K. A., Kingsley, R., & Schilling, J.-G. (2013). Composition of plume-in fl uenced mid-ocean ridge lavas and glasses from the Mid-Atlantic Ridge, East Pacific Rise, Galápagos Spreading Center, and Gulf of Aden. *Geochemistry, Geophysics, Geosystems*, *14*, 223–242. http://doi.org/10.1029/2012GC004415

Kersten, M., Xiao, T., Kreissig, K., Brett, A., Coles, B. J., & Rehkämper, M. (2014). Tracing Anthropogenic Thallium in Soil Using Stable Isotope Compositions. *Environmental Science & Technology*, *48*, 9030–9036. http://doi.org/10.1021/es501968d

Kiseeva, E. S. & Wood, B. J. (2013). A simple model for chalcophile element partitioning between sulphide and silicate liquids with geochemical applications. Earth and Planetary Science Letters, 383, 68–81. http://dx.doi.org/10.1016/j.epsl.2013.09.034

Law, S., & Turner, A. (2011). Thallium in the hydrosphere of south west England. *Environmental Pollution*, *159*(12), 3484–3489. http://doi.org/10.1016/j.envpol.2011.08.029

Lide, D. R. (2009) CRC Handbook of Chemistry and Physics. CRC Press Inc, 90th ed., 2804 p. ISBN 978-1-420-09084-0

Lin, T.-S., & Nriagu, J. (1998a). Speciation of thallium in natural waters. In *Thallium in the Environment*, 31–43. Edited by J. O. Nriagu. John Wiley & Sons, Inc. New York

Lin, T.-S., & Nriagu, J. (1998b). Revised Hydrolysis Constants for Thallium(I) and Thallium(III) and the Environmental Implications. *Journal of the Air & Waste Management Association*, *48*(2), 151–156. http://doi.org/10.1080/10473289.1998.10463658

Lin, T.-S., & Nriagu, J. (1999). Thallium Speciation in the Great Lakes. *Environmental Science & Technology*, *33*(19), 3394–3397. http://doi.org/10.1021/es981096o

Lis, J., Pasieczna, A., Karbowska, B., Zembrzuski, W., & Lukaszewski, Z. (2003). Thallium in soils and stream sediments of a Zn-Pb mining and smelting area. *Environmental Science and Technology*, *37*(20), 4569–4572. http://doi.org/10.1021/es0346936

Liu, J., Lippold, H., Wang, J., Lippmann-Pipke, J., & Chen, Y. (2011). Sorption of thallium(I) onto geological materials: Influence of pH and humic matter. *Chemosphere*, *82*(6), 866–871. http://doi.org/10.1016/j.chemosphere.2010.10.089

Liu, J., Wang, J., Chen, Y., Xie, X., Qi, J., Lippold, H. & Wu, Q. (2016). Thallium transformation and partitioning during Pb-Zn smelting and environmental implications. *Environmental Pollution*, *212*, 77–89. http://doi.org/10.1016/j.envpol.2016.01.046

McGoldrick, P. J., Keays, R. R., & Scott, B. B. (1979). Thallium: a sensitive indicator of rock/seawater interaction and of sulfur saturation of silicate melts. *Geochimica et Cosmochimica Acta*, *43*(8), 1303–1311. http://doi.org/10.1016/0016-7037(79)90120-0

Montes, S., Soriano, L., Ríos, C., & Monroy-Noyola, A. (2007). Endogenous thiols enhance thallium toxicity. *Archives of Toxicology*, *81*(10), 683–687. http://doi.org/10.1007/s00204-007-0203-8

Nielsen, S. G., Rehkämper, M., Porcelli, D., Andersson, P., Halliday, A. N., Swarzenski, P. W. Latkoczy, C., Günther, D. (2005). Thallium isotope composition of the upper continental crust and rivers—An investigation of the continental sources of dissolved marine thallium. *Geochimica et Cosmochimica Acta*, *69*, 2007–2019. http://doi.org/10.1016/j.gca.2004.10.025

Nielsen, S. G., Rehkämper, M., Teagle, D. A. H., Butterfield, D. A., Alt, J. C., & Halliday, A. N. (2006a). Hydrothermal fluid fluxes calculated from the isotopic mass balance of thallium in the ocean crust. *Earth and Planetary Science Letters*, *251*, 120–133. http://doi.org/10.1016/j.epsl.2006.09.002

Nielsen, S. G., Rehkämper, M., Norman, M. D., Halliday, A. N., & Harrison, D. (2006b). Thallium isotopic evidence for ferromanganese sediments in the mantle source of Hawaiian basalts. *Nature*, *439* (7074), 314–317. http://doi.org/10.1038/nature04450

Nielsen, S. G., Rekhämper, M., Brandon, A. D., Norman, M. D., Turner, S. & O'Reilly, S. Y. (2007). Thallium isotopes in Iceland and Azores lavas — Implications for the role of altered crust and mantle. *Earth and Planetary Science Letters*, 236, 332–345. http://doi.org/10.1016/j.epsl.2007.10.008

Nielsen, S. G., Mar-Gerrison, S., Gannoun, A., LaRowe, D., Klemm, V., Halliday, A. N., Burton, K. W., Hein, J. R. (2009a). Thallium isotope evidence for a permanent increase in marine organic carbon export in the early Eocene. *Earth and Planetary Science Letters*, *278*, 297–307. http://doi.org/10.1016/j.epsl.2008.12.010

Nielsen, S. G., Williams, H. M., Griffin, W. L., O'Reilly, S. Y., Pearson, N., & Viljoen, F. (2009b). Thallium isotopes as a potential tracer for the origin of cratonic eclogites. *Geochimica et Cosmochimica Acta*, *73*(24), 7387–7398. http://doi.org/10.1016/j.gca.2009.09.001

Nielsen, S. G., Shimizu, N., Lee, C. T. A., & Behn, M. D. (2014). Chalcophile behavior of thallium during MORB melting and implications for the sulfur content of the mantle. *Geochemistry, Geophysics, Geosystems*, *15*, 4905–4919. http://doi.org/10.1002/2014GC005536

Nielsen, S. G., Klein, F., Kading, T., Blusztajn, J., & Wickham, K. (2015). Thallium as a tracer of fluid-rock interaction in the shallow Mariana forearc. *Earth and Planetary Science Letters*, *430*, 416–426. http://doi.org/10.1016/j.epsl.2015.09.001

Nielsen, S. G., Yogodzinski, G., Prytulak, J., Plank, T., Kay, S. M., Kay, R. W. Blusztajn, J., Owens, J. D., Auro, M. & Kading, T. (2016). Tracking along-arc sediment inputs to the Aleutian arc using thallium isotopes. *Geochimica et Cosmochimica Acta*, *181*, 217–237. http://doi.org/10.1016/j.gca.2016.03.010

Nielsen, S. G., Prytulak, J., Blusztajn, J., Yunchao, S., Auro M., Regelous, M. & Walker, J. (2017). Thallium isotopes as tracers of recycled materials in subduction zones: Review and new data for lavas from Tonga-Kermadec and Central America. *Journal of Volcanology and Geothermal Research, 339*, 23–40. http://doi.org/10.1016/j.jvolgeores.2017.04.024

Hu, N., Huang, P., Liu, J., & Shi, X. (2016). Distribution of thallium in the Bohai Sea : Implications for hydrodynamic forces and anthropogenic impact. *Environmental Earth Sciences*, *75*, 903–915. http://doi.org/10.1007/s12665-016-5727-x

Nriagu, J. O. (1998a), Thallium in the Environment. Wiley Series in Advances in Environmental Science and Technology, 29, 284p. John Wiley & Sons, Inc. New York

Nriagu, J. O. (1998b). History, Production and Uses of Thallium. In Thallium in the Environment, 1–14. Edited by J. O. Nriagu. John Wiley & Sons, Inc. New York

Noll, P. D., Newson, H. E., Leeman, W.P. & Ryan, J. G. (1996). The role of hydrothermal fluids in the production of subduction magmas: Evidence from siderophile and chalcophile trace elements and boron. *Geochimica et Cosmochimica Acta*, 60, 587–611.

Peacock, C. L., & Moon, E. M. (2012). Oxidative scavenging of thallium by birnessite: Explanation for thallium enrichment and stable isotope fractionation in marine ferromanganese precipitates. *Geochimica et Cosmochimica Acta*, *84*, 297–313. http://doi.org/10.1016/j.gca.2012.01.036

Pearson, R. G. (1968). Hard and Soft Acids and Bases, HSAB, Part II – Underlying theories. *Journal of Chemical Education*, *45*(10), 643–648. http://doi.org/10.1021/2Fed045p643

Peter, a. L. J., & Viraraghavan, T. (2005). Thallium: a review of public health and environmental concerns. *Environment International*, *31*(4), 493–501. http://doi.org/10.1016/j.envint.2004.09.003

Pomerol, C., Lagabrielle, Y. & Renard, M. (2006). Eléments de Géologie, 13ème édition. *UniverSciences*, Dunod, Paris, 762p. ISBN 2-10-048658-6

Prytulak, J., Nielsen, S. G., Plank, T., Barker, M., & Elliott, T. R. (2013). Assessing the utility of thallium and thallium isotopes for tracing subduction zone inputs to the Mariana arc. *Chemical Geology*, *345*, 139–149. http://doi.org/10.1016/j.chemgeo.2013.03.003

Prytulak, J., Brett, A., Webb, M., Plank, T., Rehkämper, M., Savage, P. S., & Woodhead, J. (2017). Thallium elemental behavior and stable isotope fractionation during magmatic processes. *Chemical Geology*, *448*, 71–83. http://doi.org/10.1016/j.chemgeo.2016.11.007

Radtke, A. S., Dickson, F. W. & Slack, J. F. (1978). Occurrence and formation of avicennite, Tl_2O_3, as a secondary mineral at the Carlin gold deposit, Nevada. *Jour. Research U.S. Geol. Survey*, *6*, 241–246

Rehkämper, M., Frank, M., Hein, J. R., Porcelli, D., Halliday, a., Ingri, J., & Liebetrau, V. (2002). Thallium isotope variations in seawater and hydrogenetic, diagenetic, and hydrothermal ferromanganese deposits. *Earth and Planetary Science Letters*, *197*(1-2), 65–81. http://doi.org/10.1016/S0012-821X(02)00462-4

Rehkämper, M., & Nielsen, S. G. (2004). The mass balance of dissolved thallium in the oceans. *Marine Chemistry*, *85*, 125–139. http://doi.org/10.1016/j.marchem.2003.09.006

Rodríguez-Mercado, J. J., Altamirano-Lozano, M. A. (2013). Genetic toxicology of thallium : a review. *Drug and Chemical Toxicology* *36*, 369–383. http://doi.org/10.3109/01480545.2012.710633

Rudnik, R. L. & Gao, S. (2003). Composition of the Continental Crust. *Treatise in Geochemistry*, *3*, 1–64.

Sahl, K., Albuquerque, C. A. R., & Shaw, D. M. (1978). Thallium. *Handbook of Geochemistry*, *Ed. KH Wedepohl*, Springer-Verlag, Berlin, Germany.

Sighinolfi G. P. & Santos, A. M. (1974). Thallium in deep-seated crustal rocks, *Geochimica et Cosmochimica Acta*, *38*, 641–646.

Shannon, R. D. (1976). Revised Effective Ionic Radii and Systematic Studies of Interatomic Distances in Halides and Chalcogenides. *Acta Cryst.*, *32*, 751-767.

Shaw, D. M. (1952). The geochemistry of thallium. *Geochimica et Cosmochimica Acta*, *2*, 118–154

Shaw, D. M. (1957). The geochemistry of gallium, indium, thallium—a review. *Physics and Chemistry of the Earth*, *2*, 164–211. http://doi.org/http://dx.doi.org/10.1016/0079-1946(57)90009-5

Shotyk, W., & Krachler, M. (2004). Atmospheric deposition of silver and thallium since 12370 C-14 years BP recorded by a Swiss peat bog profile, and comparison with lead and cadmium. *Journal of Environmental Monitoring*, *6*, 427–433. http://doi.org/10.1039/b315084b

Shu, Y., Nielsen, S. G., Zeng, Z., Shinjo, R., Blusztajn, J., Wang, X. & Chen, S. (2017). Tracing subducted sediment inputs to the Ruykyu arc-Okinawa Through system: Evidence from thallium

isotopes. *Geochimica et Cosmochimica Acta*, *217*, 462–491. http://dx.doi.org/10.1016/j.gca.2017.08.035

Smeaton, C. M., Walshe, G. E., Fryer, B. J., & Weisener, C. G. (2012). Reductive Dissolution of Tl(I) − Jarosite by *Shewanella putrefaciens* : Providing New Insights into Tl Biogeochemistry, *Environmental Science & Technology*, *46*, 11086–11094. dx.doi.org/10.1021/es302292d

Smith, D. S., Bell, R. A., & Kramer, J. R. (2002). Metal speciation in natural waters with emphasis on reduced sulfur groups as strong metal binding sites. *Comparative Biochemistry and Physiology Part C*, *133*(1-2), 65–74. http://doi.org/10.1016/S1532-0456(02)00108-4

Turner, A., Cabon, A., Glegg, G. a., & Fisher, A. S. (2010). Sediment–water interactions of thallium under simulated estuarine conditions. *Geochimica et Cosmochimica Acta*, *74*(23), 6779–6787. http://doi.org/10.1016/j.gca.2010.09.004

Twining, B. S., Twiss, M. R., & Fisher, N. S. (2003). Oxidation of thallium by freshwater plankton communities. *Environmental Science & Technology*, *37*(12), 2720–6. http://doi.org/10.1021/es026145i

Vaněk, A., Chrastný, V., Mihaljevič, M., Drahota, P., Grygar, T., & Komárek, M. (2009). Lithogenic thallium behavior in soils with different land use. *Journal of Geochemical Exploration*, *102*, 7–12. http://doi.org/10.1016/j.gexplo.2008.10.004

Vaněk, A., Komárek, M., Vokurková, P., Mihaljevič, M., Sebek, O., Panuskova, G., Chrastný, V. & Drabek, O. (2011). Effect of illite and birnessite on thallium retention and bioavailability in contaminated soils. *Journal of Hazrdous Materials*, *191*, 170–176. http://doi.org/10.1016/j.jhazmat.2011.04.065

Vaněk, A., Komárek, M., Chrastný, V., Galu, I., Mihaljevi, M., Drahota, P., Tejnecký, V., & Vokurková, P. (2012). Effect of low-molecular-weight organic acids on the leaching of thallium and accompanying cations from soil – A model rhizosphere solution approach. *Journal of Geochemical Exploration*, *112*, 212–217. http://doi.org/10.1016/j.gexplo.2011.08.010

Vaněk, A., Chrastný, V., Komárek, M., Penížek, V., Teper, L., Cabala, J. & Drábek O. (2013). Geochemical position of thallium in soils from a smelter-impacted area. *Journal of Geochemical Exploration*, *124*, 176–182. http://doi.org/10.1016/j.gexplo.2012.09.002

Vaněk, A., Grösslová, Z., Mihaljevič, M., Ettler, V., Chrastný, V., Komárek, M., … Ash, C. (2015). Thallium contamination of soils/vegetation as affected by sphalerite weathering: A model rhizospheric experiment. *Journal of Hazardous Materials*, *283*, 148–156. http://doi.org/10.1016/j.jhazmat.2014.09.018

Vaněk, A., Grösslová, Z., Mihaljevic, M., Trubac, J., Teper, L., Cabala, J., Rohovec, J., & Ash, C. (2016). Isotopic Tracing of Thallium Contamination in Soils A ff ected by Emissions from Coal-Fired Power Plants. http://doi.org/10.1021/acs.est.6b01751

Vaněk, A., Grösslová, Z., Mihaljevič, M., Ettler, V., Trubač, J., Chrastný, V., … Ash, C. (2017). Thallium isotopes in metallurgical wastes/contaminated soils: A novel tool to trace metal source and behavior. *Journal of Hazardous Materials*. http://doi.org/10.1016/j.jhazmat.2017.09.020

Vink, B. W. (1993). The behavior of thallium in the (sub)surface environment in terms of Eh and pH. *Chemical Geology*, *109*, 119–123.

Vink, B. W. (1998). Thallium in the (sub)surface environment: its mobility in term of Eh and pH. In *Thallium in the Environment*, 45–58. Edited by J. O. Nriagu. John Wiley & Sons, Inc. New York

Voegelin A., Pfenninger N., Petrikis J., Majzlan J., Plötze M., Senn A.-C. and Göttlicher J. (2015). Thallium speciation and extractability in a thallium- and arsenic-rich soil developed from mineralized carbonate rock. *Environmental Science & Technology* **49**, 5390–5398.

Wedepohl, K. H. (1995). The composition of the continental crust. *Geochimica et Cosmochimica Acta*, *59*, 1217–1232. http://doi.org/10.1016/0016-7037(95)00038-2

Xiao, T., Guha, J., Boyle, D., Liu, C., & Chen, J. (2004a). Environmental concerns related to high thallium levels in soils and thallium uptake by plants in southwest Guizhou, China. The Science of the Total Environment, 318(03), 223–244. http://doi.org/10.1016/S0048-9697(03)00448-0

Xiao, T., Guha, J., Boyle, D., Liu, C., Zheng, B., Wilson, G. C., Rouleau, A. & Chen, J. (2004b). Naturally occurring thallium : a hidden geoenvironmental health hazard ? *Environment International*, *30*, 501–507. http://doi.org/10.1016/j.envint.2003.10.004

Xiao, T., Yang, F., Li, S., Zheng, B., & Ning, Z. (2012). Thallium pollution in China: A geo-environmental perspective. *Science of The Total Environment*, *421-422*, 51–58. http://doi.org/10.1016/j.scitotenv.2011.04.008

Xiong, Y. (2007). Hydrothermal thallium mineralization up to 300 ° C : A thermodynamic approach, *32*, 291–313. http://doi.org/10.1016/j.oregeorev.2006.10.003

Xiong, Y. (2009). The aqueous geochemistry of thallium : speciation and solubility of thallium in low temperature systems, 441–451. http://doi.org/10.1071/EN08086

Yang, C., Chen, Y., Peng, P., Li, C., Chang, X., & Xie, C. (2005). Distribution of natural and anthropogenic thallium in the soils in an industrial pyrite slag disposing area. *Science of The Total Environment*, *341*(1-3), 159–172. http://doi.org/10.1016/j.scitotenv.2004.09.024

Zhang, Z., Zhang, B., Long, J., Zhang, X., & Chen, G. (1998). Thallium pollution associated with mining of thallium deposits. *Sci China*, *Ser. D*, *41*(1), 75–81

Zhou, T., Fan, Æ. Y., Yuan, Æ. F., & Cooke, Æ. D. (2008). A preliminary investigation and evaluation of the thallium environmental impacts of the unmined Xiangquan thallium-only deposit in Hexian , China, 131–145. http://doi.org/10.1007/s00254-007-0800-0

PARTIE 2 : LE RADIUM

De nombreuses études existent sur la géochimie du Ra (Porcelli *et al*, 2014 ; Fesenko *et al*., 2014), le parti pris a été de ne pas être exhaustif et l'objectif de cette partie est de donner un bref aperçu de cet état de l'art.

1. DECOUVERTE DU RADIUM

Le radium est un élément qui appartient à l'histoire puisqu'il est associé à la découverte de la radioactivité. Il a été découvert sur un minerais de pechblende par Pierre et Marie Curie en 1898 (Porcelli *et al*., 2014). Le radium est un métal alcalino-terreux de numéro atomique 88. Tous ses isotopes sont radioactifs mais seulement quatre existent dans l'environnement, ^{223}Ra, ^{224}Ra, ^{226}Ra et ^{228}Ra (Porcelli *et al*., 2014). ^{226}Ra appartient à la chaîne de désintégration de ^{238}U, ^{228}Ra et ^{224}Ra à la chaîne de ^{232}Th, quant à ^{223}Ra il est dans le chaîne de désintégration de ^{235}U (Porcelli *et al*., 2014). Le comportement et la répartition de ces éléments dans les environnements terrestres va donc dépendre de l'élément avec la plus longue demi-vie de la chaîne de désintégration (Porcelli *et al*., 2014).

L'isotope du radium le plus répandu et le plus susceptible d'avoir un impact pour l'environnement est le 226 (Porcelli *et al*., 2014). C'est l'isotope à la durée de demi-vie la plus longue, 1602 ans (Porcelli *et al*., 2014). Le radium appartient au groupe des radionucléides naturellement présents dans l'environnement (Fesenko *et al*., 2014). Ces éléments, en raison de leurs demi-vies relativement courtes sont responsables d'une part importante des radiations (émetteur gamma) reçues par l'espèce humaine (Fesenko *et al*., 2014). Ce sont donc des éléments très étudiés dans l'environnement. Le radium est lui-même toxique en plus des radiations qu'il émet et peut notamment s'accumuler dans les os des mammifères (Jia et Jia, 2012). Il est aussi très étudié à cause de son élément fils, le radon 222, un gaz responsable du cancer des poumons principalement (Darby *et al*., 2004).

2. LE CYCLE DU RADIUM SUR TERRE

2.1. Le radium dans les roches de la lithosphère

La répartition des isotopes du radium dans les roches de la lithosphère va dépendre du comportement de leurs éléments pères, et principalement le ^{232}Th et l'^{238}U. Dans les processus ignés, ils sont à l'équilibre avec leurs précurseurs mais certains facteurs environnementaux comme l'érosion peuvent changer les ratios entre ^{226}Ra et ^{238}U et entre ^{228}Ra et ^{232}Th (Fesenko *et al*., 2014). Les roches les plus riches en ^{226}Ra (tableau 6) sont les shales, schistes bitumineux et les roches riches en phosphates (Fesenko *et al*., 2014; Issa *et al*., 2014). Les charbons sont aussi relativement riches en radium (Pluta, 2001 ; Chalupnik *et al*., 2001; Lauer *et al*., 2015).

Tableau 6 : Concentrations en ^{226}Ra dans différent types de roches (d'après Fesenko *et al*., 2014)

Type de roche	[^{226}Ra] (Bq.kg^{-1})	[^{226}Ra] (ppt)
Roches volcaniques	48 - 137	1,31 – 3,74
Granites	0,037 – 185	0,001 – 5,05
Basaltes	11 – 48	0,30 – 1,31
Shales	14,8 – 2220	0,40 – 60,66
Schistes bitumineux	629 – 1040	17,19 – 28,42
Roches sédimentaires	9,2 - 15	0,25 – 0,41
Chaux	5 – 18	0,14 – 0,49
Grès	7 – 55	0,19 – 1,50
Roches phosphatées	148 – 1480	4,04 – 40,44
Carbonates	26 – 30	0,71 – 0,82
Roches argileuses	55	1,50

2.2. Les sources de radium

Les sources naturelles de radium sont liées à l'érosion et à l'altération de roches, sols ou systèmes hydrothermaux riches en précurseurs du radium (^{238}U et/ou ^{232}Th) ou en radium lui-même (Fesenko *et al*., 2014).

Les sources anthropiques du radium sont plus diverses mais sont toutes liées à l'exploitation des ressources naturelles (Fesenko *et al*., 2014). L'exploitation de gisements métalliques ou non métalliques et la séparation entre le minerais et les résidus peuvent entraîner des élévations importantes des concentrations de radium à proximité des sites d'exploitation (Azouazi *et al*., 2001 ; Arogunjo *et al*., 2009 ; Gao *et al*., 2010 ; Okeji *et al*., 2012 ; Déjeant *et al*., 2014 ; Fesenko *et al*., 2014 ; Cuvier *et al*., 2015). La production d'engrais phosphatés (Okeji *et al*., 2012 ; Fesenko *et al*., 2014), les procédés de purification d'eau potable, l'extraction de fluide pour la

production d'énergie géothermique et enfin la fabrication de matériaux de construction sont aussi des sources anthropogéniques de thallium (Fesenko *et al*., 2014).

La production d'énergie fossile est également une source importante de radium (Fesenko *et al*., 2014). L'exploitation de gisement de charbon en mine profonde entraine une circulation importante d'eau qui va se charger en radium avant d'être évacuée en surface pour les besoin d'exploitation (Chalupnik *et al*., 2008). Ces eaux, chargées vont considérablement augmenter les concentrations en radium dans les systèmes aquatiques et pouvoir impacter des régions entières comme ce fut le cas dans le bassin Silésien en Pologne (Chalupnik *et al*., 2001 ; Pluta, 2001 ; Chalupnik *et al*., 2008 ; Dinh Chau *et al*., 2012 ; Bzowski et Michalik, 2015). L'exploitation d'hydrocarbures aussi bien conventionnelles que non conventionnelles vont rejeter des eaux radioactives notamment lors de l'utilisation de la fracturation hydraulique (Warner *et al*., 2013 ; Kondash *et al*., 2014 ; Zhang *et al*., 2015 ; Abdullah *et al*., 2016). Enfin, la combustion de charbon dans les centrales thermiques va générer une accumulation de radium dans les cendres (Fesenko *et al*., 2014 ; Lauer *et al*., 2014).

2.3. Le radium dans les environnements de surface

2.3.1. Le radium dans les sols et sédiments

La concentration ou l'activité du radium dans les sols va dépendre de la roche mère mais aussi d'éventuelles sources de contamination comme des déchets miniers ou des rejets d'eau polluée ou les engrais (Fesenko *et al*., 2014). L'activité moyenne en radium 226 pour les sols à l'échelle du globe est de 32 $Bq.kg^{-1}$ soit 0,87 ppt (Fesenko *et al*., 2014). Dans les sols où aucun impact anthropique n'a été identifié, l'activité moyenne en ^{226}Ra varie entre 3,7 $Bq.kg^{-1}$ (0,10 ppt) dans les sols riches en chaux et 70-126 $Bq.kg^{-1}$ (1,90 – 3,44 ppt) dans des sols sableux (Fesenko *et al*., 2014). Dans des régions impactées par des rejets miniers, comme le plateau de Jos au Nigéria, l'activité du radium (226) dans les sols peut varier entre 410 ± 100 et 4200 ± 600 $Bq.kg^{-1}$ soit respectivement 11,20 ± 2,73 et 114,75 ± 16,39 ppt (Arogunjo *et al*., 2009).

2.3.2. Le radium dans les eaux naturelles

Les eaux souterraines vont se charger en radium en circulant dans les aquifères par le lessivage des roches (Almeida *et al*., 2004 ; Fesenko *et al*., 2014 ; Schrag, 2017). Le radium est

particulièrement soluble et peut ainsi se retrouver enrichi dans les eaux souterraines de plusieurs ordres de grandeurs par rapport à ses précurseurs, notamment l'uranium (Fesenko *et al*., 2014). Lors de l'exploitation des mines en profondeurs la modification de la circulation des eaux souterraines peut engendrer d'importantes contaminations en radium dans les aquifères (Pluta, 2001 ; Chalupnik *et al*., 2001 ; Warner *et al*., 2013 ; Fesenko *et al*., 2014). Ces différents facteurs vont induire une gamme importante de concentration en radium dans les eaux souterraines. Pour ^{226}Ra, ces valeurs varient globalement entre $1{,}34.10^{-16}$ (1,11 mBq.L^{-1}) et $9{,}48.10^{-13}$ mol.L^{-1} (7840 mBq.L^{-1}) dans des zones naturelles mais cela peut aller jusqu'à plus de $6{,}00.10^{-12}$ mol.L^{-1} (~55000 mBq.L^{-1}) dans eaux provenant de la fracturation hydraulique (Fesenko *et al*., 2014).

Les concentrations en ^{226}Ra dans les eaux douces entre $6{,}04.10^{-17}$ mol.L^{-1} et $2{,}41\ .10^{-15}$ mol.L^{-1} (Fesenko *et al*., 2014). Dans le bassin Silésien, en Pologne, où des rejets de radium dans les eaux de surface par l'exploitation du charbon ont eu lieu (Pluta, 2001. Chalupnik *et al*., 2008), des concentrations allant jusqu'à environ $9{,}0.10^{-14}$ mol.L^{-1} (~750 mBq.L^{-1}) ont été mesurées (Dinh Chau *et al*., 2012). Des valeurs encore plus importantes peuvent être observées dans des régions où l'uranium est exploité. Au Saskatchewan par exemple, des concentrations atteignant $3{,}60\ .10^{-13}$ mol.L^{-1} (3000 mBq.L^{-1}) ont été mesurées à proximité des mines (Fesenko *et al*., 2014).

Les concentrations en ^{226}Ra mesurées pour les différents océans mondiaux sont résumées dans le tableau 7. La principale source de radium pour les océans sont les rivières mais des sources additionnelles provenant d'effluents miniers ou d'aquifères pollués peuvent également intervenir (Fesenko *et al*. 2014) dans les zones côtières.

Tableau 7 : Concentrations en ^{226}Ra dans les différents océans (d'après Fesenko *et al*., 2014)

	^{226}Ra (mBq.L^{-1})	^{226}Ra (mol.L^{-1})
O. Atlantique (surface)	0,135 ± 0,014	$1{,}63 \pm 0{,}16\ .10^{-17}$
O. Indien (surface)	0,147 ± 0,029	$1{,}78 \pm 0{,}35\ .10^{-17}$
O. Pacifique (surface)	0,122 ± 0,024	$1{,}47 \pm 0{,}29\ .10^{-17}$
O. Antarctique (surface)	0,258 ± 0,050	$3{,}12 \pm 0{,}60\ .10^{-17}$
O. Atlantique Nord (profondeur)	0,253 ± 0,045	$3{,}06 \pm 0{,}54\ .10^{-17}$
O. Atlantique Sud (profondeur)	0,330 ± 0,056	$3{,}99 \pm 0{,}68\ .10^{-17}$
O. Antarctique (profondeur)	0,365 ± 0,015	$4{,}41 \pm 0{,}18\ .10^{-17}$
O. Indien Nord (profondeur)	0,476 ± 0,098	$5{,}75 \pm 1{,}09\ .10^{-17}$
O. Indien Sud (profondeur)	0,459 ± 0,053	$5{,}55 \pm 0{,}64\ .10^{-17}$
O. Pacifique Nord (profondeur)	0,592 ± 0,079	$7{,}16 \pm 0{,}96\ .10^{-17}$
O. Pacifique Sud (profondeur)	0,431 ± 0,063	$5{,}21 \pm 0{,}76\ .10^{-17}$

2.3.2. Le radium dans l'atmosphère

La principale source de radium pour l'atmosphère provient de l'érosion des particules de sols (Fesenko *et al*.,2014). Fesenko *et al*., (2014) ont estimé celle de l'atmosphère à 1,5 $\mu Bg.m^{-3}$ en se basant sur l'activité moyenne des sols. Cependant, le climat et l'environnement local, comme les villes ou les zones industrielles peuvent faire varier l'activité de ^{226}Ra dans l'air (Fesenko *et al*., 2014). Lors de la combustion des charbons dans les centrales thermiques destinées à la production d'énergie, le radium se retrouve concentré dans les cendres (Fesenko *et al*., 2014; Lauer *et al*., 2014). Dans les cendres volantes, l'activité en ^{226}Ra peut atteindre 2400 $Bq.kg^{-1}$ (65,57 ppt) et ainsi devenir une source de contamination locale (Fesenko *et al*., 2014).

3. SPECIATION DU RADIUM

Le radium appartient aux alcalino-terreux et n'a qu'un état d'oxydation (+2) dans la nature (Porcelli *et al*., 2014). Le radium (en coordinence VIII) à un rayon ionique de 1,48 Å, proche de celui du baryum à 1,42 Å (Shannon, 1976). Cette similitude entraîne un comportement similaire entre les deux éléments et le baryum a souvent été utilisé comme analogue au radium (Porcelli *et al*., 2014).

3.1. Espèces aqueuses de radium

Les espèces aqueuses de radium sont principalement associés au sulfates chlorure et carbonates comme le montre le tableau 8. Compte tenu des constantes de stabilité, les complexes $RaCO_3$ (aq) et $RaSO_4$ (aq) semblent être les plus répandus (Langmuir et Riese, 1985).

Table 8 : Constantes de stabilité des différents complexes aqueux de radium

Réaction	log*K* (298.15 K)	
	Langmuir et Riese, 1985	Benes et al., 1982
$Ra^{2+} + OH^- \leftrightarrow RaOH^+$	0,5	-
$Ra^{2+} + SO_4^{2-} \leftrightarrow RaSO_4(aq)$	2,75	2,43
$Ra^{2+} + Cl^- \leftrightarrow RaCl^+$	-0,10	-
$Ra^{2+} + CO_3^{2-} \leftrightarrow RaCO_3$ (aq)	2,5	2,48
$Ra^{2+} + HCO_3^- \leftrightarrow RaHCO_3^+$	-	2,89

Les calculs spéciation du radium dans une eau de rivière (sans pollution), montre que la totalité du radium est sous forme libre (fig. 6A) tandis que l'espèce $RaSO_4$ est l'unique espèce de radium dissous dans les océans (fig. 6B). Il est donc probable que $RaSO_4$ soit également l'espèce

dominante dans les effluents de forage ou de fracturation hydraulique qui sont des eaux très salines (Fesenko *et al*., 2014 ; Porcelli *et al*., 2014).

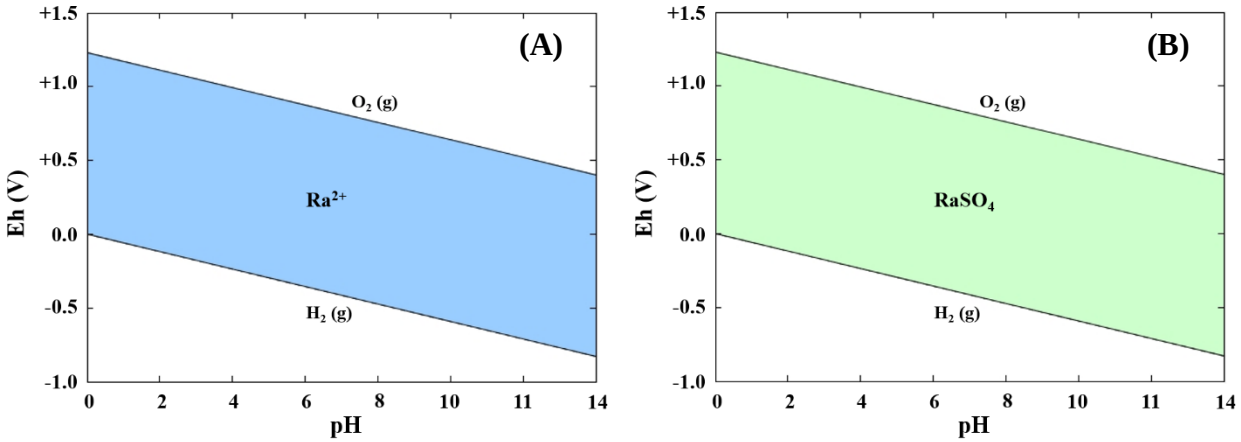

Figure 6 : Spéciation du radium dissous en fonction du pH et de l'Eh (V). (A) dans une eau de rivière et (B) dans une eau de mer. Les constantes proviennent du tableau 8 et les compositions des eaux sont de Kaplan et Mattigod (1998). La concentration en radium pour l'eau de mer correspond à la moyenne des valeurs du tableau 7 et pour les eaux douce à 6,0 $.10^{-17}$ $mol.L^{-1}$ (Fesenko *et al*., 2014). Les calculs ont été réalisés avec le logiciel JCHESS 2.0 sans composés organiques.

3.2. Précipitation du radium

Il n'existe pas de minéraux propres au radium et ce dernier va généralement co-précipiter avec des minéraux formés par d'autres alcalino-terreux présents en plus grande quantité (Porcelli *et al*., 2014). Dans des eaux riches en sulfates, le radium va co-précipiter avec la barite ($BaSO_4$) sous forme de solution solide (Ba, Ra)SO_4 (Fesenko *et al*., 2014 ; Porcelli *et al*., 2014). Ce processus est celui qui contrôle le plus la solubilité du radium dans les eaux naturelles (Porcelli *et al*., 2014). Il arrive également dans les saumures qu'en plus de la barite, Ra^{2+} précipite en solution solide avec des sulfates de strontium $SrSO_4$ (Porcelli *et al*., 2014). Dans les eaux riches en carbonates, le radium va précipiter avec ces derniers (Porcelli *et al*., 2014).

3.3. Complexation et adsorption du radium

3.3.1. Les minéraux argileux

Les interactions entre le Ra^{2+} et les minéraux argileux de types kaolinite, smectite et illite sont dominées par les échanges d'ions (Porcelli *et al*., 2014 ; Reinoso-Maset et Ly, 2016). Le

comportement du radium vis-à-vis des phases argileuses est dépendant de la force ionique et du pH (Ames *et al*., 1983a ; Porcelli *et al*., 2014 ; Reinoso-Maset et Ly, 2016). Lorsque la force ionique augmente, la quantité de radium adsorbée sur les argiles diminue, montrant l'importance des effets de compétition avec les éléments majeurs (Ames *et al*., 1983a ; Porcelli *et al*., 2014). Des études ont aussi montré que plus le pH augmente, plus le radium est adsorbé (Porcelli *et al*., 2014 ; Reinoso-Maset et Ly, 2016). Si l'on compare les phases argileuses entre elles, plus de radium sera piégé sur la smectite que sur la kaolinite tandis que la quantité de radium adsorbée sur l'illite sera similaire à une smectite (Porcelli *et al*., 2014). Dans de nombreux cas, les argiles constituent des phases importantes dans la sorption du radium dans les sols (Nathwani et Phillips, 1979 ; Vandenhove *et al*., 2007 ; Porcelli *et al*., 2014).

3.3.2. La matière organique

Les interactions entre le radium et la matière organique naturelle ont été relativement peu étudiées (Porcelli *et al*., 2014). Cependant la matière organique a été identifiée comme une des phases dominantes dans la rétention du radium dans les sols (Nathwani et Phillips, 1979 ; Greeman *et al*., 1999).

3.3.3. Les oxyhydroxydes de fer et de manganèse

L'adsorption du radium sur les oxyhydroxydes de fer est fortement dépendante du pH, et ne devient significative qu'au-dessus de pH 8 (Porcelli *et al*., 2014). Ces processus suivent également une isotherme de Freundlich (Ames *et al*., 1983b). Les oxydes de manganèse sont aussi connus pour adsorber fortement le radium sans dépendance au pH (Porcelli *et al*., 2014). Cependant, Vinson *et al*. (2009), ont montré que les processus d'adsorption du radium étaient dépendants des effets de compétition et des conditions d'oxydo-réduction du milieu. Dans des conditions anoxiques, les interactions entre le Ra^{2+} et les oxyhydroxydes de fer et de manganèse sont limitées et ces derniers sont moins efficaces pour un éventuel piégeage du radium (Vinson *et al*., 2009). Enfin, il est intéressant de noter que l'affinité du radium pour les oxydes de manganèse est telle qu'ils sont souvent utilisés comme outils de pré-concentration lors des analyses de radium (Porcelli *et al*., 2014).

REFERENCES

Abdullah, J. Al, Al-masri, M. S., Amin, Y., Awad, I., & Sheaib, Z. (2016). Chemical fractionation of radium-226 in NORM contaminated soil from oil fi elds. *Journal of Environmental Radioactivity*, *165*, 47–53. http://doi.org/10.1016/j.jenvrad.2016.09.003

Almeida, R. M. R., Lauria, D. C., Ferreira, a. C., & Sracek, O. (2004). Groundwater radon, radium and uranium concentrations in Região dos Lagos, Rio de Janeiro State, Brazil. *Journal of Environmental Radioactivity*, *73*(3), 323–334. http://doi.org/10.1016/j.jenvrad.2003.10.006

Ames, L. L., McGarrah, J. E. & Walker, B. A. (1983a). Sorption of trace constituents from aqueous solutions onto secondary minerals. *Chemical Geology*., *40*, 135–148

Ames, L. L., McGarrah, J. E., Walker, B. A. & Salter, P. F. (1983b). Uranium and radium sorption on amorphous ferric oxyhydroxides. *II, Radium, Clays Clay Miner*., *31*, 335–342

Arogunjo, A. M., H??llriegl, V., Giussani, A., Leopold, K., Gerstmann, U., Veronese, I., & Oeh, U. (2009). Uranium and thorium in soils, mineral sands, water and food samples in a tin mining area in Nigeria with elevated activity. *Journal of Environmental Radioactivity*, *100*(3), 232–240. http://doi.org/10.1016/j.jenvrad.2008.12.004

Azouazi, M., Ouahidi, Y., Fakhi, S., Andres, Y., Abbe, J. C., & Benmansour, M. (2001). Natural radioactivity in phosphates, phosphogypsum and natural waters in Morocco. *Journal of Environmental Radioactivity*, *54*(2), 231–242. http://doi.org/10.1016/S0265-931X(00)00153-3

Benes, P., Obdrzalek, M. & Cejchanova, M. (1982). The physico-chemical forms of traces of radium in aueous solutions containing chlorides, sulfates and carbonates. *Radiochem. Radioanal. Lett.*, *50*, 227–241.

Bzowski, Z., & Michalik, B. (2015). Mineral composition and heavy metal contamination of sediments originating from radium rich formation water. *Chemosphere*, *122*, 79–87. http://doi.org/10.1016/j.chemosphere.2014.10.077

Chalupnik, S., Michalik, B., Wysocka, M., Skubacz, K. & Mielnikow, A. (2001). Contamination of settling ponds and rivers as a result of discharge of radium-bearing waters from Polish coal mines. Journal of Environmental Radioactivity, 54, 85–98. https://doi.org/10.1016/S0265-931X(00)00168-5

Chalupnik, S., & Wysocka, M. (2008). Radium removal from mine waters in underground treatment installations. *Journal of Environmental Radioactivity*, *99*(10), 1548–1552. http://doi.org/10.1016/j.jenvrad.2007.12.024

Chau, N. D., Lucyna, R., Jakub, N., & Paweł, J. (2012). Radium isotopes in the Polish Outer Carpathian mineral waters of various chemical composition. *Journal of Environmental Radioactivity*, *112*, 38–44. http://doi.org/10.1016/j.jenvrad.2012.03.010

Cuvier, A., Panza, F., Pourcelot, L., Foissard, B., Cagnat, X., Prunier, J., van Beek, P., Souhaut, M. & Le Roux, G. (2015). Uranium decay daughters from isolated mines: Accumulation and

sources. *Journal of Environmental Radioactivity*, *149*, 110–120. http://doi.org/10.1016/j.jenvrad.2015.07.008

Darby, S., Hill, D., Auvinen, A., Baysson, H., Bochicchio, F., Deo, H., … Doll, R. (2004). Radon in homes and risk of lung cancer: collaborative analysis of individual data from 13 European case-control studies. Br. Med. J., 330, 223–228. http://doi.org/10.1136/bmj.38308.477650.63

Déjeant, A., Bourva, L., Sia, R., Galoisy, L., Calas, G., Phrommavanh, V. & Descotes, M. (2014). Field analyses of U-238 and Ra-226 in two uranium mill tailings piles from Niger using portable HPGe detector. *Journal of Environmental Radioactivity*, *137*, 105–112. http://doi.org/10.1016/j.jenvrad.2014.06.012

Fesenko, S., Carvalho, F., Martin, P., Moore, W. S., Yankovich, T. (2014). Radium in the Environment. In The Environmental Behaviour of Radium: Revised Edition, 33–105. IAEA, Vienna

Gao, Y., Baeyens, W., De Galan, S., Poffijn, a., & Leermakers, M. (2010). Mobility of radium and trace metals in sediments of the Winterbeek: Application of sequential extraction and DGT techniques. *Environmental Pollution*, *158*(7), 2439–2445. http://doi.org/10.1016/j.envpol.2010.03.022

Greeman, D. J., Rose, A. W., Washington, J. W., Dobos, R. R., & Ciolkosz, E. J. (1999). Geochemistry of radium in soils of the Eastern United States. *Applied Geochemistry*, *14*, 365–385

Issa, S. A. M., Mostafa, A. M. A., & Lotfy, A. E. M. (2015). Radiological impacts of natural radioactivity in phosphate rocks from El-Sibaiya and Red Sea coast mines, Egypt. *J. Radioanal. Nucl. Chem.*, *303*, 53–61. http://doi.org/10.1007/s10967-014-3312-x

Jia, G., & Jia, J. (2012). Determination of radium isotopes in environmental samples by gamma spectrometry, liquid scintillation counting and alpha spectrometry: A review of analytical methodology. Journal of Environmental Radioactivity, 106, 98–119. http://doi.org/10.1016/j.jenvrad.2011.12.003

Kondash, A. J., Warner, N. R., Lahav, O., & Vengosh, A. (2014). Radium and Barium Removal through Blending Hydraulic Fracturing Fluids with Acid Mine Drainage. *Environmental Science & Technology*, *48*, 1334–1342. dx.doi.org/10.1021/es403852h

Langmuir, D., & Riese, A. C. (1985). The thermodynamic properties of radium. *Geochimica et Cosmochimica Acta*, *49*(7), 1593–1601. http://doi.org/10.1016/0016-7037(85)90264-9

Lauer, N. E., Hower, J. C., Hsu-kim, H., Taggart, R. K., & Vengosh, A. (2015). Naturally Occurring Radioactive Materials in Coals and Coal Combustion Residuals in the United States. *Environmental Science & Technology*, *49*, 11227–11233. http://doi.org/10.1021/acs.est.5b01978

Okeji, M. C., Agwu, K. K., & Idigo, F. U. (2012). Assessment of Natural Radioactivity in Phosphate Ore , Phosphogypsum and Soil Samples Around a Phosphate Fertilizer Plant in Nigeria, 1078–1081. http://doi.org/10.1007/s00128-012-0811-8

Pluta, I. (2001). Barium and radium discharged from coal mines in the Upper Silesia, Poland. *Environmental Geology*, *40*(3), 345–348. http://doi.org/10.1007/s002540000175

Porcelli, D., Kim, C. K., Martin, P., Moore, W. S., Phaneu, M. (2014). Properties of Radium. In The Environmental Behaviour of Radium: Revised Edition, 6–32. IAEA, Vienna

Rachkova, N. G., Shuktomova, I. I., & Taskaev, a. I. (2010). The state of natural radionuclides of uranium, radium, and thorium in soils. *Eurasian Soil Science*, *43*(6), 651–658. http://doi.org/10.1134/S1064229310060050

Reinoso-Maset, E., & Ly, J. (2016). Study of uranium (VI) and radium (II) sorption at trace level on kaolinite using a multisite ion exchange model. *Journal of Environmental Radioactivity*, *157*, 136–148. http://doi.org/10.1016/j.jenvrad.2016.03.014

Schrag, J. M. (2017). Naturally occurring radium (Ra) in home drinking-water wells in the Sandhills region of South Carolina, USA: Can high concentrations be predicted?. *GeoHealth*, *1*, 1–13. http://doi.org/10.1002/2017GH000069

Shannon, R. D. (1976). Revised Effective Ionic Radii and Systematic Studies of Interatomic Distances in Halides and Chalcogenides. *Acta Cryst*., *32*, 751-767.

Vandenhove, H., & Van Hees, M. (2007). Predicting radium availability and uptake from soil properties. *Chemosphere*, *69*(4), 664–674. http://doi.org/10.1016/j.chemosphere.2007.02.054

Vinson, D. S., Vengosh, A., Hirschfeld, D., & Dwyer, G. S. (2009). Relationships between radium and radon occurrence and hydrochemistry in fresh groundwater from fractured crystalline rocks, North Carolina (USA). *Chemical Geology*, *260*(3-4), 159–171. http://doi.org/10.1016/j.chemgeo.2008.10.022

Warner, N. R., Christie, C. a., Jackson, R. B., & Vengosh, A. (2013). Impacts of shale gas wastewater disposal on water quality in Western Pennsylvania. *Environmental Science and Technology*, *47*(20), 11849–11857. http://doi.org/10.1021/es402165b

Zhang, T., Hammack, R. W., & Vidic, R. D. (2015). Fate of Radium in Marcellus Shale Flowback Water Impoundments and Assessment of Associated Health Risks. *Environmental Science & Technology*, *49*, 9347–9354. http://doi.org/10.1021/acs.est.5b01393

PARTIE 3 : OBJECTIFS DE LA THESE

Le thallium et le radium sont deux polluants qui peuvent avoir un impact sur l'environnement et les êtres vivants. Le thallium est un élément classé dans les polluants d'intérêt prioritaire par l'agence états-unienne de protections de l'environnement et comme élément stratégique pour les nouvelles technologies (TCEs: *Technological Critical Elements*) par le l'action européenne COST[6] (Cobelo-Garcia *et al*., 2015). Le radium 226 appartient lui au NORM (Naturally Occuring Radioactive Materials) et fait l'objet de nombreuses études depuis sa découverte, notamment à cause de sa radiotoxicité et du radon 222, gaz toxique issus de sa désintégration radioactive.

Pour ces deux éléments, leur cycle naturel dans l'environnement peut être perturbé par les activités anthropiques et les conséquences sur leur dispersion ne sont pas encore totalement prédictibles.

Le thallium est un élément qui a suscité de l'intérêt pour les scientifiques à cause de son comportement à la fois proche des éléments lithophiles et de ceux chalcophiles. Les limites de détections élevées ont été pendant longtemps un frein à son étude dans l'environnement. Aujourd'hui que ces verrous sont levés, de nombreuses études ont mesuré les concentrations en thallium et sa répartition dans les différents compartiments qui composent le globe est mieux connue (Belzile et Chen, 2017). La spéciation du thallium et son comportement sont de mieux en mieux contraints. Dans les environnements de (sub)surface, les interactions avec les oxyhydroxides de fer et les oxydes de manganèse sont relativement bien connus. Cependant, beaucoup d'hypothèses sont faites sur les interactions du thallium avec d'autres phases porteuses comme les argiles et la matière organique naturelle. Les phases porteuses du radium ainsi que son comportement dans l'environnement sont aussi bien connus. Son association avec la matière organique naturelle et notamment les substances humiques reste pourtant mal quantifiée.

Les premières questions qui résultent de l'étude bibliographique concernent les interactions entre le thallium et le radium avec la matière organique naturelle. Dans le cas du thallium, ces mêmes questions se posaient vis-à-vis des minéraux argileux. Ces questions sont les suivantes :

[6]European Cooperation in Science and Technology

(1) Quels sont les processus intervenant dans l'adsorption/complexation du thallium et du radium avec la matière organique et les argiles ?

(2) Quelles places occupent ces interactions dans le cycle de ces éléments ?

Une des autres problématiques liées à l'étude du devenir du radium dans l'environnement concerne sa mobilité et l'évolution de sa concentration dans les sols, les systèmes aquatiques et les sédiments. Il est donc important d'étudier le Ra à l'interface de ces différents compartiments. L'étude du Ra à ces interfaces est délicate à cause notamment, des faibles volumes disponibles (interface eau-sédiment, zone hyporhéique, etc.) et des très faibles concentrations de cet élément dans l'environnement (Fesenko *et al*., 2014). En effet, pour mesurer le Ra, il est souvent nécessaire d'échantillonner de grands volumes d'eau et d'utiliser des résines pour pré-concentrer cet élément. Cependant il existe des outils permettant de s'affranchir de ces contraintes, comme la pré-concentration *in situ* mais il existe peu d'études sur ce sujet. L'un des objectifs de cette thèse a donc été d'adapter un capteur *in-situ* permettant de mesurer le radium à ces interfaces et de tester les limites de fonctionnement du capteur dans des conditions de concentrations ou de redox variables par exemple.

Dans le chapitre II, nous présentons l'étude de la complexation du thallium et du radium avec un acide humique purifié à différent pH et différentes concentrations. Nous avons pour se faire utiliser la *Donnan Membrane Technique* ou DMT (Temminghoff *et al*., 2000) pour permettre la séparation de la fraction libre du thallium(I) ou du radium(II) de la fraction complexée avec l'acide humique. Nous avons ensuite utilisé le modèle NICA-Donnan (Benedetti *et al*., 1996) pour décrire cette complexation. Suivant le formalisme du modèle, des constantes ont pu être extraites pour la première pour le radium et le thallium. Ces constantes ont permis de nouvelles interprétations de la spéciation du radium et du thallium dans les solutions de sols et les eaux naturelles. Enfin, le comportement du thallium(I) étant souvent comparé à celui de l'argent(I), nous avons également déterminé les constantes pour ces deux éléments à partir de données expérimentales. Tl^+ et Ag^+ étant tous les deux des éléments chalcophiles, ils sont suspectés d'interagir avec les groupes sulfurés de la Matière Organique Naturelle (MON). Nous avons donc proposé une façon de les considérer dans le cadre déjà existant du modèle NICA-Donnan.

Parallèlement à ces études de complexation nous avons également étudié les processus de sorption du thallium avec deux argiles de références, l'illite du Puy et la smectite du Wyoming. Chacune de ses argiles a été conditionnée en fonction d'un cation majeur. Nous avons choisi de travailler avec Na^+ et Ca^{2+} pour se rapprocher des environnements aquatiques. Des isothermes en fonction du pH et de la concentration en thallium à force ionique constante ont été réalisées. Les isothermes ont été réalisées par des expériences en « batch » où ^{204}Tl, isotope radioactif du thallium, a été utilisé comme traceur. Ces résultats ont été complétés par une modélisation des interactions à l'aide de la théorie des échangeurs d'ions. Les coefficients de sélectivité extraits de cette étude sont les premiers disponibles pour Tl^+. De plus cela nous a permis de mieux comprendre les processus en jeu lors de la sorption du thallium par ces deux minéraux argileux et surtout quels types de sites réactifs étaient impliqués et l'impact que cela aurait sur la mobilité du thallium. Cette étude est présentée dans le chapitre III.

Dans le chapitre IV, nous avons cherché à développer et faciliter la mesure du radium dans l'environnement par l'intermédiaire de la technique des *Diffusive Gradient in Thin-films* ou DGT (Davison et Zhang, 1994). Nous avons pour cela adapté une couche réactive faite de nano-oxydes de manganèse censés rendre cette couche plus spécifique au radium par rapport à d'autres cations. L'utilisation de ce capteur passif étant destinée aux études de l'interface eau-sédiment, nous avons mené une série de tests spécifiques nous permettant d'appréhender les limites de leurs utilisations en fonction de la force ionique (compétitions avec les autres cations) et les conditions d'oxydo-réduction du milieu. L'utilisation des capteurs de types DGT en contexte de surveillance environnementale posait également la question de leurs réponses dans des régimes de concentrations variables au cours du temps. Nous avons donc utilisé un logiciel permettant le calcul du transport-réactif (COMSOL Multiphysic®) pour modéliser le comportement du DGT et son enregistrement des signaux transitoires.

Le thallium étant un élément souvent associé au gisement de sulfures, nous avons choisis d'étudier l'ancien site minier des Rosiers situé dans la région de Pontgibaud (Puy de Dôme) en France. Trois zones ont été identifiées en fonction de la concentration en thallium. La rivière en amont et en aval du site, une retenue d'eau où les concentrations en thallium sont les plus élevées et la zone de mélange entre l'évacuation de la retenue et la rivière. En plus de la spéciation du

thallium dans les eaux, nous avons estimé son flux de transfert entre les sédiments et la colonne d'eau. L'ensemble de ces résultats est présenté dans le chapitre V.

REFERENCES

Benedetti, M. F., Van Riemsdijk, W. H., & Koopal, L. K. (1996). Humic substances considered as a heterogeneous Donnan gel phase. *Environmental Science and Technology*, *30*(6), 1805–1813. http://doi.org/10.1021/es950012y

Belzile, N., & Chen, Y. (2017). Applied Geochemistry Thallium in the environment : A critical review focused on natural waters , soils , sediments and airborne particles. *Applied Geochemistry*, *84*, 218–243. http://doi.org/10.1016/j.apgeochem.2017.06.013

Cobelo-García, A., Filella, M., Croot, P., Frazzoli, C., Du Laing, G., Ospina-Alvarez., N., Rauch, S., Salaun, P., Schäfer, J., Zimmermann, S. (2015). COST action TD1407 : network on technology-critical elements (NOTICE) - from environmental processes to human health threats. *Environ. Sci. Pollut. Res*, *22*, 15188–15194. http://doi.org/10.1007/s11356-015-5221-0

Davison, W., & Zhang, H. (1994). In-situ speciation measurements of trace components in natural waters using thin-film gels. *Nature*, *237*, 546 – 548.

Fesenko, S., Carvalho, F., Martin, P., Moore, W. S., Yankovich, T. (2014). Radium in the Environment. In The Environmental Behaviour of Radium: Revised Edition, 33–105. IAEA, Vienna

Temminghoff, E. J. M., Plette, A. C. C., Van Eck, R., & Van Riemsdijk, W. H. (2000). Determination of the chemical speciation of trace metals in aqueous systems by the Wageningen Donnan Membrane Technique. *Analytica Chimica Acta*, *417*(2), 149–157. http://doi.org/10.1016/S0003-2670(00)00935-1

Chapter II: Effect of Natural Organic Matter on Thallium and Radium Speciation in Aquatic Systems

Loïc A. Martin[1], *Caroline Simonucci*[2], *Eric Viollier*[1], *Setareh Rad*[3] *and Marc F. Benedetti*[1*]

[1]Institut de Physique du Globe de Paris – USPC- UMRCNRS7154, Paris, France

[2]IRSN, PSE-ENV/SIRSE/LER-Nord, BP 17, 92262 Fontenay-aux-Roses Cedex, France

[3]BRGM, Avenue Claude Guillemin, 45100 Orléans

*Corresponding author. *Email address :* benedetti@ipgp.fr

Article en preparation pour soumission dans Environmental Science & Technology

1. RESUME

La matière organique naturelle est connue pour jouer un rôle important dans le transport et l'adsorption des éléments traces métalliques dans les sols et les environnements aquatiques. De plus, il apparait que ces phases porteuses sont très peu étudiées pour le thallium et le radium. En conséquences, l'objectif de cette étude est de s'intéresser à la complexation du thallium(I) et du radium(II) avec un acide humique purifié (AH). La *Donnan Membrane Technique* a donc été utilisée au cours des expériences pour séparer la forme libre des cations étudiés de la solution totale. Ces expériences ont été conduites à plusieurs pH et concentrations mais à force ionique et concentration en acide humique constante. Les résultats ont ensuite été décrits avec le modèle NICA-Donnan et le logiciel ECOSAT. La complexation du thallium a été comparée à celle de l'argent en suivant le même formalisme de modélisation avec NICA-Donnan et des données provenant de la littérature. Les paramètres propres à ces trois cations ont donc été calculés pour la première fois pour ce type de modèle. Le thallium montre une faible complexation avec les acides humiques tandis que l'argent complexe suffisamment pour entrer en compétition avec des cations divalents. De plus, la spéciation du thallium dans la fraction dissoute montre une dominance de l'espèce libre Tl^+ alors que le complexe Tl-AH représente à peine 10% des espèces de Tl(I) en solution. Des résultats similaires ont été calculés pour la spéciation du thallium dans des solutions de sols. Au contraire, le radium forme plus de complexes avec les acides humiques et les résultats sont similaires aux autres alcalino-terreux. Enfin, le complexe $Ra\text{-}AH^+$ semble être une des espèces dominantes du radium dans les solutions de sols.

2. ABSTRACT

Natural organic matter (NOM) is known to play an important role in the transport and binding of trace metal elements in aquatic and soil systems. This bearing phases appears to be few studied in respect to thallium and radium. Consequently, this study aim to investigate thallium(I) and radium(II) complexation to a purified humic as proxy for NOM. Experiments were performed with the Donnan Membrane Technique to separate the free form of the studied cations from the bulk solution. Various pH and concentrations were investigated at constant ionic strength and constant humic concentrations in solution. Then experimental results were described with NICA-Donnan model and ECOSAT software. Thallium complexation was compared to silver complexation from data from literature following the same formalism with NICA-Donnan. Consequently, parameters were calculated for the first time for the three cations. Results displays low thallium complexation to humic acid while silver could compete with divalent cations for complexation. Calculated speciation for dissolved thallium highlight the dominance of free thallium (Tl^+) in solution whereas Tl-HA complex contribute to roughly 10% of Tl(I) species. Results are similar in soil solutions. On the contrary, radium shows greater complexation to humic acid, similar to others alkaline earth metals. Finally, it appears that $Ra\text{-}HA^+$ species could be one of the major radium species in soil solutions.

3. INTRODUCTION

Thallium (Tl) is a trace element and is widely distributed in the environment with average concentrations of 0.49 ppm and 0.013 ppm in the continental and oceanic crusts respectively [1]. Tl occurs in two oxidation states, Tl(I) and Tl(III) [2]. Tl(I) exhibits both lithophile and chalcophile behaviors [3] but it is strongly dependent of the geological context [3-7]. Tl^+ has a large ionic radius (1.49 Å), similar to K^+, Rb^+ and Cs^+ [10]. Classically, Tl substitutes for K^+ in biotite, K-feldspar and plagioclase from volcanic rocks and granite systems [7]. This also suggests that Tl^+ would substitute for K^+ on secondary clays [7-8].

Thallium is univalent in the deep environment, from the mantle to the non-altered crust [7]. In the (sub) surface environment, Tl(I) is relatively soluble, mobile and bioavailable [9-11]. Some studies have demonstrated that Tl(I) is the most dominant and thermodynamically stable species in aquatic systems and soils [12-14]. However, in some environments, mainly those affected by Tl contamination, Tl(III) is also present in various quantities [11, 15-17]. Tl(III) is supposed to be present only in high oxidative environment [12] but photochemically reactions in surface waters [18] or microbiological processes [19] may oxidize Tl(I). Then, Tl(III) may be stabilized by colloid formation [15] or sorption to Fe(III)-colloids [18]. Tl(I) can also be oxidized when in contact with certain Mn(IV)-oxides and Tl(III) is stabilized when incorporated into those oxides [16].

Thallium has two main sources. Firstly, weathering of K-rich rocks [20] and/or S-rich minerals and more rarely Tl-rich sulfide deposits [11,21]. Anthropogenic sources may be the main source of thallium for the (sub) surface environment. Tl contamination results from non-ferrous and ferrous metal mining [14,17,22], from coal and cement combustion and from smelting activities [22-24]. Nielsen *et al.*[25] calculated an average Tl concentration of $\sim 2.94 .10^{-11}$ $mol.L^{-1}$ from 16 worldwide large river systems. However, in highly impacted area, Tl concentration can reach $\sim 1.62 .10^{-6}$ $mol.L^{-1}$ [14]. In soils, Tl concentrations are widespread. In non-anthropogenic impacted areas with a Tl-bearing bedrock, Tl concentration in soils is around 1.5 ppm [20] but can reach 6000 ppm [11]. On another hand, in anthropogenically impacted area Tl contents in soils can range from 5 ppm up to 124 ppm [21,22,24].

Radium (Ra) is a radionuclide of concern found in naturally occurring radioactive materials (NORM). Radium has only radioactive isotopes. Four isotopes are naturally occurring, ^{223}Ra, ^{224}Ra, ^{226}Ra and ^{228}Ra. ^{223}Ra belongs to ^{235}U series, ^{226}Ra to ^{238}U series and ^{224}Ra and ^{228}Ra are part of ^{232}Th series. ^{226}Ra isotopes are the most abundant on Earth [26]. ^{226}Ra is therefore a major environmental concern due to his relatively long half life (1602 years), his radiotoxicity and his daughter isotopes, ^{222}Rn. Ra is easily incorporated and accumulated into bones of mammals [27] and ^{222}Rn is a major cause of lung cancer [28]. High radium concentrations result mainly from anthropogenic activities such as mining and milling of metallic ores, mainly uranium, phosphate productions, extraction and purification of water (for drinking water or for geothermy) and extraction/production of coal, oil and gas [29-35]. These contexts are particularly important concerning ^{226}Ra. Releases from storage of nuclear waste, nuclear medicine and nuclear industries are also sources of radium in the environment [30].

Radium is a widely spread ultra-trace element on Earth. As ^{226}Ra is the most abundant and is in radioactive equilibrium with ^{238}U, the average Ra concentration in Earth's crust is close to 32.9 $Bq.kg^{-1}$ [30]. Ra is strongly enriched in U, Th rich-granites or in shales and coal rich rocks [30,33]. Fesenko *et al.* [30], documented a large database of environmental levels of radium in various compartments from soils to groundwater. Girault *et al.* [36], also well reviewed the occurrence of ^{226}Ra in waters. In the environment, radium occurs only at one oxidation state, Ra(II) [26].

Both thallium and radium are toxic trace elements for the surface environment [1,27-28,37]. Processes that drive their chemical speciation and mobility are well documented but some questions remain [10-11,14,17,26,30]. Some are about its interactions with natural organic matter (NOM) [9, 26, 38]. It is known that NOM plays an important role in the fate of metal ions and can control ion mobility and concentrations in soils and natural waters [39-40] and NOM is a complex mixture of compounds but the most studied and the most reactive fraction is the humic substances (HS) with the humic (HA) and fulvic (FA) acids [40-41].

Kaplan and Mattigod [42] first gave constants for Tl(I)-fulvate complex with $\log K_{Tl\text{-}Ful1}$ = 4.83 and $\log K_{Tl\text{-}Ful2}$ = 3.32. Then they made some previsions to assess the impact of natural organic matter on thallium speciation. According to those predictions, up to 67 % of Tl(I) is bound to organic compounds in bog water [42]. Thus, NOM seems to play a non-negligible part

in Tl(I) speciation. In an article published in 2005, Jacobson *et al*. [9] showed low Tl^+ complexation with a peat soils. Liu *et al.* [38] also studied Tl sorption onto two purified humic acids and their results suggested also weak Tl interactions with these kinds of ligand. Both attributed Tl chalcophile behavior as Tl complexation to humic susbtances, assuming interactions with rich-sulfur groups such as thiols [9, 38]. However, these studies only worked with high Tl concentrations, which are relevant in some rare polluting events but investigations with lower level of Tl could allow understanding the role of NOM in Tl speciation in the environment.

Fewer studies exist for Ra binding to NOM [26]. Sorption studies on a peat bog [43] and coir pitch with humic acid [44] display medium adsorption. However the role of humic substances or organic matter (OM) in general is largely unknown and assumption of its impact on radium mobility are usuals.

In this study, the main purpose was to study the mechanisms that drive radium and thallium complexation on humic substances. In order to do that, complexation of Ra^{2+} and Tl^+ with a purified humic acid (HA) was investigated in multiple pH range and concentration conditions. Experimentations were conducted with Donnan Membrane Technique (DMT;[45]) to calculate the amount of ion complexed to HA. These observations were completed with NICA-Donnan modelling to predict mechanisms of complexation. The role of NOM in Ra and Tl cycles will also be further discussed. In addition, thallium (I) complexation was compared with silver (I) to humic acid. Indeed, both are monovalent heavy metals and softs cations[46], both are non-essentials and trace elements with lithophile and chalcophile behaviors [9,47]. Considering this, Ag sorption to various humic acid [48] was described with NICA-Donnan and ECOSAT. Despite previous papers studying Ag(I) complexation to humic substance, it is going to be the first work with this element and NICA-Donnan [49-50].

4. MATERIALS AND METHODS

4.1. Donnan Membrane Technique.

Temminghoff *et al.*[45] first described the principle and the design of a cation exchange cell. This cell, so-called the “lab DMT” consists of two chambers, a donor and an acceptor, separated by a cation exchange membrane [45,51]. The membrane is negatively charged and allows free cations to go through it [45]. Later a new cell was designed, derived from the first one and called

"field DMT". In this case, there is only the acceptor chamber separated from the sample solution (the donor) by cation exchange membranes on the two sides [52-53]. Both are based on Donnan equilibrium principle and theoretical basis has been described elsewhere [45,51].

The donor solution contains the total concentration of dissolved metals, with the free and the complexed fractions, while the acceptor solution only contains the free metal. At Donnan equilibrium, equation 1 [45] is valid and can be used to calculate the concentration of free metal in the donor, based on the effect of ionic strength differences between the two compartments.

$$\left(\frac{C_{i,don}}{C_{i,acc}}\right)^{\frac{1}{z_i}} = \left(\frac{C_{j,don}}{C_{j,acc}}\right)^{\frac{1}{z_j}} \quad (1)$$

Here $C_{i,don}$ and $C_{i,\ acc}$ are the concentrations of free metal ion *i* in donor and acceptor solutions and z_i its charge. $C_{j,don}$, $C_{j,\ acc}$ are the analogous values for cation *j*. Assuming that this cation does not form complexes with ligands, the total concentration of j is equal to the free concentration. In this study, K^+ was chosen to be the reference cation *j* for Tl experiments and Ca^{2+} was for Ra experiments. After correction, the concentrations of metal complexed to the ligand were calculated by differences between total concentrations ($C_{dissolved}$) and corrected free metal ion concentrations (C_{free})[54] (equation 2):

$$C_{complexed} = C_{dissolved} - C_{free} \quad (2)$$

Prior to experiments with humic acids, it is mandatory to evaluate the time to reach equilibrium. Thus, experiments with only free Tl and Ra in a background electrolyte (KNO_3 50 mmol.L^{-1} or KNO_3 50 mmol.L^{-1} plus $Ca(NO_3)_2$ 2 mmol.L^{-1}) were performed and showed that equilibrium was reached after 24 hours for thallium and 72 hours for radium (SI, Figure S1).

4.2. Reagents and chemicals.

In order to have Tl(I) in all experiments, all sources of thallium are from Tl(I)NO_3 salt (99.9 %, Sigma Aldrich). Radium in solution was spiked from a standard radium solution (EB95 Eurostandard from Czech Metrology Institute). Background electrolyte solutions were prepared with salt of KNO_3 (VWR Chemical) and $Ca(NO_3)_2$ (VWR Chemical) dissolved in ultrapure water (milli Q, Millipore). pH was adjusted with distilled 0.1 M HNO_3 and 0.5 M NaOH (VWR

Chemical). A peat purified humic acid (fully purified) from the Mogi river region of Ribeirão Preto, São Paulo State, Brazil was used in all experiments. Detailed of purification procedures and chemical compositions are described in [55].

Tl calibration standards were diluted from a thallium ICP standard solution (TraceCERT®, Sigma Aldrich). The EB95 standard (EB95 Eurostandard from Czech Metrology Institute**)** was used for Ra calibration standards. Blanks of chemicals were analyzed with HR-ICP-MS Element 2 (Thermo Scientific) and no thallium or radium was detected.

4.3. Isotherms.

Two kinds of experiments at room temperature (between 23 ± 1°C) and open to atmosphere were performed. Radium and thallium experiments were made in separated tanks. For radium, only complexation dependence over pH was investigated. Thus, pH varied from 4 to 8 with an initial radium concentration of $3.0.10^{-13}$ mol.L^{-1}. Concerning Tl experiments, both pH and concentration dependencies were tested. In pH isotherms, pH ranged from 3.98 to 7.89 at initial Tl concentration equals to $2.0.\ 10^{-10}$ mol.L^{-1}. In concentration isotherms, pH was fixed at 7.35 ± 0.05 and concentration ranged from ~$2.0\ .10^{-11}$ to ~$2.0\ .10^{-6}$ mol.L^{-1}. Background electrolyte in both donor and acceptor was made with KNO_3 $5.0\ 10^{-2}$ mol.L^{-1} and $Ca(NO_3)_2$ $2.0\ .10^{-3}$ mol.L^{-1} in Ra experiments. In Tl experiments, only KNO_3 at $5.0\ .10^{-2}$ mol.L^{-1} was used in order to avoid any competitive effect with Ca^{2+}. Experiments with Ra^{2+} were conducted with 50 mg.L^{-1} of purified humic acid and it was 150 mg.L^{-1} for Tl^{+} experiments. For each experimental point duplicates of DMT were done.

4.4. Measurements of cations in solution.

Thallium and radium were both measured with an HR-ICP-MS Element 2 (Thermo scientific) in a white room with a solution of ^{115}In 5 ppb as internal standard. For each samples, 9 measurements in a row are done (3 x 3 passes, SI table 2). Then, the average is used as concentration value and the standard deviation is used as measurement error. Concentration are corrected from signal derivation by internal standard. No matrix effects were observed due to the presence of humic acid in solutions. Certified materials TM23.4 and TM24.4 (Environment Canada) validated Tl analysis. An IRSN (Institut de Radioprotection et de Sureté Nucléaire, Fontenay aux Roses, France) certified standard was used for ^{226}Ra HR-ICP-MS analysis

validation. Limits of quantification were respectively between 2.5 $.10^{-12}$ $mol.L^{-1}$ to 7.5 $.10^{-12}$ $mol.L^{-1}$for Tl and 3.0 $.10^{-14}$ $mol.L^{-1}$ for Ra. Major cations (K, Na and Ca) were analyzed with an ICP-AES ICAP 6200 (Thermo scientific). More details of HR-ICP-MS measurement for Ra and Tl can be found in SI (table S2).

4.5. Experimental procedure.

DMT devices [51-52] were used in duplicate for every experimental points. All cells, bottles and tanks for sample solution (donor) were washed before use with 0.1 M Suprapur HNO_3 and ultrapure water (milliQ). The cation exchange membranes (551652U, VWR Chemicals) were prepared by successive washing. Firstly with 0.1 M HNO_3, and 1 M $Ca(NO_3)_2$ then several times with the background electrolyte solution at experiment concentrations. The experimental set-up consisted in a tank filled with donor solution where two field DMTs were immerged. Donor solution was stirred continuously during the entire experiment. For pH isotherms, after pH equilibration, field DMTs stayed immerge in solution during the estimated time in order to reach Donnan equilibrium (24 h for Tl and 72 h for Ra). For concentration isotherms, the procedure is the same. At each pH or concentration steps, two new DMT cells were added in the donor and the two were removed. Then acceptor and donor solutions were sampled. Finally, each sample was acidified to pH~1 with distilled HNO_3 2 %, diluted when necessary and stored for further analysis. No addition of Tl or Ra is made during experiments, so concentrations slowly decreased at each steps and after basic pH adjustments, small amount of Na (from NaOH addition) appeared in sampled solutions. Therefore, at each change of DMT, Tl and Ra concentrations were measured in donor. Na concentrations were only checked at the end of each experiment. Previous modelling confirms that only free Ra and free Tl are found in acceptor solution, without dissolved $RaOH^+$ or TlOH (SI, table S4).

Every species in solution for each isotherm is sum up in supporting information (table S3) like experimental data (tables S5 and S6). Experimental errors are calculated according the propagation of uncertainties theory, as in equation A1 in SI.

4.6. NICA-Donnan modelling.

Metal ions binding to humic substances (HS, mix of humic and fulvic acids) is assumed to occur through specific interactions between cations and negative charges from the surface

functional groups and by nonspecific Coulombic binding to any residual negative charge [56]. The model merges the Non-ideal Competitive Adsorption (NICA) isotherm with the Donnan model. The first (NICA isotherm) describes competitive binding of protons and cations to HS taking into account binding site heterogeneity and the second (Donnan model) details the electrostatic interactions within the structure of HS considered as a water-permeable gel [40, 57].

For humic substances, the model accounts for binding sites heterogeneity by including two different groups of binding sites each with a continuous affinity distribution: type 1 and 2, corresponding to carboxylic (low affinity) and phenolic (high affinity) sites respectively [39]. The model equation is (equation 3):

$$Q_i = \frac{n_{i,1}}{n_{H,1}} Q_{max1,H} \frac{(\tilde{K}_{i,1} c_i)^{n_{i,1}}}{\sum_i (\tilde{K}_{i,1} c_i)^{n_{i,1}}} \frac{\left[\sum_i (\tilde{K}_{i,1} c_i)^{n_{i,1}}\right]^{p_1}}{1+\left[\sum_i (\tilde{K}_{i,1} c_i)^{n_{i,1}}\right]^{p_1}} + \frac{n_{i,2}}{n_{H,2}} Q_{max2,H} \frac{(\tilde{K}_{i,2} c_i)^{n_{i,2}}}{\sum_i (\tilde{K}_{i,2} c_i)^{n_{i,2}}} \frac{\left[\sum_i (\tilde{K}_{i,2} c_i)^{n_{i,2}}\right]^{p_2}}{1+\left[\sum_i (\tilde{K}_{i,2} c_i)^{n_{i,2}}\right]^{p_2}} \quad (3)$$

where the amount of bound ion *i*, Q_i (mol.kg^{-1}) at solution concentration c_i (mol.L^{-1}) is given by the sum of two identical binding expressions. The first for carboxylic-type (subscript 1) and the second for phenolic-type (subscript 2) site distributions. Four parameters describe intrinsic heterogeneity of HS ($Q_{max1, H}$, $Q_{max2, H}$, p_1 and p_2) and four ion specific parameters ($\tilde{K}_{i,1}$, $\tilde{K}_{i,2}$, $n_{i,1}$ and $n_{i,2}$) portray ion binding. p_1 and p_2 are the widths of the affinity distributions and condense the intrinsic heterogeneity of humic substances. $Q_{max1, H}$ and $Q_{max2, H}$ (mol.kg^{-1}) are the maximum proton binding capacity of HS. $\tilde{K}_{i,1}$ and $\tilde{K}_{i,2}$ are the median values of the affinity distributions for ion *i*, and $n_{i,1}$ and $n_{i,2}$ express the non-idealities of the ion-binding to each distribution. When those last four parameters are unknown for a given cation, it is possible to estimate them with empirical equations (equations 4 to 7) using the hydrolysis constant K_{OH} [58]. Details for K_{OH} calculations can be found in supporting information (table S7).

$$n_{i,1} = 0.14 - 0.055 \log K_{OH} \quad (4)$$

$$n_{i,2} = 0.76 n_{i,1} \quad (5)$$

$$n_{i,1} \log \tilde{K}_{i,1} = 0.26 \log K_{OH} + 2.59 \quad (6)$$

$$n_{i,2} \log \widetilde{K}_{i,2} = 0.41 \log K_{OH} + 4.98 \qquad (7)$$

The residual net charge of humic molecule is neutralized by the specific binding of counter-ions and the exclusion of co-ions within the Donnan volume V_D ($L.kg^{-1}$) [40]. This is given by the following relationship (equation 8):

$$\log V_D = b(1 - \log I) - 1 \qquad (8)$$

where I is the ionic strength of the solution and *b* is an empirical parameter detailing how the Donnan volume varies with ionic strength [40].

In this study, modeling is performed using ECOSAT software [59]. The four ion specific parameters ($\widetilde{K}_{i,1}$, $\widetilde{K}_{i,2}$, $n_{i,1}$ and $n_{i,2}$) developed in equations 4, 5, 6 and 7 were calculated for thallium, radium and potassium. In addition to thallium and radium, all other cation complexation present in the donor was modeled in order to consider all competitive effect. Input data were total concentrations (Ra, Tl, Ca or K, depending of the donor) for every cation in solution, pH and ionic strength. Each pH or concentration step is considered as one-modeled experiment, with its own inputs. Hydrolysis constant for thallium and radium were calculated with thermodynamic data from Brown and Ekberg's book [60]. For competitive cations (Ca^{2+} and/or K^{+}), parameters stayed as calculated. However for radium and thallium $\widetilde{K}_{i,1}$, $\widetilde{K}_{i,2}$, $n_{i,1}$ and $n_{i,2}$ were adjusted in order to fit experimental data. Root Mean Square Error (*RMSE*, SI equation A2) was used to estimate the gap between experimental and modeled data. Parameters specific to the purified humic acid and proton binding are from [55] and are presented in SI (tables S8 and S9). Initial ion specific parameters are also summarized in supporting information (Table S8).

5. RESULTS AND DISCUSSION

5.1. Thallium (I) and silver (I).

Thallium complexation to humic acid increases with increasing Tl concentrations (fig. 1A). However, as the line slope of experimental is below 1, it means the amount of bound thallium is higher at low Tl concentrations than at high Tl concentrations (fig. 1A). Tl complexation to HA is also pH-dependent as it is suggested by figure 1B where more thallium is complexed with

increasing pH. In all cases however (fig. 1A and 1B), the amount of complexed thallium is low and always below 50 % of the total Tl in solution.

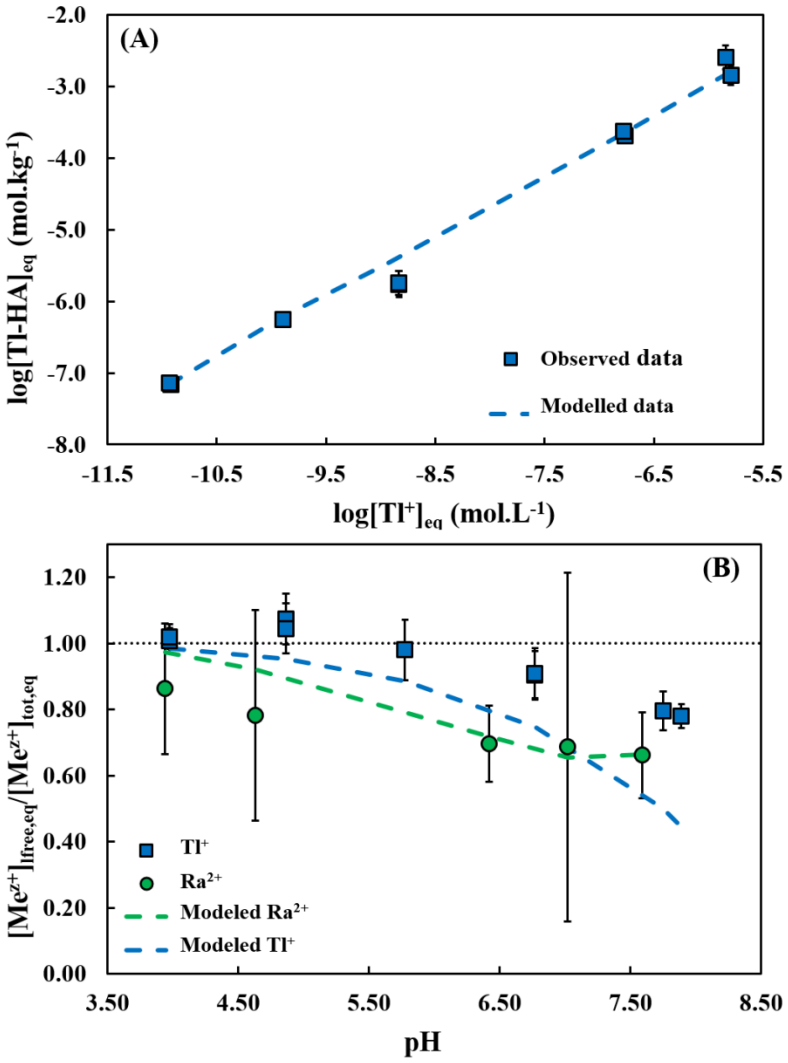

Figure 1: (A) Evolution of free thallium in function of bound thallium. pH for observed data was 7.3 ±0.08 with [HA] = 150 mg.L^{-1}. For free Tl: *RMSE*=0.04 (n=9) and for bound Tl: *RMSE*=0.16 (n=9). (B) Evolution of free thallium and radium in DMT over pH. Input concentrations were 2.0 .10^{-10} mol.L^{-1} and 3.0 .10^{-13} mol.L^{-1} for Tl and Ra respectively. Error bars are ± 2σ for A and B.

Ion specific parameters in NICA-Donnan modelling were adjusted to fit Tl concentration isotherm values (figure 1A) instead of pH isotherm data. In this case, data would be fitted with a width range of thallium concentrations (6 order of magnitude), which is more accurate. Thus, free data are better matched than bound data with respective *RMSE* of 0.04 and 0.16 (table 1). It also appears that the associated description (dashed line in fig. 1B) of pH isotherm is over

experimental data (fig. 1B). This suggests an underestimation of bound thallium at multiple pH with experimental data. In this study, within the ion specific parameters, only $\log\widetilde{K}_{Tl,1}$ and $\log\widetilde{K}_{Tl,2}$were adjusted to limit the set of results. Values are summarized in table 1. The ability to model others experimental data with this set of data (table 1), was successfully tested with Liu's study[38]. Results are in SI (figure S14 and table S15).

Table 1: Ion specific parameters for NICA equation selected after adjustment with experimental data.

Element	$\text{Log}\widetilde{K}_{i,1}$	$n_{i,1}$	$\log\widetilde{K}_{i,2}$	$n_{i,2}$	*RMSE* for free metal	*RMSE* for bound metal
Tl^{+}	0.1	0.88	2.15	0.84	0.04 (n=9)	0.16 (n=9)
Ag^{+}	-0.13	0.59	4.76	0.71	-	0.02 (n=62)
Ra^{2+}	-1.02	0.78	-0.65	0.75	0.04 (n=5)	0.37 (n=5)

The same exercise was done with silver, Ag(I). Experimental data were from Sikora *et al.* [48]. In this study, they performed concentrations isotherms at pH 6.5 for three different humic acids. Then, as humic acids were not in ECOSAT database, parameters describing HS heterogeneity along with both proton and silver specific parameters needed to be adjusted. Values for $Q_{max1,H}$ associated to carboxylic type sites were from Sikora *et al.* [48] and never optimized. Silver specific parameters were adjusted only for the first humic acid. Finally, $Q_{max2,H}$ values, as like as p_1, p_2, $\log\widetilde{K}_{H,1}$, and $\log\widetilde{K}_{H,2}$ were optimized within the range of parameters given by Milne *et al.* [61] in his generic humic acid definition. The procedure is summarized in SI, table S13. Figure 2 displays the results and optimized Ag(I) specific parameters are in table 1.

In donor solution, at pH below 6 (fig. 1B), few Tl is complexed but the majority is on carboxylic sites. Then at higher pH (> 6) and independently of thallium concentrations (fig. 1A and 1B), the larger amount of thallium is bound on phenolic type-sites with more than 65 % (of complexed Tl). Those results are confident with the median values of affinity distribution calculated for Tl, which highlight a much higher values for phenolic like sites than carboxylic like sites (table 1). A small role is also played by the donnan gel, at either low pH or high Tl concentrations without overtaking 10 % of complexed thallium. In Sikora's paper [48] conditions (pH = 6.5), Ag(I) is almost exclusively bound to high affinity sites (phenolic) and only residues (≤ 5 % of complexed silver) are bound to low affinity sites or are in the gel. Then it appears Ag binding to humic acid is strongly controlled by phenolic sites, more than for Tl. The amount of bound Ag(I) is also much higher than Tl(I) (fig. 3). Silver has a higher affinity for organic matter

than Tl and its mobility is strongly influenced by this type of ligand [9,48]. Figure 3 also suggests that Ag, a monovalent cation, could compete with divalent cation to complex humic substances. The pH-dependence in Ag complexation is less pronounced than divalent and at neutral pH, it may compete with cobalt for instance (fig. 3). At acidic pH, silver has more affinity for HA than cobalt, manganese and cadmium (fig. 3).

As mentioned in introductions, both Ag(I) and Tl(I) are soft cations [46,62] with a chalcophile behavior. Then, assumptions are made regarding the role of S-rich compound such as thiol groups from humic substances [9,36,47,49]. Although Ag-S binding is evidenced for Ag [49] and despite high affinity for thiolate [49,62], its relative importance is not so obvious [47-49]. Moreover, Tl(I) affinity to sulfur-containing organic compounds such as cysteine for instance is still under investigation and no data were found for thiol [37,47,63-66]. Finally, characterizing S-rich functional group in NOM is challenging and many questions remain [67]. Two latest studies had determined thiol group concentrations in natural organic matter (NOM)[68-69]. Rao *et al.*[68] calculated a concentrations of 0.7 $\mu mol.g^{-1}$ (of NOM) for Suwanee River NOM and 3.6 $\mu mol.g^{-1}$ (of NOM) for a soil humic acid. In their study, Joe-Wong *et al.*[69] estimated that thiol groups represent 0.535 $mmol.g^{-1}$ of dissolved organic matter (DOM). Consequently, due to their abundance and their pKa at 8[62,68-69], thiol groups can be easily considered within the phenolic type sites in the continuous distribution of the NICA-Donnan model [39-40,57]. Thus, the high affinity of Tl(I) and Ag(I) for hydroxyl functional groups is emphasized in this study (table 1). It is also coherent regardless whether assumptions of the role of S-rich groups would be later confirmed or not.

In this study, Tl(I) aqueous speciation in various natural water systems from Kaplan and Mattigod [42] was revisited (table 2). DOM was calculated from DOC considering a ratio DOM to DOC of 2:1. Then, according to Perdue and Ritchie [70], 60 % of DOM is assimilated to Humic Substances (HS) and simplified as strictly humic acids. The remaining 40 % are non-reactive [70]. Constants for others complexes than Tl-HA aqueous species are summarized in SI (table S16). Results (table 2) show that only two dissolved aqueous species of Tl(I) exist in freshwater systems, Tl^+ and Tl-HA. Amount of free thallium are over 90 % of total thallium whereas Tl-HA complex are below 10% (table 2). In groundwater, thallium is mostly free like in bog waters. The latest system point out the main difference with Kaplan and Mattigod's results

[42]. Indeed, in this study, Tl-HA complex is more important in river or lake waters and not in bog water due to too acidic conditions (pH<4). In seawater, only half of thallium is free and the other half is aqueous complexes with chlorides (table 2). Differences with Kaplan and Mattigod's study [42] are also due to different source of constant for Tl(I) species and emphasize the need of a consensus in thallium speciation studies. Moreover, the role of colloids is not taken in consideration here.

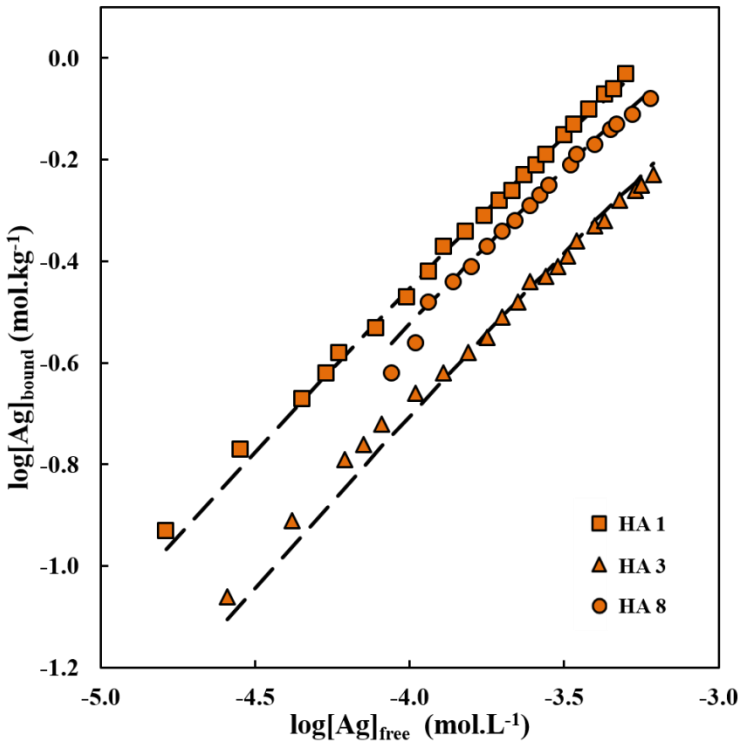

Figure 2: Bound silver versus free silver. Points are experimental from Sikora *et al.* [48]. Background electrolyte was KNO3 0.1 mol.L-1, pH was 6.5 and [HA] = 0.5 g.L^{-1}. Dashed black lines are adjusted values with NICA-Donnan model in same conditions as experimental data.

Speciation of thallium is soil solution was also modeled. Composition of solutions was from Kinniburgh *et al*. [72]. Various Tl concentrations relevant with natural systems (polluted or not) were taken into consideration. Details of constants, compositions and results are presented in SI (tables S16 and S18). Many species are reunited as DOM in soil solutions. According to Ren *et al*. [54], approximately 29% are humic substances, 66 % are hydrophilic acids and 5% are non-reactive. In this study hydrophilic acids were equally divided in acetic acid, citric acid and oxalic acid, three low-molecular weight organic acids (LMWOAs). Thallium does not complex with those organic acids as it was already observed [71]. Therefore, as for natural water systems, only

two dissolved species of Tl(I) are present, Tl^+ and Tl-HA. At low Tl concentrations ($\leq 10^{-9}$ mol.L^{-1}), it seems that up to 25% of thallium could complex humic acid. On the contrary at high Tl concentrations ($\geq 10^{-9}$ mol.L^{-1}), less than 10 % is complexed.

These results confirm that in the surface environment, Tl(I) is predominantly free and labile. In highly thallium impacted systems (anthropically or naturally) the role of natural organic matter in thallium mobility seems limited as suggested [11,20,24,71]. Moreover, in opposition to its dual behavior (lithophile and chalcophile) in the deep environment, Tl(I) seems to behave more as a lithophile element close to alkali metals (K^+, Rb^+ and Cs^+). This suggestion is supported by the idea that illitic clays seem to control the mobility of Tl^+ in many environments [9,11,20]. However many questions remain regarding Tl, especially concerning Tl(III) and its abundance/stability in the environment [15,18-19]. In this context, the role of natural organic matter still needs to be investigated, as a ligand and about its involvement in Tl sorption mechanism onto clays and oxihydroxides (Fe and Mn).

Table 2: Calculated distribution of Tl(I) species (% of total) in various natural water systems. Revisited from Kaplan and Mattigod [42]. Association constants for complexes are summarized in SI and waters compositions are as in Kaplan and Mattigod [42]. Only complexes with more than 1% of total thallium are presented here. No precipitation of Tl minerals occurs. TlOH(aq), $TlCO_3^-$, $TlHCO_3$, $Tl(CO_3)_2^{3-}$, $TlHPO_4^-$ and $TLPO_4^{2-}$ do not contribute in Tl(I) speciation.

	pH	[Tl(I)] (nmol.L^{-1})	HA (mg.L^{-1})	Tl^+	$TlSO_4^-$	TlCl(aq)	$TlCl_2$	Tl-HA
Groundwater	7.14	35.5	0.91	98.4	1.3	-	-	-
River water	8.01	9.8 .10^{-2}	6.5	91.8	-	-	-	7.9
Eutrophic lake water	7.70	9.8 .10^{-2}	13.00	90.0	-	-	-	9.6
Bog water	3.60	9.8 .10^{-2}	39.00	96.5	-	-	-	3.5
Seawater	8.22	6.4 .10^{-2}	0.65	49.8	3.9	36.1	10.0	-

5.2. Radium (II).

More radium is complexed to humic acids (fig.1B). At low pH (< 6), the amount of bound Ra increases from 13.7 % to 21 %. At pH over 6, this amount is steadier and reached a maximum at pH=7.59 with 33 % of complexed Ra (fig. 1B). Error bars for Ra concentrations (fig. 1B) are high due to HR-ICP-measurements close to limit of quantification (LOD) and low Ra counting

values. Then, measurement errors are propagated and generate high uncertainties in the end.. When Ra concentration measurements are closer to LOD, the uncertainties increase.

Adjusted parameters for Ra(II) complexation with HA function of pH are summarized in table 1. Free Ra is better calculated than complexed Ra with *RMSE* = 0.04 for the former and 0.37 for the latter (table 1) where the fitting is less precise at pH < 5 (fig. 1B and more details in SI, figure S12). Indeed, under these experimental conditions, few complexations occur and the amount of free Ra is close to total Ra in solution, increasing uncertainties on the calculated complex species. Results from calculation with NICA-Donnan model display a stronger dependence to pH (fig 1B) than expected with experimental values. At acidic pH, the little radium bound to HA is almost totally onto carboxylic type sites of HA, with a small fraction in the gel (~10%). At neutral and basic pH carboxylic type sites still complexed the majority of Ra^{2+} (more than 70% of complexed Ra), but phenolic like sites have a bigger part as pH increases.

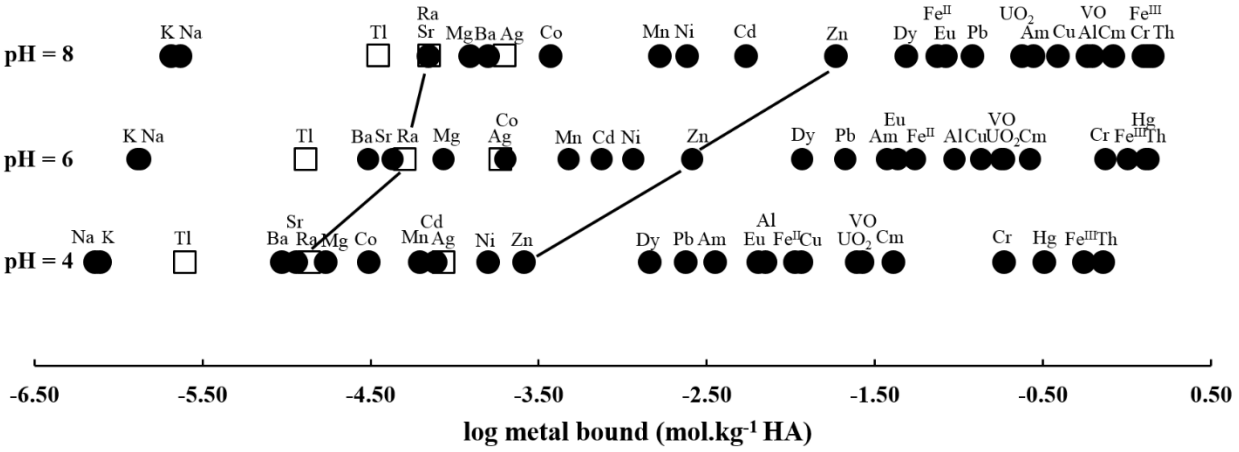

Figure 3: Calculated metal bound to a generic humic acid for with 10 nmol.L^{-1} of a given metal and presence of 1 mmol.L^{-1} of Ca^{2+}. Figure adapted from Milne *et al.* [58]. Tl, Ra and Ag values are from this study, other metals are from Milne *et al.*[58]

Compared to other divalent cations, Ra forms weak interactions with humic substances (fig. 3). According to previous observations, Ra display the same behavior as others heavy alkali earth elements (fig. 3) and may compete with them for complexation as it is for other bearing phases [26]. Ra seems to have however a high affinity for organic matter in the environment, particularly in soil. In a soil solution, revisited from Kinniburgh *et al.* [72] (details in SI, tables S17 and S19)

at pH≥7, more than 60 % of Ra is bind to humic acid at high Ra concentrations (>1.0 10^{-13} $mol.L^{-1}$). At low Ra concentrations (<1.0 10^{-13} $mol.L^{-1}$), it is up to 87 % of Ra that is bound. When not bound to HA, Ra is mainly free in solution and a small fraction (less than 2 %) is complexed to sulfates. Besides, radium does not complex with LMWOAs, highlighting the high reactivity of humic substances with this elements. These results concur with other studies that showed an important role of organic matter in Ra speciation [26,43-44,74] and especially in soils where humic substances may retain Ra [73-75]. However the impact of other bearing phases (not taken in consideration here), and mainly clay minerals [26,74-76] with natural organic matter needs to be investigated to fully understand Ra cycle.

ACKNOWLEDGEMENTS

The authors thank IRSN, CEA, BRGM and IPGP for funding this research. Parts of this this work were supported by IPGP multidisciplinary program PARI and by Region Ile de France SESAME Grant no. 12015908.

REFERENCES

[1]Peter, a. L. J., Viraraghavan, T. (2005). Thallium: a review of public health and environmental concerns. *Environment International*, *31*(4), 493–501. http://doi.org/10.1016/j.envint.2004.09.003

[2]Nriagu, J. O. (1998). Thallium in the Environment. Ed. John Wiley & Sons: New York.

[3]McGoldrick, P. J., Keays, R. R., & Scott, B. B. (1979). Thallium: a sensitive indicator of rock/seawater interaction and of sulfur saturation of silicate melts. *Geochimica et Cosmochimica Acta*, *43*(8), 1303–1311. http://doi.org/10.1016/0016-7037(79)90120-0

[4]Baker, R. G. A., Rehkämper, M., Ihlenfeld, C., Oates, C. J., & Coggon, R. (2010). Thallium isotope variations in an ore-bearing continental igneous setting : Collahuasi Formation , northern Chile, *74*, 4405–4416. http://doi.org/10.1016/j.gca.2010.04.068

[5]Biagioni, C., D'Orazio, M., Vezzoni, S., Dini, A., & Orlandi, P. (2013). Mobilization of TI-Hg-As-Sb-(Ag,Cu)-Pb sulfosalt melts during low-grade metamorphism in the Alpi Apuane (Tuscany, Italy). *Geology*, *41*(7), 747–750. http://doi.org/10.1130/G34211.1

[6]Hettmann, K., Marks, M. a. W., Kreissig, K., Zack, T., Wenzel, T., Rehkämper, M., Jacob, D. E., Markl, G. (2014). The geochemistry of Tl and its isotopes during magmatic and hydrothermal processes: The peralkaline Ilimaussaq complex, southwest Greenland. *Chemical Geology*, *366*, 1–13. http://doi.org/10.1016/j.chemgeo.2013.12.004

[7]Prytulak, J., Brett, A., Webb, M., Plank, T., Rehkämper, M., Savage, P. S., Woodhead, J. (2017). Thallium elemental behavior and stable isotope fractionation during magmatic processes. *Chemical Geology*, *448*, 71–83. http://doi.org/10.1016/j.chemgeo.2016.11.007

[8]Shaw, D. M. (1952). The geochemistry of thallium. *Geochimica et Cosmochimica Acta*, *2*, 118–154

[9]Jacobson, A. R., McBride, M. B., Baveye, P., & Steenhuis, T. S. (2005). Environmental factors determining the trace-level sorption of silver and thallium to soils. *Science of The Total Environment*, *345*(1-3), 191–205. http://doi.org/10.1016/j.scitotenv.2004.10.027

[10]Coup, K. M., & Swedlund, P. J. (2015). Demystifying the interfacial aquatic geochemistry of thallium(I): New and old data reveal just a regular cation. *Chemical Geology*, *398*, 97–103. http://doi.org/10.1016/j.chemgeo.2015.02.003

[11]Voegelin, A., Pfenninger, N., Petrikis, J., Majzlan, J., Plötze, M., Senn, A.-C., … Göttlicher, J. (2015). Thallium speciation and extractability in a thallium- and arsenic-rich soil developed from mineralized carbonate rock. *Environmental Science & Technology*, *49*(9), 5390–8. http://doi.org/10.1021/acs.est.5b00629

[12]Vink, B. W. (1993). The behavior of thallium in the (sub) surface environment in terms of Eh and pH. *Chemical Geology*, *109*, 119–123.

[13]Xiong, Y. (2009). The aqueous geochemistry of thallium : speciation and solubility of thallium in low temperature systems. *Environ. Chem.*, *6*, 441–451. http://doi.org/10.1071/EN08086

[14]Casiot, C., Egal, M., Bruneel, O., Verma, N., Parmentier M., Elbaz-Poulichet, F. (2011). Predominance of Aqueous Tl(I) Species in the River System Downstream from the Abandoned Carnoulès Mine (Southern France). *Environmental Science & Technology*, *45*(1), 2056–2064. dx.doi.org/10.1021/es102064r |

[15]Lin, T.-S., & Nriagu, J. (1999). Thallium Speciation in the Great Lakes. *Environmental Science & Technology*, *33*(19), 3394–3397. http://doi.org/10.1021/es981096o

[16]Peacock, C. L., & Moon, E. M. (2012). Oxidative scavenging of thallium by birnessite: Explanation for thallium enrichment and stable isotope fractionation in marine ferromanganese precipitates. *Geochimica et Cosmochimica Acta*, *84*, 297–313. http://doi.org/10.1016/j.gca.2012.01.036

[17]Campanella, B., Casiot, C., Onor, M., Perotti, M., Petrini, R., & Bramanti, E. (2017). Talanta Thallium release from acid mine drainages : Speciation in river and tap water from Valdicastello mining district (northwest Tuscany). *Talanta*, *171*(May), 255–261. http://doi.org/10.1016/j.talanta.2017.05.009

[18]Karlsson, U., Karlsson, S., & Düker, A. (2006). The effect of light and iron(II)/iron(III) on the distribution of Tl(i)/Tl(iii) in fresh water systems. *Journal of Environmental Monitoring*, *8*(6), 634. http://doi.org/10.1039/b516445a

[19]Twining, B. S., Twiss, M. R., & Fisher, N. S. (2003). Oxidation of thallium by freshwater plankton communities. *Environmental Science & Technology*, *37*(12), 2720–6. http://doi.org/10.1021/es026145i

[20]Vaněk, A., Chrastný, V., Mihaljevič, M., Drahota, P., Grygar, T., & Komárek, M. (2009). Lithogenic thallium behavior in soils with different land use. *Journal of Geochemical Exploration*, *102*, 7–12. http://doi.org/10.1016/j.gexplo.2008.10.004

[21]Xiao, T., Guha, J., Boyle, D., Liu, C., & Chen, J. (2004). Environmental concerns related to high thallium levels in soils and thallium uptake by plants in southwest Guizhou, China. *The Science of the Total Environment*, *318*(03), 223–244. http://doi.org/10.1016/S0048-9697(03)00448-0

[22]Lis, J., Pasieczna, A., Karbowska, B., Zembrzuski, W., & Lukaszewski, Z. (2003). Thallium in soils and stream sediments of a Zn-Pb mining and smelting area. *Environmental Science and Technology*, *37*(20), 4569–4572. http://doi.org/10.1021/es0346936

[23]Cheam, V. (2001). Thallium Contamination of Water in Canada, *Water Qual. Res. J. Canada*, *36*(4), 851–877.

[24]Vaněk, A., Chrastný, V., Komárek, M., Penížek, V., Teper, L., Cabala, J. & Drábek O. (2013). Geochemical position of thallium in soils from a smelter-impacted area. *Journal of Geochemical Exploration*, *124*, 176–182. http://doi.org/10.1016/j.gexplo.2012.09.002

[25]Nielsen, S. G., Rehkämper, M., Porcelli, D., Andersson, P., Halliday, A. N., Swarzenski, P. W., Latkoczy, C., Günther, D. (2005). Thallium isotope composition of the upper continental crust and rivers—An investigation of the continental sources of dissolved marine thallium. *Geochimica et Cosmochimica Acta*, *69*(8), 2007–2019. http://doi.org/10.1016/j.gca.2004.10.025

[26]Porcelli, D., Kim, C. K., Martin, P., Moore, W. S., Phaneu, M. (2014). Properties of Radium. In *The Environmental Behaviour of Radium: Revised Edition*, 6–32. IAEA, Vienna

[27]Jia, G., & Jia, J. (2012). Determination of radium isotopes in environmental samples by gamma spectrometry, liquid scintillation counting and alpha spectrometry: A review of analytical methodology. *Journal of Environmental Radioactivity*, *106*, 98–119. http://doi.org/10.1016/j.jenvrad.2011.12.003

[28]Darby, S., Hill, D., Auvinen, A., Baysson, H., Bochicchio, F., Deo, H., … Doll, R. (2004). Radon in homes and risk of lung cancer: collaborative analysis of individual data from 13 European case-control studies. Br. Med. J., 330, 223–228. http://doi.org/10.1136/bmj.38308.477650.63

[29]Gao, Y., Baeyens, W., De Galan, S., Poffijn, a., & Leermakers, M. (2010). Mobility of radium and trace metals in sediments of the Winterbeek: Application of sequential extraction and DGT techniques. *Environmental Pollution*, *158*(7), 2439–2445. http://doi.org/10.1016/j.envpol.2010.03.022

[30]Fesenko, S., Carvalho, F., Martin, P., Moore, W. S., Yankovich, T. (2014). Radium in the Environment. In *The Environmental Behaviour of Radium: Revised Edition*, 33–105. IAEA, Vienna

[31]Manakhov, D. V., & Egorova, Z. N. (2014). Speciation of radium-226 in podzols of northeastern Sakhalin in the impact zone of the oil field. *Eurasian Soil Science*, *47*(6), 608–612. http://doi.org/10.1134/S106422931404005X

[32]Cuvier, A., Panza, F., Pourcelot, L., Foissard, B., Cagnat, X., Prunier, J., … Le Roux, G. (2015). Uranium decay daughters from isolated mines: Accumulation and sources. *Journal of Environmental Radioactivity*, *149*, 110–120. http://doi.org/10.1016/j.jenvrad.2015.07.008

[33]Lauer, N. E., Hower, J. C., Hsu-kim, H., Taggart, R. K., & Vengosh, A. (2015). Naturally Occurring Radioactive Materials in Coals and Coal Combustion Residuals in the United States. http://doi.org/10.1021/acs.est.5b01978

[34]Zhang, T., Hammack, R. W., & Vidic, R. D. (2015). Fate of Radium in Marcellus Shale Flowback Water Impoundments and Assessment of Associated Health Risks. http://doi.org/10.1021/acs.est.5b01393

[35]Chalupnik, S., Wysocka, M., Janson, E., Chmielewska, I. & Wiesner, M. (2017). Long term changes in the concentration of radium in discharge waters of coal mines and Upper Silesian rivers. *Journal of Environmental Radioactivity*, *171*, 117–123

[36]Girault, F., Perrier, F., & Przylibski T. A. (2016). Radon-222 and radium-226 occurrence in water: a review. In *Radon, Health and Natural Hazards*, Special Publication *451*. Geoogical Society, London.

[37]Rodríguez-Mercado, J. J., Altamirano-Lozano, M. A. (2013). Genetic toxicology of thallium : a review. *Drug and Chemical Toxicology* *36*, 369–383. http://doi.org/10.3109/01480545.2012.710633

[38]Liu, J., Lippold, H., Wang, J., Lippmann-Pipke, J., & Chen, Y. (2011). Sorption of thallium(I) onto geological materials: Influence of pH and humic matter. *Chemosphere*, *82*(6), 866–871. http://doi.org/10.1016/j.chemosphere.2010.10.089

[39]Benedetti, M. F., Milne, C. J., & Kinniburgh, D. G. (1995). Metal ion binding to humic substances: application of the non-ideal competitive adsorption model. *Environmental Science & Technology*, *29*(2), 446–457. http://doi.org/10.1021/es00002a022

[40]Benedetti, M. F., Van Riemsdijk, W. H., & Koopal, L. K. (1996a). Humic substances considered as a heterogeneous Donnan gel phase. *Environmental Science and Technology*, *30*(6), 1805–1813. http://doi.org/10.1021/es950012y

[41]Koopal, L. K., Saito, T., Pinheiro, J. P., & Van Riemsdijk, W. H. (2005). Ion binding to natural organic matter: General considerations and the NICA-Donnan model. *Colloids and Surfaces A: Physicochemical and Engineering Aspects*, *265*(1-3), 40–54. http://doi.org/10.1016/j.colsurfa.2004.11.050

[42]Kaplan, D. I., & Mattigod S. V. (1998). Aqueous geochemistry of thallium. In *Thallium in the Environment*, 15–29. Edited by J. O. Nriagu. John Wiley & Sons, Inc. New York

[43]Beaucaire, C. (2013). Sorption Properties of Peat for U (VI) and 226Ra in U Mining Areas areas. *Procedia Earth and Planetary Science*, *7*(February 2017), 85–88. http://doi.org/10.1016/j.proeps.2013.03.121

[44]Laili, Z., Yasir, M. S., Omar, M., Mohd Zaidi, I., & Philip, E. (2010). Influence of humic acids on radium adsorption by Coir Pith in aqueous solution. *Sains Malaysiana*, *39*(1), 99–106.

[45]Temminghoff, E. J. M., Plette, A. C. C., Van Eck, R., & Van Riemsdijk, W. H. (2000). Determination of the chemical speciation of trace metals in aqueous systems by the Wageningen Donnan Membrane Technique. *Analytica Chimica Acta*, *417*(2), 149–157. http://doi.org/10.1016/S0003-2670(00)00935-1

[46]Pearson, R. G. (1968). Hard and Soft Acids and Bases, HSAB, Part II – Underlying theories. *Journal of Chemical Education*, *45*(10), 643–648. http://doi.org/10.1021/2Fed045p643

[47]Jacobson, A. R., Klitzke, S., McBride, M. B., Baveye, P., & Steenhuis, T. S. (2005). The desorption of silver and thallium from soils in the presence of a chelating resin with thiol functional groups. *Water, Air, Soil Pollut.*, *160*, 41–54. http://doi.org/10.1007/s11270-005-3860-3

[48]Sikora, F. J., Stevenson, F. J. (1988). Silver Complexation by Humic Substances : Conditional Stability Constants and Nature of Reactive Sites. *Geoderma*, *42*, 353–363.

[49]Kleja, D. B., Nakata, S., Persson, I., & Gustafsson, J. P. (2016). Silver(I) Binding Properties of Organic Soil Materials Are Different from Those of Isolated Humic Substances. *Environmental Science and Technology*, *50*, 7453–7460. http://doi.org/10.1021/acs.est.6b00970

[50]Chen, Z., Campbell, P. G. C., & Fortin, C. (2012). Silver binding by humic acid as determined by equilibrium ion-exchange and dialysis. *Journal of Physical Chemistry A*, *116*(25), 6532–6539. http://doi.org/10.1021/jp212403r

[51]Weng, L., Van Riemsdijk, W. H., & Temminghoff, E. J. M. (2005). Kinetic aspects of Donnan membrane technique for measuring free trace cation concentration. *Analytical Chemistry*, *77*(9), 2852–2861. http://doi.org/10.1021/ac0485435

[52]Kalis, E. J. J., Temminghoff, E. J. M., Van Riemsdijk, W. H., & Weng, L. (2007). Measuring Free Metal Ion Concentrations in Multicomponent Solutions Using the Donnan Membrane Technique Measuring Free Metal Ion Concentrations in Multicomponent Solutions Using the Donnan Membrane Technique. *Analytical Chemistry*, *40*(3), 955–955. http://doi.org/10.1021/ac0615403

[53]Kalis, E. J. J., Weng, L., Dousma, F., Temminghoff, E. J. M., & Van Riemsdijk, W. H. (2006). Measuring Free Metal Ion Concentrations in Situ in Natural Water Using the Donnan Membrane Technique. *Environ. Sci. Technol*, *40*(3), 955–961. http://doi.org/10.1021/ac0615403

[54]Ren, Z.-L., Tella, M., Bravin, M. N., Comans, R. N. J., Dai, J., Garnier, J.-M., … Benedetti, M. F. (2015). Effect of dissolved organic matter composition on metal speciation in soil solutions. *Chemical Geology*, *398*, 61–69. http://doi.org/10.1016/j.chemgeo.2015.01.020

[55]Botero, W. G., Pineau, M., Janot, N., Domingos, R., Mariano, J., Rocha, L. S., Groenenberg, J. E., Benedetti, M. F., & Pinheiro, J. P. Binding behavior of trace metals with a peat soil humic acid: effect of the HF/HCl isolation treatment. *To be submitted Under Review??*.

[56]Kinniburgh, D. G., Milne, C. J., Benedetti, M. F., Pinheiro, J. P., Filius, J., Koopal, L. K., & Van Riemsdijk, W. H. (1996). Metal Ion Binding by Humic Acid: Application of the NICA-Donnan Model. *Environmental Science & Technology*, *30*(5), 1687–1698. http://doi.org/10.1021/es950695h

[57]Benedetti, M. F., Van Riemsdijk, W. H., Koopal, L. K., Kinniburgh, D. G., Gooddy, D. C., & Milne, C. J. (1996b). Metal ion binding by natural organic matter: From the model to the field. *Geochimica et Cosmochimica Acta*, *60*(14), 2503–2513. http://doi.org/10.1016/0016-7037(96)00113-5

[58]Milne, C. J., Kinniburgh, D. G., van Riemsdijk, W. H., & Tipping, E. (2003). Generic NICA-Donnan Model Parameters for Metal-Ion Binding by Humic Substances. *Environmental Science & Technology*, *37*(5), 958–971. http://doi.org/10.1021/es0258879

[59]Keizer, M. G., Van Riemsdjik, W. H. (1994). *A Computer Program for the Calculation of Chemical Speciation and Transport in Soil-Water Systems (ECOSAT 4.7)*. Wageningen Agricultural University: Wageningen, The Netherlandd.

[60]Brown, P. L., Ekberg, C. (2016). Hydrolysis of Metal Ions. *Wiley VCM*, p217-218 & p825

[61]Milne, C. J., Kinniburgh, D. G., & Tipping, E. (2001). Generic NICA-Donnan model parameters for proton binding by humic substances. *Environmental Science and Technology*, *35*(10), 2049–2059. http://doi.org/10.1021/es000123j

[62]Smith, D. S., Bell, R. A., & Kramer, J. R. (2002). Metal speciation in natural waters with emphasis on reduced sulfur groups as strong metal binding sites. *Comparative Biochemistry and Physiology Part C*, *133*(1-2), 65–74. http://doi.org/10.1016/S1532-0456(02)00108-4

[63]Gharib, F. (2010). Solvent Effects on Protonation and Complexation of Penicillamine and Thallium (I) in Different Aqueous Solutions of Methanol. *J. Chem. Eng. Data.*, *55*, 1547–1553.

[64]Gharib, F., & Shamel, A. (2009). Solvent Effects on Protonation and Complexation of Cysteine and Thallium (I) in Different Aqueous Solutions of Methanol. *J. Chem. Eng. Data.*, *54*, 933–939.

[65]Montes, S., Soriano, L., Ríos, C., & Monroy-Noyola, A. (2007). Endogenous thiols enhance thallium toxicity. *Archives of Toxicology*, *81*(10), 683–687. http://doi.org/10.1007/s00204-007-0203-8

[66]Garcia Bugarin, M. G., Casas, J. S., Sordo, J. Filella M. (1989). Thallium (I) Interactions in Biological Fluids : A Potentiometric Investigation of Thallium (I) Complex Equilibria with Some Sulphur-containing Amino Acids. *Journal of Inorganic Biochemistry*, *35*, 95–105.

[67]Aiken, G. R., Hsu-Kim, H., & Ryan, J. N.(2011). Influence of Dissolved Organic Matter on the Environmental Fate of Metals, Nanoparticles, and Colloids. . *Environmental Science and Technology*, *45*, 3196–3201. http://doi.org/10.1021/es103992s

[68]Rao, B., Simpson, C., Lin, H., Liang, L., & Gu, B. (2014). Determination of thiol functional groups on bacteria and natural organic matter in environmental systems. *Talanta*, *119*, 240–247. http://doi.org/10.1016/j.talanta.2013.11.004

[69]Joe-Wong, C., Shoenfelt, E., Hauser, E. J., Crompton, N., & Myneni, S. C. B. (2012). Estimation of reactive thiol concentrations in dissolved organic matter and bacterial cell membranes in aquatic systems. *Environmental Science and Technology*, *46*(18), 9854–9861. http://doi.org/10.1021/es301381n

[70]Perdue, E. M., & Ritchie, J. D. (2003). Dissolved organic matter in freshwaters. *Treatise on geochemistry*, *5*, 605.

[71]Vaněk, A., Komárek, M., Chrastný, V., Galu, I., Mihaljevi, M., Drahota, P., Tejnecký, V., & Vokurková, P. (2012). Effect of low-molecular-weight organic acids on the leaching of thallium and accompanying cations from soil – A model rhizosphere solution approach. *Journal of Geochemical Exploration*, *112*, 212–217. http://doi.org/10.1016/j.gexplo.2011.08.010

[72]Kinniburgh, D. G., & Miles, D. L. (1983). Extraction and chemical analysis of interstitial water from soils and rocks. *Environmental Science & Technology*, *17*(6), 362–368. http://doi.org/10.1021/es00112a011

[73]Greeman, D. J., Rose, A. W., Washington, J. W., Dobos, R. R., & Ciolkosz, E. J. (1999). Geochemistry of radium in soils of the Eastern United States. *Applied Geochemistry*,*14*, 365-385.

[74]Vandenhove, H., & Van Hees, M. (2007). Predicting radium availability and uptake from soil properties. *Chemosphere*, *69*(4), 664–674. http://doi.org/10.1016/j.chemosphere.2007.02.054

[75]Carvalho, F., Chambers, D., Fesenko, S., Moore, W. S., Porcelli, D., Vandenhove, H. & Yankovich, T. (2014). Environmental pathways and corresponding models. In *The Environmental Behaviour of Radium: Revised Edition*, 1066–32. IAEA, Vienna

[76]Reinoso-Maset, E., & Ly, J. (2016). Study of uranium (VI) and radium (II) sorption at trace level on kaolinite using a multisite ion exchange model. *Journal of Environmental Radioactivity*, *157*, 136–148. http://doi.org/10.1016/j.jenvrad.2016.03.014

APPENDIX 1: Time to equilibrium for Tl^+ and Ra^{2+} (Donnan Membrane Technique)

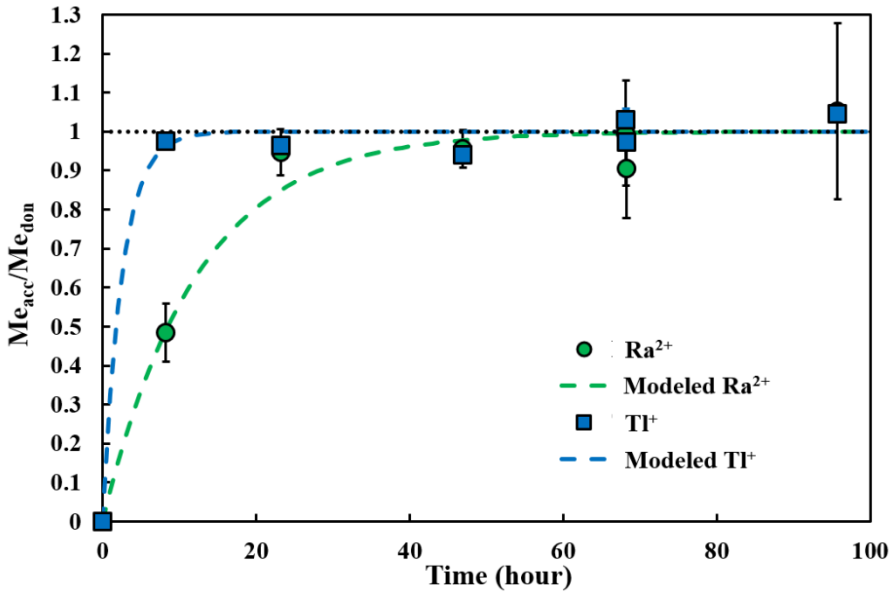

Figure S1: Time to reach equilibrium for Tl^+ and Ra^{2+}, at pH = 4.0 ± 0.1 without humic acid. Error bars are ±2σ of the experimental data. Time to reach equilibrium is **24 hours** for **Tl** and **72 hours** for **Ra**. Dashed lines correspond to the modeled variation of cation concentrations during experiments (Temminghoff et al., 2000[7]). For Tl, $t_{1/2}$ was 0.75 hours and for Ra, it was 8.5 hours

[7]Temminghoff, E. J. M., Plette, A. C. C., Van Eck, R., & Van Riemsdijk, W. H. (2000). Determination of the chemical speciation of trace metals in aqueous systems by the Wageningen Donnan Membrane Technique. *Analytica Chimica Acta*, *417*(2), 149–157. http://doi.org/10.1016/S0003-2670(00)00935-1

APPENDIX 2: ^{205}Tl and ^{226}Ra measurements with HR-ICP-MS Element 2 (Thermo Scientific)

Table S2: Operating conditions and data acquisition parameters for HR-ICP-MS Element 2 used for ^{205}Tl and ^{226}Ra measurements. Thallium was measured only in low resolution mode. Radium was measured in low and medium resolution modes.

HR-ICP-MS		
Rf power (W)	1350	
Sample uptake rate (mL.min^{-1})	0.2	
Argon flow rates (L.min^{-1})		
Cool	16	
Auxiliary	1.0	
Sample	Between 0.9 and 1.0 (depends of sensibility)	
Torch	Quartz torch with a separate quartz injector tube	
Nebulizer	PFA ST microflow nebulizer	
Spray chamber	Quartz Cyclo spray chamber	
Sampler cone	Nickel	
Skimmer cone	Nickel	
Data acquisition	*Low Resolution*	*Medium Resolution*
No. of passes	3	3
Mass window (%)	20	125
Search window (%)	0	60
Integration window (%)	20	20
Samples per peak	25	20
Sample time (s)	1.5 (^{226}Ra); 1.0 (^{205}Tl)	0.5

APPENDIX 3: Composition and calculated speciation of experimental solutions

Table S3: Compositions of donor and acceptor solutions at t=0

	Tl isotherms	Ra Isotherms
Donor	Tl^+, K^+, NO_3^-, Humic Acids, Na^+(after basic pH)	Ra^{2+}, Ca^{2+}, K^+, NO_3^-, Humic Acids, Na^+(after basic pH)
Acceptor	K^+, NO_3^-	Ca^{2+}, K^+, NO_3^-

Table S4: Tl or Ra species in acceptor. Modeled with CHESS 2.0. Only specie with more than 1% of total concentrations are presented here. Saturations indices showed no precipitation during experiments. K_{OH} for Ra^{2+} were from annex 1. Additional constants came from Casiot *et al.* (Casiot *et al.*, 2011[8]) for Tl and from Porcelli *et al.* (Porcelli *et al.*, 2014[9]) for Ra

Element	Total concentration ($mol.L^{-1}$)	Species	Abundance in % of total						
			pH = 3	pH = 4	pH = 5	pH = 6	pH = 7	pH = 8	pH = 9
Thallium	$2.\ 10^{-10}$	Tl^+	100	100	100	100	100	100	99.99
	$2.\ 10^{-6}$	Tl^+	100	100	100	100	100	100	99.99
Radium	$1.\ 10^{-13}$	Ra^{2+}	100	100	100	100	100	100	100

[8]Casiot, C., Egal, M., Bruneel, O., Verma, N., Parmentier M., Elbaz-Poulichet, F. (2011). Predominance of Aqueous Tl(I) Species in the River System Downstream from the Abandoned Carnoulès Mine (Southern France). *Environmental Science & Technology*, *45*(1), 2056–2064. dx.doi.org/10.1021/es102064r |

[9]Porcelli, D., Kim, C. K., Martin, P., Moore, W. S., Phaneu, M. (2014). Properties of Radium. In *The Environmental Behaviour of Radium: Revised Edition*, 6–32. IAEA, Vienna

APPENDIX 4: Experimental data

Table S5: Experimental data acquired for Tl(I) and used for calculations

$[Tl]_{donor, eq}$ ($mol.L^{-1}$)	$[Tl]_{acceptor, eq}$ ($mol.L^{-1}$)	$[Tl]_{free,don, eq}$ ($mol.L^{-1}$)	$[Tl]_{complexed}$ ($mol.kg^{-1}$)	$log[Tl]_{free}$ ($mol.L^{-1}$)	$log[Tl]_{complexed}$ ($mol.kg^{-1}$)	T_{avg} (°C)	pH
2.24E-11	1.67E-11	1.210E-11	6.84E-08	-10.92	-7.17	24.4	7.39
2.24E-11	1.68E-11	1.16E-11	7.17E-08	-10.94	-7.14	24.4	7.39
2.11E-10	3.08E-10	1.27E-10	5.59E-07	-9.90	-6.25	23.5	7.40
1.73E-09	2.59E-09	1.47E-09	1.74E-06	-8.83	-5.76	24.2	7.35
1.73E-09	2.57E-09	1.46E-09	1.81E-06	-8.84	-5.74	24.2	7.35
2.03E-07	2.78E-07	1.72E-07	2.05E-04	-6.76	-3.69	23.1	7.31
2.03E-07	2.76E-07	1.67E-07	2.39E-04	-6.78	-3.62	23.1	7.31
1.82E-06	2.79E-06	1.60E-06	1.43E-03	-5.79	-2.84	23.4	7.31
1.82E-06	2.62E-06	1.43E-06	2.57E-03	-5.84	-2.59	23.4	7.31
1.71E-10	1.81E-10	1.73E-10	0.00	-9.76	-	20.9	3.98
1.71E-10	1.84E-10	1.75E-10	0.00	-9.76	-	20.9	3.98
1.57E-10	1.57E-10	1.69E-10	0.00	-9.77	-	21.6	4.87
1.57E-10	1.55E-10	1.65E-10	0.00	-9.78	-	21.6	4.87
1.45E-10	1.39E-10	1.43E-10	1.88E-08	-9.85	-7.73	22.3	5.78
1.48E-10	1.28E-10	1.33E-10	9.49E-08	-9.88	-7.02	20.9	6.77
1.48E-10	1.29E-10	1.34E-10	8.93E-08	-9.87	-7.05	20.9	6.77
1.74E-10	1.22E-10	1.38E-10	2.38E-07	-9.86	-6.62	22.5	7.75
1.34E-10	1.13E-10	1.04E-10	1.96E-07	-9.98	-6.71	22.0	7.89
3.17E-11	2.89E-11	2.84E-11	2.16E-08	-10.55	-7.67	22.3	7.5
3.17E-11	2.75E-11	2.78E-11	2.60E-08	-10.56	-7.59	22.3	7.5

Table S6: Experimental data acquired for Ra(II) and used for calculations

$[Ra]_{donor,eq}$ ($mol.L^{-1}$)	$[Ra]_{acceptor, eq}$ ($mol.L^{-1}$)	$[Ra]_{free,donor,eq}$ ($mol.L^{-1}$)	$[Ra]_{complexed}$ ($mol.kg^{-1}$)	$log[Ra]_{free}$ ($mol.L^{-1}$)	$log[Ra]_{complexed}$ (mol/L)	T_{avg} (°C)	pH
3.03E-13	2.60E-13	2.61E-13	8.30E-10	-12.58	-13.38	21.5	3.94
2.72E-13	2.08E-13	2.13E-13	1.19E-09	-12.67	-13.23	20.8	4.63
2.10E-13	1.55E-13	1.46E-13	1.28E-09	-12.83	-13.19	21.8	6.42
1.61E-13	1.06E-13	1.11E-13	1.01E-09	-12.96	-13.30	21.8	7.02
4.54E-13	3.02E-13	3.00E-13	3.07E-09	-12.52	-12.81	22.2	7.59

APPENDIX 5: Estimation of experimental errors and *RMSE* calculations

Uncertainties reported in this section have only been calculated from the propagation of known measurements or lab errors following the same approach as Reinoso-Maset *et al*[10]. These didn't take into account the humic acid variabilities. Experimental errors were hence calculated for each experimental point following the propagation errors theory. The variance of a G function of different x_i variable can be calculated from the variances of the variables x_i using the following expression:

$$\sigma_G^2 = \sum_{i=1}^{n} \left(\frac{\partial G}{\partial x_i}\right)^2 \sigma_i^2 + 2 \sum_i \sum_j \frac{\partial G}{\partial x_i} \frac{\partial G}{\partial x_j} \sigma_{ij} \qquad \text{(A1)}$$

where $(\delta G/\delta x_i)$ is the partial derivative of G with respect to x_i, σ^2 is the variance of xi and σ_{ij} the covariance of the x_i and x_j variables. If these variables are independents, the covariance term is then equal to zero.

Root Mean Square Error (*RMSE*, equations 4) was calculated to assess the gap between experimental and modelled values for each series.

$$RMSE = \sqrt{\frac{1}{n} \sum_{i=1}^{n} \left(\log[\mathrm{Me}^{z+}]_{i,\mathrm{measured}} - \log[\mathrm{Me}^{z+}]_{i,\mathrm{modelled}}\right)^2} \qquad \text{(A2)}$$

[10] Reinoso-Maset, E., Ly, J. (2014). Study of major ions sorption equilibria to characterize the ion exchange properties of kaolinite. *Journal of Chemical and Engineering Data*, *59*(12), 4000–4009. http://doi.org/10.1021/je5005438

APPENDIX 6: Calculations of hydrolysis constants for Tl^+ and Ra^{2+}

The following reactions are used for calculation of Tl^+ and Ra^{2+} hydrolysis constants (KOH):

$$Tl^+ + OH^- \leftrightarrow TlOH^0 \qquad (A3)$$

$$Ra^{2+} + OH^- \leftrightarrow RaOH^+ \qquad (A4)$$

Equation A1 is used to determine the equilibrium constant from the hydrolysis reaction. The Gibbs free energy for the reaction ($\Delta_R G^0$ in kJ.mol^{-1}) is adjusted with the standard enthalpy for formation ($\Delta G^0_{f...}$ en kJ.mol^{-1}, equation A2). All values are from Brown and Ekberg's book (Brown and Ekberg 2016[11]). Then, equilibrium constants are used to calculate hydrolysis constants as in equation A3. All results are summarized in table S1.

$$\ln K = -\frac{\Delta_R G^0}{RT} \qquad (A5)$$

$$\Delta_R G^0 = \Delta G^0_{f\,MOH^{n-1}} - \Delta G^0_{f\,M^{n+}} - \Delta G^0_{f\,OH^-} \qquad (A6)$$

$$\log K_{OH} = \log K - \log K_e \qquad (A7)$$

Table S7: Thermodynamic properties used for K_{OH} calculation. $\Delta G^0_{f\,OH^-}$ = -157,3 k.mol^{-1} and logK_e = 14.0. T = 298.15 K. R = 8.314472 J.K^{-1}.mol^{-1}.

	$\Delta_R G^0$ (kJ.mol^{-1})	$\Delta G^0_{f\,MOH^{n-1}}$ (kJ.mol^{-1})	$\Delta G^0_{f\,M^{n+}}$ (kJ.mol^{-1})	K	K_{OH}
Ra^{2+}	-2,4	-721,7	-561,5	$10^{0,500}$	$10^{-13,49}$
Tl^+	-3,6	-193,3	-32,4	$10^{0,631}$	$10^{-13,37}$

[11]Brown, P. L., Ekberg, C. (2016). Hydrolysis of Metal Ions. *Wiley VCM*, p217-218 & p825

APPENDIX 7: Parameters for NICA-Donnan modelling

Table S8: Parameters used during modeling for ion specific binding. K^+, Tl^+, Ag^+ and Ra^{2+} are estimated parameters (in italic) according to Milne et al. (Milne et al., 2003[12]). Tl^+, Ag^+ and Ra^{2+} were adjusted during modelling. H^+ parameters are specific to the purified humic acids used in experiments. So no adjustment were made. Ca^{2+} is already adjusted from previous study (Milne *et al.*, 2003[13]). K^+ remains estimated.

	$\log\widetilde{K}_{i,1}$,	$log\widetilde{K}_{i,2}$,	$n_{i,1}$	$n_{i,2}$	K_{OH}	References
H^+	3.65	8.07	0.84	0.65	-	Botero *et al.*,submitted
Tl^+	*-0.78*	*-0.55*	*0.88*	*0.67*	*$10^{-13.37}$*	This study
K^+	*-1.26*	*-1.14*	*0.94*	*0.72*	*$10^{-14.50}$*	This study
Ag^+	*-0.67*	*0.07*	*0.80*	*0.61*	*$10^{-12.04}$*	This study
Ra^{2+}	*-1.04*	*-0.61*	*0.88*	*0.68*	*$10^{-13.49}$*	This study
Ca^{2+}	-1.37	-0.43	0.78	0.75	$10^{-12.85}$	Milne *et al.*, 2003

Table S9: Purified humic acids specific parameters used during modelling (Botero *et al.*, submitted[14]).

A	β	$Q_{max,1}$ (mol.kg^{-1})	$Q_{max,2}$ (mol.kg^{-1})	p_1	p_2
0.60	-0.27	3.18	3.02	0.79	0.44

[12]Milne, C. J., Kinniburgh, D. G., van Riemsdijk, W. H., & Tipping, E. (2003). Generic NICA-Donnan Model Parameters for Metal-Ion Binding by Humic Substances. *Environmental Science & Technology*, *37*(5), 958–971. http://doi.org/10.1021/es0258879

[13]Op.cit.

[14]Botero, W. G., Pineau, M., Janot, N., Domingos, R., Mariano, J., Rocha, L. S., Groenenberg, J. E., Benedetti, M. F., & Pinheiro, J. P. Binding behavior of trace metals with a peat soil humic acid: effect of the HF/HCl isolation treatment. *Submitted*.

APPENDIX 8: Figures for thallium and radium complexation with humic acids

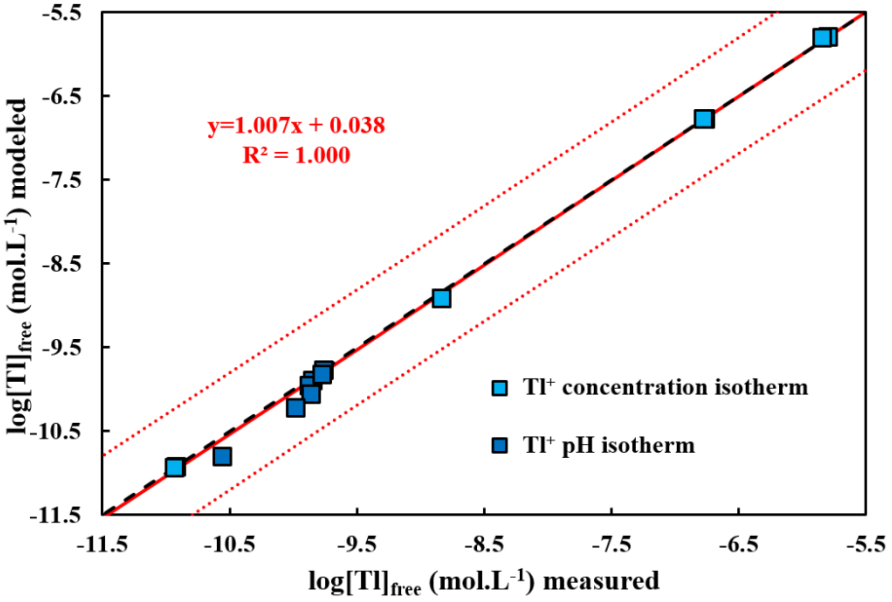

Figure S10: Measured vs. modeled for free thallium. Red line is the regression line from concentration isotherm (n=9). Dashed red lines correspond to the confidence area of the regression. The dashed black line is the one to one line. Error bars are ± 2σ.

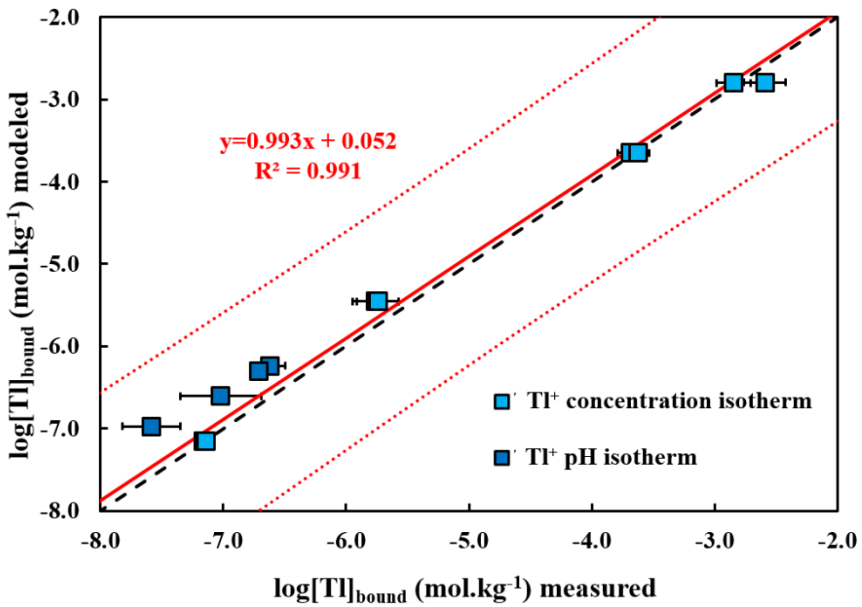

Figure S11: Measured vs. modeled for bound thallium. Red line is the regression line from concentration isotherm (n=9). Dashed red lines correspond to the confidence area of the regression. The dashed black line is the one to one line. Error bars are ± 2σ.

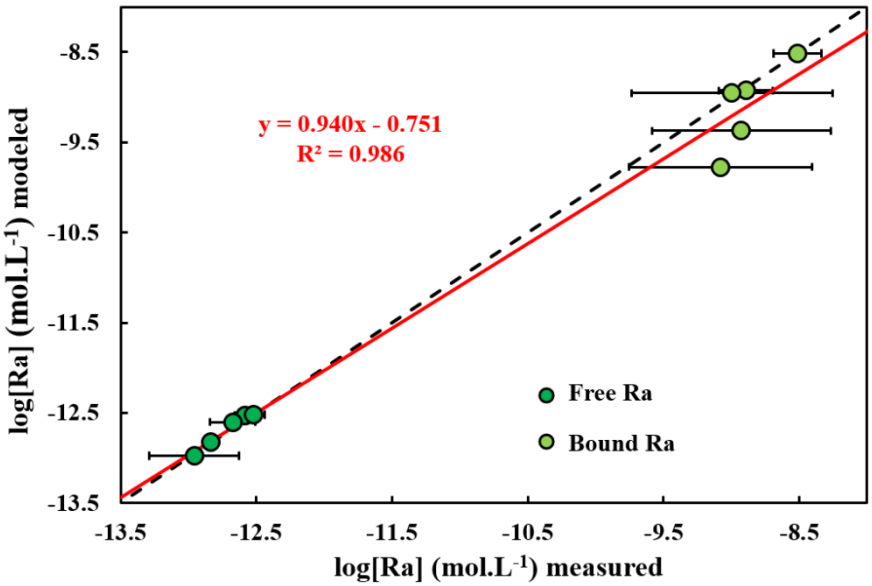

Figure S12: Measured vs. modeled for radium. Red line is the regression line for all values (n=10). Confidence area is out of the window graph. The dashed black line is the one to one line. Error bars are ± 2σ

APPENDIX 9: Silver complexation with humic acids

Table S13: Parameters used during modeling with ECOSAT software for experimental data of silver complexation to three humic acids from Sikora *et al*. (1988[15]). In all simulations, pH=6.5, background electrolyte was KNO_3 0.1 mol.L^{-1} and HA concentration was 0.5 g.L^{-1}. Values in bold and italic are those that were adjusted. $m_i = n_i p_i$ (Benedetti *et al.*, 1995[16])

	HA1	HA3	HA8
B	0.49	0.49	0.49
$Q_{max1, H}$	4.43 (from Sikora *et al.*, 1988)	3.95 (from Sikora *et al.*, 1988)	3.95
p_1	0.62	***0.79***	0.62
$\log \widetilde{K}_{H,1}$	3.00	3.00	3.00
$n_{H,1}$	0.81	0.81	0.81
$Q_{max2, H}$	3.30	3.30	3.30
p_2	0.41	0.41	0.41
$\log \widetilde{K}_{H,2}$	7.00	***7.53***	***7.19***
$n_{H,2}$	0.63	0.63	0.63
$\log \widetilde{K}_{K,1}$	-1.26	-1.26	-1.26
$n_{K,1}$	0.94	0.94	0.94
$\log \widetilde{K}_{K,2}$	-1.14	-1.14	-1.14
$n_{K,2}$	0.72	0.72	0.72
$\log \widetilde{K}_{Ag,1}$	***-0.13***	-0.13	-0.13
$n_{Ag,1}$	***0.59***	0.59	0.59
$\log \widetilde{K}_{Ag,2}$	***4.76***	4.76	4.76
$n_{Ag,2}$	***0.71***	0.71	0.71
m_1	0.50	0.64	0.50
m_2	0.26	0.26	0.26

[15]Sikora, F. J., Stevenson, F. J. (1988). Silver Complexation by Humic Substances : Conditional Stability Constants and Nature of Reactive Sites. *Geoderma, 42*, 353–363.

[16]Benedetti, M. F., Milne, C. J., & Kinniburgh, D. G. (1995). Metal ion binding to humic substances: application of the non-ideal competitive adsorption model. *Environmental Science & Technology*, *29*(2), 446–457. http://doi.org/10.1021/es00002a022

APPENDIX 10: Comparison with data from Liu *et al.* 2011[17]

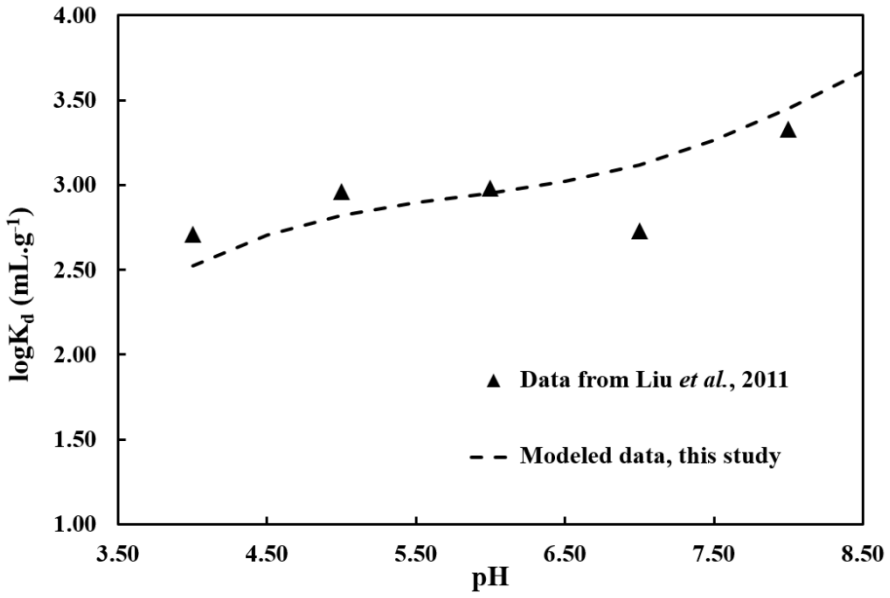

Figure S14: Sorption of Tl(I) onto humic acids. Black triangles are Liu et al. (2011[18]) data and describe sorption of Tl(I] onto a purified humic acids (GZHA, Liu et al., 2010[19] and 2011[20]). Dashed line is modeled data with NICA-Donnan and ECOSAT. Ion specific parameters used for Tl are these presented in this study (table1). Details of humic acid parameters used during modelling are in table S20.

Table S15: GZHA parameters, $Q_{max1,H}$ and $Q_{max2,H}$ are Liu *et al.* (2010[21]). The rest of the parameters are in the same range of Milne et al. (2001[22]) work and are adjusted to fit Liu's data.

m_1	m_2	$n_{1,H}$	$n_{2,H}$	$\log \tilde{K}_{H,1}$	$\log \tilde{K}_{H,2}$	$Q_{max,1}$ (mol.kg^{-1})	$Q_{max,2}$ (mol.kg^{-1})	p_1	p_2
0.42	0.26	0.81	0.63	2.1	8.6	3.18	3.02	0.52	0.41

[17]Liu, J., Lippold, H., Wang, J., Lippmann-Pipke, J., & Chen, Y. (2011). Sorption of thallium(I) onto geological materials: Influence of pH and humic matter. *Chemosphere*, *82*(6), 866–871. http://doi.org/10.1016/j.chemosphere.2010.10.089
[18]Op.cit.
[19]Liu, J., Wang, J., Chen, Y., Lippold, H., & Lippmann-Pipke, J. (2010). Comparative characterization of two natural humic acids in the Pearl River Basin, China and their environmental implications. *Journal of Environmental Sciences*, *22*(11), 1695–1702. http://doi.org/10.1016/S1001-0742(09)60308-9
[20]Op.cit.
[21]Op.cit.
[22]Op.cit.

APPENDIX 11: Constants and associated references used in this paper

Table S16: Table of constant used in Tl speciation modelling with ECOSAT

Reaction	log*K* (298.15 K)	Reference
$Tl^+ + OH^- \leftrightarrow TlOH$	0.63	This study
$Tl^+ + SO_4^{2-} \leftrightarrow TlSO_4^-$	1.37	[19]
$Tl^+ + Cl^- \leftrightarrow TlCl(aq)$	0.51	[19]
$Tl^+ + 2Cl^- \leftrightarrow TlCl_2^-$	0.28	[19]
$Tl^+ + CO_3^{2-} \leftrightarrow TlCO_3^-$	2.16	[19]
$Tl^+ + 2CO_3^{2-} \leftrightarrow Tl(CO_3)_2^{3-}$	0.11	[19]
$Tl^+ + HCO_3^- \leftrightarrow TlHCO_3$	0.90	[19]
$Tl^+ + HPO_4^{2-} \leftrightarrow TlHPO_4^-$	1.27	[17]
$Tl^+ + PO_4^{3-} \leftrightarrow TlPO_4^{2-}$	3.54	[18]
$Tl^+ + F^- \leftrightarrow TlF$	0.10	[18]
$Tl^+ + Cit^{3-} \leftrightarrow TlCit^{2-}$	2.00	[23]
$Tl^+ + Ox^{2-} \leftrightarrow TlOx^-$	1.39	[17]
$Tl^+ + Ac^- \leftrightarrow TlAc^0$	-0.11	[18]
$Tl^+ + 2SO_4^{2-} + 3Fe^{3+} + 6OH \leftrightarrow TlFe_3(SO_4)_2(OH)_6(s)$	3.36	[24*]
$Tl^+ + 2SO_4^{2-} + 3Al^{3+} + 24H^+ \leftrightarrow TlAl(SO_4)_2{\cdot}12H_2(s)$	7.46	[18*]
$Tl^+ + OH^- \leftrightarrow TlOH(s)$	1.08	[18*]
$Tl^+ + Cl^- \leftrightarrow TlCl(s)$	-3.65	[17*]
$2Tl^+ + CO_3^{2-} \leftrightarrow Tl_2CO_3(s)$	3.84	[25]
$2Tl^+ + SO_4^{2-} \leftrightarrow Tl_2SO_4(s)$	3.79	[19]
$Tl^+ + NO_3^- \leftrightarrow TlNO_3(s)$	1.06	[17*]
*Calculated from Gibbs free energy of formation		

Table S17: Table of constant used in Ra speciation modelling with ECOSAT

Reaction	log*K* (298.15 K)	Reference
$Ra^{2+} + OH^- \leftrightarrow RaOH^+$	0.51	This study
$Ra^{2+} + SO_4^{2-} \leftrightarrow RaSO_4(aq)$	2.75	[20]
$Ra^{2+} + Cl^- \leftrightarrow RaCl^+$	-0.10	[20]
$Ra^{2+} + Cit^{3-} \leftrightarrow RaCit^-$	2.36	[26]
$Ra^{2+} + Ox^{2-} \leftrightarrow RaOx$	1.20	[20]
$Ra^{2+} + Ac^- \leftrightarrow RaAc^+$	0.00	[2à]

[23]Xiong, Y. (2009). The aqueous geochemistry of thallium : speciation and solubility of thallium in low temperature systems, 441–451. http://doi.org/10.1071/EN08086

[24]Xiong, Y. (2007). Hydrothermal thallium mineralization up to 300 ° C : A thermodynamic approach, *32*, 291–313. http://doi.org/10.1016/j.oregeorev.2006.10.003

[25]Corine Casiot. (2012). Predominance of Aqueous Tl(I) Species in the River System Downstream from the Abandoned Carnoul è s Mine (Southern France) ", (I), 2475–2476.

[26]Porcelli, D., Kim, C. K., Martin, P., Moore, W. S., Phaneu, M. (2014). Properties of Radium. In *The Environmental Behaviour of Radium: Revised Edition*, 6–32. IAEA, Vienna

APPENDIX 12: Modelling with soil solutions

Table S18: Calculated dissolved thallium (I) speciation in soil solution with ECOSAT. Compositions of solutions and soils characteristics are in Kinniburgh *et al*. (1983[27]). DOM (Dissolved organic matter) is composed of 29.3% of humic substances, 66.2% of hydrophilic acids and 4.5% is considered non-reactive according to average from Ren *et al*. (2015[28]) and Groenenberg *et al*. (2010[29]). Humic substances are simplified as only humic acids and hydrophilic acids are simplified (one third for each) as combination of citric acid (Cit), oxalic acid (Ox) and acetic acid (Ac). Tl minerals taken in consideration are lanmuchangite, dorallcharite, TlCl(s), $TlNO_3$(s) and Tl_2SO_4(s). No precipitation occurred. Only species with more than 1% are presented. Tl-Cit^{2-}, Tl-Ox^{-}, Tl-Ac, TlCl(aq), TlOH and $TlSO_4^{-}$ are negligeable. Constants (minerals and dissolved complexes) used in calculation are summarized in table S16.

Soil	pH	HA ($mg.L^{-1}$)	[Tl]total ($nmol.L^{-1}$)	Tl-HA (% Tl total)	Tl^{+} (% Tl total)
Icknield	7.8	27.0	$1.00 .10^{-2}$	25.5	74.2
			0.16	18.3	81.4
			1.26	14.0	85.6
			10.00	10.7	88.9
			158.49	7.4	92.2
			1258.90	5.6	94
Denchworth	7.0	32.8	$1.00 .10^{-2}$	12.4	86.9
			0.16	8.8	90.4
			1.26	6.8	92.5
			10.00	5.2	94
			158.49	3.7	95.5
			1258.90	2.9	96.4
Southampton	4.3	50.4	$1.00 .10^{-2}$	3.9	95.7
			0.16	2.9	96.6
			1.26	2.4	97.2
			10.00	1.9	97.6
			158.49	1.5	98.0
			1258.90	1.3	98.3

[27]Kinniburgh, D. G., & Miles, D. L. (1983). Extraction and chemical analysis of interstitial water from soils and rocks. *Environmental Science & Technology*, *17*(6), 362–368. http://doi.org/10.1021/es00112a011

[28]Ren, Z.-L., Tella, M., Bravin, M. N., Comans, R. N. J., Dai, J., Garnier, J.-M., … Benedetti, M. F. (2015). Effect of dissolved organic matter composition on metal speciation in soil solutions. *Chemical Geology*, *398*, 61–69. http://doi.org/10.1016/j.chemgeo.2015.01.020

[29]Groenenberg, J. E., Koopmans, G. F., & Comans, R. N. J. (2010). Uncertainty Analysis of the Nonideal Competitive Adsorption−Donnan Model: Effects of Dissolved Organic Matter Variability on Predicted Metal Speciation in Soil Solution. *Environmental Science & Technology*, *44*(4), 1340–1346. http://doi.org/10.1021/es902615w

Table S19: Calculated dissolved radium (II) speciation in soil solution with ECOSAT. Compositions of solutions and soils characteristics are in Kinniburgh *et al*. (1983[30]). DOM (Dissolved organic matter) is composed of 29.3% of humic substances, 66.2% of hydrophilic acids and 4.5% is considered non-reactive according to average from Ren *et al*. (2015[31]) and Groenenberg *et al*. (2010[32]). Humic substances are simplified as only humic acids and hydrophilic acids are simplified (one third for each) as combination of citric acid (Cit), oxalic acid (Ox) and acetic acid (Ac). Ra minerals taken in consideration are only co-precipitation with barite ($BaSO_4$, logK_s from ECOSAT database. No precipitation occurred. Only species with more than 1% are presented. Ra-Cit$^-$, Ra-Ox, Ra-Ac$^+$, RaCl$^+$, RaOH$^+$ are negligeable. Constants (minerals and dissolved complexes) used in calculation are summarized in table S17.

Soil	pH	HA ($mg.L^{-1}$)	[Ra]total ($fmol.L^{-1}$)	Ra-HA$^+$ (% Ra total)	Ra^{2+} (% Ra total)	$RaSO_4$(aq) (% Ra total)
Icknield	7.8	27.0	7.94	86.8	12.7	-
			15.85	84.5	15.0	-
			63.10	79.0	20.3	-
			125.89	75.7	23.4	-
			501.19	68.5	30.4	1.0
Denchworth	7.0	32.8	7.94	82.8	16.4	-
			15.85	80.0	19.1	-
			63.10	73.5	25.2	1.2
			125.89	69.9	28.7	1.4
			501.19	62.0	36.2	1.7
Southampton	4.3	50.4	7.94	71.1	28.0	-
			15.85	67.5	31.5	-
			63.10	59.9	38.9	1.2
			125.89	56.0	42.7	1.3
			501.19	48.3	50.2	1.5

[30]Op.cit.
[31]Op.cit.
[32]Op.cit.

Chapitre III: Thallium (Tl) Sorption onto Illite and Smectite - Implications for Tl Mobility in the Environment

Loïc A. Martin[a*], *Aubéry Wissocq*[b], *Marc. F. Benedetti*[a], *Chritelle Latrille*[b]

[a]Institut de Physique du Globe de Paris – USPC- UMRCNRS7154, Paris, France

[b]Den-Service d'étude du Comportement des Radionucléides (SECR), CEA, Université Paris-Saclay, F91191, Gif-sur-Yvette, France

* Corresponding author. IPGP, Equipe de Biogéochimie Environnementale, 1 rue Jussieu, 75238 Paris Cedex 05, France. *E-mail address*: martin@ipgp.fr *Tel*: +33 (0)1 83 95 74 39

Soumis dans Geochimica et Cosmochimica Acta

1. RESUME

Les argiles sont connues pour jouer un rôle important dans le transport et l'adsorption des éléments traces métalliques et l'illite a été spécifiquement identifiée comme une importante phase porteuse du thallium dans les sols. L'objectif ici est d'étudier la sorption du thallium, sous sa forme Tl(I), sur l'illite et la smectite. Des expériences en « batch » ont donc été menées dans plusieurs conditions de pH et de concentrations en thallium à force ionique constante (0,01 $mol.L^{-1}$). Na^+ et Ca^{2+} ont été utilisés comme cations de fond tandis que le thallium 204 a été utilisé comme radiotraceur. Les résultats montrent que l'illite est le minéral qui a le plus d'affinité pour le thallium par rapport à la smectite. Les coefficients de partage (K_d en $L.kg^{-1}$) varient entre $10^{2.75 \pm 0.17}$et $10^{4.0 \pm 0.17}$ dans les solutions de NaCl alors qu'ils varient entre $10^{2.25 \pm 0.17}$ and $10^{3.0 \pm 0.17}$ dans celles de $CaCl_2$. Pour la smectite, les K_d (in $L.kg^{-1}$) varient entre $10^{2.50 \pm 0.16}$ et $10^{3.20 \pm 0.16}$ et entre $10^{1.25 \pm 0.16}$ et $10^{1.95 \pm 0.16}$ dans les solutions de NaCl et $CaCl_2$ respectivement. La sorption a ensuite été décrite avec le model d'Echange d'Ion Multi-Site et des coefficients de sélectivité par rapport aux protons ont été calculés pour la première fois dans le cas du thallium. Dans tous les cas, indépendamment de la solution de fond, les sites de faibles capacités ont été identifiés comme les sites dominants pour la sorption du thallium, montrant ainsi l'affinité du thallium pour ces sites. De plus, ces interactions étant échangeables et réversibles, elles suggèrent que le thallium pourrait être remis en solution en cas de conditions d'équilibres changeantes. Le rôle des minéraux argileux dans le cycle environnemental du thallium est évident et l'illite est bien une phase porteuse majeur pour le thallium pouvant même entrer en compétition avec les oxydes de manganèse dans certains cas. Les phases porteuses du thallium peuvent être classées ainsi: MnO_2> illite> smectite ~ ferrihydrite ~> Al_2O_3 ~ goethite> SiO_2.

2. ABSTRACT

Clay minerals play a relevant role in the transport and trace trapping of elements and illite has been referred as an important Tl bearing phase in soils. However, mechanisms and affinity of thallium for clay minerals remain poorly known. This study aimed to investigate the sorption behavior of thallium as Tl(I) onto illite and smectite, two clay minerals occurred mainly in soils and sediments. Different sorption experiments were carried out under various pH conditions and Tl concentrations, in competition with sodium and calcium at a constant ionic strength of 0.01 $mol.L^{-1}$. Our results showed that illite displayed more affinity for thallium than smectite. With illite, the distribution coefficients (K_d in $L.kg^{-1}$) varied between $10^{2.75 \pm 0.17}$ and $10^{4.0 \pm 0.17}$ in Na solutions versus between $10^{2.25 \pm 0.17}$ and $10^{3.0 \pm 0.17}$ in Ca solutions, depending on pH. With smectite, K_d (in $L.kg^{-1}$) ranged between $10^{2.50 \pm 0.16}$ and $10^{3.20 \pm 0.16}$ and between $10^{1.25 \pm 0.16}$ and $10^{1.95 \pm 0.16}$ in Na and Ca solutions respectively. Sorption behavior was described with the Multi-Site Ion Exchanger model and selectivity coefficients in respect to protons were calculated for the first time. In all cases, independently of clay mineral and background electrolyte, low capacity but highly reactive sites were dominant in thallium uptake, highlighting Tl affinity for those sites. Moreover, the exchangeable and reversible interactions between Tl^+ and clays reactive sites suggested that in changing conditions, thallium could be released in solution. The role of clay minerals in thallium environmental cycle is evident and confirmed illite to be a dominant Tl bearing phases, in some environment competing with manganese oxides. Compared to others Tl bearing phases, clays are ranked as follow: MnO_2> illite> smectite ~ ferrihydrite ~> Al_2O_3 ~ goethite> SiO_2

3. INTRODUCTION

Thallium (Tl) is a heavy metal which can be highly toxic for mammals mainly due to the close behavior of Tl^+ compared to K^+ in biological processes (Rodríguez-Mercado and Altamirano-Lozano, 2013). It is recognized to be as toxic as lead, cadmium, mercury or arsenic (Rodríguez-Mercado and Altamirano-Lozano, 2013).

Thallium is a widely distributed trace element on earth with an average concentration of 0.49 ppm in the continental crust and 0.13 ppm in the oceanic crust (Peter and Viraraghavan, 2005). Thallium exhibits both chalcophile and lithophile behavior (McGoldrick *et al.*, 1979; Baker *et al.*, 2010; Biagioni *et al.*, 2013; Hettmann *et al.*, 2014; Prytulak *et al.*, 2017). Tl^+ has a large ionic radius (1.49 Å), similar to K^+, Rb^+ and Cs^+ (Shaw 1952). Classically, Tl substitutes for K^+ in biotite, K-feldspar and plagioclase from volcanic rocks and granite systems (Prytulak *et al.*, 2017). It occurs in two oxidation states, Tl(I) and Tl(III) (Vink, 1993; Kaplan and Mattigod, 1998) with Tl(I) the only specie issued from the mantle to the non-altered crust (Prytulak *et al.*, 2017). Tl(I) is the most dominant and thermodynamically stable specie in the sub-surface environment (Vink, 1993; Xiong, 2009; Casiot *et al.*, 2011). However, in some environments, mainly those affected by Tl contamination, Tl(III) is detected in various amounts (Lin *et al.*, 1999; Peacock *et al.*, 2012; Voegelin *et al.*, 2015; Campanella *et al.*, 2017).

Thallium has two main sources in sub-surface environments. The first one corresponds to the weathering of K-rich rocks (Vaněk *et al.*, 2009) and/or S-rich minerals and more rarely Tl-rich sulfides deposit (Kaplan and Mattigod, 1998; Xiao *et al.*, 2004; Voegelin *et al.*, 2015) and the second one corresponds to anthropogenic sources. Contaminations result from mining of ferrous and non-ferrous sulfide ores (Lis *et al.*, 2003; Casiot *et al.*, 2011; Karbowska *et al.*, 2016; Campanella *et al.*, 2017), from smelting activities, coal combustion and cement production (Cheam, 2001; Lis *et al.*, 2003; Vaněk *et al.*, 2013; Karbowska *et al.*, 2016) as well as effluents of industry which use thallium compounds (Bennett 2017).

Nielsen et al. (Nielsen *et al.*, 2005) reported an average concentration of thallium ca. $3.00 \pm 2.64.10^{-11}$ $mol.L^{-1}$ for sixteen rivers worldwide. However, in highly impacted area, in particular in acid mine drainage, concentration can reach ~$1.0\ 10^{-6}$ $mol.L^{-1}$ (Casiot *et al.*, 2011). In non-anthropogenic impacted soils formed from Tl-bearing bedrocks, Tl contents are widespread,

varying from around 1.5 ppm (Vaněk *et al.*, 2009) to 6000 ppm (Voegelin *et al.*, 2015). Those ranges largely depend on the geological background. Conversely, in anthropogenically impacted soils without Tl-bearing bedrocks, Tl concentrations range between 5 ppm and 124 ppm (Lis *et al.*, 2003; Xiao *et al.*, 2004; Vaněk *et al.*, 2013).

The dominant aqueous specie of thallium is Tl^+ (Vink 1993; Kaplan and Mattigod 1998; Xiong 2007; Casiot *et al.*, 2011). Indeed, thallium makes few complexes with anions (Kaplan and Mattigod 1998; Casiot *et al.*, 2011) except with Cl^- in seawater and therefore Tl remains mostly as a free and bioavailable ion in solution (Vink 1993; Jacobson *et al.*, 2005; Casiot *et al.*, 2011; Voegelin *et al.*, 2015). However, in the particulate and colloidal fractions in waters or in soils, thallium interacts with various bearing phases. Thallium has strong affinity for manganese oxides (Bidoglio *et al.*, 1993; Jacobson *et al.*, 2005; Liu *et al.*, 2011; Peacock *et al.*, 2012; Voegelin *et al.*, 2015) and Mn(IV)-oxides, such as birnessite, which are known to oxidize Tl(I) in Tl(III) resulting in Tl_2O_3 precipitation (Peacock *et al.*, 2012; Voegelin *et al.*, 2015). Iron oxy-hydroxides (Liu *et al.*, 2011; Cassiot *et al.*, 2011; Coup *et al.*, 2015) and aluminum oxides have medium affinity for thallium. They are mostly known to sorb Tl(I) (Bidoglio *et al.*, 1993; Casiot *et al.*, 2011; Coup *et al.*, 2015) though iron reduction might oxidize Tl(I) and stabilize the resulting Tl(III) (Karlsson *et al.*, 2006).

Few studies gained insight into relationships between Tl and clay minerals though Tl uptake by illite in soils (Jacobson *et al.*, 2005; Voegelin *et al.*, 2015) was highlighted. Moreover, due to its lithophile behavior and a close ionic radius, Tl^+ might substitute K^+ in secondary clay minerals (Shaw 1952; Prytulak *et al.*, 2017). In clay minerals, K^+ takes place as counter ion on the negative surface charges and is strongly linked to the structure in the interlayer space. Based on the chemical similarity between Tl^+ and K^+, chemical adsorption of Tl^+ on clay minerals is likely to have an impact on the Tl mobility in the environment and mainly in waters. Nevertheless, mechanisms and affinity of thallium for clays remain poorly known and further studies are needed (Voegelin *et al.*, 2015). Consequently, in this study we have chosen to study thallium sorption onto two major clay minerals, illite and smectite, present in soils and river sediments. The purpose has been, (1) to assess the clay mineral exchange properties that drive the uptake on those surfaces and, (2) to evidence the affinity of Tl for the minerals. In order to be close to environmental conditions, Ca and Na bulk solutions at 10^{-2} $mol.L^{-1}$ were chosen for batch

experiments. Radioactive ^{204}Tl was used as radiotracer to minimize the measurement uncertainty. Then, sorption and its reversibility were tested over a large pH range and Tl concentrations. Finally, a multi-site ion exchanger model has been used to describe experimental data and the impact on Tl cycle in the sub-surface environment has been discussed.

4. EXPERIMENTAL

4.1. Thallium species and isotopes in batch solutions

As mentioned in introduction, Tl(I) dominates thallium speciation in the environment (Vink, 1993; Kaplan and Mattigod, 1998). Figure 1 shows Tl speciation in aqueous systems containing 10 mM $CaCl_2$ (Fig. 1A and 1B) or 10 mM NaCl (Fig. 1C and 1D). In those systems, similar to those of batch experiments (see below), Tl^+ is likely the most stable specie under those conditions (fig. 1). At low pH and high Eh, Tl^{3+} is stable under aqueous $TlCl_3$ (in NaCl) or $TlCl_4^-$ (in $CaCl_2$). At high pH, Tl^+ is hydrolyzed (TlOH) as is Tl^{3+} at higher Eh values forming $TlOH_3$ and $TlOH_4^-$ aqueous complexes (Fig. 1). Thallium concentrations seem to have no effect on its speciation in those cases (Fig. 1A, 1B, 1C and 1D).

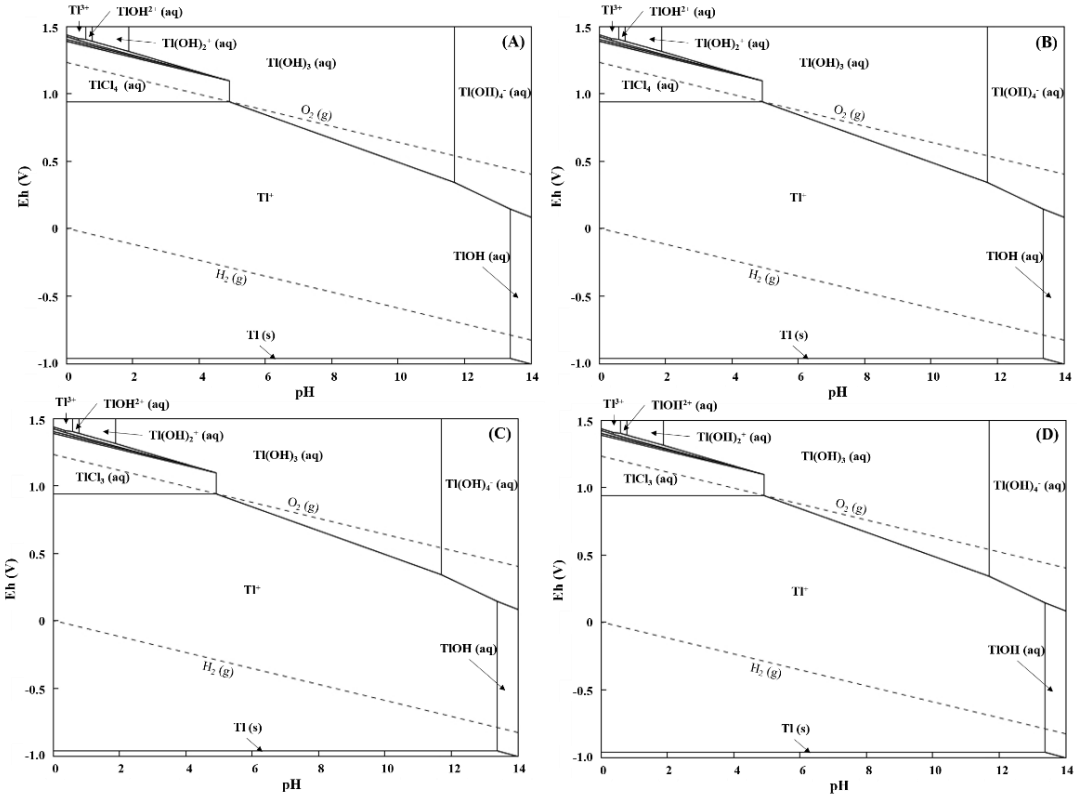

Figure 1: Eh-pH diagrams for thallium. A Tl-Ca-Cl-H_2O system is described for A and B with [$CaCl_2$] = 10 mM. In A, [Tl] = 100 nM and in B, [Tl] = 0.1 nM. C and D describe a Tl-Na-Cl-H_2O system with [NaCl] = 10 mM and [Tl] = 100 nM for C and 0.1 nM forD. Tl constants database is from Casiot *et al*. (2011) except for TlOH(aq) which is calculated from Brown and Ekberg's book (2016). Diagrams are made with JChess v2.0.

During experiments (pH 3 to 11), redox potentials (Eh in V) were measured with a Pt electrode (Metrohm) on random samples. Average value (at T = 20.1 °C) was 195.7 ± 4.3 mV (n = 3). This condition placed in Tl diagrams (fig. 1) confirms that Tl(I) would be the main specie of thallium. Moreover, Tl speciation function of pH (fig. 2A, 2B, 2C and 2D) give Tl^+ as the only Tl(I) specie in solution for batch experiments.

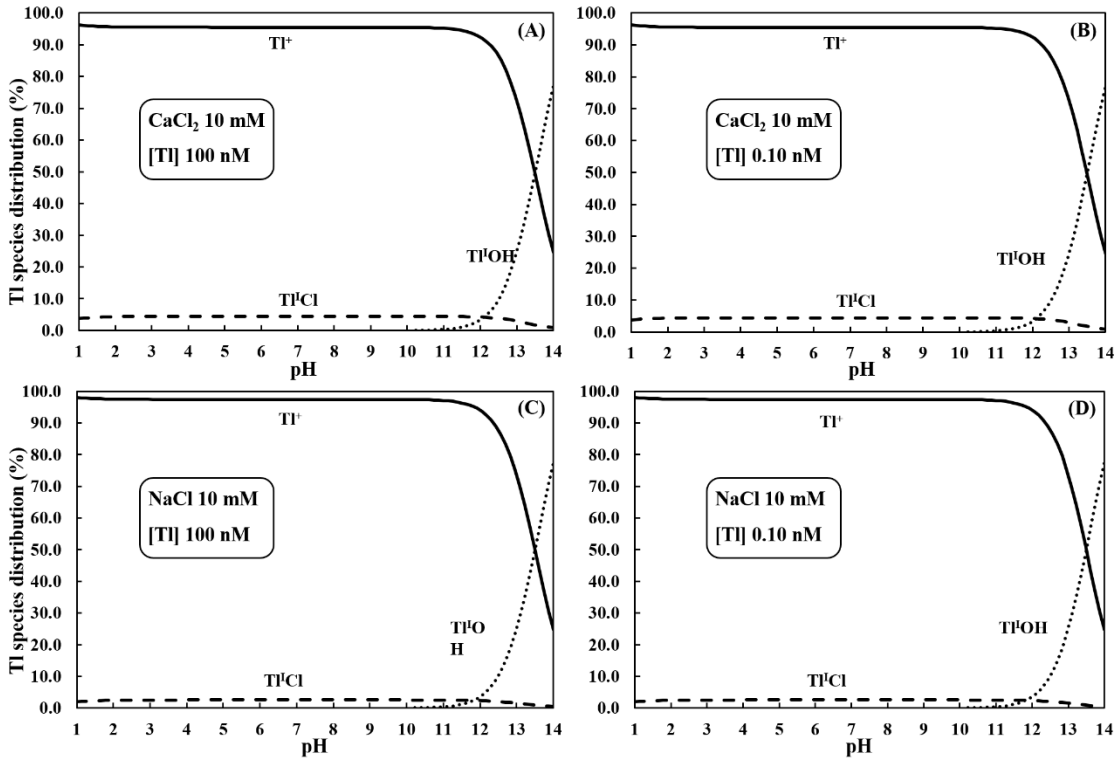

Figure 2: Thallium aqueous speciation at Eh = + 0.2 V. A and B are in [$CaCl_2$] = 10 mM whereas C and D are in NaCl 10 mM. Tl(I) is the only species calculated in solution. Species < 1% of total species are not represented and no precipitation of TlOH(s), TlCl(s) or $TlCl_2$(s) occurred. Database of Tl constant in Casiot *et al*. (2011) except for TlOH(aq) calculated from Brown and Ekberg's book (Brown and Ekberg 2016). Diagrams made with JChess v2.0.

Radioactive and stable Tl solutions were used in this study. Tl occurs in the environment only with two stable isotopes, ^{203}Tl (29.5%) and ^{205}Tl (70.5%) (Rehkämper and Nielsen, 2004). The radioisotope ^{204}Tl, used here as radiotracer, does not exist naturally but only after neutron activation of stable thallium. Its half-life is 3.78 years. Therefore, a ^{204}Tl solution of 4.90 MBq in 1M HCl (Eckert & Ziegler®, source # 1876-98, 07/01/16; initial Tl concentration of 2.80 $.10^{-7}$ mol.L^{-1}) was used. Two daughter solutions were made with 1mL of parent solution diluted in 10mL of ultrapure water (milli Q 18.2 MΩ.cm^{-2}, Millipore®). They were composed of ~ 0.1M HCl (dilution factor of 9.80 for solution 1 and 9.92 for solution 2) for an initial activity of 1.01MBq ([Tl] = 3.19 $.10^{-8}$ mol.L^{-1}) and 0.99 MBq ([Tl] = 3.14 $.10^{-8}$ mol.L^{-1}), respectively. The solution of stable thallium was made by dissolving a Tl(I)Cl salt (99.999%, Sigma Aldrich®) and acidified with diluted ultrapure HNO_3. Thallium concentration was confirmed at 4.76 ± 0.08 10^{-4} mol.L^{-1} by HR-ICP-MS Element 2 (Thermo Scientific®) measurements.

4.2. Reagents

Every salt solution and then every dilution were made with ultrapure water (milli-Q, 18.2 $M\Omega.cm^{-2}$, Millipore®). Salts of NaCl (VWR Chemical), $CaCl_2$ (VWR Chemical), NaOH (VWR Chemical) and $Ca(OH)_2$ (VWR Chemical) were used. Acidification was done with ultrapure nitric acid (ULTREX Ultrapure Reagent, J.T. Baker), diluted at appropriate concentrations when needed. Ultima Gold™ (Perkin Elmer®) as scintillant was used. Blanks of every solution were analyzed for Tl at HR-ICP-MS Element 2 and no thallium was detected.

4.3. Materials and conditioning process

The clay materials selected for this study are Illite du Puy and a Wyoming smectite. The latter is the montmorillonite extracted from the MX80 bentonite and similar to those previously extensively studied (Baeyens and Bradbury 1997; Bradbury and Baeyens 2002, Karnland, 2010). Synthesis of the MX80 bulk mineralogical composition, based on X-ray diffraction analyses, revealed around 83.5% montmorillonite, 0.7% illite, 1.1% gypsum, 2.5% muscovite, 4.7% plagioclase, 0.9% pyrite, 2.8% quartz and 3.1% tridymite (Karnland, 2010). Illite du Puy was extracted from the Oligocene geological formation located in the region of Le Puy-en-Velay (Haute-Loire, France). Its raw mineralogical composition contains illite with impurities such as kaolinite, carbonates, quartz and feldspars (Gabis, 1958; Van Olphen and Fripiat, 1979; Poinssot et al., 1999).

Natural illite and smectite were initially purified and conditioned to the homo-ionic Na- and Ca-forms. Raw Illite du Puy and MX80 were finely crushed and suspended in ultrapure water for one night and sieved at 25 µm. Both < 25µm suspensions were centrifuged. Then, illite du Puy was decarbonized with HCl 10% (weight, Merck) and heated to remove calcite and dolomite. Illite and smectite were dispersed three times each during 24h in a 1 M solution of NaCl or $CaCl_2$. Following this step, they were washed in NaOH or in $Ca(OH)_2$ solutions at pH~8 overnight. Then, they were rinsed in ultrapure water (milli-Q, Millipore®) again for 24h before suspension in NaCl or $CaCl_2$ 10^{-2} M for another 24h. Finally, conditioned illite and smectite were dispersed in ethanol overnight, dried and crushed. Between each step, illite was centrifuged at 10596 *g* for 30 minutes and smectite at 16556 *g* for 45 minutes.

XRD analyses were performed to check the purity of the final material and confirmed that < 25µm Ca- and Na-smectite contained pure montmorillonite with tridymite in trace and Ca- and Na-illite, mainly illite and significant kaolinite and quartz. Whatever the significant impurities of kaolinite and quartz, their sorption properties are very low compared to illite and consequently are neglected. Cation exchange capacity (CEC) was measured by K/Cs exchange at pH8, firstly conditioned materials were saturated with K (1M KCl) and secondly K was exchanged with Cs. Then, for smectite the value was 0.896 ± 0.040 $eq.kg^{-1}$ whereas it was 0.268 ± 0.014 $eq.kg^{-1}$ for illite.

At neutral pH (~7) in bulk solution, blanks of thallium released (in duplicates) by materials were performed and the bulk solution was analyzed with HR-ICP-MS Element 2 (Thermo Scientific®) after six days. The Tl content in material was 2.50 ± 2.11 $.10^{-8}$ $mol.kg^{-1}$ in Na-smectite, 8.62 ± 0.34 $.10^{-9}$ $mol.kg^{-1}$ in Ca-smectite, 1.06 ± 1.03 $.10^{-10}$ $mol.kg^{-1}$ in Na-illite and 1.52 ± 0.08 $.10^{-9}$ $mol.kg^{-1}$ in Ca-illite. Total thallium concentrations measured in the supernatant during batch experiments were therefore corrected according to the latest values.

4.4. ^{204}Tl measurement by liquid scintillation

The β emission of ^{204}Tl radioisotope was used to measure ^{204}Tl activity in every sample by liquid scintillation counting. Thus, 1mL of solution was sampled and displayed in 4 mL of UltimaGold™ scintillant. The scintillation counter used was a PACKARD Tricarb 2700. Before experiments, the source solution was measured three times with this protocol. The measured activity was compared to the expected activity and a yield of 97% was calculated. Then, each measured activity during experiments was corrected with the latest yield.

4.5. Stable thallium measurement

Solutions with only stable isotopes were analyzed by using an HR-ICP-MS Element 2 (Thermo Scientific®) in a clean room at mass 205 in low resolution. A solution of ^{115}In 5ppb served as an internal standard. Dilutions of samples, when needed, as well as standard preparations were made with distilled nitric acid. Final solutions were in a matrix of 1.0 to 1.5 % (weight) of HNO_3. Calibration standards were diluted from a thallium ICP standard solution (TraceCERT®, Sigma Aldrich®) Certified solutions TM23.4 (Environment Canada) validated Tl

analysis and calibration. The limit of detection was 7.5 $.10^{-13}$ $mol.L^{-1}$ and limit of quantification was 2.5 $.10^{-12}$ $mol.L^{-1}$.

4.6. Sorption isotherms

The effects of concentrations and pH on sorption were investigated by sorption isotherms and conducted for each matrix, Na-illite, Ca-illite, Na-smectite and Ca-smectite. At each step, batches were weighted in order to precisely calculate each solution component's concentration.

Firstly, 100 mg of solid material was dispersed in 5mL of bulk solution at 10 mM ($CaCl_2$ or NaCl) in a 10 mL ultracentrifuge tube in Nalgene (Oak Ridge Centrifuge Tube, Thermo Scientific). Tubes were sequentially weighted in order to maintain a constant mass over volume ratio in each batch. Then, acidic pHs were adjusted with 50µL of HNO_3 diluted at needed concentrations to introduce the proper amount of protons for every targeted pH, taking into account the additional protons coming from Tl solutions and radiotracer solution. Basic pHs were adjusted with 50 to 200 µL of NaOH 0.1M solution for Na matrices while 120 to 1500 µL of $Ca(OH)_2$ 0.01M solution were used in Ca matrixes. This solution was previously bubbled with N_2 gas to avoid carbonate precipitation into the batches.

In order to optimize the measurement uncertainty of ^{204}Tl in solution at equilibrium, stable and radiotracer concentrations introduced were based on results obtained on Cs sorption towards illite and smectite in similar physico-chemical conditions, extracted from literature (Poinssot *et al.*, 1999). Higher sorption was estimated onto illite than smectite as well as higher cation exchange in Na^+ media than in Ca^{2+} media. Consequently, different amounts of stable Tl and radioisotope were adjusted depending on matrices and background solutions.

For pH isotherms with illite, 50µL of a stable Tl solution at 4.66 ± 0.08 $.10^{-6}$ $mol.L^{-1}$ was added to increase total thallium in solution. Then 100µL of radiotracer solution (solution 1: 1.01MBq in 0.1M HCl) was introduced in batches with Na matrices and 50µL in batches with Ca matrices.

Eight stable Tl solutions (concentrations in SI, table S1) were used to create a range of Tl concentrations from 2.52 ± 0.11 10^{-10} to 8.39 ± 0.15 10^{-6} $mol.L^{-1}$ for concentration isotherms. Depending on background solution and matrices, stable Tl solutions added were 50 or 100µL.

Finally, 100µL or 50µL of radiotracer (solution 1) was introduced in Na and Ca bulk solutions respectively. Only radiotracer was injected in the two batches containing the lowest Tl concentrations. pH was only buffered by illite.

The operating condition was basically the same applied for experiments with Wyoming smectite, except that no stable Tl was added in solutions for pH isotherm experiments. Radiotracer (solution 2: 0.99MBq in 0.1M HCl) volumes were 50 µL for every experiment independently of the bulk solutions or the type of isotherms. Total Tl concentrations (between $2.52 \pm 0.06\ 10^{-10}$ and $1.04 \pm 0.02\ 10^{-5}$ mol.L-1) introduced in concentration isotherms were adjusted by adding 50 to 100µL of height different Tl solutions (SI, table S1). pH was only buffered by smectite.

After six days of continuous shaking at room temperature, tubes were ultra-centrifuged (Beckman Coulter Optima XPN-80 ultracentrifuge with a Type Ti70 rotor) for 45 minutes at 10596 *g* for illite and 16556 *g* for smectite. Then, pH (±0.10) was measured (for each tube) using a combined glass pH microelectrode (Metrohm) incorporating an Ag/AgCl reference electrode. Electrode calibration was made with buffer solutions (Certipur®, Merck) at pH 4.01, 7.00 and 12.00. 1mL of supernatant was sampled and mixed with 4mL of scintillant. Finally, ^{204}Tl activity is measured by liquid scintillation.

4.7. Desorption isotherms

We attempted to verify that the desorption reaction at equilibrium remained the same solid to solution partitioning as obtained with sorption reaction under the same chemical conditions. Following the sorption isotherm, the remaining supernatant was removed. Then, the residual solids and small liquid fraction (as hydrated clays minerals) were weighted. Bulk solutions were added with acid/base solutions to adjust pH to be as close as possible to those measured in sorption isotherms. Volumes were calculated to keep the same solid/solution ratio as in sorption experiments. Lastly, tubes were shaken continuously during six days and then, centrifuged and sampled following the same procedure described in the sorption isotherms section.

Desorption isotherms are necessary to check the sorption reversibility. Thus, cation exchange is verified as expressed in equation 6 (see below). When this condition is met, the thermodynamic multi-site ion exchanger model may be applied.

4.8. Sorption kinetics

Kinetics of Tl sorption onto illite and smectite in all tested matrices (Na and Ca) were performed to determine the time to achieve equilibrium. Batch experiments used the same polycarbonate centrifuge tube as isotherms and were done using stable Tl. Thus, 100 mg of conditioned clay minerals were dispersed in 5mL of $CaCl_2$ or NaCl at 10 mmol.L^{-1}. Duplicates were performed at a set of contact times. Tested contact times were 0, 2, 6, 10 and 15 days for Ca-illite and Na-illite. They were 0, 2, 7, 11 and 15 days for Ca-smectite ad Na-smectite. Initial Tl concentrations were ~1.0 10^{-7} mol.L^{-1}. pH was buffered by conditioned illite and smectite used in this study. Solutions were shaken continuously. At each investigated time, tubes were centrifuged (as in section 2.7.). Details of experimental conditions and figures are presented in Appendix 2 (fig. S2 and S3). Nevertheless, sorbed concentrations achieved equilibrium in all cases within 2 days. To insure time to equilibrium, in all isotherms experiments, contact time was imposed at six days.

4.9. Calculations of experimental parameters

Both sorption and desorption isotherm (experimental) results are expressed in term of distribution coefficient, calculated following the equation 1:

$$K_d = \frac{A_{ini} - A_{sup,eq}}{A_{sup,eq}} \times \frac{V}{m} \qquad \text{(Eq. 1)}$$

Where K_d is expressed in L.kg^{-1}. A_{ini} (Bq.L^{-1}) is the initial activity of the solution and $A_{sur,eq}$ (in Bq.L^{-1}) is the supernatant solution activity calculated with the measured activity of 1 mL of supernatant (A_{mes}, equation 2, in Bq.L^{-1}) reported to the total solution volume V (in L).

$$A_{sup,eq} = A_{mes} \times V \qquad \text{(Eq. 2)}$$

Then m (in kg) is the dry mass of conditioned clay minerals. In this study, V/m was maintained constant at 50.0 ± 3.8 L.kg^{-1}. Equation 1 can be simplified in equation 3. The corresponding equation with thallium concentration is also reported in equation 3.

$$K_d = \left(\frac{A_{ini}}{A_{sur,eq}} - 1\right) \times \frac{V}{m} = \left(\frac{[Tl]_{t=0}}{[Tl]_{free,eq}} - 1\right) \times \frac{V}{m} \qquad \text{(Eq. 3)}$$

$[Tl]_{free,eq}$ (mol.L^{-1}) is the thallium concentration in the supernatant and calculated by adding ^{204}Tl radiotracer and of the stable thallium concentration in solution. Details of its calculations are provided in supporting information (SI). $[Tl]_{t=0}$ (in mol.L^{-1}) corresponds to the thallium concentration at the beginning of each experiments.. $[Tl]_{sorbed}$ in mol.kg^{-1} was also calculated as in equation 4.

$$[Tl]_{sorbed} = K_d \times [Tl]_{free,eq} \quad \text{(Eq. 4)}$$

Two blank sets were associated with each sorption isotherms and contained only bulk solutions ($CaCl_2$ or NaCl 10 mmol.L^{-1}), radiotracers and when necessary stable thallium solutions. They were used as reference to calculate, for each isotherm, the initial Tl concentration ($[Tl]_{t=0}$) considering the ^{204}Tl source activity diluted in batch samples (A_{ini}). More details of equations and associated corrections for sorption and desorption isotherms are presented in SI.

4.10. Estimation of experimental uncertainties

Uncertainties reported in this section have only been calculated from the propagation of known measurements or lab errors following the same approach as Reinoso-Maset and Ly (2014). However, these are missing the variability in minerals properties. Experimental errors were hence calculated for each batch following the propagation errors theory. The variance of a G function of different x_i variable can be calculated from the variances of the variables x_i using this expression:

$$\sigma_G^2 = \sum_{i=1}^{n} \left(\frac{\partial G}{\partial x_i}\right)^2 \sigma_i^2 + 2 \sum_i \sum_j \frac{\partial G}{\partial x_i} \frac{\partial G}{\partial x_j} \sigma_{ij} \quad \text{(Eq. 5)}$$

where $(\partial G/\partial x_i)$ is the partial derivative of G with respect to x_i, σ^2 is the variance of x_i and σ_{ij} the covariance of the x_i and x_j variables. If these variables are independents, the covariance term is then equal to zero. In this study, logK_d (in L.kg^{-1}) experimental errors were between 0.01 and 0.05 log units for illite and between 0.01 and 0.07 for smectite. $\log[Tl]_{free,eq}$ (in mol.L^{-1}) experimental errors were from 0.02 to 0.07 log units. Finally, errors on $\log[Tl]_{sorbed}$ (in mol.kg^{-1}) were between 0.02 and 0.09 log units for illite and from 0.03 to 0.05 log units for smectite. Sets of repeated measurements indicated that ± 0.17 log units for illite and ± 0.16 log units for smectite yielding the spread in logK_d values. Those values were taken as error bars values. $[Tl]_{sorbed}$ is calculated with coefficient distribution, so accordingly, it would have the same

variability. Consequently, errors bars for $[Tl]_{sorbed}$ are ± 0.17 log units for illite and ± 0.16 log units for smectite.

For pH, uncertainties for each measurement are ± 0.10 pH unit. In results, for pH isotherms, due to measurement in each batch, the latest value is taken as error. However for pH related to concentration isotherms, averages are displayed. Then, errors are standard deviations of series averaged.

5. MULTI-SITE ION EXCHANGER MODEL

The Multi-Site Ion Exchanger model is based on the thermodynamics of chemical equilibria, and considers minerals as ion-exchangers described by negatively charged adsorption sites. For a complete description of the approach, readers can refer to Gorgeon (1994); Motellier *et al.* (2003) and Jacquier *et al.* (2004). This theory is only based on a macroscopic description, and does not consider any structural hypothesis of minerals (Motellier *et al.*, 2003). Thus, the exchange behavior of each cation (here, Na^+, Ca^{2+} and Tl^+) has to be studied individually as a function of pH and concentration on purified clay minerals (Motellier *et al.*, 2003; Jacquier *et al.*, 2004). Then, H^+ protons are taken as reference cations (Motellier *et al.*, 2003).

Classically, cation exchange between H^+ and M^{m+} for a given sites X_i^- is expressed by equation 6.

$$\{(X_i^-)_m - M^{m+}\} + mH^+ \leftrightarrow m\{X_i^- - H^+\} + M^{m+} \qquad \text{(Eq. 6)}$$

Then, the equilibrium constant of this reaction is written as follow in equation 7:

$$K^i_{M^{m+}/H^+} = \frac{(X_i^- - H^+)^m (M^{m+})}{\left((X_i^-)_m - M^{m+}\right)(H^+)^m} = \frac{[X_i^- - H^+]^m [M^{m+}] f^m_{(X_i^- - H^+)} \gamma_{M^{m+}}}{\left[(X_i^-)_m M^{m+}\right][H^+]^m f_{\left((X_i^-)_m M^{m+}\right)} \gamma^m_{H^+}} \qquad \text{(Eq. 7)}$$

where K^i is the selectivity coefficient, *i* is the type of sorption site. () and [] represent activities and concentrations of species, respectively. Species in solution are in $mol.L^{-1}$ whereas adsorbed species are in $mol.kg^{-1}$ (of dry clay mineral). *f* (in $kg.mol^{-1}$) is the activity coefficient of each adsorbed species and γ (in $L.mol^{-1}$) is the activity coefficient of the species in solution. All *f*'s are unknown but their ratios are expected to be constant. Consequently, a corrected selectivity

coefficient ($K^{*i}_{M^{m+}/H^+}$) is calculated (equation 8). Activity coefficients for species in solution are calculated according to Davis theory.

$$K^{*i}_{M^{m+}/H^+} = \frac{[X_i^- - H^+]^m [M^{m+}] \gamma_{M^{m+}}}{\left[(X_i^-)_m - M^{m+}\right] [H^+]^m \gamma^m_{H^+}} \quad \text{(Eq. 8)}$$

In this study, three cations are in solution, Tl^+, Na^+ or Ca^{2+}, each exchanging with H^+ according to equations 9, 10 and 11. In our experimental physico-chemical conditions, thallium is expected only in free form, Tl^+, avoiding some hydroxide forms of thallium (fig. 1 and 2). So a correction with Ringböm coefficient (Jacquier *et al.*, 2004; Tertre *et al.*, 2009) is neglected.

$$\{(X_i^-)_m - Tl^+\} + H^+ \leftrightarrow \{X_i^- - H^+\} + Tl^+ \quad \text{(Eq. 9)}$$

$$\{(X_i^-)_m - Na^+\} + H^+ \leftrightarrow \{X_i^- - H^+\} + Na^+ \quad \text{(Eq. 10)}$$

$$\{(X_i^-)_m - Ca^{2+}\} + 2H^+ \leftrightarrow 2\{X_i^- - H^+\} + Ca^{2+} \quad \text{(Eq. 11)}$$

Therefore, selectivity coefficients are calculated as follows:

$$K^{*i}_{Tl^+/H^+} = \frac{[X_i^- - H^+][Tl^+] \gamma_{Tl^+}}{[X_i^- - Tl^+][H^+] \gamma_{H^+}} \quad \text{(Eq. 12)}$$

$$K^{*i}_{Na^+/H^+} = \frac{[X_i^- - H^+][Na^+] \gamma_{Na^+}}{[X_i^- - Na^+][H^+] \gamma_{H^+}} \quad \text{(Eq. 13)}$$

$$K^{*i}_{Ca^{2+}/2H^+} = \frac{[X_i^- - H^+]^2 [Ca^{2+}] \gamma_{Ca^{2+}}}{\left[(X_i^-)_2 - Ca^{2+}\right] [H^+]^2 \gamma^2_{H^+}} \quad \text{(Eq. 14)}$$

Corrected selectivity coefficients ($K^{*i}_{Ca2+/2H+}$ and $K^{*i}_{Na+/H+}$) of each X_i sorption site characterizing the four matrices (Ca-illite, Ca-smectite, Na-illite and Na-smectite) are acquired in 10 mmol.L^{-1} solutions, while those of Tl^+ required estimation. Compiles data from a previous study were used (Wissocq *et al.*, accepted) andare recapitulated in table 1. In this study, only Tl selectivity coefficients with reference to protons were adjusted from both sorption curves over pH and over concentration by non-linear regression using Excel solver. Uncertainties of selectivity coefficient obtained by Excel solver were calculated with the Excel macro Solver Aid. Results are given in table 1.

Cations, here Tl^+, Na^+ and H^+ or Tl^+, Ca^{2+} and H^+, can saturate a sorption site X_i^- capacity (Tertre *et al.*, 2009). The capacity of major sorption sites are generally deduced from

experimental saturation curves, implying cation in major concentration (i.e. Na^+, Ca^{2+}, H^+). Those sites are characterized by plateau in pH isotherms when saturation occurs. Thus, site capacity, CE_i, is calculated with the sum of adsorbed species (equations 15 and 16).

$$CE_i = [X_i^- - Tl^+] + [X_i^- - Na^+] + [X_i^- - H^+] \quad \text{(Eq. 15)}$$

$$CE_i = [X_i^- - Tl^+] + [(X_i^-)_2 - Ca^{2+}] + 2[X_i^- - H^+] \quad \text{(Eq. 16)}$$

Sorbed cation concentrations may be expressed by relations according to cation valence of electrolyte, and taking into account pH, CEC, corrected selectivity coefficient (for Ca^{2+} and Na^+) (Wissocq *et al.*, 2017). In case of trace element, as for thallium competing with major element, sorbed concentration is directly estimated from experimental results (equation 4). The capacity of low capacity sites are then determined on experimental data expressed in terms of sorbed concentration versus concentration in solution at equilibrium or by fitting the combination of equations 12 to 16 on experimental isotherms. In case of multi-sites, the sum of CE_i has to be equal to the exchange capacity (CEC) of the clay minerals. Given that sorption properties of illite du Puy and Wyoming smectite were extensively studied and our conditioned clay CEC comparable to those of previous studies, the CE_i of major sorption sites are those determined by Gorgeon (1994) for illite and Nolin (1997) for smectite. Usually, three major sorption sites are used to describe the illite exchanger (Brouwer *et al.*, 1983). However, it is common to add a fourth site, of lower capacity and higher affinity to describe experimental data (Maes *et al.*, 1985) both on illite (Savoye *et al.*, 2012) and on smectite (Maes *et al.*, 1985; Tertre *et al.*, 2009).

In this study, four sites were necessary to model experimental data: three major sites and one minor site, with high affinity and low capacity. The latest (X_0 or X_s) was estimated with graphs support (fig. 7A and 7B) by considering the slope break of the $Log[Tl]_{sorbed}$ vs. $Log[Tl]_{free,eq}$ curves (Poinssot *et al.*, 1999; Missana *et al.*, 2014a). The value of $Log[Tl]_{sorbed}$ read (arrows in fig. 3A and 3B) at the slope break is used as X_0 and X_s site capacity and refined by adjusting simultaneously this CE_i and the $K^{*i}_{Tl+/H+}$ of four sites for pH and concentration isotherms. For each mineral, data from all matrices (Na-illite and Ca-illite on one hand and Na-smectite and Ca-smectite on another hand) were treated together. Consequently, CE_is for X_0 or X_s were adjusted as one as they are intrinsic properties of minerals and cannot depend on the conditioning state (Na or Ca). CE_i values for major sites (X_1, X_2 and X_3 or X_a, X_b and X_c) determined by Gorgeon (1994) and Nolin (1997) are summarized in table 1 and were taken as published.

6. RESULTS

6.1. Sites descriptions and selectivity coefficient for thallium

In the case of Tl, illite and smectite have to be described as cation exchangers with four sites. Although, smectite expresses a larger cation exchange capacity than illite (table 1), the estimated minor sites capacities (X_s and X_0) are close for both clay minerals, reaching 0.20 meq.kg^{-1} and 0.25 meq.kg^{-1}, respectively (table 1). Their capacities were estimated graphically on log $[Tl]_{sorbed}$ vs. Log $[Tl]_{eq}$ curves, at the slope break (pointed by arrows) in figures 3A for smectite and 3B for illite. In this study, shifts are small but more obvious when Na^+ is the background cation (fig. 3A and 3B) and correspond to site saturations by the trace cation (Wissocq *et al.*, accepted; Missana et al., 2014a), here thallium.

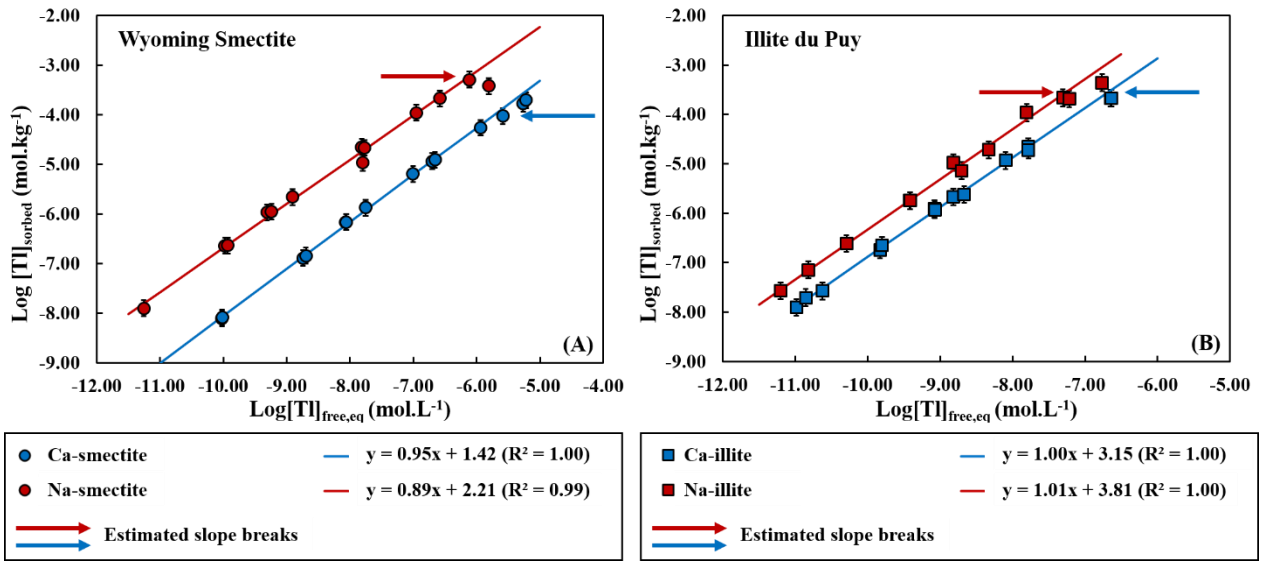

Figure 3: Results in $log[Tl]_{sorbed} = f([Tl]_{free,eq})$ for smectite (A) and illite (B). Error bars correspond to the variability of Tl sorbed.

Considering selectivity coefficient (K^{*i}) values, the X_0 or X_s sites show the most affinity for Tl (table 1). For the two studied clays, the sites selectivity can be ordered as, $X_0 > X_1 > X_2 > X_3$ (table 1) for illite and as $X_s > X_a > X_b > X_c$ for smectite (table 1). However the main difference between illite and smectite affinity for thallium comes from K^{*i} values for X_0 and X_s. Values are respectively $10^{-3.87}$ for the first and $10^{-2.31}$ for the last (table 1) when reported to protons. When reported to electrolyte cations, thallium affinity for low capacity and high reactivity sites (X_0 and X_s) is also higher than any other sites except for Ca-smectite (table 1). Nevertheless, thallium

affinity for major sites remains higher than for sodium and calcium but lesser than for protons, which induces some pH-dependence. As indicated by negative selectivity coefficient, illite and smectite have more affinity for thallium than for calcium, sodium (table 1).

Table 1: Sites capacity and selectivity coefficients calculated in this study. Equations for $\log K^{*i}_{Tl^+/Na^+}$ and $\log K^{*i}_{Tl^+/Ca^{2+}}$, not used during modelling are summarized in Appendix 5 (eq. I and J)

Mineral	Sites	CE_i (eq.kg^{-1})	$\log K^{*i}_{Tl^+/H^+}$	$\log K^{*i}_{Na^+/H^+}$ [C]	$\log K^{*i}_{Ca^{2+}/2H^+}$ [C]	$\log K^{*i}_{Tl^+/Na^+}$	$\log K^{*i}_{2Tl^+/Ca^{2+}}$
Illite	X_0	2.5 .10^{-4}	-3.87 ± 0.03	0.87 ± 0.14	0.40 ± 1.98	-4.74 ± 0.77	-3.97 ± 19.50
	X_1	0.13[A]	0.18 ± 0.05	2.77 ± 0.13	2.17 ± 0.07	-2.60 ± 0.79	-1.69 ± 0.49
	X_2	0.04[A]	1.13 ± 0.11	4.19 ± 0.18	4.31 ± 0.272	-3.07 ± 0.44	-2.88 ± 0.39
	X_3	0.07[A]	6.20 ± 1.03	8.95 ± 3.78	11.75 ± 0.21	-2.75 ± 1.62	-5.24 ± 0.96
	$\sum_i CE_i$	*0.25*					
Smectite	X_s	2.0 .10^{-4}	-2.31± 0.25	2.59 ± 0.23	0.22 ± 0.18	-4.90 ± 0.95	-2.23 ± 2.10
	X_a	0.39[B]	0.13 ± 0.81	0.26 ± 0.04	0.49 ± 0.49	-0.14 ± 0.92	-0.06 ± 0.45
	X_b	0.36[B]	1.52± 0.29	2.62 ± 0.089	4.35 ± 0.03	-1.10 ± 0.25	-2.53 ± 0.50
	X_c	0.14[B]	6.35 ± 0.21	8.45 ± 0.18	14.84 ± 0.06	-2.10 ± 0.12	-8.19 ± 0.31
	$\sum_i CE_i$	*0.89*					

A from Gorgeon, 1994
B from Nolin, 1997
C from Wissocq *et al*., accepted

6.2. Thallium adsorption as function of pH

In all cases, Tl adsorption is pH dependent. LogK_d are lower at low pH and higher at basic pH (fig. 4A, 5A, 6A and 7A). This highlights the competition with protons for sorption sites, according to the electrolyte (Na or Ca) and the progressive exchange with thallium on sorption sites. Besides, two kinds of behavior are identified, depending on the background cation. When it is Na^+, whatever clay mineral is in suspension, the pH effect on Tl uptake is significant below pH 6.0 by the lowest K_d values; whereas at higher pH a plateau with roughly constant logK_d is reached (fig. 4A and 6A). Corresponding maximal logK_d values are ~3.16 ± 0.16 L.kg^{-1} for smectite and~4.00 ± 0.17 L.kg^{-1} for illite. In Na-smectite (fig. 4A), from pH 3.5 to 6.0, logK_d (in L.kg^{-1}) are between 2.51 and 3.10 (± 0.16). For Na-illite below pH 6.0, logK_d range between 1.89

± 0.17 to 4.00 ± 0.17. On the contrary, when Ca^{2+} is the background cation, K_d evolution is gradual over the range of investigated pH (fig. 5A and 7A). Except at low pH (< 4.0), the amount of thallium adsorbed onto clay minerals is more important on Na-illite, then on Na-smectite and Ca-illite almost in the same ranges. Ca-smectite holds the smallest amount of sorbed thallium.

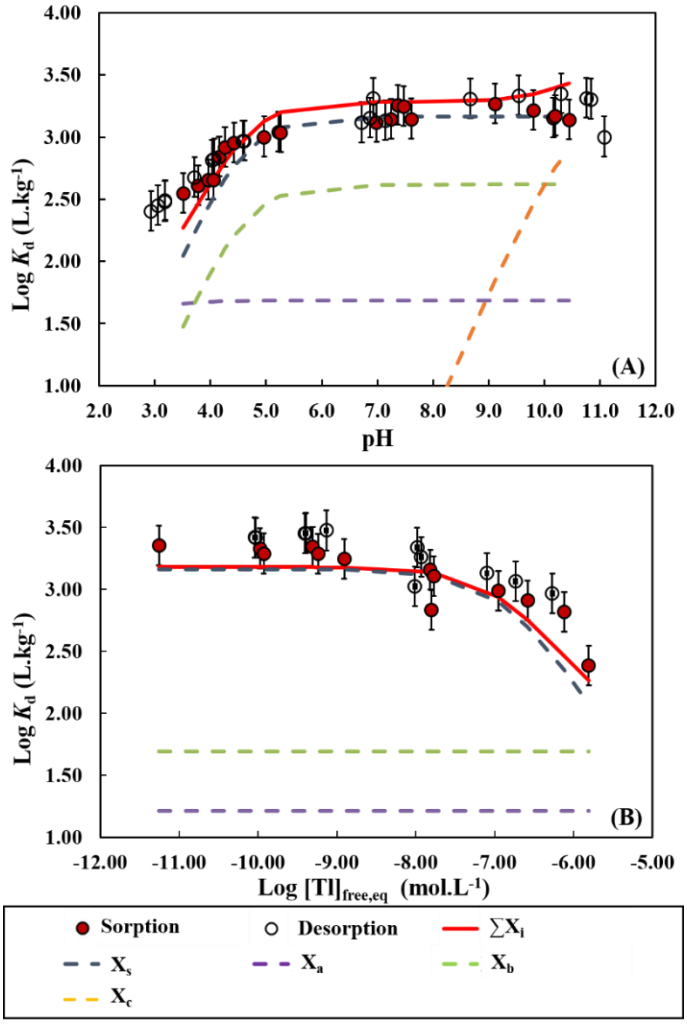

Figure 4: Results for **Na-smectite** in logK_d = f(pH) (A) and in logK_d = f([Tl]$_{free,eq}$) (B). In A, introduced average Tl concentration is $[Tl]_{t=0}$ = 2.24 ± 0.08 .10^{-10} mol.L^{-1}. In B, sorption average pH was 7.34 ± 0.40 and was 6.11 ± 0.40 during desorption. Dashed colorful lines correspond to the individual modeled reactive sites contributions. Red lines are the sum of each site contribution. Error bars correspond to the K_d variability.

The four sites considered in the model allow correct fitting of the smectite experimental data, both with Na^+ and Ca^{2+} (fig. 3A and 4A). Individual site contributions show that the high reactive site (X_s) is one which uptakes the most thallium by smectite in all pH conditions (fig. 4A and

5A). They follow the same profile as experimental data with growing logK_d values before reaching a plateau for pH > 5.0. X_a and X_b also play a significant role in Tl uptake but only the logK_d for X_b site varies at low pH and remains constant above pH 5.0 (fig. 4A and 5A). The X_a site displays a steady logK_d along the range of tested pH (fig. 4A and 5A). X_c becomes more important at higher pH and its role increases with increasing pH. In Na-smectite, it is significant from pH ~ 8.0 and at pH 10.0 and then occupies the second site contribution, express in term of logK_d values, after X_s site (fig. 4A). Observations are similar for Ca-smectite but the X_c site appears at pH 7.0 and equal the X_s site in term of logK_d from pH 10.0 (fig. 4A). In figure 5A, two experimental points at pH over 10.0 are well above the general trend (logKd ~ 2.50 L.kg^{-1}) and were not considered in the study. It seems that calcite precipitations occurred in batches during pH adjustment with $Ca(OH)_2$.

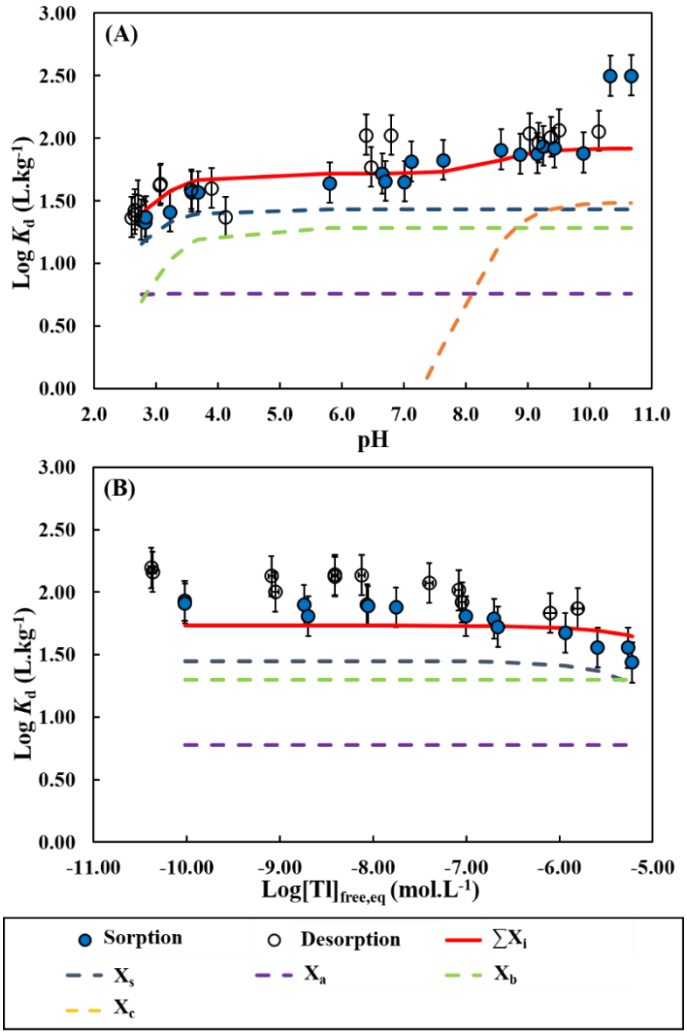

Figure 5: Results for **Ca-smectite** in $\log K_d = f(pH)$ (A) and in $\log K_d = f([Tl]_{free,eq})$ (B). In A, introduced average Tl concentration, $[Tl]_{t=0} = 2.12 \pm 0.29 .10^{-10}$ mol.L^{-1}. In B, sorption average pH was 7.89 ± 0.20 and was 7.97 ± 0.04 during desorption. Dashed colorful lines correspond to contribution of individual modeled reactive sites. Red lines are the sum of each site contribution. Error bars correspond to the K_d variability.

The combined contribution of all sites (red line, fig. 6A and 7A) describes effectively the experimental data. In Na-illite, Tl sorption is driven by high reactive site X_0 at pH less than 3.0 (fig. 6A). Then, a significant role is played by the X_1 site, as it dominates Tl uptake for pHs between 4.0 and 7.0. A similar trend is observed for X_2 (fig. 6A) but from pH 4.0. It reaches Tl saturation around pH 8.0 and uptakes as much thallium as the X_1 site. From pH 8.0, X_3 starts to uptake Tl but never reaches saturation under our conditions (fig. 6A). The case of Ca-illite is different. X_0 seems to uptake the majority of the thallium as it almost corresponds to the overall trend (fig. 7A). Despite low $\log K_d$ (< 1.50 L.kg^{-1}) the uptakes by sites X_1 and X_2 remain significant considering their exchange capacities (fig. 7A). No role from the X_3 site is observed here (fig. 7B).

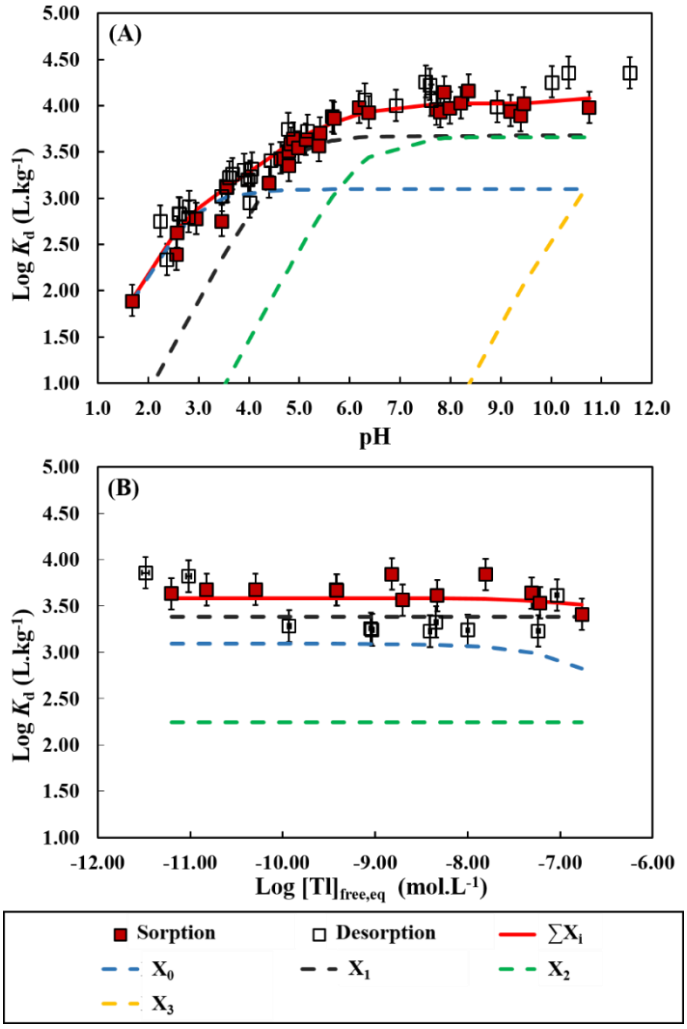

Figure 6: Results for **Na-illite** in logK_d = f(pH) (A) and ion logK_d = f([Tl]$_{free,eq}$) (B). In A, introduced average Tl concentration, [Tl]$_{t=0}$ = 4.01 ± 0.95 .10^{-8} mol.L^{-1}. In B, sorption average pH was 5.00 ± 0.10. For desorption, it was 5.00 ± 0.46 for points with log[Tl]$_{free,eq}$ < -10 and for the point (-7.03; 3.62). Then, it was 3.94 ± 0.19 for points with log[Tl]$_{free,eq}$ > -10. Dashed colorful line correspond to contributions of individual modeled reactive sites. Red lines are the sum of each sites. Error bars correspond to the variability of the K_d.

6.3. Thallium adsorption as function of Tl concentrations

In this section, partitioning coefficients are expressed in function of thallium concentrations measured at sorption equilibrium in the supernatant at fixed pH. LogK_d values in comparable pH and Tl concentrations are similar to those from pH isotherms in all experiments (fig. 4, 5, 6 and 7). Observations are the same with modeling results and for all matrices, the highly reactive site

(X_0 or X_s) mainly contributes to uptake thallium at all concentrations (fig. 4B, 5B and 7B) except for Na-illite where X_1 is dominant (fig. 6B). LogK_d values remain constant until free thallium concentration reaches 10^{-8} (-8 in log scale) mol.L^{-1}. Smooth declines in logKd are observed when Ca^{2+} is the background cation, from 10^{-8} mol.L^{-1} and from 10^{-7} mol.L^{-1} of free Tl for illite (fig. 7B) and for smectite (fig. 7A), respectively. No logKd decrease is seen on illite in sodic conditions (fig. 6B) suggesting that no sites saturation is achieved in the studied concentrations. On the contrary, a clear break is evidenced for Na-smectite (fig. 4B) implying that less thallium is adsorbed up to 10^{-8} mol.L^{-1} of free cation.

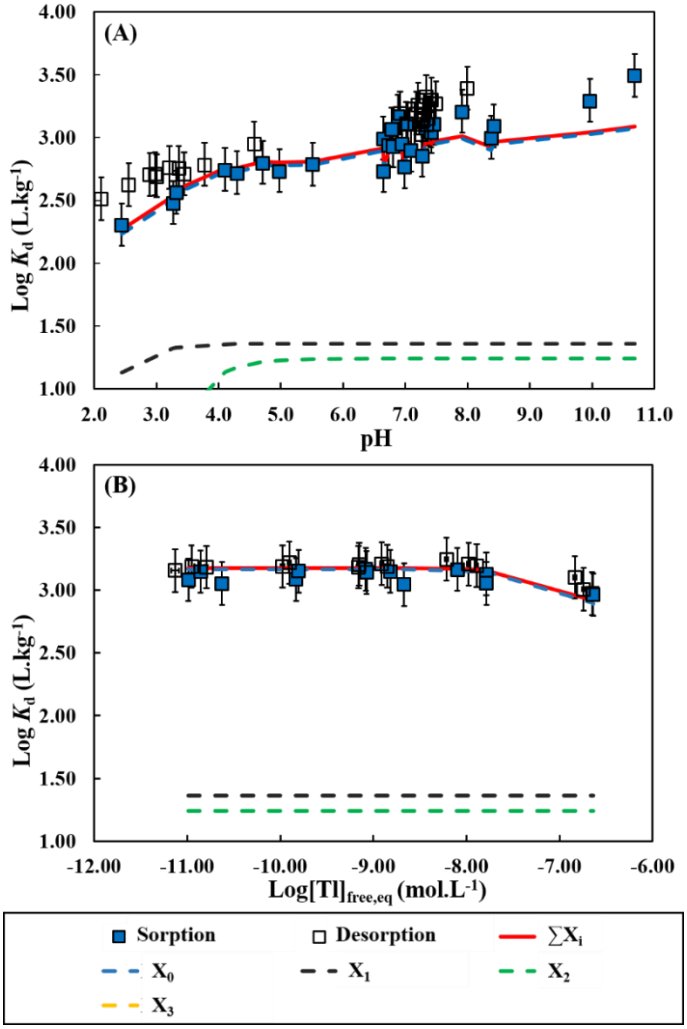

Figure 7: Results for **Ca-illite** in logK_d = f(pH) (A) and in logK_d = f([Tl]$_{free,eq}$) (B). In A, introduced average Tl concentration, [Tl]$_{t=0}$ = 4.37 ± 0.18 .10^{-8} mol.L^{-1}. In B, sorption average pH was 7.18 ± 0.08 and was 7.14 ± 0.19 during desorption. Dashed colorful lines correspond to LogK_d for each modeled reactive sites. Red lines are the sum of each site contribution. Error bars correspond to the K_d.variability

6.4. Adsorption reversibility

From figures 3 to 6, both sorption and desorption data are presented. When thallium uptake by clay minerals is studied in function of pH, the desorption K_d values are in the same range as sorption within error bars of each data set (fig 4A, 5A, 6A and 7A). Results are similar when thallium uptake is studied in function of Tl concentrations (fig. 4B, 5B, 6B, 7B). Those results indicate that thallium sorption on clay minerals, both illite and smectite is reversible in all tested conditions.

Variability observed for desorption data in figure 6B is explained by different pH conditions within the set of batch experiments. The three values over logK_d at 3.50 L.kg^{-1} were acquired at pH 5.00 ± 0.46 while the other values (logK_d < 3.50 L.kg^{-1}) where acquired at pH 3.94 ± 0.19. When compared to the same pH conditions in figure 6A, the reversibility is attested.

7. DISCUSSION

This study represents the first description of thallium sorption with two major clay minerals in the sub-surface environment, such as illite and smectite. Hence, the set of selectivity coefficients obtained for thallium/protons exchange is also the first available up to our knowledge.

7.1. Estimations of low capacity sites

As mentioned previously, a low capacity site is evidenced at trace concentrations and is intrinsic to mineral properties (Bradbury and Baeyens 1997; Poinssot *et al*., 1999; Tertre *et al*., 2009). Thus, no distinct site capacity value depending on physico-chemical conditions is expected as verified by low site capacity values that remain the same both in Na and Ca bulk solutions. Results with illite gave a value at $2.5.10^{-4}$ eq.kg^{-1} (table 1) which is close to values obtained by Missana *et al*. (2014b) at $3.0 .10^{-4}$ eq.kg^{-1} and by Poinssot *et al*. (1999) at $5.5 .10^{-4}$ eq.kg^{-1} with Cs. On another hand, they were estimated at $5.0.10^{-3}$ eq.kg^{-1} by Wissocq *et al*. (2017) with Sr sorption experiments and at $2.0 .10^{-3}$ eq.kg^{-1} for Zn experiments (Altmann *et al*., 2015). For smectite, Baeyens (1997) calculated their capacity at $2.0 .10^{-3}$ eq.kg^{-1} (Zn experiments) whereas it was evaluated at $1.2.10^{-4}$ eq.kg^{-1} by Missana *et al*. (2014), $1.0 .10^{-4}$ by Wissocq *et al*. (accepted) and finally at $5.0 .10^{-4}$ eq.kg^{-1} by Peynet (2003), each issue of Cs sorption

experiments. Values from this study are in the same range as those from literature. However, it appears that estimations calculated during sorption experiments with divalent cations give values roughly one order of magnitude higher than with monovalent.

7.2. Thallium sorption behavior towards clay minerals comparing with other cations.

7.2.1. Thallium sorption behavior

Thallium sorption behavior can be described by combining two main factors, affinity for the minerals and competition with a major element (here Ca^{2+} and Na^{+}) for sorption sites. When normalized by mineral CEC (table 2), it appears that Tl affinity for illite is one order of magnitude higher than for smectite for both Ca^{2+} and Na^{+} matrices. However, experimental data clearly show that thallium uptake by smectite can equal thallium uptake by illite depending on the background cation. Similarly, based on thallium affinity for the mineral and *vice-versa*, illite in $CaCl_2$ should uptake as much thallium as illite in NaCl but it does not. In the latest case, thallium and sodium exchange easily because they are both monovalent and only one Tl^{+} is needed to exchange with one Na^{+}. On the contrary, in a $CaCl_2$ solution, two Tl^{+} are necessary to replace one Ca^{2+} and consequently, thallium uptake is limited. This phenomenon is also highlight in Na-smecite experiments where almost the same amount is taken up compared to an illite in $CaCl_2$.

Tableau 2: Thallium affinity in moles of sorbed element normalized by CEC ($mol.eq^{-1}$) for illite and smectite at pH = 7.

Background cation	Illite	Smectite
Na^{+}	$2.09 .10^{-7}$	$5.65 .10^{-8}$
Ca^{2+}	$2.03 .10^{-7}$	$2.60 .10^{-8}$

Competition between a trace and a major cation is somehow the greater limiting factor in thallium uptake by clay minerals. Depending on pH, thallium is first adsorbed onto X_0 and X_s sites, while they represent respectively 0.1% and 0.02% of illite and smectite CEC (table 1 and fig. 4 to 7), those sites dominate thallium uptake by clay minerals. Then, when X_0 and X_s are saturated, major sites control Tl sorption depending of their protonation state. Nevertheless, competition for those sites is higher and the intrinsic properties of the major cation in solution get important. With sodium, exchange is easier and the site's affinity is less overtaken by the competitive effect, so major sites uptake more thallium. However, with calcium, exchange is more difficult and the competitive effect with other cation is greater than site's affinity for

thallium. Consequently, thallium uptake is limited. This dual effect (competition vs. affinity) also explains why thallium uptake by Ca-smectite is dominated by major sites at high pH (> 7). Indeed, thallium has higher affinity for X_3 ($K^{i*}_{Tl^+/Ca^{2+}} = 10^{-8.19}$, table 1) sites than calcium and so more Tl is taken up.

Thallium concentration has a limited effect on the sorption behavior because it remains in trace concentrations compared to the electrolyte cation. However, we can expect that that the ionic strength could influence the amount of adsorb thallium as observed for other trace elements (Missana *et al*., 2014a; Missana *et al*., 2014b; Altmann *et al*., 2015). Then, thallium uptake would decrease with higher ionic strength. In various environments, thallium is assumed to substitute potassium in secondary minerals (e.g. Nielsen *et al*., 2006; Prytulak *et al*., 2017; Nielsen *et al*., 2017). Based on the discussion so far, we can expect similar behavior of thallium in a KCl electrolyte for instance. Nevertheless, thallium and potassium share some similar behavior mostly due to close ionic radii (Shanon 1976). Then, the competition for site would increase and less thallium uptake is expected. This phenomenon was observed for cesium for instance (Missana *et al*., 2014a).

In other studies, when modeling is performed with the surface complexation theory, X_0 and X_s sites are akin to frayed edge type-sites (FES) for illite (Poinssot *et al*., 1999) and smectite (Missana *et al*., 2014a). Interpretations from multi-site ion exchanger theory allow only macroscopic descriptions of the sorption without any structural considerations. Consequently, the sites described in this study and involved in thallium sorption cannot be attributed to FES type or interlayer sites for instance.

7.2.2. Comparison with other trace cations

Tl(I) with its main dissolved species Tl^+, have a ionic radii of 1.50Å, close to Rb (1.52Å) and Cs (1.67Å; Shannon 1976). Consequently, its behavior is often compared to alkali metals (e.g. Prytulak *et al*., 2017). Over the three cations, Tl is the one less sorbed on illite independently of the background cations (Brouwer *et al*., 1983, Poinssot *et al*., 1999; Missana *et al*., 2014b). For instance, in similar conditions (trace concentrations and ionic strength at 0.01M), cesium onto Na-illite shows logK_d varying between ~ 4.5 to ~ 5.0 L.kg^{-1} in function of pH (Poinssot *et al*., 1999), corresponding to one order of magnitude higher than thallium. Then, alkali metals

sorption onto illite can be ranked as follow, Cs> Rb> Tl. For smectite, observations are similar and cesium sorption is greater than thallium (Missana et al., 2014a; Wissocq *et al*., accepted).

In the studied context, no chalcophile vs. lithophile behavior (McGoldrick *et al*., 1979; Prytulak *et al*., 2017) for Tl can be involved. Thallium behaves as expected for other cations (Rb, Cs and K) with large ionic radii and displays weaker sorption interactions with the studied clay minerals.

7.2.3. Comparison to other thallium bearing phases

Thallium sorption onto illite and smectite in NaCl was compared to other bearing phases extracted from Bidoglio *et al*. (1993), Liu *et al*. 2011 and Casiot *et al*. (2011). Figures are presented in Appendix 6 (fig. S3 and S4).Note that ionic strengths are different for some phases, so thallium uptake by illite and smectite is probably overestimated (around one order of magnitude; Missana *et al*., 2014a; Altmann *et al*., 2015) in respect to goethite, δ-MnO_2, γ-Al_2O_3 and SiO_2. Nevertheless, it appears that manganese (here δ-MnO_2) oxides adsorb the most Tl(I) whereas silica adsorbs less. Aluminium oxides could compete in controlling Tl in solution with both illite and smectite at alkaline pH (>10). Casiot *et al*., (2011), evidenced a weak thallium sorption to ferrihydrite that is similar to smectite (same ionic strength) at pH> 7 (SI fig. S4). At near neutral (in natural waters conditions) and acidic pH, thallium sorption is dominated first by manganese oxides and then by clay minerals. Bearing phases in natural waters conditions could be ranked as follow (order of decreasing sorption): δ-MnO_2> illite> smectite ~ ferrihydrite ~> γ-Al_2O_3 ~ goethite> SiO_2.

Few studies address Tl sorption mechanisms, mostly on manganese oxides and iron oxihydroxides (Bidoglio *et al*., 1993; Lin and Nriagu, 1998; Casiot *et al*., 2011; Peacock and Moon, 2012; Coup *et al*., 2015) so far. Thallium (I) is known to have weak interactions with ligands in aqueous solution due to its shell electron configuration and its large ionic radii (Persson *et al*., 2002). Peacock and Moon (2012) identified weak interactions by outer sphere complexes for thallium with ferrihydrite, triclinic birnessite and todorokite. Those types of complexes could be expected for thallium on the sites of both illite and smectite. Indeed, adsorption reversibility is total in our experiments and evidences that thallium sorption with clay minerals is driven by exchange reactions. In conclusion, thallium displays weak binding to clay

minerals, possibly because of outer sphere complexes but more data are necessary to perfectly understand the mechanisms involved here.

7.3. Implications for thallium mobility in the environment

Thallium has mainly been studied in soils in which clay minerals were suggested as potential bearing phases (Tremel *et al*., 1997; Vaněk *et al*., 2011; Voegelin *et al*., 2015). Voegelin *et al* (2015) and Vaněk *et al* (2011) identified illite and birnessite as the main thallium pedogenic Tl-bearing phases. The present study confirms that illite is an important bearing phase for Tl. Moreover, it seems thallium goes preferentially on illite clays instead of smectite (Voegelin *et al*., 2015) which is in accordance with the lower Tl affinity evidenced in this study. However, the exchangeable interactions between thallium and clays suggest that in changing environmental conditions, thallium could be released from bearing phases. This process may contribute to the thallium bioavailability and could explain the limited contribution of illite on thallium trapping in several soils (Vaněk *et al*., 2011). In a Tl-rich soil, Tl uptake by illlite appears to be dominant over other pedogenic phases such as Mn-oxides for instance (Voegelin *et al*., 2015). The Tl/Mn ratio is known to be determinant in Tl sorption onto manganese oxides. Tl excess saturates Mn oxide sorption sites, which constrains its retention effect in soils for instance (Peacock and Moon, 2012; Voegelin *et al*., 2015). Due to higher Tl affinity for Mn oxides, Tl is expected to be trapped preferentially by those minerals. Then, clays and especially illite, could have an important role in controlling Tl uptake at high concentrations (i.e. polluted soils, sediments or in acid mine drainage).

The role of clay minerals in other environmental compartments is not clear due to lack of studies. In rivers, aqueous Tl(I) species are mainly dissolvedand the thallium loaded in particulate matter seems limited (Law and Turner, 2011). Nevertheless, in lake and river sediments, we can assume that clay minerals are dominant bearing phases and can be responsible for thallium output fluxes from water column as in oceans (Rehkämper and Nielsen, 2004). In estuarine conditions where particles are small and often re-suspended, thallium seems mostly fixed on particles (Law and Turner, 2011). In this context, illite or smectite, given their quick exchange kinetics with thallium (roughly two days) could play an important role, especially in freshwater where Tl seems to mostly be sorbed on particles (Turner *et al*., 2010).

8. SUMMARY AND CONCLUSIONS

Illite du Puy and Wyoming smectite were used in this study to assess the sorption behavior of thallium as Tl(I) to clays. Batch experiments at a constant ionic strength of 0.01 mol.L^{-1}, with various pH and Tl concentration conditions were performed. Na^+ or Ca^{2+} was used as background cations for all experiments. Experimental results were interpreted with the help of a multi-site ion exchanger model. Our results showed that illite is the mineral with more affinity for thallium while smectite has less affinity. In both cases, independently of the background electrolyte, low capacity but highly reactive sites were dominant in thallium uptake highlighting Tl affinity for those sites. The exchange reversibility and weak interactions between Tl^+ and reactive clay sites suggested similarity with outer sphere complexes as dominant mechanism.

The role of clay minerals in thallium environmental cycle is evident but more studies are needed to understand all the mechanism involved. On one hand, more descriptions of thallium interactions with clays in various environments such as lake, river and estuary sediments and particulate matter would be interesting. New environmental measurements will benefit from our database and modeling approach and Tl-clay interactions will be modeled to gain a better understanding of Tl behavior. In parallel, studies to evidence the sorption mechanisms are important especially concerning the type of bonding and the possible thallium migration in interlayers of clay minerals. Finally, thallium substitution of potassium is prevalent in geogenic processes and is present in weathering products of various K-bearing minerals. Thus, it would be interesting in the future to distinguish the source of thallium in illite, for instance, and to know whether it was already present in the parent mineral or thallium complex due to sub(surface) environmental processes.

ACKNOWLEGDEMENTS

The authors thank IRSN, CEA, BRGM and IPGP for funding this research. Parts of this this work were supported by IPGP multidisciplinary program PARI and by Region Ile de France SESAME Grant no. 12015908. Logan Rand is acknowledged for his helpful English proofreading.

APPENDIX A. SUPPLEMENTARY MATERIAL

REFERENCES

Altmann S., Aertsens M., Appelo T., Bruggeman C., Gaboreau S., Glaus M., Jacquier P., Kupcik T., Maes N., Montoya V. *et al*. (2015). Processes of cation migration in clayrocks. *Final Scientic Report of the CatClay European Project*. 140p.

Baeyens B. and Bradbury M. H. (1997). A mechanistic description of Ni and Zn sorption on Part I : Titration and sorption measurements. *Journal of Contaminant Hydrology* **27**, 199–222.

Bradbury M. H. and Baeyens B. (2002). Sorption of Eu on Na- and Ca-montmorillonites : Experimental investigations and modelling with cation exchange and surface complexation. *Geochimica et Cosmochimica Acta* **66**, 2325–2334.

Baker R. G. A., Rehkämper M., Ihlenfeld C., Oates C. J. and Coggon R. (2010). Thallium isotope variations in an ore-bearing continental igneous setting : Collahuasi Formation, northern Chile. *Geochimica et Cosmochimica Acta* **74**, 4405–4416.

Bennett S. M. (2017). Thallium. US Geological Survey, *Mineral Commodity Summaries*, 170–171.

Biagioni C., D'Orazio M., Vezzoni S., Dini A. and Orlandi P. (2013). Mobilization of TI-Hg-As-Sb-(Ag,Cu)-Pb sulfosalt melts during low-grade metamorphism in the Alpi Apuane (Tuscany, Italy). *Geology* **41**, 747–750.

Bidoglio G., Gibson P. N., O'Gorman M. and Roberts K. J. (1993). X-ray absorption spectroscopy investigation of surface redox transformations of thallium and chromium on colloidal mineral oxides. *Geochimica et Cosmochimica Acta* **57**, 2389–2394.

Brouwer E., Baeyens B., Maes A. and Cremers A. (1983). Cesium and rubidium ion equilibriums in illite clay. *The Journal of Physical Chemistry* **87**, 1213–1219.

Brown P. L. and Ekberg C. (2016). Hydrolysis of Metal Ions. *Wiley VCM*, p217-218 & p825

Campanella B., Casiot C., Onor M., Perotti M., Petrini R. and Bramanti E. (2017). Talanta Thallium release from acid mine drainages : Speciation in river and tap water from Valdicastello mining district (northwest Tuscany). *Talanta* **171**, 255–261.

Casiot C., Egal M., Bruneel O., Verma N., Parmentier M. and Elbaz-Poulichet F. (2011). Predominance of Aqueous Tl(I) Species in the River System Downstream from the Abandoned Carnoulès Mine (Southern France). *Environmental Science & Technology* **45**, 2056–2064.

Cheam V. (2001). Thallium Contamination of Water in Canada, *Water Qual. Res. J. Canada* **36**, 851–877.

Coup K. M. and Swedlund P. J. (2015). Demystifying the interfacial aquatic geochemistry of thallium(I): New and old data reveal just a regular cation. *Chemical Geology* **398**, 97–103.

Gabis V. (1958). Etude préliminaire des argiles oligocènes du Puy-en-Velay (Haute-Loire). *Bull. Soc. Franç. Minéral. Cristallog*. **81**, 183-185.

Gorgeon L. (1994). Contribution à la modélisation physico-chimique de la rétention de radioéléments à vie longue par des matériaux argileux. *PhD thesis*, 189p. Université Paris 06, France.

Jacquier P., Ly J. and Beaucaire C. (2004). The ion-exchange properties of the Tournemire argilliteI. Study of the H, Na, K, Cs, Ca and Mg behaviour. *Applied Clay Science* **26**, 163–170.

Jacobson A. R., McBride M. B., Baveye P. and Steenhuis T. S. (2005). Environmental factors determining the trace-level sorption of silver and thallium to soils. *Science of the Total Environment* **345**, 191–205.

Hettmann K., Marks M. A. W., Kreissig K., Zack T., Wenzel T., Rehkämper M., Jacob D. E. and Markl G. (2014). The geochemistry of Tl and its isotope during magmatic and hydrothermal processes: The peralkaline Ilimaussaq complex, southwest Greenland. *Chemical Geology* **366**, 1–13.

Kaplan D. I. and Mattigod S. V. (1998). Aqueous geochemistry of thallium. In *Thallium in the Environment*, 15–29. Edited by J. O. Nriagu. John Wiley & Sons, Inc. New York

Karbowska B. (2016). Presence of thallium in the environment : sources of contaminations, distribution and monitoring methods. *Environmental Monitoring and Assessment* **164**, 640–658.

Karlsson U., Karlsson S. and Düker A. (2006). The effect of light and iron(II)/iron(III) on the distribution of Tl(i)/Tl(iii) in fresh water systems. *Journal of Environmental Monitoring* **8**, 634–640.

Karnland, O. (2010). Chemical and mineralogical characterization of the bentonite buffer for the acceptance control procedure in a KBS-3 repository (No. SKB-TR-10-60). *Swedish Nuclear Fuel and Waste Management* Co. http://www.iaea.org/inis/collection/NCLCollectionStore/_Public/43/003/43003619.pdf

Law S. and Turner A. (2011). Thallium in the hydrosphere of south west England. *Environmental Pollution* **159**, 3484–3489.

Lin T.-S. and Nriagu J. (1998). Speciation of thallium in natural waters. In *Thallium in the Environment*, 15–29. Edited by J. O. Nriagu. John Wiley & Sons, Inc. New York.

Lin T.-S. and Nriagu J. (1999). Thallium Speciation in the Great Lakes. *Environmental Science & Technology* **33**, 3394–3397.

Lis J., Pasieczna A., Karbowska B., Zembrzuski W. and Lukaszewski Z. (2003). Thallium in soils and stream sediments of a Zn-Pb mining and smelting area. *Environmental Science and Technology* **37**, 4569–4572.

Liu J., Lippold H., Wang J., Lippmann-Pipke J. and Chen, Y. (2011). Sorption of thallium(I) onto geological materials: Influence of pH and humic matter. *Chemosphere* **82**, 866–871.

Maes A., Verheyden D. and Cremers A. (1985). Formation of Highly Selective Cesium-Exchange Sites in Montmorillonites. *Clays and Clay Minerals* **33**, 251–257.

McGoldrick P. J., Keays R. R. and Scott B. B. (1979). Thallium: a sensitive indicator of rock/seawater interaction and of sulfur saturation of silicate melts. *Geochimica et Cosmochimica Acta* **43**, 1303–1311.

Meunier A. (2003). Argiles. *Collection Géosciences*, 436p. Editions Scientifiques GB-SGF, Paris.

Missana T., Benedicto A., Garcia-Gutiérrez M. and Alonso U. (2014a). Modeling cesium retention onto Na- , K- and Ca-smectite : Effects of ionic strength, exchange and competing cations on the determination of selectivity coefficients. *Geochimica et Cosmochimica Acta* **128**, 266–277.

Missana T., Garcia-Gutiérrez M. and Alonso U. (2014b). Modelling of Cs sorption in natural mixed-clays and the effects of ion competition. *Applied Geochemistry* **49**, 95–102.

Motellier S., Ly J., Gorgeon L., Charles Y., Hainos D., Meier P. and Page, J. (2003). Modelling of the ion-exchange properties and indirect determination of the interstitial water composition of an argillaceous rock. Application to the Callovo-Oxfordian low-water-content formation. *Applied Geochemistry* **18**, 1517–1530.

Nielsen S. G., Rehkämper M., Porcelli D., Andersson P., Halliday A. N., Swarzenski P. W., Latkoczy C. and Günther D. (2005). Thallium isotope composition of the upper continental crust and rivers - An investigation of the continental sources of dissolved marine thallium. *Geochimica et Cosmochimica Acta* **69**, 2007–2019.

Nielsen S. G., Rehkämper M., Teagle D. A. H., Butterfield D. A., Alt J. C. and Halliday A. N. (2006). Hydrothermal fluid fluxes calculated from the isotopic mass balance of thallium in the ocean crust. *Earth and Planetary Science Letters* **251**, 120–133.

Nielsen S. G., Prytulak J., Blusztajn J., Yunchao S., Auro M., Regelous M. and Walker J. (2017). Thallium isotopes as tracers of recycled materials in subduction zones: Review and new data for lavas from Tonga-Kermadec and Central America. *Journal of Volcanology and Geothermal Research* **339**, 23–40.

Nolin D. (1997). Rétention de radioéléments à vie longue par des matériaux argileux. Influence d'anions contenus dans les eaux naturelles. *PhD thesis*, 219p. Université Paris 6, France.

Peacock C. L. and Moon, E. M. (2012). Oxidative scavenging of thallium by birnessite: Explanation for thallium enrichment and stable isotope fractionation in marine ferromanganese precipitates. *Geochimica et Cosmochimica Acta* **84**, 297–313.

Persson I., Jalilehvand F. and Sandström M. (2002). Structure of the Solvated Thallium(I) Ion in Aqueous, Dimethyl Sulfoxide, *N*,*N*-Dimethylpropyleneurea, and *N*,*N*-Dimethylthiolformanide Solution. *Inorganic chemistry* **41**, 192–197.

Peter A. L. J. and Viraraghavan T. (2005). Thallium: a review of public health and environmental concerns. *Environment International* **31**, 493–501.

Peynet V. (2003) Rétention d'actinide et de produits de fission par des phases solides polyminérales. *PhD thesis*, 256p. Université Paris 6, France.

Poinssot C., Baeyens B. and Bradbury M. H. (1999). Experimental and modelling studies of caesium sorption on illite. *Geochimica et Cosmochimica Acta* **63**, 3217–3227.

Prytulak J., Brett A., Webb M., Plank T., Rehkämper M., Savage P. S. and Woodhead J. (2017). Thallium elemental behavior and stable isotope fractionation during magmatic processes. *Chemical Geology* **448**, 71–83.

Rodríguez-Mercado J. J. and Altamirano-Lozano M. A. (2013). Genetic toxicology of thallium : a review. *Drug and Chemical Toxicology* **36**, 369–383.

Reinoso-Maset E. and Ly J. (2014). Study of major ions sorption equilibria to characterize the ion exchange properties of kaolinite. *Journal of Chemical and Engineering Data* **59**, 4000–4009.

Rehkämper M. and Nielsen S. G. (2004). The mass balance of dissolved thallium in the oceans. *Marine Chemistry* **85**, 125–139.

Savoye S., Beaucaire C., Fayette A., Herbette M. and Coelho D. (2012). Mobility of cesium through the callovo-oxfordian claystones under partially saturated conditions. *Environmental Science and Technology* **46**, 2633–2641.

Shannon R. D. (1976). Revised Effective Ionic Radii and Systematic Studies of Interatomic Distances in Halides and Chalcogenides. *Acta Cryst*. **32**, 751-767.

Shaw D. M. (1952). The geochemistry of thallium. *Geochimica et Cosmochimica Acta* **2**, 118–154.

Tertre E., Beaucaire C., Coreau N. and Juery A. (2009). Modelling Zn(II) sorption onto clayey sediments using a multi-site ion-exchange model. *Applied Geochemistry* **24**, 1852–1861.

Tremel A., Masson P., Sterckeman T., Baize D. and Mench M. (1997). Thallium in French Agrosystems–I. Thallium contents in arable soils. *Environmental Pollution* **95**, 293–302.

Turner A., Cabon A., Glegg G. A. and Fisher A. S. (2010). Sediment–water interactions of thallium under simulated estuarine conditions. *Geochimica et Cosmochimica Acta* **74**, 6779–6787.

Vaněk A., Chrastný V., Mihaljevič M., Drahota P., Grygar T. and Komárek M. (2009). Lithogenic thallium behavior in soils with different land use. *Journal of Geochemical Exploration* **102**, 7–12.

Vaněk A., Komárek M., Vokurková P., Mihaljevič M., Sebek O., Panuskova G., Chrastný V. and Drabek O. (2011). Effect of illite and birnessite on thallium retention and bioavailability in contaminated soils. *Journal of Hazardous Materials* **191**, 170–176.

Vaněk A., Chrastný V., Komárek M., Penížek V., Teper L., Cabala J. and Drábek O. (2013). Geochemical position of thallium in soils from a smelter-impacted area. *Journal of Geochemical Exploration* **124**, 176–182.

Van Olphen H. and Fripiat J. J. (1979). Data handbook for clay materials and other non-metallic minerals: providing those involved in clay research and industrial application with sets of authoritative data describing the physical and chemical properties and mineralogical composition of the available reference materials. *Pergamon Press*, 346p. Oxford, United Kingdom.

Vink B. W. (1993). The behavior of thallium in the (sub) surface environment in terms of Eh and pH. *Chemical Geology* **109**, 119–123.

Voegelin A., Pfenninger N., Petrikis J., Majzlan J., Plötze M., Senn A.-C. and Göttlicher J. (2015). Thallium speciation and extractability in a thallium- and arsenic-rich soil developed from mineralized carbonate rock. *Environmental Science & Technology* **49**, 5390–5398.

Wissocq A., Beaucaire C. and Latrille C. (2017). Ca and Sr sorption on Ca-illite: experimental study and modelling. *Procedia Earth and Planetary Science* **17**, 662–665.

Wissocq A., Beaucaire C. and Latrille C. (accepted). Application of the multi-site ion exchanger model to the sorption of Sr and Cs on a natural sandstone. *Applied Geochemistry*.

Xiao T., Guha J., Boyle D., Liu C. and Chen J. (2004). Environmental concerns related to high thallium levels in soils and thallium uptake by plants in southwest Guizhou, China. *The Science of the Total Environment* **318**, 223–244.

Xiong Y. (2009). The aqueous geochemistry of thallium : speciation and solubility of thallium in low temperature systems. *Environmental Chemistry* **6**, 441–451.

SUPPORTING INFORMATION 1: Parent solutions concentrations used in concentrations isotherms

Table S1: Concentration of parent solutions (stable Tl) used to create ranges of Tl concentrations in batch experiments for concentrations isotherms. Italic and bold values are for solutions where Tl concentrations were measured with HR-ICP-MS Element 2 (Thermo Scientific). Associated errors are measurements uncertainties. For others solutions, errors correspond to propagated uncertainties from parent solutions.

WS batches, [Tl] ($mol.L^{-1}$)	IdP batches, [Tl] ($mol.L^{-1}$)
4.76 ± 0.08 .10^{-4}	***4.76 ± 0.08 .10^{-4}***
2.41 ± 0.04 .10^{-4}	2.37 ± 0.04 .10^{-4}
4.77 ± 0.08 .10^{-5}	4.74 ± 0.08 .10^{-5}
2.40 ± 0.04 .10^{-5}	2.34 ± 0.04 .10^{-5}
4.66 ± 0.08 .10^{-6}	***4.66 ± 0.08 .10^{-6}***
2.35 ± 0.04 .10^{-6}	2.63 ± 0.04 .10^{-6}
4.66 ± 0.08 .10^{-7}	4.67 ± 0.08 .10^{-7}
4.76 ± 0.08 .10^{-8}	3.72 ± 0.06 .10^{-8}

Supporting Information 2: Sorption Kinetics

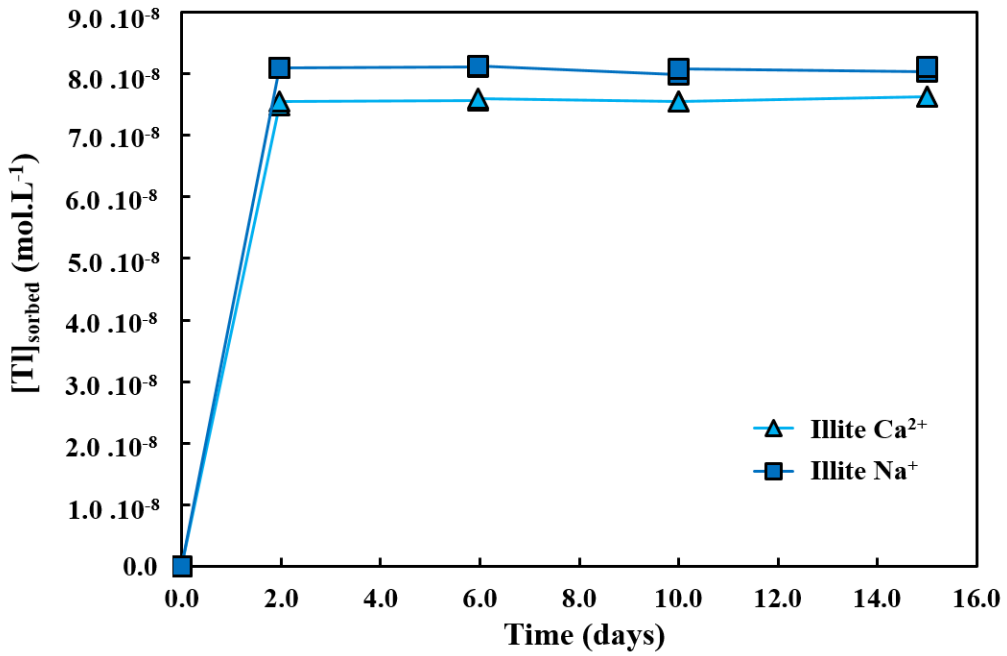

Figure S1: Kinetics of Tl sorption with illite du Puy in $CaCl_2$ and NaCl 10mM. For Na-illite, $[Tl]_{initial}$ = 8.17 ± 0.1 .10^{-8}M and pH = 7.76 ± 0.23. For Ca-illite, $[Tl]_{initial}$ = 8.03 ± 0.23 .10^{-8}M and pH = 7.72 ± 0.11. Error bars are ± 2σ and correspond to uncertainties of measured thallium.

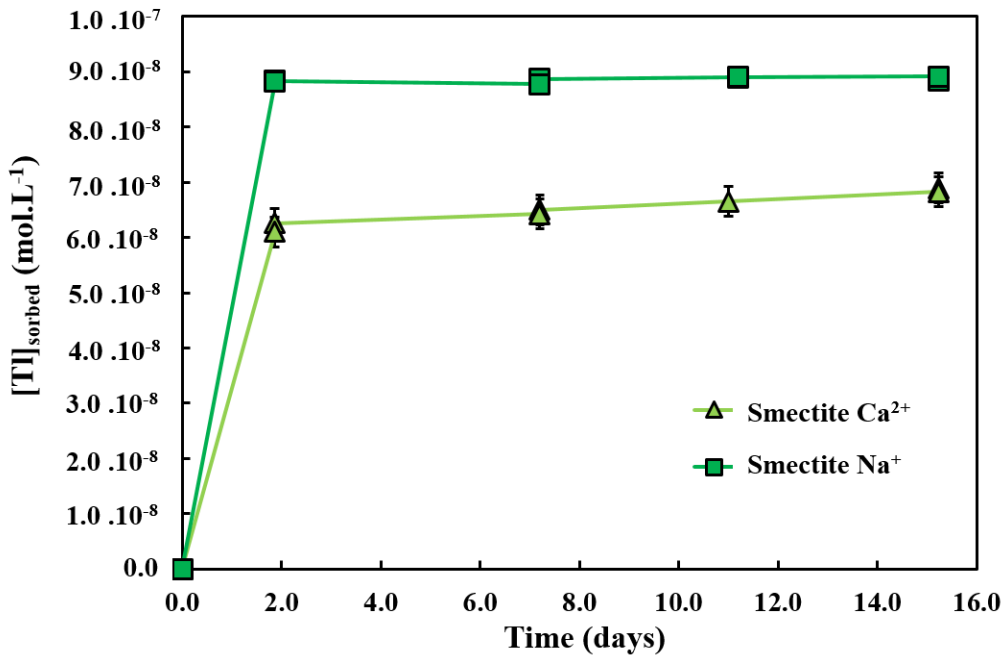

Figure S2: Kinetics of Tl sorption with Wyoming smectite in $CaCl_2$ and NaCl 10mM. For Na-smectite, $[Tl]_{initial}$ = 9.08 ± 0.1 $.10^{-8}$M and pH = 7.57 ± 0.48. For Ca-Sm, $[Tl]_{initial}$ = 9.77 ± 0.27 $.10^{-8}$M and pH = 7.80 ± 0.01. Error bars are ± 2σ and correspond to uncertainties of measured thallium

SUPPORTING INFORMATION 3: Details of equations used in batch experiments

$$A_{ini} = \overline{A_{source}} \times \frac{V_{source,\ added}}{V_{source}} \qquad \text{(Eq. S1)}$$

$\overline{A_{source}}$ (in $Bq.L^{-1}$) is the average activity calculated for the two blanks of a series. V_{source} (in L) correspond to the total volume of the ^{204}Tl in 0.1 M HCL solution. $V_{source,\ added}$ (in L) is the volume of ^{204}Tl in 0.1 M HCl added in each batches. Thallium concentration sorbed ($[Tl]_{sorbed}$ in $mol.kg^{-1}$) onto the clay mineral was also calculated as follow

$$[Tl]_{free,eq} = [Tl]_{t=0} \times \frac{A_{ini}}{A_{sup,eq}} \qquad \text{(Eq. S2)}$$

$[Tl]_{free,eq}$ is the thallium concentration in the supernatant. $[Tl]_{t=0}$ (in $mol.L^{-1}$) corresponds to the thallium concentration at the beginning of each experiments.

$$[Tl]_{t=0} = \left[^{204}Tl\right] + \left(\frac{[Tl_{stable}] \times V_{Tl_{stable}}}{V}\right) \qquad \text{(Eq. S3)}$$

[^{204}Tl] corresponds to the thallium concentrations in diluted source solutions (from solutions 1 and 2) in 0.1 HCl. $[Tl]_{stable}$ correspond to stable thallium concentration and $V_{Tlstable}$ is the added volume of this solution.

A_{sorbed} (in Bq.L-1) is calculated as in equation D.

$$A_{sorbed} = A_{ini} + A_{sup,eq} \quad \text{(Eq. S4)}$$

Distribution coefficient during desorption, $K_{d,des}$ is calculated with the same equation as K_d in sorption experiments. Residual activity (A_{res}, in Bq.L^{-1}) from the solution remaining in the hydrated clays (V_{res} in L) was calculated as follow in equation D.

$$A_{res} = A_{mes} \times V_{res} \quad \text{(Eq. S5)}$$

$$[Tl]_{desorbed} = \frac{Tl_{released}}{V_{des}} + \left([Tl]_{t=0} - [Tl]_{free,eq}\right) \times \left(\frac{A_{sup,eq,des}}{A_{ini,des}} - A_{res}\right) \quad \text{(Eq. S6)}$$

$[Tl]_{desorbed}$ and is in mol.L^{-1}. $Tl_{released}$ (in mol) is the amount of thallium released from the clay, which was initially present (see section 2.4) normalized with the mass m (in kg) of clay for each batch. V_{des} (in mol.L^{-1}) is the volume of bulk solution for each batch during desorption. $[Tl]_{t=0}$ (in mol.L^{-1}) and $[Tl]_{free,eq}$ (in mol.L^{-1}) are respectively the initial thallium concentration and the free thallium concentration at equilibrium both during sorption experiments. $A_{sup,eq,des}$ (in Bq.L^{-1}) is the measured activity of ^{204}Tl in the supernatant at desorption equilibrium. It is calculated with the same formula as in equation 2. $A_{ini,des}$ (in Bq.L^{-1}) is calculated as follow:

$$A_{ini,des} = A_{sorbed} + A_{res} \quad \text{(Eq. S7)}$$

$[Tl]^*_{desorbed}$ is the amount of desorbed thallium in mol.kg^{-1} of material. It is calculated as in equation G:

$$[Tl]^*_{des} = K_{d,des} \times [Tl]_{desorbed} \quad \text{(Eq. S8)}$$

SUPPORTING INFORMATION 4: Calculation of selectivity coefficient in respect to Na^+ and Ca^{2+}

$$K^{*i}_{Tl^+/Na^+} = K^{*i}_{Tl^+/H^+} / K^{*i}_{Na^+/H^+} \quad \text{(Eq. S9)}$$

$$K^{*i}_{2Tl^+/Ca^{2+}} = 2\, K^{*i}_{Tl^+/H^+} / K^{*i}_{Ca^{2+}/2H^+} \quad \text{(Eq. S10)}$$

SUPPORTING INFORMATION 5: Comparison to other Tl bearing phases

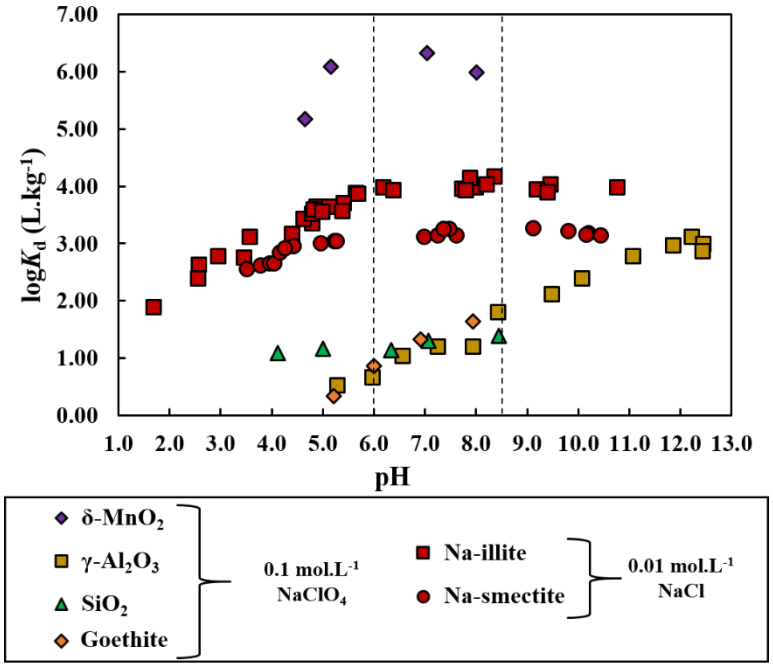

Figure S3: Thallium sorption onto different mineral phase function of pH. SiO_2, δ-MnO_2 and γ-Al_2O_3 data are from Bidoglio *et al*. (1993) and goethite is from Liu *et al*. (2011). Total thallium concentrations in those bacth experiments was 1.2 .10^{-7} mol.L^{-1}. Illite and smectite data are from this study. Dashed lines correspond to the range of natural waters pH (freshwater + seawater).

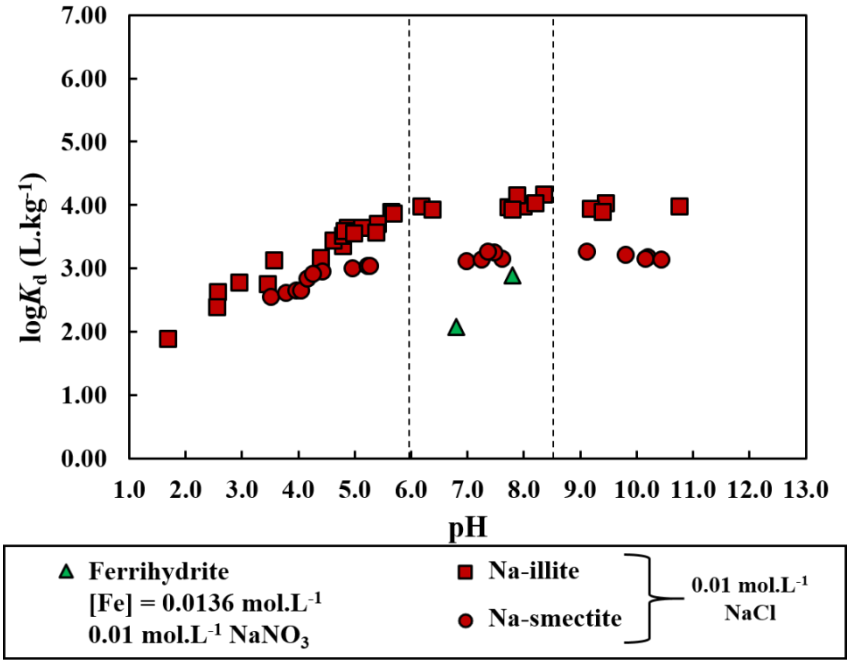

Figure S4: Thallium sorption onto ferrihydrite (Casiot *et al*., 2011 and clay minerals of pH. Dashed lines correspond to the range of natural waters pH (freshwater + seawater).

REFERENCES

Bidoglio G., Gibson P. N., O'Gorman M. and Roberts K. J. (1993). X-ray absorption spectroscopy investigation of surface redox transformations of thallium and chromium on colloidal mineral oxides. *Geochimica et Cosmochimica Acta* **57**, 2389–2394.

Casiot C., Egal M., Bruneel O., Verma N., Parmentier M. and Elbaz-Poulichet F. (2011). Predominance of Aqueous Tl(I) Species in the River System Downstream from the Abandoned Carnoulès Mine (Southern France). *Environmental Science & Technology* **45**, 2056–2064.

Liu J., Lippold H., Wang J., Lippmann-Pipke J. and Chen Y. (2011). Sorption of thallium(I) onto geological materials: Influence of pH and humic matter. *Chemosphere* **82**, 866–871.

Chapter IV: Limits of MnO_2-DGT for measuring radium in aquatic environments

Martin Loïc A.[1], *Simonucci Caroline*[2*], *Benedetti Marc F.*[1], *Gourgiotis Alkiviadis*[3], *Rad Setareh*[4], *Viollier Eric*[1]

[1]Institut de Physique du Globe de Paris – USPC- UMRCNRS7154, Paris, France

[2]IRSN/PSE-ENV/SIRSE/LER-Nord, BP 17, 92262 Fontenay aux Roses Cedex, France

[3]IRSN/PSE-ENV/SEDRE/LELI, BP 17, 92262 Fontenay aux Roses Cedex, France

[4]BRGM, Orléans France

* Corresponding author. *E-mail address:* caroline.simonucci@irsn.fr

Article en preparation pour soumission dans Applied Geochemistry

1. RESUME

Durant leur extraction, les gisements de charbon, de phosphate et d'uranium sont sources de radium pour l'environnement. A proximité de ces sites, les concentrations en radium peuvent être supérieures de plusieurs ordres de grandeurs au fond géochimique. La surveillance du radium dissous dans l'environnement requiert des traitements préliminaires ainsi qu'un conditionnement spécifique de l'échantillon et, dans le cas de la mesure par spectrométrie gamma, de long temps de comptage. De plus, d'importants volumes d'échantillon (1 to 100L) sont nécessaires pour pré-concentrer l'espèce dissoute que ce soit par co-précipitation ou par adsorption sur des résines échangeuses d'ions. Dans le but de remédier à ces contraintes et d'améliorer la mesure du radium dans les systèmes aquatiques, il a été testé dans cette étude l'efficacité d'un capteur de type DGT utilisant MnO_2 comme couche accumulatrice dans plusieurs environnements aquatiques. La première étape a été de tester les potentiels effets de compétition dans différentes matrices en laboratoire. Ensuite, le comportement de la phase accumulatrice en condition d'anoxie a été testé dans le Lac Pavin en France. Enfin un modèle numérique a été adapté pour prévoir la réponse du capteur aux signaux transitoires de concentrations Les résultats montrent qu'un important effet de compétition avec les ions majeurs, empêche la pré-concentration du radium par le DGT. De plus, la phase accumulatrice en dioxyde de manganèse (MnO_2) est soumise à la réduction de Mn qui entraîne une perte de l'agent fixateur en condition anoxique. Dans ces conditions, l'adsorption du radium devient impossible. Enfin, il semble que les DGT soient capables d'enregistrer aussi bien des signaux transitoires de concentration que des signaux constants. Cependant, le temps de déploiement et la qualité de l'agent chélateur sont des paramètres à ne pas négliger lors de leur utilisation. Cette étude a donc permis de démontrer que les oxydes de manganèse n'étaient probablement pas le meilleur agent chélatant à utiliser pour le DGT appliqué à la mesure du radium dans l'environnement.

2. ABSTRACT

Coal, phosphate or uranium ores are sources of radium (Ra) during extraction and in these areas, radium concentrations can be three orders of magnitude higher than the background level (close to 1 $fmol.L^{-1}$). Environmental monitoring of dissolved radium requires preliminary treatment, a specific conditioning of the sample and in some cases gamma spectrometry long counting time is required. Besides, large volumes of sample (1 to 100 L) are required to pre-concentrate the dissolved species by co-precipitation or adsorption onto different types of ion exchange resins. In order to overcome these issues and improve radium measurements in aquatic systems, this study tested the efficiency of Diffusive Gradient in Thin films (DGT) devices using MnO_2 as a trapping layer in various aquatic environments. The first step was to test possible competition effects and the capacity of the binding agent in laboratory with different aqueous matrices. Then the redox response of the device was tested in Pavin Lake (France). This study also focused on the Ra-DGT response to transient signals, as it can be used in dynamic aquatic systems. It seems that there is a strong matrix effect inhibiting radium enrichment onto Ra-DGT and under anoxic conditions Ra-DGT binding agent seems to be affected by manganese reduction, which induces a loss of Mn-oxides. No radium adsorption was possible there. These results appear as major drawbacks. Nevertheless, according to our model, Ra-DGT design is appropriate to record steady or transient radium concentration signals in aquatic environments. This work shows that MnO_2 may not be the best chelating agent to use for Ra-DGT in natural environments or it should be restricted to specific environments with very soft and oxic water conditions.

3. INTRODUCTION

In mining areas, especially where coal, phosphate or uranium ores are extracted, radium concentrations can be three order of magnitude higher than the background level (close to 1 $fmol.L^{-1}$; Azouazi *et al.*, 2001; Pluta, 2001; Vandenhove *et al.*, 2006; Carvalho *et al.*, 2007; Chaplunik & Wysocka, 2008; Cuvier *et al.*, 2015). ^{226}Ra is the most abundant radium isotope and due to its radiotoxicity (St-Amant *et al.*, 2011; Jia & Jia, 2012) and to its carcinogen daughter isotope (^{222}Rn) has become a targeted element in mining monitoring (Vinson *et al.*, 2009). Existing speciation studies tend to demonstrate that free Ra^{2+} and labile complexes are the dominant forms of radium in aquatic systems (Sturchio *et al.*, 2001; Martin *et al.*, 2003; Almeida *et al.*, 2004; Manakhov & Egorova, 2014).

To analyze ^{226}Ra, large volumes of sample (1 to 100 L) are required to pre-concentrate the dissolved species by co-precipitation or adsorption onto different types of ion exchange resins (Moon *et al.*, 2003; Decaillon *et al.*, 2004; Waska *et al.*, 2008; Van Beek *et al.*, 2010; Jia & Jia, 2012). To facilitate sample pretreatment and to increase the number of measurements in impacted watersheds or to collect data from compartments where sample volume is low (sediment, soil, hyporheic zone), a DGT (Diffusive Gradient in Thin-films) probe, which consists of a gel combined to a chelating gel, was designed according to the DGT theory (Davison & Zhang, 1994; Zhang & Davison, 1995; Harper *et al.*, 1998). The DGT technique was already applied to trace metals monitoring and more recently to radium by using a MnO_2 trapping layer (Leermakers *et al.*, 2009; Gao *et al.*, 2010; Leermakers *et al.*, 2016). These previous studies showed that MnO_2 can sorb specifically radium in natural waters and soils, and it was first tested in (Leermarkers et al., 2009) as a chelating agent for DGT development. Another advantage of MnO_2 shown in (Leermarkers et al., 2009) is to pre-concentrate specifically radium over barium or strontium which could interfere at m/z 226 in HR-ICP-MS measurements (Leermakers *et al.*, 2009). In these previous studies (Leermakers *et al.*, 2009; Gao *et al.*, 2010; Leermakers *et al.*, 2016) the type of MnO_2 that was used was not detailed, so we choose to precipitate MnO_2 directly in the gel and we have tested the limitation of the DGT theory of these devices under our field conditions (redox conditions, competition effect, binding agent capacity, and the monitoring at different time scales).

In small watershed, some events such as heavy rain during a storm could modify metal concentrations from a steady state to transient signal (Gu *et al*., 2008; Ward *et al*., 2012). For instance, big amount of metals could be re-suspended from an external sources and a contamination plume could be release in the system. On the contrary, heavy rains could dilute the signal. In both examples, metal concentrations vary and are not stable at a small time scale. Many models were developed to describe and interpret DGT's functioning (DIFS: Harper *et al*., 2000; 2D-DIFS: Sochazcewski *et al*., 2007; DGT-PROFS: Ciffroy *et al*., 2011), but they focused either on processes inside the sensor (Mongin *et al*., 2011, 2013; Galceran & Puy, 2015) or when DGTs are deployed in soils (Ernstberger *et al*., 2002; Letho *et al*., 2006a). But scarce studies were published to describe the behavior of the sensor regarding transient signal concentrations in bulk solution (Letho *et al*., 2006b; Puy *et al*., 2016).

The aims of the present study are (i) to develop a DGT probe to assess radium *in-situ*, in different natural waters from rivers to pore water. The probe is required to work over a wide range of pH, in different matrices and under anoxic conditions and above all, with small volume of water. The use of a nano-dispersed MnO_2 in agarose gel presents the advantage of being cheap, easy to prepare, and highly adaptable to many DGT geometry. And (ii) to answer another major question in the use of DGTs in dynamic aquatic systems (rivers, etc.): does the sensor respond to transient signals (Allan *et al*., 2007; Davison & Zhang, 2012, 2016)?

4. MATERIALS AND METHODS

4.1. Gel preparation

DGT probe consisted of an agarose (1.5 wt %; VWR Chemicals) diffusive layer and a layer composed with nano-MnO_2 included in agarose (2.5 wt %) gel. The trapping layer is composed of 0.1 $mol.L^{-1}$ potassium permanganate (Merck) solution mixed with a heated agarose solution (2.5 wt % at roughly 70°C). The aim is to reduce $KMn^{VII}O_4$ to $Mn^{IV}O_2$ dispersed nano-cristal with agarose as electron donor. Then, 2 mL of the mix between trapping layer and diffusive layer solution were poured directly in Petri dishes (diameter 34 mm) until cooling, sedimentation of the trapping agent and solidification of agarose. A PVDF filter was used to protect the gel when deployed *in situ*.

4.2. Laboratory tests

DGT devices were set in different mineral spring waters in order to investigate their selectivity against competitor ions. To this end, three different natural waters were spiked with radium (EB95 Eurostandard, Czech Metrology Institute) to obtain a final radium concentration of $2.0.10^{-13}$ mol.L^{-1}. Natural water from Volvic®, Evian® and Hépar® commercial springs and ultrapure water (milli Q; Millipore) were used (composition in table 1).

Table 1: Composition of mineral spring waters used in experiments. Concentrations are in mmol/L.

	Ca^{2+}	Mg^{2+}	Na^{+}	K^{+}	Ba^{2+}	SO_4^{2-}	HCO_3^{-}	NO_3^{-}	Cl^{-}	F^{-}
Volvic®	0.287	0.329	0.505	0.159	$2.0.10^{-4}$	0.084	1.130	0.102	0.381	0.012
Evian®	1.996	1.069	0.283	0.026	$2.0.10^{-4}$	0.146	5.900	0.061	0.282	< D.L
Hépar®	13.698	4.896	0.618	0.105	$2.0.10^{-4}$	15.927	6.289	0.069	0.530	0.021

Triplicates were immerged and agitated in each tank, with a total volume equal to 1L, corresponding to one type of water, during 24 hours at room temperature (22.0 ± 1.0 °C). pH was adjusted to 6.0 ± 0.1 with Suprapur HNO_3 (Merck) in order to be as close as natural waters conditions. After 24 hours, triplicates were removed from each tank, MnO_2 gels were isolated and dissolved in 4.0 mL of 0.22 mol.L^{-1} HNO_3 (diluted from distilled HNO_3) during additional 24 hours prior analysis using an HR-ICP-MS Element 2 (Thermo Scientific®). For each DGT, a Ra pre-concentration factor was defined with the quotient of radium concentration in dissolved residue (ready for analysis) over radium concentration in tank. As each media contains triplicates a Ra mean pre-concentration factor (Ra-MPF) was calculated with an arithmetic average of the three Ra pre-concentration factors.

4.3. Radium measurement

Radium was measured with an HR-ICP-MS Element 2 (Thermo scientific) in a white room with a solution of ^{115}In 5 ppb as internal standard. For each samples, 9 measurements in a row are done (3 x 3 passes, Appendix 1, table A1) in two resolutions, low and medium.

At low resolution, three main polyatomic interferences could interfere at m/z 226: $^{208}Pb^{18}O$, $^{138}Ba^{88}Sr^{+}$ and $^{186}W^{40}Ar$. $^{138}Ba^{88}Sr^{+}$ is problematic due to the abundance of barium in natural water (Leermakers *et al.*, 2009) and its behavior similar to radium in the environment. However,

the interference occurs above 1 ppm of total barium (Appendix 1, Table A2). The $^{186}W^{40}Ar$ interference was also observed after 1 ppm of tungsten in matrix solution (Park *et al.*, 1999). In this study, no lead or tungsten was present in tested solution and the only sources of barium and strontium were from standard solution but diluted during experiment. Then, no interference is observed due to matrix solution.

Then, only results in low resolution were used in this study. Concentrations are corrected from signal derivation by internal standard. An IRSN (Institut de Radioprotection et de Sureté Nucléaire, Fontenay aux Roses, France) certified standard was used for ^{226}Ra HR-ICP-MS analysis validation. Limit of quantification (in low resolution) was $3.0 .10^{-14}$ mol.L^{-1} for Ra. More details of HR-ICP-MS measurement for Ra can be found in supporting information (Appendix 1, table A1).

4.4. Redox effect test

MnO_2 binding layer stability regarding redox conditions was tested in a meromictic lake (Pavin Lake, Puy de Dôme, France), which has a deep sulfidic anoxic layer all year long (Alberic *et al.*, 2000; Buka-Nakic *et al.*, 2009) beneath 60 meters depth (Michard *et al.*, 1994; Viollier *et al.*, 1995). It was tested at 30 m depth (oxic) and 60 m depth (anoxic) in April 2016, and kinetic experiments were conducted during about 24h. Concerning kinetic experiments, an assumption was made of a decrease of manganese IV in MnO_2 binding layer driven by manganese reduction (as describe in equation 1). Thus, a first order kinetics law was defined (equation 2).

$$Mn^{4+} + 2e^- \leftrightarrow Mn^{2+} \quad (1)$$

$$[Mn^{4+}](t) = [Mn^{4+}]_{t=0}\exp^{-kt} \text{ with } \ln[Mn^{4+}] = -k^{Mn}t + \ln[Mn^{4+}]_{t=0} \quad (2)$$

It is then possible to calculate a kinetic constant k for MnO_2 binding layer reduction function of time and depth.

One set of four sensors was not immerged and was used as reference for the manganese concentrations at the beginning of the deployment. Remaining manganese was totally extracted from Ra-DGTs by HNO_3 0.1 mol.L^{-1} and measured with an ICP-AES ICAP 6200 (Thermo scientific) after appropriate dilution.

5. MODELLING

5.1. Theory

Transport of species in diffusive gradient in thin-films occurs solely by molecular diffusion according to Fick's Law (Letho *et al*., 2006b; Mongin *et a*l., 2013), either in the diffusive layer or in the resin layer (Letho *et al*., 2006b; Mongin *et al*., 2013). In addition to transport, chemical reactions may affect species concentration function of time. Thus, solute concentration evolves as follow:

$$\frac{\delta C}{\delta t} = D_{s\_m}\frac{\delta^2 C}{\delta x^2} + R_E \qquad (3)$$

where R_E is the reaction term which obey to a first order kinetics. D_{s_m} is the diffusion coefficient of species (s) in a medium (m) in $m^2.s^{-1}$. This coefficient is specific for each species in a given medium and is temperature dependent. x is the location of species in the gel and depends of the object geometry. In this study, an element is modeled with two species. M represents the mobile one. It diffuses through both diffusive and resin layers and M gathers all labile species of solute that can diffuse through gel pores (Uribe *et al*., 2011). MR is the immobile complex made between M and the resin R. R describes the immobile resin binding sites. Thus, in the resin layer, complexation reactions between the mobile species (M) and resin binding sites (R) would depend of the affinity for the resin and the available binding sites. The latest is given by R concentration and can be adjusted.

In the diffusive layer, the time to reach steady state specific to DGT depends on Ds_m and the rate of the complexation reaction. Equation 3 expresses the equilibrium between concentrations during complexation in the resin layer:

$$\mathrm{M} + \mathrm{R} \leftrightarrow \mathrm{MR} \qquad (4)$$

$$\frac{[\mathrm{MR}]}{[\mathrm{M}][\mathrm{R}]} = K_{\mathrm{R}} = \frac{k_f}{k_{diss}} \qquad (5)$$

Concentrations are in $mol.L^{-1}$. k_{f_r} ($L.mol^{-1}.s^{-1}$) is the complex formation rate constant and k_{diss_r} (s^{-1}) is the complexation dissociation rate constant. K_R ($L.mol^{-1}$) is the complex stability constant and defines M affinity for the resin. R and MR are immobiles (Letho *et al*., 2006b) and

thus, belong only to the resin domain. Their concentrations evolve with time only by complex formation/dissociation. On the contrary, M is mobile in all domains. Reactive transport equations for each species are described in table 2.

Table 2: Equations describing the behavior of the solute M, the Resin R,the complex resin-solute MR in the gel and resin domains during modelling.

Species	Domain geometry	Equation	N°
M is diffusive gel	$0 < x < x_1$	$\frac{\partial[M_x]}{\partial t} = \frac{\partial}{\partial x}\left(D_{M\_gel}\frac{\partial[M_x]}{\partial x}\right)$	5
M in resin	$x_2 < x < 0$	$\frac{\partial[M_x]}{\partial t} = k_{diss}[MR_x] - k_f[M_x][R_x] + \frac{\partial}{\partial x}\left(D_{M\_gel}\frac{\partial[M_x]}{\partial x}\right)$	6
R in resin	$x_2 < x < 0$	$\frac{\partial[R_x]}{\partial t} = k_{diss}[MR_x] - k_f[M_x][R_x]$	7
MR complex in resin	$x_2 < x < 0$	$\frac{\partial[MR_x]}{\partial t} = k_f[M_x][R_x] - k_{diss}[MR_x]$	8

3.2. Designed and boundary conditions

The DGT was represented by 1D geometry (unit is in meter), divided in two domains with three boundaries (fig. 1). On a line, 0 is the interface between the gel and the resin domains. This boundary is open and the flux of solute in the gel is equal to the flux in the resin and *vice versa*. Between 0 and x_1 (x_1>0), is the gel domain corresponding to the diffusive layer of the DGT (fig. 1). The interface between the gel domain and the bulk solution in x_1, corresponds to the entry point of any solutes in the modeled sensor (fig. 1). Finally, the domain defines between 0 and x_2 (x_2<0) is the resin layer. In x_2, the boundary is closed and and no flux of solute is allowed. x_1 and x_2 can be adjusted as wanted to create various DGT geometries (fig. 1). Both the gel and the resin domains are considered as water and consequently, water diffusive coefficients are applied. Diffusion in the resin equals to diffusion in the gel ($D_{M\_gel} = D_{M\_resin}$), hence diffusive coefficient is $5.0 .10^{-10}$ $m^2.s^{-1}$ (Letho *et al*., 2006b).

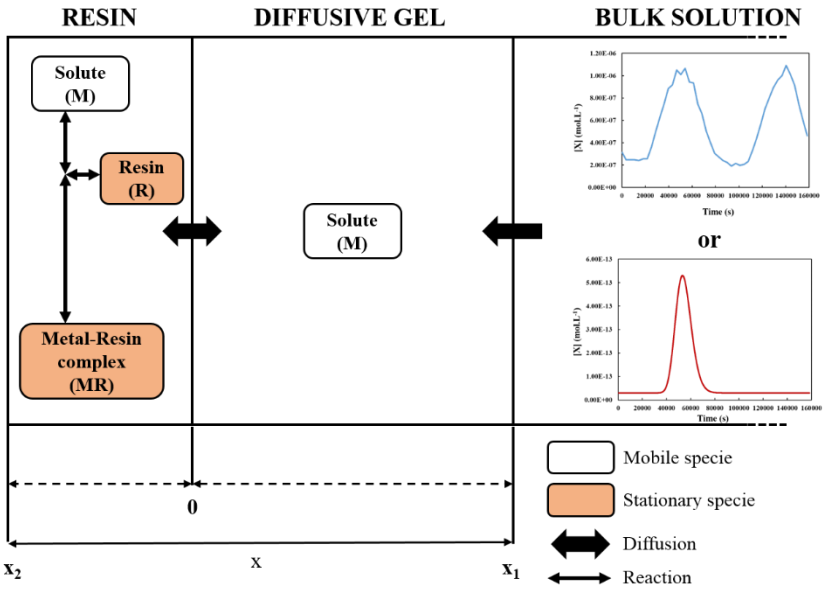

Figure 1: Simplified representation of the DGT model used in this study

In order to assess the impact of transient signal, three kinds of functions were used as entry at point x_1 (fig. 1). A steady function was used to compare the model outputs to DGT theory as defined in Davison and Zhang (1994). Then, two transients function were computed. The first one is taken from Borrok *et al.* (2008) and represents the evolution of solute in trace concentrations in a polluted river. The second signal is defined to model the evolution of a solute concentration in a small watershed when a contaminant plume passes through. Functions and equations are summarized in appendix 2. The first signal, extracted from Borrok *et al.* (2008), displays ranges of concentrations for zinc (between roughly 10^{-7} to 10^{-6} mol.L^{-1}). The second type of transient signal was designed with radium- range of concentrations (between 10^{-14} to 10^{-12} mol.L^{-1}). The shape of the signal is also different. The Zn-type signal is related to natural variations (Borrok *et al.*, 2008). The second signal is designed to represent a plume of contamination. As results, the DGT sensitivity to transient signal was studied in a wide range of trace metal concentrations.

5.3. Software and model solution

COMSOL Multiphysics® version 5.0 with "Chemical Reaction Engineering" module and "Transport Species in Porous Media" was used. An optimization procedure was carried out to determine the most accurate mesh and the most efficient step time. The mesh was fixed at 10^{-6}

cm in the resin domain whereas it was fixed at 10^{-3} cm in the gel domain. The step time was fixed at 1000 seconds. The total time of calculation was adjusted to the time definition of the concentration input.

5.4. Tested hypothesis and outputs

During modeling, various parameters were changed. Firstly, in order to assess the role of the solute affinity for the resin, multiple complex (resin-solute) stability constants were tested (table A7, appendix 2). Secondly, the resin site density was investigated with three [R] values 100, 50 and 1 mol.m^{-3}. The highest corresponds to Chelex (Letho *et al*., 2006b), the second is a fictive value and the lowest is similar to Mn concentrations in the reactive layer tested in this study.

6. RESULTS AND DISCUSSION

6.1. Binding agent capacity test:

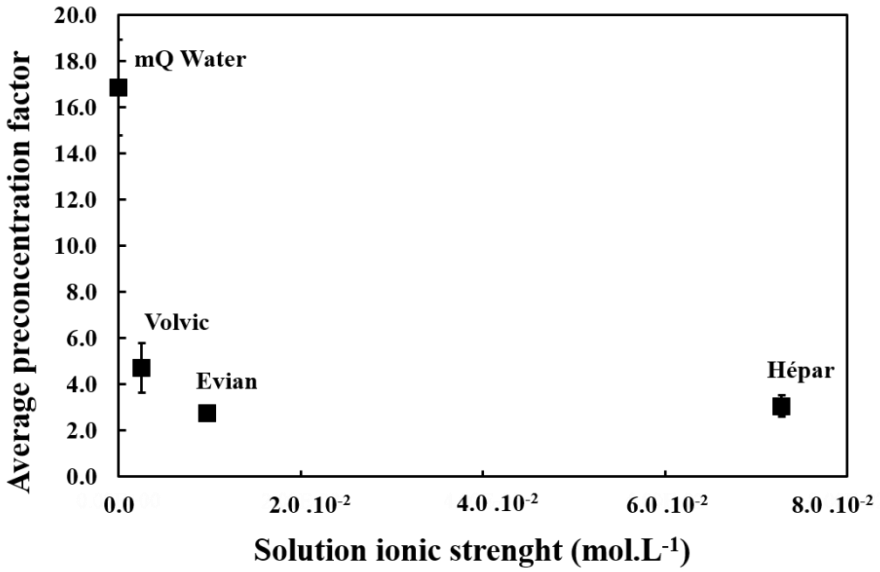

Figure 2: Measured evolution of radium average pre-concentration factor (APF) in various natural waters (Hépar® and Evian® springs) and milliQ® water. Error bars equal standard deviation of triplicates.

In order to test the capacity of the binding agent for Ra, Mn-oxides were exposed to different analytes, until equilibrium was reached. The effective binding capacity is determined in the presence of potentially competing ions (e.g. HCO_3^-, H^+, SO_4^{2-}, etc.), which can compete for

binding sites and reduce the number available (Bennett *et al*., 2016). Mn-oxides were tested in various matrices: milliQ® water, Evian® water, Volvic® water and Hépar® water. The composition of these matrices is well known (table 1). Hépar® water is the hardest water (table 1) followed by Evian®, Volvic® and milliQ® water as the opposite end-member.

Figure 2 presents the evolution of radium average pre-concentration factor (APF) in the different matrices and it clearly shows that Ra is fixed on Mn-oxides in milliQ® water (around 17 APF), whereas for all other matrices Ra-APF is rather low, between 3 and 5. Hence, Ra is not specifically bound to the Mn-oxides when the matrix is complex. Volvic® water contains fewer ions than the two other mineral waters which can explain that its Ra APF is slightly higher. But this test cannot determine which ion is responsible for the competition effect. For radium, contradictory matrix effects were also observed in (Varga, 2007). The amount of trapped radium onto MnO_2 was the same in seawater and in ultra-pure water. However, pH was optimized to 8, as it is the best pH for radium adsorption onto manganese oxides (Varga, 2007). On the contrary, matrix effects were observed in brine or in ion-charged water (Nelson *et al.*, 2014) and divalent cations were pointed as main competitors (Kiro *et al.*, 2012; Nelson *et al.*, 2014). MnO_2 seems to efficiently trap radium only with important volumes of water (Varga, 2007; Kiro *et al.*, 2012; Nelson *et al*., 2014) and under optimized environmental condition (in term of pH for instance), which is hardly compatible with natural environments. According to our results Mn-oxides may not be the best binding agent for Ra pre-concentration in natural waters. 6.2. Redox effect on MnO_2 binding layer stability (Pavin Lake, France)

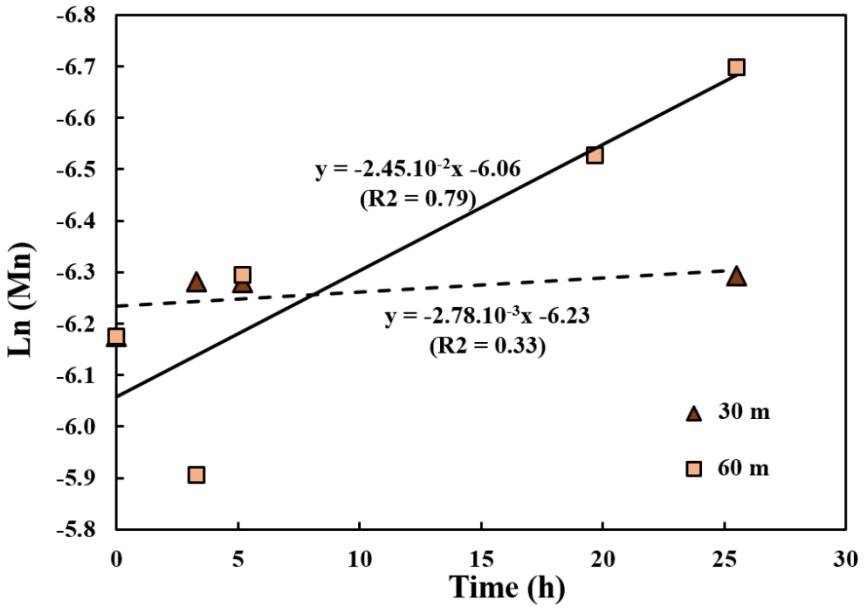

Figure 3: Evolution of Neperian logarithm of manganese concentrations (mol.L^{-1}) with time in Lake Pavin experiment. Error bars are included in the symbols

Mn-oxides (MnO_2) binding layer stability regarding redox conditions was tested in Pavin Lake (France). Ra-DGTs were deployed in the water column at two different depths, 30 m (oxic) and 60 m (anoxic) in April 2016 (fig. 3). Ra-DGTs deployed at 30 m depth (oxic part) showed constant Mn concentrations with time (fig. 3) and a brownish color (fig. 4), whereas Mn concentrations obtained at 60 m depth, in the anoxic part of the lake, increased (fig. 3) with time and retrieved Ra-DGTs were orange (fig. 4). These results can be explained by a difference of behavior according to the oxygen conditions. The loss of the dark brownish color, in comparison with blank Ra-DGT sample, under the oxic-anoxic interface certainly shows the loss of MnO_2 binding agent from the gel. In Pavin Lake, it was shown by Viollier *et al*. (1995) that there is a large enrichment of the lower layer in dissolved manganese (Mn^{2+}), which means that in the lower layer reduction of Mn-oxides take place. In Pavin Lake lower layer (below 60 meters depth) different studies showed a lack of dissolved oxygen and the presence of a sulfidic anoxic layer all year long below 60 meters (Michard *et al.*, 1994; Viollier *et al.*, 1995, Alberic *et al*., 2000; Buka-Nakic *et al.*, 2009.

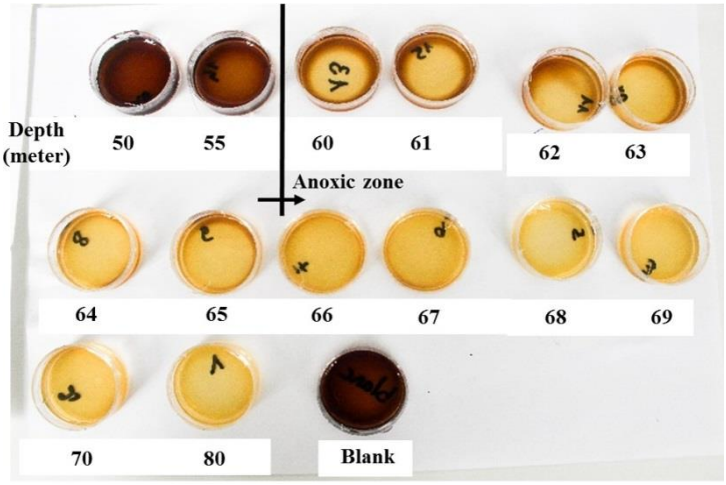

Figure 4: Ra-DGT coloration changes with depth. Disappearance of MnO_2 binding agent in Ra-DGTs at the oxic-anoxic interface (60 meters depth), after 24 hours in the Pavin Lake water column in April 2015 (courtesy of E. Lascar).

The fact that there is a redox interface, transition from oxic to anoxic condition, can explain the reduction of MnO_2 in dissolved Mn^{2+} (Patrick & Henderson, 1980; Stumm & Morgan, 1995). According to several studies, sulfide can also reduce abiotically or biotically Mn-oxides (Ghiorse, 1988; Nealson *et al*., 1989; King, 1990; Ehrlich, 1990; Lovley, 1991; Gounod, 1994; Stumm & Morgan, 1995). Another parameter to consider is the presence of ferrous iron (Fe^{2+}) in the lower part of the Lake (Viollier *et al*., 1995) and according to (Lovley & Phillips, 1988; Golden *et al*., 1988; Ghiorse, 1988; Ehrlich, 1990; Lovley, 1991; Gounod, 1994) it can be responsible for Mn-oxides reduction (biotic or abiotic pathways). It is quite unlikely that Mn-oxides are biotically reduced in agarose gel because agarose gel pores are around 74 nano-meters (Fatin-Rouge *et al*., 2004; Narayanan *et al*., 2006; Labille *et al*., 2007; Davison & Zhang, 2016) and so no bacteria can go through. The most likely assumption is that Mn-oxides are reduced via abiotically reduction pathways catalyzed mainly by sulfide and ferrous irons and by the lack of dissolved oxygen (redox interface). The loss of Mn-oxides binding layer would hence preclude to any radium enrichment/accumulation onto its surface. The use of Ra-DGT based on MnO_2(s) is not recommended in anoxic environments

6.3. Transient signals

The figures (Fig. 5A, 5B, 6A, 6B) clearly show that less solute is accumulated with decreasing K_{resin} values. The "ideal behavior" according to Fick's law represented in Figures 5 and 6 corresponds to the total accumulation over tested time according to DGT theory from Davison and Zhang (1994). A slope lower than the perfect sink indicates that an amount of solute, which diffuses through the gel, is not bind to the chelating agent (Puy *et al*., 2016). In cases described in Figures 5 and 6, the complex stability is too weak and a fraction of the solute diffuses out of the binding layer to the outer media. However this effect is limited to low K_{resin} ($\leq 10^6$ $L.mol^{-1}$) and when the stability constant for the complex resin-solute is higher (Appendix 2, Table A6), the accumulation of solute is equal (within 5 % of incertitude) to the expected value (perfect sink). These results are consistent with Letho *et al*. (2006b) and Puy *et al*. (2016). Moreover, it appears that the site density of the binding agent enhanced the limited Ra-accumulation at low K_{resin} (fig. 5B) but the effect is no more relevant for higher constants. Such a result highlights the need to choose carefully the binding-agent/solute couple to avoid any low estimate of Ra-accumulation.

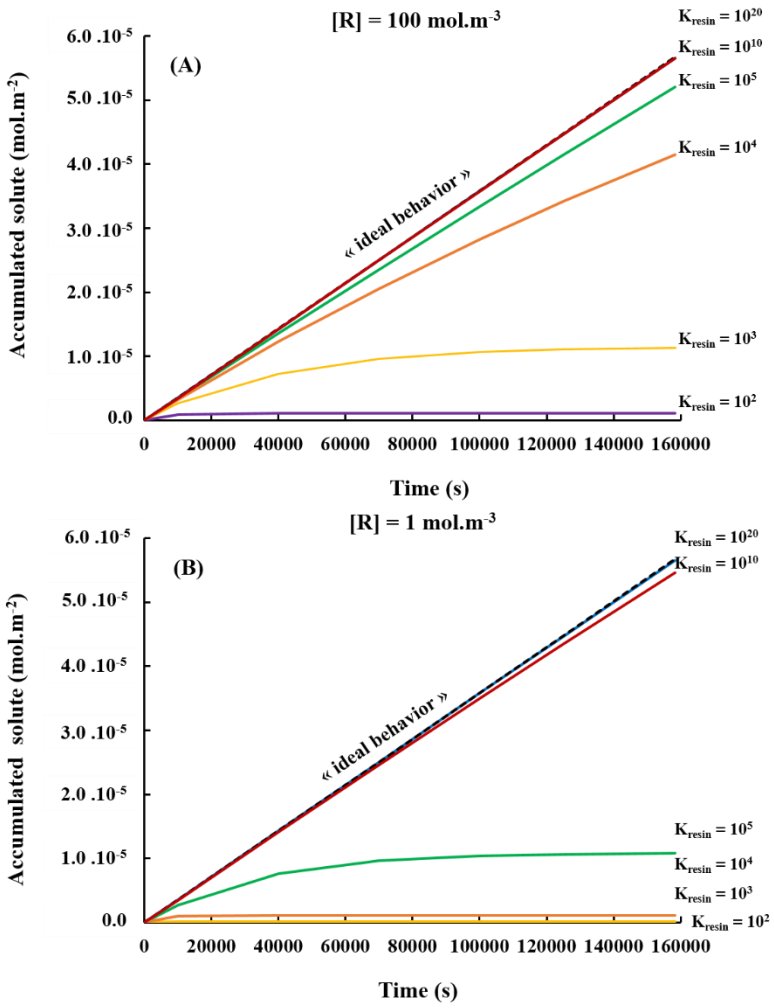

Figure 5: Outputs for the steady function ($y = 5.73.10^{-4}$). (A) Amount MR species (or solute accumulated) in the resin domain with a site density, [R] = 100 $mol.m^{-3}$. (B) Amount MR species (or solute accumulated) in the resin domain with a site density, [R] = 1 $mol.m^{-3}$. The black dashed line represents the "ideal behavior" according to Fick's law and DGT theory from Davison and Zhang (1994). K_{resin} are in $L.mol^{-1}$

Transient signals were tested and results are shown in Figures 6A and 6B. It appears that DGT accumulation is not linear and seems to depend on the shape of the applied signal (fig. 6A). The "ideal behavior" represented in these figures (black dashed lines, fig. 6A and 6B) corresponds to the total accumulation over tested time according to Fick's law. The slopes variations for the modeled scenarios can be explained by a change in the accumulation regime. Indeed, the steady accumulation regime as described in Jimenez-Piedrahita *et al.* (2017) is reached within 600 seconds - this step is not visible in our results because the considered time

scale is bigger (160 000 s) - which means DGTs are sensitive enough. The changing slope recorded in the modeling could be explained by adapting "ideal behavior" to transient signal. In addition, the accumulated solute for the total time of calculation seems to confirm the latest hypothesis (fig 6A).

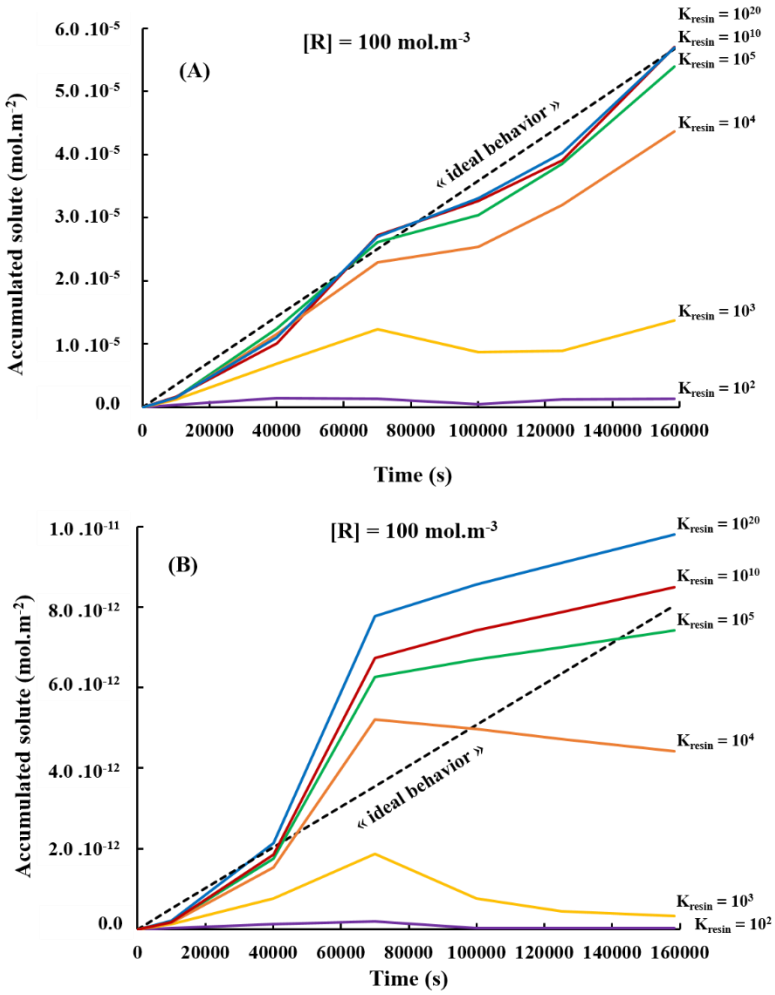

Figure 6: (A) Outputs for the first transient signal (Borrok *et al.*, 2008; appendix 2, fig. A3): Amount MR species (or solute accumulated) in the resin domain with a site density, [R] = 100 mol.m^{-3}. (B) Outputs for the second transient signal (appendix 2, fig. A4): Amount MR species (or solute accumulated) in the resin domain with a site density, [R] = 1 mol.m^{-3}. The black dashed line represents the "ideal behavior" according to Fick's law and DGT theory from Davison and Zhang (1994). K_{resin} are in L.mol^{-1}

DGT device response is clearly affected by transient signals. It seems that the key parameters are the deployment time, the length and intensity of the transient signal, and the site density on

the binding layer. Moreover, DGT can integrate transient signal without over or under estimate Ra-accumulation, if deployment time is long enough to allow DGT to reach the "ideal behavior".

7. CONCLUSIONS

It seems that a strong matrix effect is inhibiting radium transfer to DGT Mn-oxides binding layer and appears as a major drawback to the use of Ra-DGT in many environmental waters. Moreover, Ra-DGT Mn-oxides binding layer is reduced under anoxic conditions, which induces a loss of the binding agent from the agarose gel and so no radium adsorption is possible. Henceforth it is not recommended to use Ra-DGT in anoxic environments. According to our modeling results, Ra-DGT design can record steady and transient radium concentration signals in multiple aquatic environments but it is deployment time and site density dependent. However, these results suggest choosing carefully the binding agent to avoid any low estimate.

In order to use Ra-DGT, it should be restricted to specific environments with very soft and oxic water, soil or sediment conditions. Otherwise, a more radium specific binding agent needs to be investigated. This Ra specific binding agent should work on a range of environmental pH (from 4 to 9) and should not vary with redox conditions. Possible candidates could be crown-ethers fixed on a sulfonic acid cation exchange resin (Chiarizia *et al.*, 2007) or on an organic polymer (L'Anunziata, 2012), or on magnetic nanoparticles (Mesnic *et al.*, 2013). All were investigated for the rapid extraction of ^{226}Ra from water samples. It could be interesting to use it as a binding layer in a Ra-DGT.

ACKNOWLEDGMENTS

We thank Laure Cordier and Michael Tharaud (IPGP) for their analyses. We are grateful to the master students from IPGP for their help during the campaign at Pavin Lake. A special mention to Eric Lascar for his previous work on this topic. We are grateful to Christelle Courbet (INTERA) for her involvement in the project. We also thank IRSN, CEA, BRGM and IPGP for funding this research. Parts of this this work were supported by IPGP multidisciplinary program PARI and by Region Ile de France SESAME Grant no. 12015908.

REFERENCES

Alberic, P., Viollier, E., Jezequel, D., Grosbois, C., & Michard, G. (2000). Interactions between trace elements and dissolved organic matter in the stagnant anoxic deep layer of a meromictic lake. *Limnol. Oceanogr.*, *45*(5), 1088–1096.

Allan, I. J., Knutsson, J., Guigues, N., Mills, G. A., Fouillac, A.-M. & Greenwood, R. (2007). Evaluation of the Chemcatcher and DGT passive samplers for monitoring metals with highly fluctuating water concentrations. *J. Environ. Monit*., *9*, 672–681

Almeida, R. M. R., Lauria, D. C., Ferreira, a. C., & Sracek, O. (2004). Groundwater radon, radium and uranium concentrations in Região dos Lagos, Rio de Janeiro State, Brazil. *Journal of Environmental Radioactivity*, *73*(3), 323–334.

Azouazi, M., Ouahidi, Y., Fakhi, S., Andres, Y., Abbe, J. C., & Benmansour, M. (2001). Natural radioactivity in phosphates, phosphogypsum and natural waters in Morocco. *Journal of Environmental Radioactivity*, *54*(2), 231–242.

Bennett, W. W., Arsic, M., Panther, J. G., Welsh, D.T. & Teasdale, P R. (2016). Binding layer properties. In *Diffusive Gradients in Thin-films for Environmental Measurements*, ed: Davison, W. Cambrige Environmental Chemistry Series, Cambridge University Press, pp. 66-92.

Borrok, D. M., Nimick, D. A., Wanty, R. B., & Ridley, W. I. (2008). Isotopic variations of dissolved copper and zinc in stream waters affected by historical mining. *Geochimica et Cosmochimica Acta*, *72*, 329–344. http://doi.org/10.1016/j.gca.2007.11.014

Bura-Nakić, E., Viollier, E., Jézéquel, D., Thiam, A., & Ciglenečki, I. (2009). Reduced sulfur and iron species in anoxic water column of meromictic crater Lake Pavin (Massif Central, France). *Chemical Geology*, *266*(3-4), 320–326.

Carvalho, F. P., Madruga, M. J., Reis, M. C., Alves, J. G., Oliveira, J. M., Gouveia, J., & Silva, L. (2007). Radioactivity in the environment around past radium and uranium mining sites of Portugal. *Journal of Environmental Radioactivity*, *96*(1-3), 39–46.

Chalupnik, S., & Wysocka, M. (2008). Radium removal from mine waters in underground treatment installations. *Journal of Environmental Radioactivity*, *99*(10), 1548–1552.

Chiarizia, R., Dietz, M. L., Horwitz, E. P., Burnett, W. C., Cable, P. H. (1999). Radium Separation Through Complexation by Aqueous Crown Ethers and Ion Exchange or Solvent Extraction. *Separation Science And Technology*, *34*(6-7).

Ciffroy, P., Nia, Y., Garnier, J.M. (2011). Probabilistic multicompartmental model for interpretating DGT kinetics in sediments. *Environmental Science and Technology*. 45, 9558-9565.

Cuvier, A., Panza, F., Pourcelot, L., Foissard, B., Cagnat, X., Prunier, J., Le Roux, G. (2015). Uranium decay daughters from isolated mines: Accumulation and sources. *Journal of Environmental Radioactivity*, *149*, 110–120.

Davison, W., & Zhang, H. (1994). In-situ speciation measurements of trace components in natural waters using thin-film gels. *Nature, 237*, 546 – 548.

Davison, W., & Zhang, H. (2012). Progress in understanding the use of diffusive gradients in thin films (DGT) – back to basics. *Environmental Chemistry, 9*, 1-13.

Davison, W., & Zhang, H. (2016). Principles of measurements in simple solutions. In *Diffusive Gradients in Thin-films for Environmental Measurements*, ed: Davison, W. Cambrige Environmental Chemistry Series, Cambridge University Press, pp. 10-31.

Decaillon, J.-G., Bickel, M., Hill, C., & Altzitzoglou, T. (2004). Validation of methods for the determination of radium in waters and soil. *Applied Radiation and Isotopes*, *61*(2-3), 409–413.

Ehrlich, H.L. (1990). Geomicrobiology. Marcel Dekker, NY.

Ernstberger, H., Davison, W., Zhang, H., Andrew, T. Y. E., & Young, S. (2002). Measurement and dynamic modeling of trace metal mobilization in soils using DGT and DIFS. *Environmental Science and Technology*, *36*(3), 349–354.

Fatin-Rouge, N., Startchev, K. and Buffle, J. (2004). Size effects on diffusion processes within agarose gels, *Biophysical J.*, 86, 2710-2719.

Galceran, J. & Puy, J., (2015). Interpretation of diffusion gradients in thin films (DGT) measurements: a systematic approach. *Environmental Chemistry*, 12(2), 112-122.

Gao, Y., Baeyens, W., De Galan, S., Poffijn, A., & Leermakers, M. (2010). Mobility of radium and trace metals in sediments of the Winterbeek: Application of sequential extraction and DGT techniques. *Environmental Pollution*, *158*(7), 2439–2445.

Ghiorse, W.C. (1988). Microbial reduction of manganese and iron. *In*: Biology of Anaerobes (Zehnder, A.J.B., Ed), pp. 305-331. John Wiley&Sons, New York.

Golden, D.C., Chen, C.C., Dixon, J.B. and Tokashiki, Y. (1988). Pseudomorphic replacement of manganese oxides by iron oxide minerals. *Geoderma, 42*, 199-211.

Gounod, A.-M. (1994). Microbial oxidation and reduction of manganese: consequences in groundwater and applications. *FEMS Microbiology Reviews, 14*, 339-350.

Gu, C., Hornberger, G., Herman, J. S. and Mills, A. L., 2008. Influence of stream-groundwater interactions in the streambed sediments on NO3- flux to a low-relief coastal stream. *Water Resources Research, 44*, W11432.

Harper, M. P., Davison, W., Zhang, H., & Tych, W. (1998). Kinetics of metal exchange between solids and solutions in sediments and soils interpreted from DGT measured fluxes. *Geochimica et Cosmochimica Acta*, *62*(16), 2757–2770.

Jia, G., & Jia, J. (2012). Determination of radium isotopes in environmental samples by gamma spectrometry, liquid scintillation counting and alpha spectrometry: A review of analytical methodology. *Journal of Environmental Radioactivity*, *106*, 98–119.

Jiménez-Piedrahita, M., Altier, A., Cecilia, J., Puy, J., Galceran, J., Rey-Castro, C., Zhang, H. & Davison, W. (2017). Extending the Use of Diffusive Gradient in Thin Films (DGT) to Solutions Where Competition, Saturation, and Kinetics Effects Are Not Negligible. *Analytical Chemistry*, *89*, 6567–6574.

King, G.M. (1990). Effects of added manganic and ferric oxides on sulfate reduction and sulfide oxidation in intertidal sediments. *FEMS Microbiol. Ecol., 73,* 131-138.

Kiro, Y., Yechieli, Y., Voss, C. I., Starinsky, A., & Weinstein, Y. (2012). Modeling radium distribution in coastal aquifers during sea level changes: The Dead Sea case. *Geochimica et Cosmochimica Acta*, *88*, 237–254.

Labille, J., Fatin-Rouge, N. and Buffle, J. (2007). Local and average diffusion of nanosolutes in agarose gel: The effect of the gel/solution interface structure. *Langmuir*, 23, 2083-2090.

L'Annuziata, M. F. (2012). Handbook of Radioactivity Analysis. *Academic Press*, 1418 pages.

Leermakers, M., Gao, Y., Navez, J., Poffijn, a., Croes, K., & Baeyens, W. (2009). Radium analysis by sector field ICP-MS in combination with the Diffusive Gradients in Thin Films (DGT) technique. *Journal of Analytical Atomic Spectrometry*, *24*(8), 1115.

Leermakers, M., Phrommavanh, V., Drozdzak, J., Gao, Y., Nos, J. & Descostes, M. (2016). DGT as a useful monitoring tool for radionuclides and trace metals in environments impacted by uranium mining: Case study of the Sagnes wetland in France. *Chemosphere*, *155*, 142-151.

Lehto, N. J., Davison, W., Zhang, H., & Tych, W. (2006a). Theoretical Comparison of How Soil Processes Affect Uptake of Metals by Diffusive Gradients in Thinfilms and Plants. *Journal of Environmental Quality*, *35*(5), 1903–1913.

Lehto, N. J., Davison, W., Zhang, H., & Tych, W. (2006b). An evaluation of DGT performance using a dynamic numerical model. *Environmental Science and Technology*, *40*(20), 6368–6376. http://doi.org/10.1021/es061215x

Lovley, D.R. (1991). Dissimilatory Fe(III) and Mn(IV) reduction. *Microbiology Review, 55,* 259-287.

Lovley, D.R. & Philipps, E.J.P. (1988). Manganese inhibition of microbial iron reduction in anaerobic sediments. *Geomicrobiol. J., 6,* 145-155.

Manakhov, D. V., & Egorova, Z. N. (2014). Speciation of radium-226 in podzols of northeastern Sakhalin in the impact zone of the oil field. *Eurasian Soil Science*, *47*(6), 608–612.

Martin, a. J., Crusius, J., Jay McNee, J., & Yanful, E. (2003). The mobility of radium-226 and trace metals in pre-oxidized subaqueous uranium mill tailings. *Applied Geochemistry*, *18*(7), 1095–1110.

Mesnic, N., Sadi, B., Li, C., Lai, E. (2013). Application of magnetic nanoparticles for the extraction of radium-226 from water samples. *Journal of Radioanalytical and Nuclear Chemistry*, *298*(3), 1501-1509

Michard, G., Viollier, E., Jézéquel, D., & Sarazin, G. (1994). Geochemical study of a crater lake: Pavin Lake, France - Identification, location and quantification of the chemical reactions in the lake. *Chemical Geology*, *115*(1-2), 103–115.

Moon, D. S., Burnett, W. ., Nour, S., Horwitz, P., & Bond, a. (2003). Preconcentration of radium isotopes from natural waters using MnO2 Resin. *Applied Radiation and Isotopes*, *59*(4), 255–262.

Mongin, S., Uribe, R., Rey-castro, C., Cec, J., Galceran, J., Zhang, H. and Davison, W. (2011). Key role of the resin layer thickness in the lability of complexes measured by DGT. *Environmental Science & Technol*ogy, *45(11)* 4869-4875.

Mongin, S., Uribe, R., Rey-castro, C., Cec, J., Galceran, J., & Puy, J. (2013). Limits of the Linear Accumulation Regime of DGT Sensors. *Environmental Science & Technol*ogy, *47*, 10438−1044

Narayanan, J., Xiong, J.-Y., & Liu, X.-Y. (2006). Determination of agarose gel pore size: Absorbance measurements vis a vis other techniques. *Journal of Physics: Conference Series*, *28*(1), 83–86.

Nealson, K.H., Rosson, R.A. and Myers, C.R. (1989). Mechanisms of oxidation and reduction of manganese. *In:* Metals Ions and Bacteria (Beveridge, T.J. and Doyle, R.J., Eds), pp. 383-411, Wiley-Interscience, New York.

Nelson, A. W., May, D., Knight, A. W., Eitrheim, E. S., Mehrho, M., Shannon, R., Schultz, M. K. (2014). Matrix Complications in the Determination of Radium Levels in Hydraulic Fracturing Flowback Water from Marcellus Shale. *Environmental Science & Technology Letters*, *1*, 204–208.

Park, C. J., Oh, P. J., Kim, H. Y., & Lee, D. S. (1999). Determination of 226Ra in mineral waters by high-resolution inductively coupled plasma mass spectrometry after sample preparation by cation exchange. *Journal of Analytical Atomic Spectrometry*, *14*(2), 223–227.

Patrick, W.H. & Henderson, R.E. (1980). Reduction and reoxidation cycles of manganese and iron in flooded soil. *Soil Sci. Soc. Am. J., 45*, 855-859.

Pluta, I. (2001). Barium and radium discharged from coal mines in the Upper Silesia, Poland. *Environmental Geology*, *40*(3), 345–348.

Puy, J., Galceran, J. & Rey-Castro C. (2016). Interpreting the DGT Measurement. Speciation and Dynamics. Diffusive Gradient in Thin-Films for Environmental Mearus

Sochaczewski, Ł., Tych, W., Davison, B. and Zhang, H. (2007) 2D DGT induced fluxes in sediments and soils (2D DIFS). Environmental Modelling & Software 22(1), 14-23.

St-Amant, N., Whyte, J. C., Rousseau, M.-E., Lariviere, D., Kurt Ungar, R., & Johnson, S. (2011). Radiostrontium and radium analysis in low-level environmental samples following a multi-stage semi-automated chromatographic sequential separation. *Applied Radiation and Isotopes*, *69*(1), 8–17.

Stumm, W., and Morgan, J. J., 1995. Aquatic Chemistry, Chemical Equilibria and Rates in Natural Waters, Environmental Science and Technology, Wiley. 1022.

Sturchio, N. C., Banner, J. L., Binz, C. M., Heraty, L. B., & Musgrove, M. (2001). Radium geochemistry of ground waters in Paleozoic carbonate aquifers, midcontinent, USA. *Applied Geochemistry*, *16*(1), 109–122.

Uribe, R., Mongin, S., Puy, J., Cecília, J., Galceran, J., Zhang, H., & Davison, W. (2011). Contribution of partially labile complexes to the DGT metal flux. *Environmental Science and Technology*, *45*(12), 5317–5322.

Varga, Z. (2007). Preparation and characterization of manganese dioxide impregnated resin for radionuclide pre-concentration. *Applied Radiation and Isotopes*, *65*(10), 1095–1100.

Van Beek, P., Souhaut, M., & Reyss, J.-L. (2010). Measuring the radium quartet (228Ra, 226Ra, 224Ra, 223Ra) in seawater samples using gamma spectrometry. *Journal of Environmental Radioactivity*, *101*(7), 521–529.

Vandenhove, H., Sweeck, L., Mallants, D., Vanmarcke, H., Aitkulov, A., Sadyrov, O., … Aitaliev, A. (2006). Assessment of radiation exposure in the uranium mining and milling area of Mailuu Suu, Kyrgyzstan. *Journal of Environmental Radioactivity*, *88*(2), 118–139.

Vinson, D. S., Vengosh, A., Hirschfeld, D., & Dwyer, G. S. (2009). Relationships between radium and radon occurrence and hydrochemistry in fresh groundwater from fractured crystalline rocks, North Carolina (USA). *Chemical Geology*, *260*, 159–171.

http://doi.org/10.1016/j.chemgeo.2008.10.022

Viollier, E., Jézéquel, D., Michard, G., Pèpe, M., Sarazin, G., & Albéric, P. (1995). Geochernical study of a crater lake (Pavin Lake, France): Trace-element behaviour in the monimolimnion. *Chemical Geology*, *125*(1-2), 61–72.

Ward, A., Gooseff, M. .N., Voltz, T. J., Fitzgerald, M., Signha, K. and Zarnetske, J. P., 2012. How does rapidly changing discharge during storm events affect transient storage and channel water balance in a headwater mountain stream? *Water Resources Research*, *49*, 5473-5486.

Waska, H., Kim, S., Kim, G., Peterson, R. N., & Burnett, W. C. (2008). An efficient and simple method for measuring 226Ra using the scintillation cell in a delayed coincidence counting system (RaDeCC). *Journal of Environmental Radioactivity*, *99*(12), 1859–1862.

Zhang, H., Davison, W., Miller, S., & Tych, W. (1995). In situ high resolution measurements of fluxes of Ni, Cu, Fe, and Mn and concentrations of Zn and Cd in porewaters by DGT. *Geochimica et Cosmochimica Acta*, *59*(20), 4181–4192.

APPENDIX 1: Parameters and interferences in 226Ra measurement with HR-ICP-MS Element 2 (Thermo Scientific)

Table A1: Operating conditions and data acquisition parameters for HR-ICP-MS Element 2 used for ^{226}Ra measurements.

HR-ICP-MS		
Rf power (W)	1350	
Sample uptake rate ($mL.min^{-1}$)	0.2	
Argon flow rates ($L.min^{-1}$)		
Cool	16	
Auxiliary	1.0	
Sample	Between 0.9 and 1.0 (depends of sensibility)	
Torch	Quartz torch with a separate quartz injector tube	
Nebulizer	PFA ST microflow nebulizer	
Spray chamber	Quartz Cyclo spray chamber	
Sampler cone	Nickel	
Skimmer cone	Nickel	
Data acquisition	*Low Resolution*	*Medium Resolution*
No. of passes	3	3
Mass window (%)	20	125
Search window (%)	0	60
Integration window (%)	20	20
Samples per peak	25	20
Sample time (s)	1.5	0.5

Table A2: Observed isobaric interferences at mass 226 for HR-ICP-MS Element 2 in low resolution before measurements.

[Ba] & [Sr] (ppm)	[Pb] (ppb)	Apparent 226 Ra concentration ($mol.L^{-1}$)
0.01		0
0.1		0
1		$3.24 .10^{-15}$
10		$3.46 .10^{-14}$
100		$1.19 .10^{-13}$
	1	0
	10	0
	100	$1.24 .10^{-14}$

APPENDIX 2: Model inputs

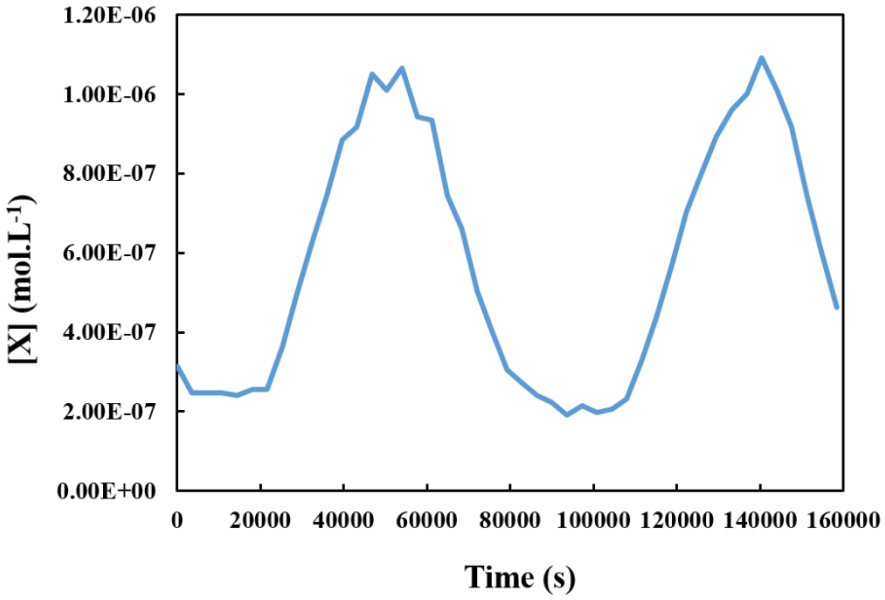

Figure A3: Evolution of a solute concentration function of time. Extracted from Borok *et al*. (2008[33]) and used as input during modelling. Total time is 158400 seconds.

[33]Borrok, D. M., Nimick, D. A., Wanty, R. B., & Ridley, W. I. (2008). Isotopic variations of dissolved copper and zinc in stream waters affected by historical mining. *Geochimica et Cosmochimica Acta*, *72*, 329–344. http://doi.org/10.1016/j.gca.2007.11.014

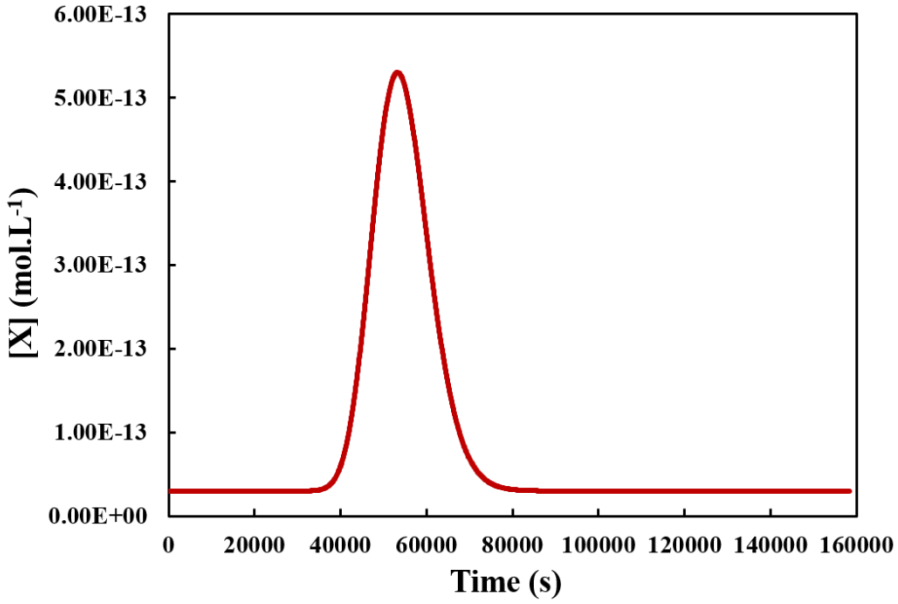

Figure A4: Transient signal designed to represent a contaminant plume. Total time is 158400 seconds. Equation is explained below and is from

Table A5: Equation and associated parameters used to define the signal in figure A4.

Equation: $g(t) = A + h \times \exp\left[-\left(\ln\left(t/t_{puls}\right)/\omega\right)^2\right]$		
Parameters	Value or interval	Comment
A	$3.0 .10^{-14}$	Correspond to the geochemical background
h	$5.0 .10^{-13}$	
tpuls	53265	
T	0 - 158400	
Ω	0.1705	

Table A6: Parameters used to model resin (R) affinity to the solute M according to equation 4

K_R (L.mol^{-1})	k_f (L.s^{-1}.mol^{-1})	k_{diss} (s^{-1})
10^{+2}	10^{+5}	10^{+3}
10^{+3}	10^{+1}	10^{-2}
10^{+4}	10^{+5}	10^{+1}
10^{+5}	10^{+9}	10^{+4}
10^{+6}	10^{+1}	10^{-5}
10^{+7}	10^{+5}	10^{-2}
10^{+8}	10^{+9}	10^{+1}
10^{+9}	10^{+1}	10^{-8}
10^{+10}	10^{+5}	10^{-5}
10^{+11}	10^{+9}	10^{-2}
10^{+12}	10^{+1}	10^{-11}
10^{+13}	10^{+5}	10^{-8}
10^{+14}	10^{+9}	10^{-5}
10^{+15}	10^{+9}	10^{-6}
10^{+16}	10^{+5}	10^{-11}
10^{+17}	10^{+9}	10^{-8}
10^{+18}	10^{+5}	10^{-13}
10^{+20}	10^{+9}	10^{-11}

Chapter V: Field experiments

1. INTRODUCTION

Thallium is known to be associated to sulfur deposits (Biagoni *et al*., 2013; Hetmann *et al*., 2014; D'Orazio *et al*., 2017) and in some area, high concentrations were measured (Casiot *et al*., 2011; Campanella *et al*., 2016; Campanella *et al*., 2017). Thanks to collaboration with BRGM (Bureau de Recherche Géologique et Minière, Orléans, France), we had access to the former French mining sites. The area of Pontgibaud was selected for its geological background rich in sulfur and its potential Tl high levels. Consequently, the area of Roure-Les Rosiers was chosen to assess the fate of thallium in a small watershed associated with sulfur deposits. Both waters and solids were sampled. Waters were analyzed and results are presented here, results on solids are not shown bu samples are still available for further investigations.

2. MINING DISTRICT OF PONTGIBAUD

The mining district of Pontgibaud is located in the western district of Clermont-Ferrand (Auvergne, France). The district was known for its mining activities since the Gallo-Roman era but achieved its prosperity during the XIXth century when it became the French first lead producer. Between 1850 and 1897, 50 000 tons of lead and 100 tons of silver were extracted. Mining activities ended in 1897 and the mine was definitively shut down in 1903.

2.1. Geological settings

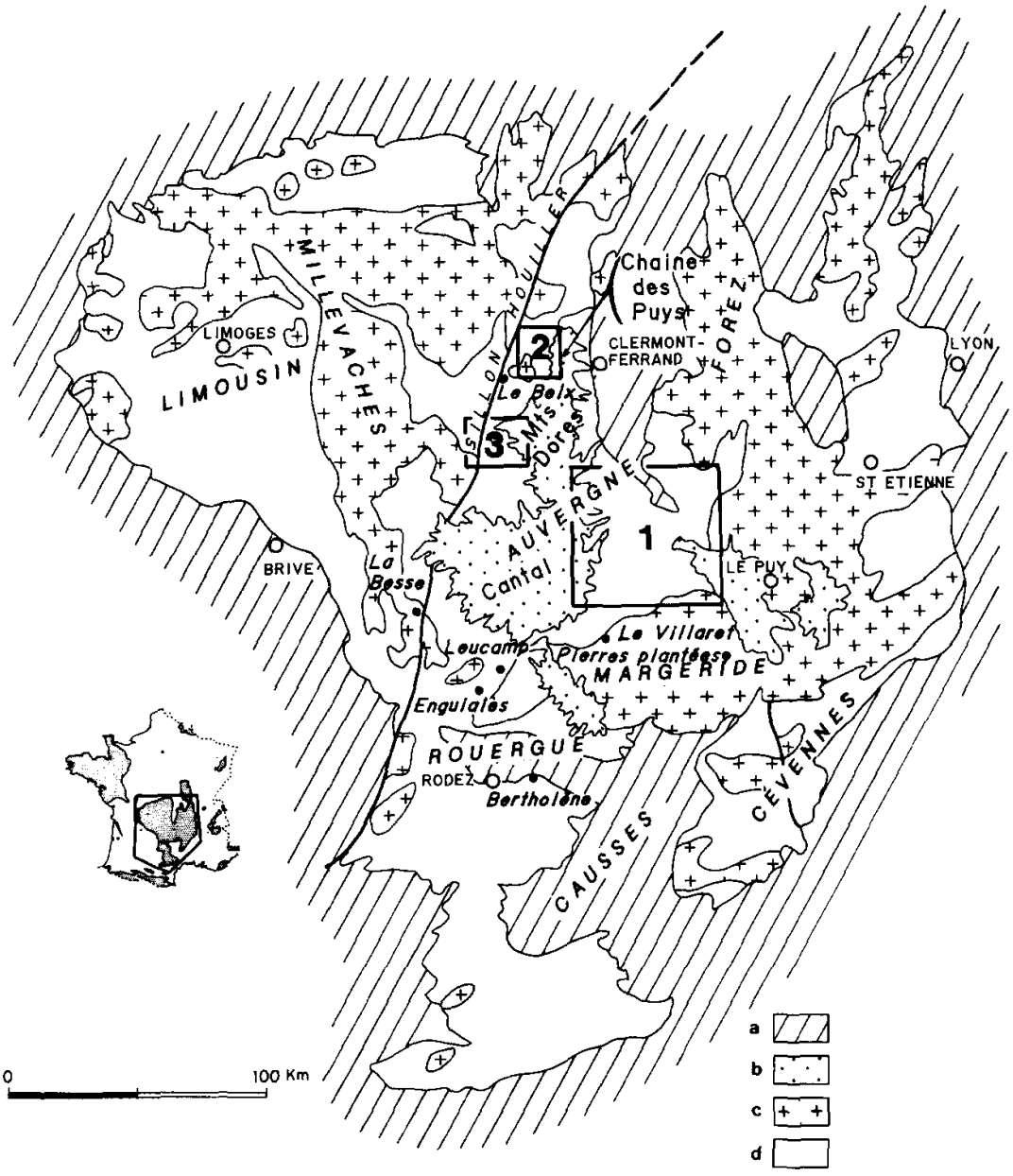

Figure 1: Geology of the French Massif Central from Bril *et al.*, 1991. *a*: sedimentary rocks from Mesozoic and Cenozoic; *b*: Neogene volcanism; *c*: granites; *d*: metamorphic base; *1*: Distric of Brioude-Massiac; *2*: District of Pontgibaud; 3: District of Pontvieux-Labessette

The district of Pontgibaud is part of the Massif Central mountainous area, which is a segment of Hercynian formation in Europe (fig. 1A). The area around Pontgibaud is standing on both metamorphic and granitic basement dated between 430 and 350 My (fig. 1; Bril *et al*., 1991). The district was later intruded by multiple mineralizations in vein due to hydrothermal activities (Bril *et al*., 1991). Three phases were identified (Négroni, 1981; Bril *et al*., 1991):

(1) High-temperature mineralization with precipitation of arsenopyrite in Les Peyrouses dated around 295 ± 6 My (fig. 2),

(2) Mineralization with formation of Ag-rich galena, pyrite and Cu-Ag sulfosalt in Brousse, Pranal, Brousse and Rosier (fig. 2). This phase was at the origin of the Pb-Ag ores exploited at Pontgibaud,

(3) Fluo-barite mineralization in the northwestern part of the district (fig. 2).

Every phase of mineralization was associated with hydrothermal alteration and secondary mineral formations such as illite, smectite, phengite and kaolinite (Bril *et al*. 1991).

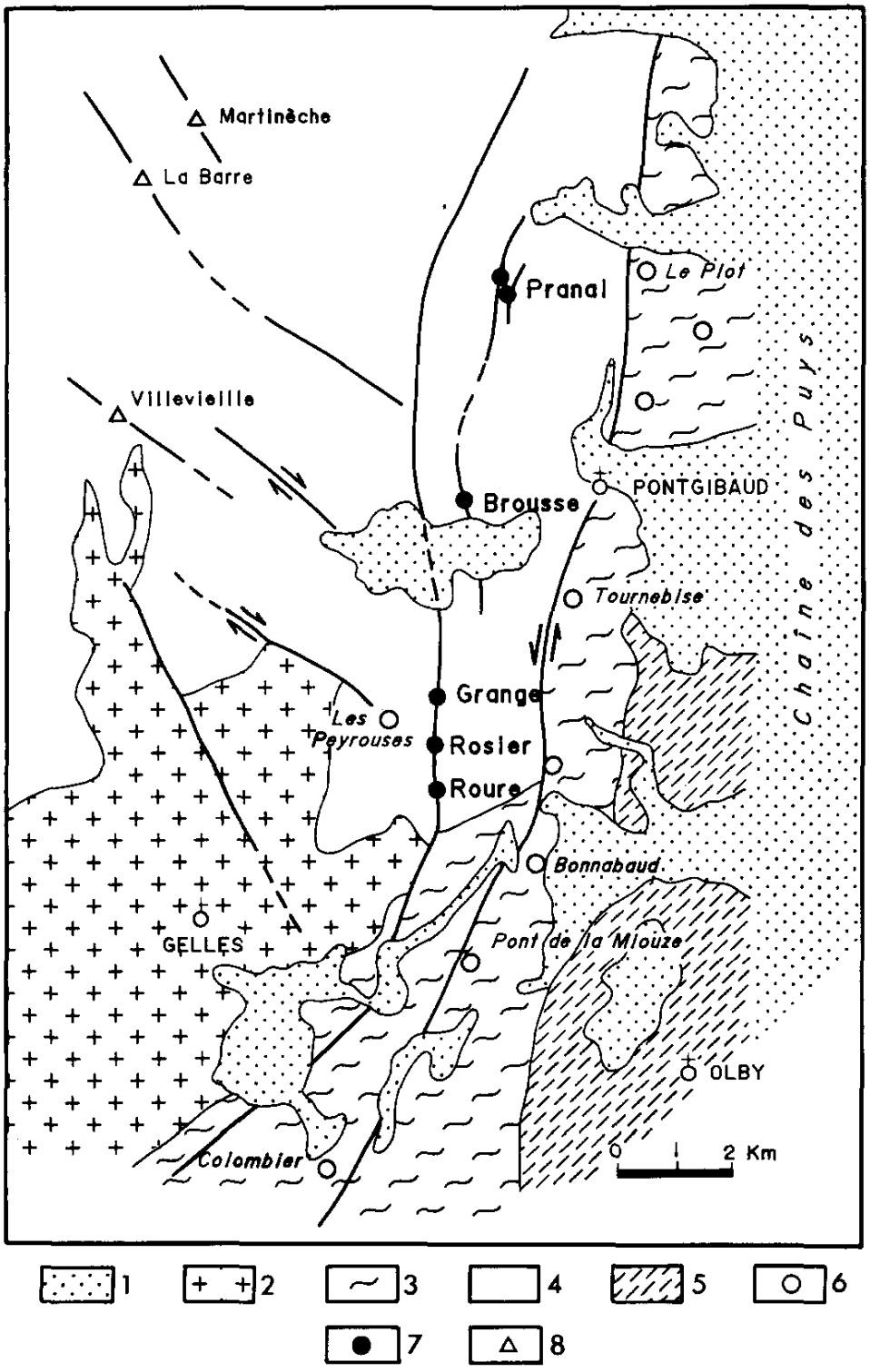

Figure 2: Geology of Pontgibaud district from Bril *et al*., (1991). *1*: Neogene volcanism; *2*: granites; *3*: biotite and sillimanite paragneiss; *4*: biotite and cordierite gneiss; *5*: biotite migmatites; *6*: As-W-Sn veins; *7*: Pb-Ag veins; *8*: fluorine veins

2.2. Sites location and description

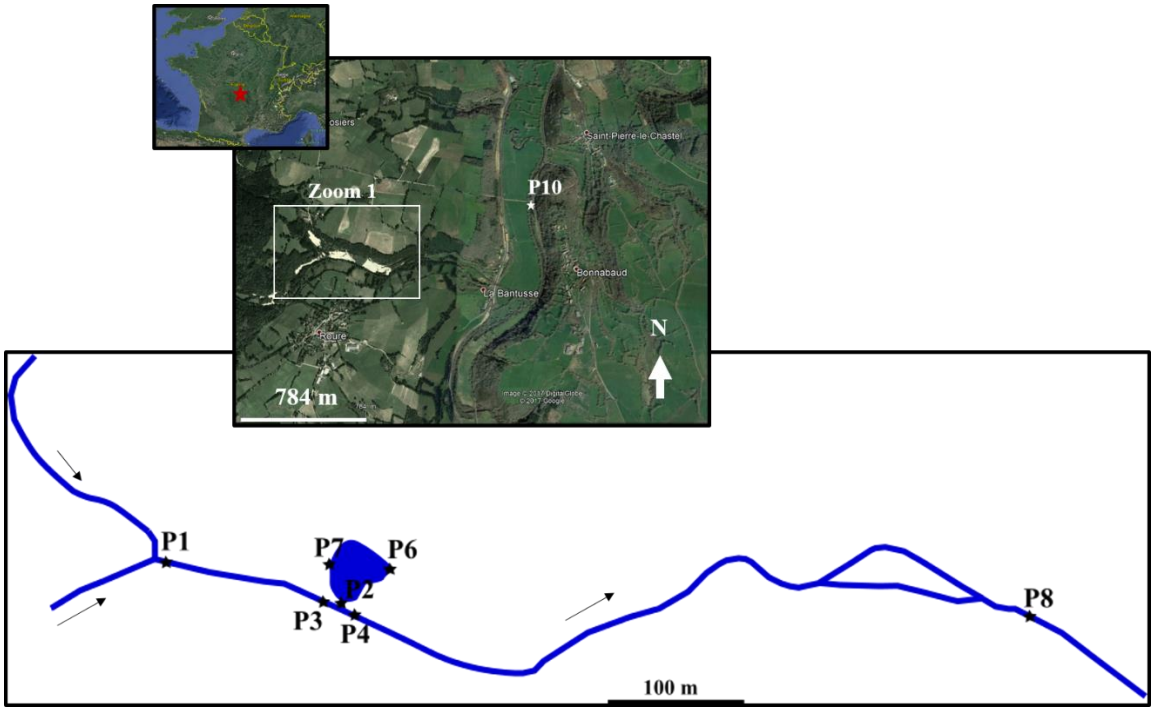

Figure 3: Sampling locations in Roure-Les Rosiers site, District of Pontgibaud (France). Black arrows show the stream flow direction.

During mining activities in the district, Roure-Les Rosiers was dedicated to the storage of mining residues. In a small valley, the thin material was stored in small hillocks along La Veyssière riverbanks (fig. 3). A pond of 2.60 meters depth on its right bank (P6, fig. 3) collects run-off of the nearby hillocks. The pond is connected to the river by a small stream identified as P2 in figure 3. Birch and pine trees were the dominant vegetation on the mining residues. Around the storage sites, land occupation was divided between forest and pasture. La Veyssière River ends in the Sioule River approximately 1.5 km after P8 sampling point (fig. 3).

3. EXPERIMENTAL SECTION

3.1. Sample collection and processing

A first campaign took place in April 2016 on the entire district of Pontgibaud to identify which sites in the different rivers (fig. 2) show the higher thallium concentrations. It appears that the sites located between Roure and Les Rosiers (fig. 2 and 3) showed the highest Tl values and were then chosen for further sampling. A second campaign was done in February 2017. The

previous selected sampling sites (P1 to P6) were sampled. P7, P8 and P10 along the Sioule River (fig. 3) were added.

At each point, water samples were sampled for total content (no filtration) and filtered at 0.22 µm, 0.45 µm (Polyethersulfone membrane, Minisart®, Satorius) then stored in tubes 14mL Polypropylene tubes (Falcon®). Major anions (SO_4^{2-}, F^-, Cl^-, NO_3^- and $\sum PO_4^{3-}$) and other elements (Ca, Na K, Mg, Mn, Fe, Al, Si, Ba and Sr) were analyzed using 0.22 µm-filtered samples. Thallium was analyzed in 0.22-µm, 0.45-µm filtered samples and in total samples. DOC (Dissolved Organic Carbon) and alkalinity were measured in the below 0.22 µm fractions and stored in fume glass bottle. Samples for other elements analysis were acidified with Suprapur nitric acid (HNO_3; Merck). Blanks of filters, syringes and acids were collected on the field. 8 Diffusive Equilibrium in Thin-films (DET; DGT Research $^{Ltd.}$) were deployed at each sampling points. Contact time was 24 hours. Two unused DET served as blanks. All liquid samples were analyzed within the week following sampling. DET compartments were gathered five pieces at a time, stored in 14 mL Polypropylene tubes (Falcon®) and diluted with 10 mL of HNO_3 2% (Merck). Between each step, tubes were weighted to calculate an accurate dilution factor.

For P1, P4, P6 and P10 water column particulate matter was collected on Glass fiber filter. At P7, sediment samples (triplicates) were drilled with a transparent PVC core tube and kept in anoxia (with corks and a high water column in the pipe), for later flux measurements. Lastly, one sample of the mining residue was collected on the hillbock nearby P7.

Water river physico-chemical parameters were collected thanks to a multi-parameter HORIBA probe (U-50 multi-parameter water quality meter): pH, conductivity, redox potential (Eh), temperature, dissolved oxygen concentration, TDS (total dissolved solid), turbidity. All samples were taken in surface.

3.3. Analytical section

Thallium was measured with an HR-ICP-MS Element 2 (Thermo Scientific) in a clean room with a solution of ^{115}In 5 ppb as internal standard. For each sample, nine measurements in a row were done (3 x 3 runs). Then, the average and the standard deviation were used as concentration value and the measurement error, respectively. Concentrations were corrected for signal drift by internal standard. Certified materials TM23.4 and TM24.4 (Environment Canada) validated Tl

analysis and the limit of quantification was $7.5.10^{-12}$ $mol.L^{-1}$ for Tl. Other elements were analyzed with an ICP-AES ICAP 6200 (Thermo scientific) whereas anions were analyzed by ionic chromatography with an ion chromatographer DIONEX ICS-1100 (Thermo Scientific). DOC was measured with a Total Carbon Analyzer TOC-V_{CHS} (Shimadzu). Alkalinity was determined by titration with a titrator, 809 Titrando (Metrohm).

Additional MEB-EDS analyses were performed on collected suspended particle samples and sediments from P7, P4 and P6. One XRD qualitative analysis was performed on bulk sediment. Total analysis of solid samples was not performed for this study.

3.2. Fluxes measurements and calculations

In the following hours of sampling sediment, sediment columns were installed at the laboratory to measure thallium fluxes between the sediment and the water column. Triplicates incubations were done. In each column, sediment top water was removed and new water from La Veyssière River was added (low Tl concentration). The water column was oxygenated by bubbling during the length of the experiment. In order to calculate flux values, water samples (15 mL) were collected after 1h40, 10h30 and 16h45. Blanks were collected at the beginning of the experiment. Samples were filtered, acidified and then stored in 14 mL Polypropylene tubes (Falcon®).

The flux (in $mol.m^{-2}.s^{-1}$) was calculated according the following equation:

$$F = \frac{\Delta[Tl]}{\Delta t} \times \frac{V}{S} \qquad \text{(Eq. 1)}$$

with V (in m^3) and S (in m^2), respectively the volume and the surface of overlaying water. $\Delta[Tl]$ is the Tl concentration variation (in $mol.m^{-3}$) and Δt (s) is time variation. Equation 1 can be simplified as:

$$F = \frac{\Delta n_{Tl}}{\Delta t} \times \frac{1}{S} \qquad \text{(Eq. 2)}$$

Δn_{Tl} correspond to the variation of thallium (in mole) in the water pipe water column. Then, for each transparent PVC core tube (Ø 17.1 cm), thallium concentrations at each sampling times were measured and converted in amounts of thallium (n_{Tl}). n_{Tl} as function of time was linear (see

appendix 1, fig. S1), so $\frac{\Delta n_{Tl}}{\Delta t}$ corresponds to the slope α (mol.s^{-1}) of this linear relationship. Then, an average flux was calculated with the duplicate (appendix 1, Table S1). The latest value was normalized by the pond surface (estimated at 2200 m^2) and converted in mole per year.

4. RESULTS AND DISCUSSION

Measured parameters, Eh, pH, dissolved oxygen, temperature, and conductivity of each sampled points are summarized in table 1. Conductivity and pH were relatively homogenous and all samples were in oxidative conditions (table 1). Eh (mV) suggests that water samples are in the stability domain of Thallium(I) (Lin and Nriagu, 1998).

Tableau 1: Physico-chemical parameters measured during February 2017 campaign.

Sample	T (°C)	pH	Cond (µS.cm^{-1})	DO (mg.L^{-1})	Eh (mV)	DOC (mg.L^{-1})
P1	6.31	6.60	77	11.07	133	2.54
P2	6.50	6.09	90	15.60	199	1.48
P3	6.01	6.03	79	14.70	83	2.64
P4	6.10	5.94	73	14.87	113	2.32
P6	7.30	6.01	89	15.70	226	1.51
P7	6.91	6.17	95	12.75	168	0.74
P8	7.29	6.02	81	15.00	114	2.55
P10	7.30	7.42	97	14.00	242	1.91

Thallium concentrations ranged between $5.28.10^{-11}$ and $1.20.10^{-9}$ mol.L^{-1} represent the fraction below 0.22 µm (table 1). Thallium concentrations are similar for the two campaigns. For all samples, thallium in the 0.22 µm fraction represents more than 75% of total thallium for all samples, meaning that thallium is mostly dissolved or complex to colloids.This oberservation is similar to others studies (Nielsen *et al*., 2005; Law and Turner, 2011; Casiot *et al*., 2011; Campanella *et al*., 2017).

P2 and P6 stations are located in the main and deepest vegetated basin of the pond and show homogeneous concentrations. P7 station corresponds to a shallow unvegetated basin (10 to 40 cm depth) where water directly overlays mine tailings. This station shows the highest Tl concentration (table 2).

Table 2: Thallium in different fractions for the water column

Sample	$Tl_{0.22}$ (. 10^{-11} mol.L^{-1})		$Tl_{0.45}$ (.10^{-11}mol.L^{-1})	Total Tl (.10^{-11} mol.L^{-1})	% of total Tl in 0.22 µm fraction
	04/2016	*02/2017*	*02/2017*	*02/2017*	
P1	5.28 ± 0.26	5.95 ± 0.41	6.41 ± 0.09	7.68 ± 0.20	78
P2	34.94 ± 1.74	33.78 ± 1.64	33.58 ± 0.58	35.12 ± 0.53	96
P3	8.92 ± 0.45	6.35 ± 0.16	6.25 ± 0.26	7.45 ± 0.20	85
P4	8.14 ± 0.41	13.16 ± 2.48	7.57 ± 0.12	8.40 ± 0.57	100
P6	34.63 ± 1.73	35.46 ± 0.90	36.03 ± 0.66	37.17 ± 0.80	95
P7	-	120.12 ± 7.27	123.61 ± 3.07	122.99 ± 3.30	98
P8	-	6.88 ± 0.64	6.66 ± 0.21	7.95 ± 0.14	86
P10	-	1.63 ± 0.08	1.56 ± 0.04	1.76 ± 0.19	93

Speciation calculation (as calculated in chapter II, section 3.1) shows that Tl^+ is the main thallium species in solution in the pond, la Veyssière River and at the sampling point in the Sioule River (table 3). Tl-HA (Tl complex with humic acid) represents less than 2 % of total dissolved thallium and $TlSO_4$ counts for less than 1 %. (table 3). Those values are low compared the concentrations measured by Casiot *et al*. (2011) or Campanella *et al*. (2017). Nevertheless, Law and Turner (2011) in partly mineralized catchements, measured thallium concentrations mostly between 2.45 .10^{-11} and 3.00 .10^{-10} mol.L^{-1}.

Table 3: Calculated Thallium(I) speciation for the fraction below 0.22 µm. ECOSAT software (Keizer, 1994) was used for modeling. TlOH, TlCl, $TlCl_2^-$, $TlCO_3$-, $TlHCO_3$, $TlHPO_4$ and $TlPO_4^{2-}$ do not contribute to Tl speciation in the system. All minerals had negative saturation index.

Sampling point	Tl^+ (% of total Tl)	Tl-HA (% of total Tl)	$TlSO_4$ (% of total Tl)
P1	98.35	1.43	0.17
P2	98.83	0.51	0.63
P3	98.58	1.12	0.18
P4	99.16	0.77	-
P6	99.54	0.37	-
P7	99.08	0.10	0.79
P8	98.41	1.35	0.19
P10	97.75	2.08	-

The average calculated flux of 1.60 ± 0.03 10^{-10} mol.y^{-1} at sediment-water interface and column displays thallium release from the sediment toward the water column. Hence, the pond is enriched in thallium by its sediment. Figure 3 shows that interstitial thallium concentrations are rather homogenous in the pond system, which is coherent with observations at the sediment-water interface. Other DETs were under limit of detection so no profiles are available. Concentrations measured at the outlet of the pond (P2, table 2) suggest that a part of the thallium

is released in the nearby river and undergo subsequent dilution along La Veyssière river until it reaches the Sioule river.

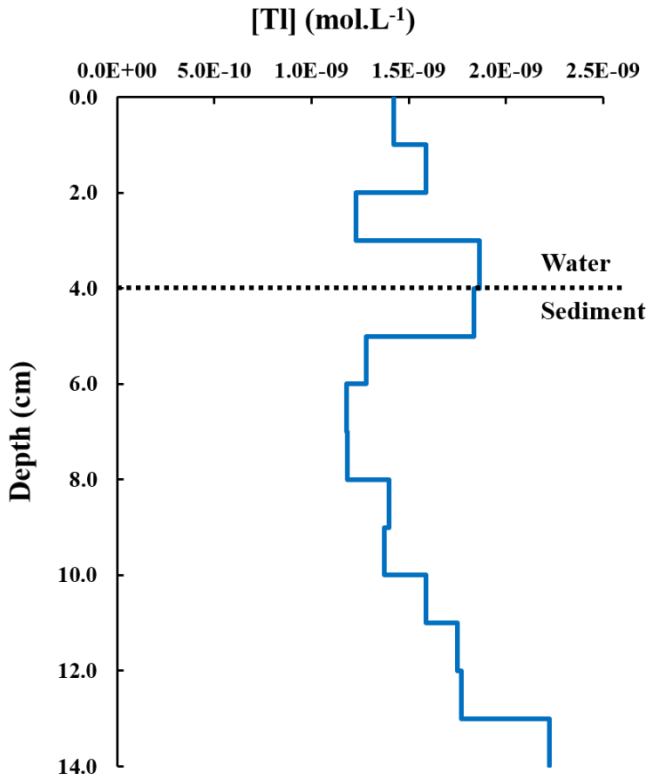

Figure 3: Thallium concentrations vs. depth at P7

XRD and MEB-EDS results identified quartz, kaolinite, illite, micas, (Ba,Sr) sulfate, bassanite ($CaSO_4$ $0.5H_2O$), lead oxides and traces of stibnite (Sb_2S_3) and arsenopyrite (FeAsS) in the sediment.

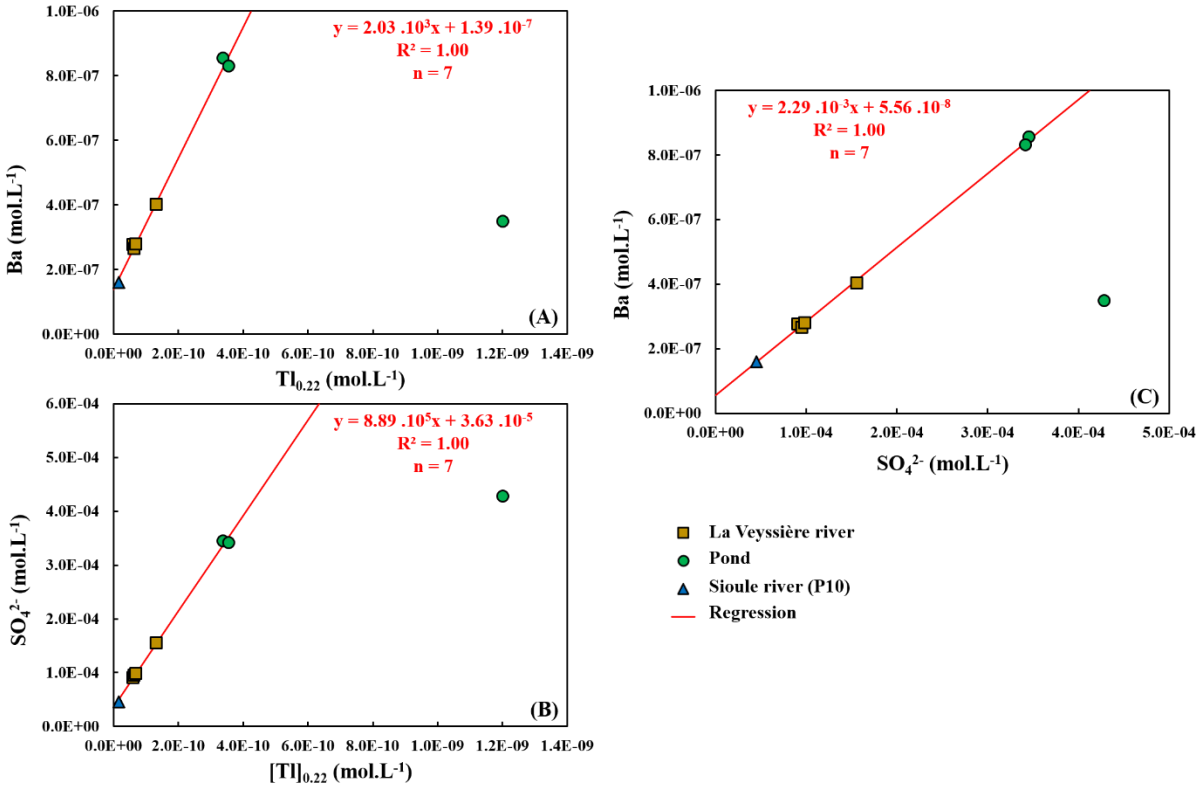

Figure 4: (A) Barium function of thallium concentrations for 0.22 µm fractions. (B) Sulfates function of thallium concentrations for 0.22 µm fractions. (C) Barium function of sulfates concentrations. Red line corresponds to regression line of the dataset.

Thallium dissolved concentrations are correlated with sulfates and barium in the three sampled systems (fig. 4A and 4B). Barium and sulfate are correlated in all systems (fig. 4C). The green point outside of the regression in figure 4A, 4B and 4C corresponds to P7. At this point, water level seemed to vary with forecast/season, which can disconnect this point to the main pond, meaning differences in the accumulation state. Figure 5A displays also thallium correlation with silica, except for the Sioule River. Lead is also correlated with thallium for the sample in the pond system (fig. 5B). This suggests that mineralization or residues containing sulfide (then oxidized in sulfates) are likely to be the source of thallium for the three systems. Nevertheless, as well in the pond and in la Veyssière River, both silica and lead (for pond system only) indicate the mining residues as Tl source. Quartz and lead oxides were identified in sediments.

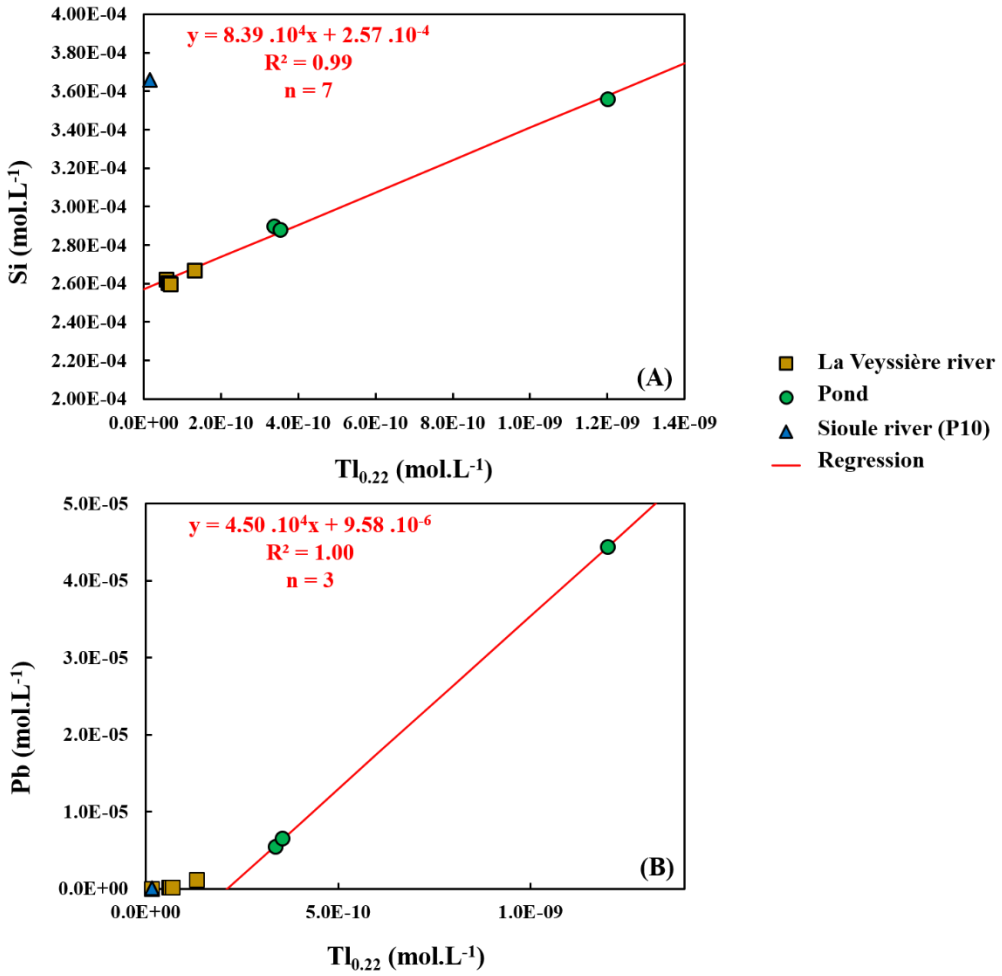

Figure 5: (A) Silica function of thallium concentrations for 0.22 µm fractions. (B) Lead function of thallium concentrations for 0.22 µm fractions. Red line corresponds to regression line of the dataset.

5. CONCLUSIONS AND PERSPECTIVES

Thallium concentrations in aquatic system from Roure-Les Rosiers was low with the higher values measured in a pond directly related to mining residues. In both the pond and the nearby river, thallium was almost exclusively free. The different observations suggest that mining residue is the source of thallium.

The next step would be to identify Tl-bearing phases in the sediment and then confirm the source of thallium for aquatic systems. Calculation of partitioning coefficient between dissolved (< 0.22 µm) and particulate matter would also be interesting, even if the majority of thallium in the water column was measured as free thallium.

Illite, smectite were identified in the sampled sediment so it would be interesting to study their interactions with thallium for this system. The first step would be to identify the source of clay minerals: whether they come from the hydrothermal alterations observed in the area (Bril *et al*., 1991) or they are secondary clays from weathering. Then, if adsorbed thallium is measured, the second step would be to distinguish geogenic thallium, from hydrothermal alteration and thallium adsorbed by clays in these sediments.

REFERENCES

Biagioni, C., D'Orazio, M., Vezzoni, S., Dini, A., & Orlandi, P. (2013). Mobilization of TI-Hg-As-Sb-(Ag,Cu)-Pb sulfosalt melts during low-grade metamorphism in the Alpi Apuane (Tuscany, Italy). *Geology*, *41*(7), 747–750. http://doi.org/10.1130/G34211.1

Bril, H., Bonhomme, M. G., Marcoux, E., Baubron, J. C. (1991). Ages K/Ar des minéralisations de Brioude-Massiac (W-Au-As-Sb; Pb-Zn), Pontgibaud (Pb-Ag; Sn), et Labessette (As-Pb-Sb-Au): Place de ces districts dans l'évolution géotectonique du Massif central français. *Mineralium Deposita*, *26*, 189-198

Campanella, B., Onor, M., D'Ulivo, A., Giannecchini, R., D'Orazio, M., Petrini, R., & Bramanti, E. (2016). Human exposure to thallium through tap water: A study from Valdicastello Carducci and Pietrasanta (northern Tuscany, Italy). *Science of the Total Environment*, *548-549*, 33–42. http://doi.org/10.1016/j.scitotenv.2016.01.010

Campanella, B., Casiot, C., Onor, M., Perotti, M., Petrini, R., & Bramanti, E. (2017). Talanta Thallium release from acid mine drainages : Speciation in river and tap water from Valdicastello mining district (northwest Tuscany). *Talanta*, *171*(May), 255–261. http://doi.org/10.1016/j.talanta.2017.05.009

Casiot, C., Egal, M., Bruneel, O., Verma, N., Parmentier, M. & Elbaz-Poulichet F. (2011). Predominance of Aqueous Tl(I) Species in the River System Downstream from the Abandoned Carnoulès Mine (Southern France). *Environ. Sci. Technol*., *45*, 2056–2064.

D'Orazio, M., Biagioni, C., Dini, A., & Vezzoni, S. (2017). Thallium-rich pyrite ores from the Apuan Alps , Tuscany , Italy : constraints for their origin and environmental concerns, 687–707. http://doi.org/10.1007/s00126-016-0697-1

Hettmann, K., Kreissig, K., Rehkämper, M., Wenzel, T., Mertz-Kraus, R. & Markl, G. (2014b). Thallium geochemistry in the metamorphic Lengenbach sulfide deposit, Switzerland : Thallium-isotope fractionation in a sulfide melt. *American Mineralogist*, *99*, 793–803. http://doi.org/10.2138/am.2014.4591

Keizer, M. G., Van Riemsdjik, W. H. (1994). *A Computer Program for the Calculation of Chemical Speciation and Transport in Soil-Water Systems (ECOSAT 4.7)*. Wageningen Agricultural University: Wageningen, The Netherlandd.

Law, S., & Turner, A. (2011). Thallium in the hydrosphere of south west England. *Environmental Pollution*, *159*(12), 3484–3489. http://doi.org/10.1016/j.envpol.2011.08.029

Lin, T.-S., & Nriagu, J. (1998). Speciation of thallium in natural waters. In *Thallium in the Environment*, 31–43. Edited by J. O. Nriagu. John Wiley & Sons, Inc. New York

Négroni, D. (1981). Le district de Pontgibaud. Cadre géologique; évolution structural et minéralogique. *Doctoral dissertation*, 291p. University of Clermont-Ferrand, France

Nielsen, S. G., Rehkämper, M., Porcelli, D., Andersson, P., Halliday, A. N., Swarzenski, P. W., … Günther, D. (2005). Thallium isotope composition of the upper continental crust and rivers—An investigation of the continental sources of dissolved marine thallium. *Geochimica et Cosmochimica Acta*, *69*(8), 2007–2019. http://doi.org/10.1016/j.gca.2004.10.025

APPENDIX 1: Data for flux calculation

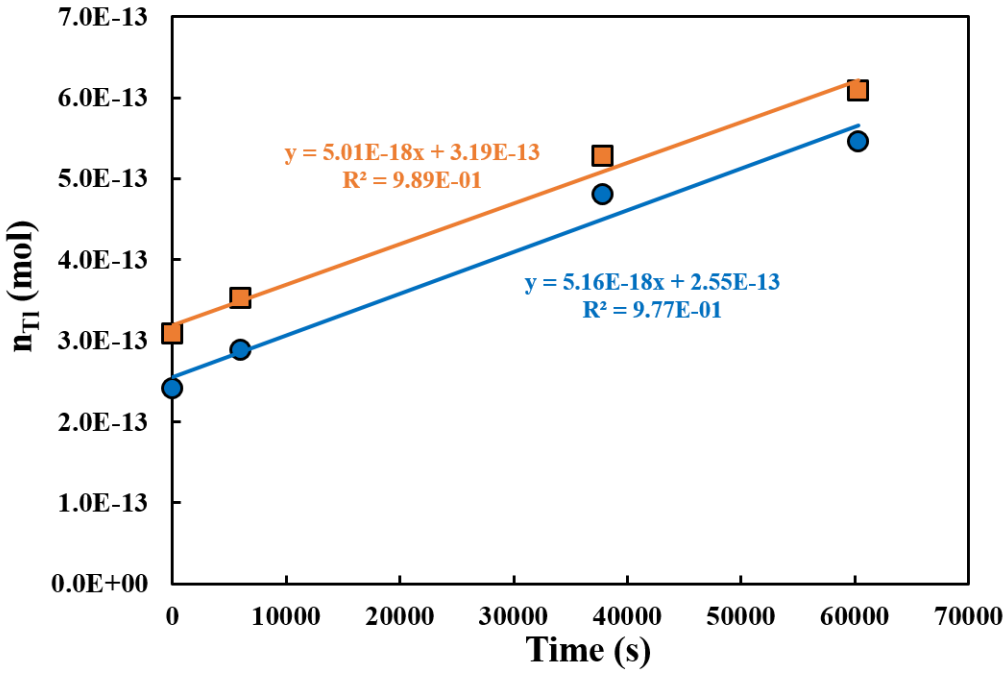

Figure S1: Evolution of thallium amounts (nTl) as function of time for pipe n°4 in orange and for pipe n°3 in blue.

Table S1: Parameters used for flux calculation between sediment and water column

Pipe n°	Height of water (m)	Initial volume of overlying water (m^3)	Flux ($mol.m^{-2}.s^{-1}$)
2	0.11	Loss of water due to a leak	
3	0.10	$5.74 .10^{-4}$	$8.73 .10^{-16}$
4	0.12	$6.89 .10^{-4}$	$8.99 .10^{-16}$
Avergage flux			$\boldsymbol{8.86 \pm 0.19 .10^{-16}}$

APPENDIX 2: Correlations between Tl and other measured elements/parameters

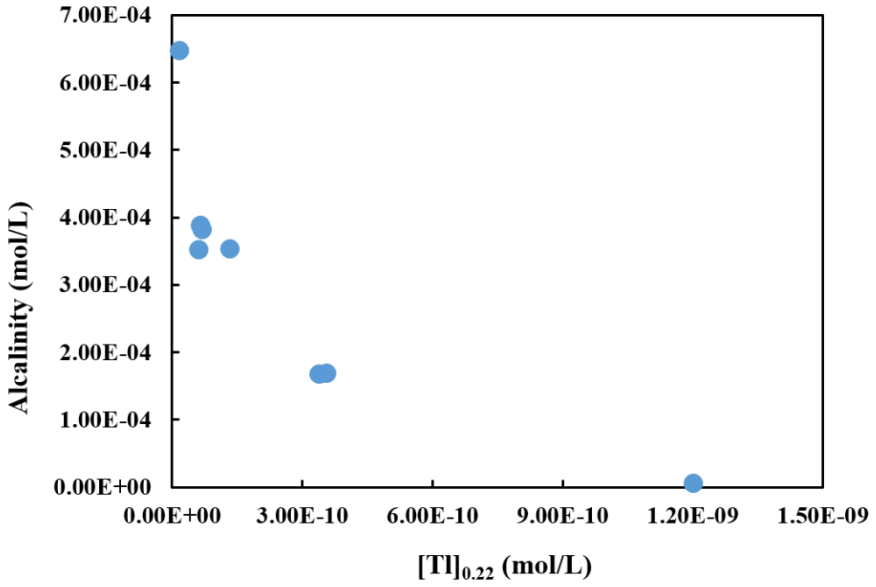

Figure S2: Alcalinity vs. Tl

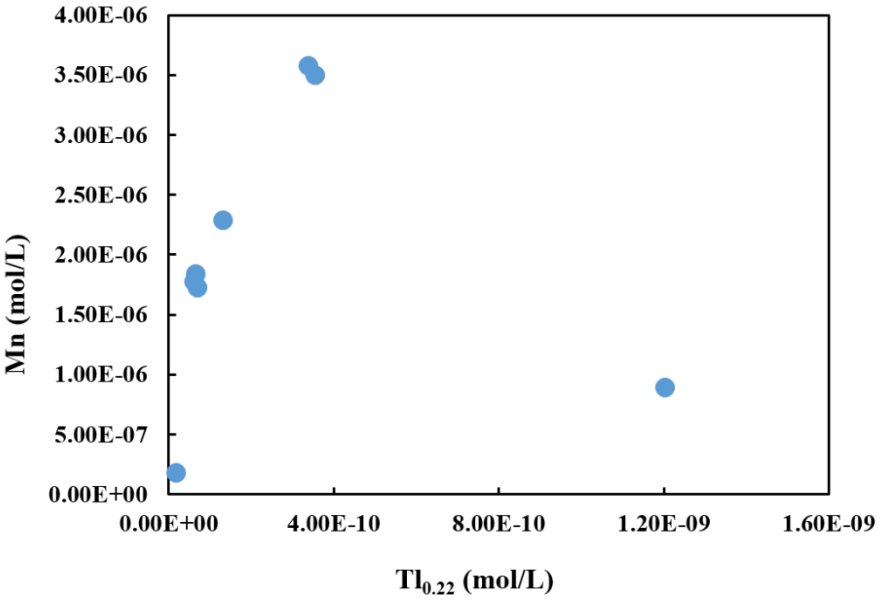

Figure S3: Mn vs. Tl

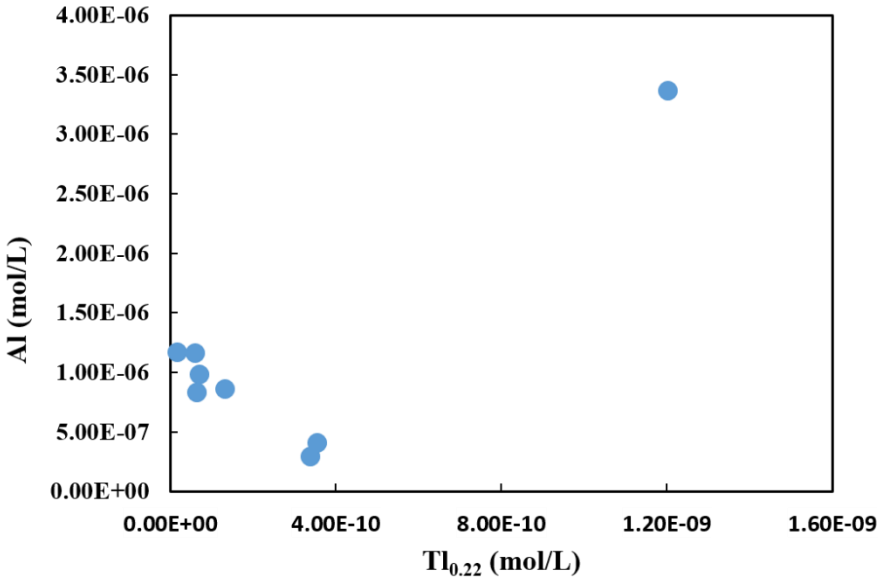

Figure S4: Al vs. Tl

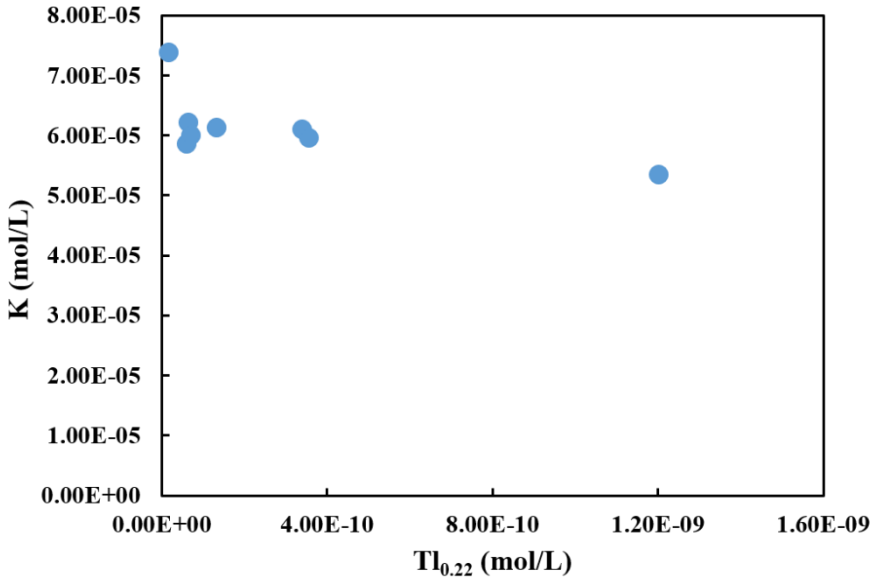

Figure S5: K vs. Tl

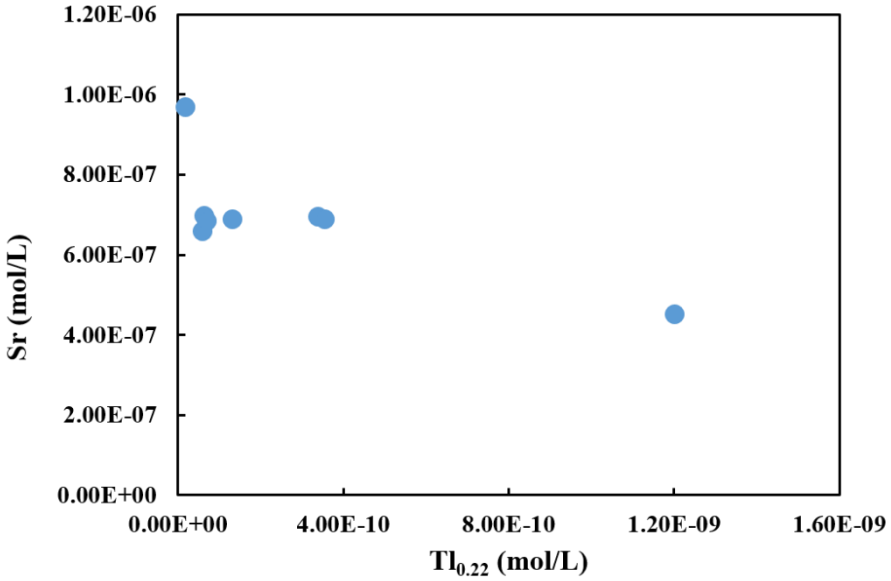

Figure S6: Sr vs. Tl

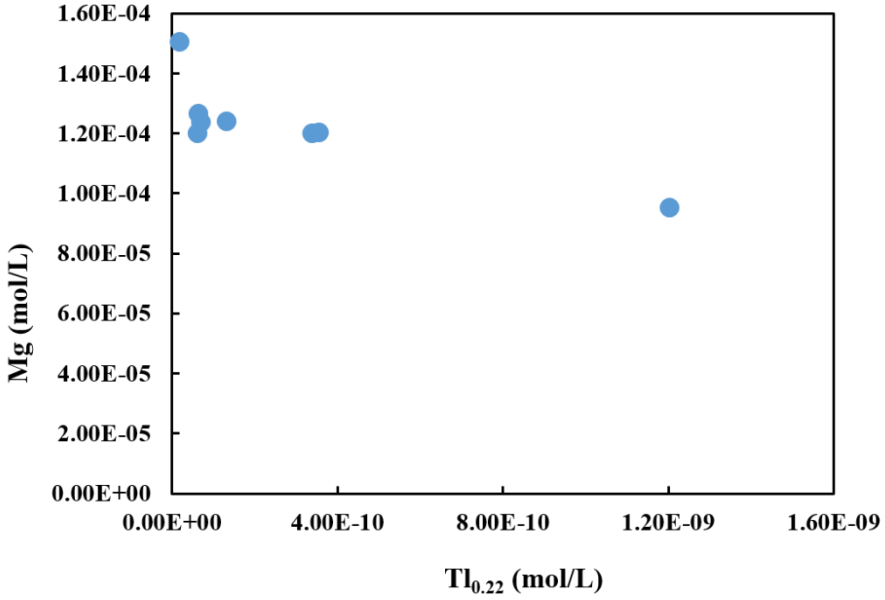

Figure S7: Mg vs. Tl

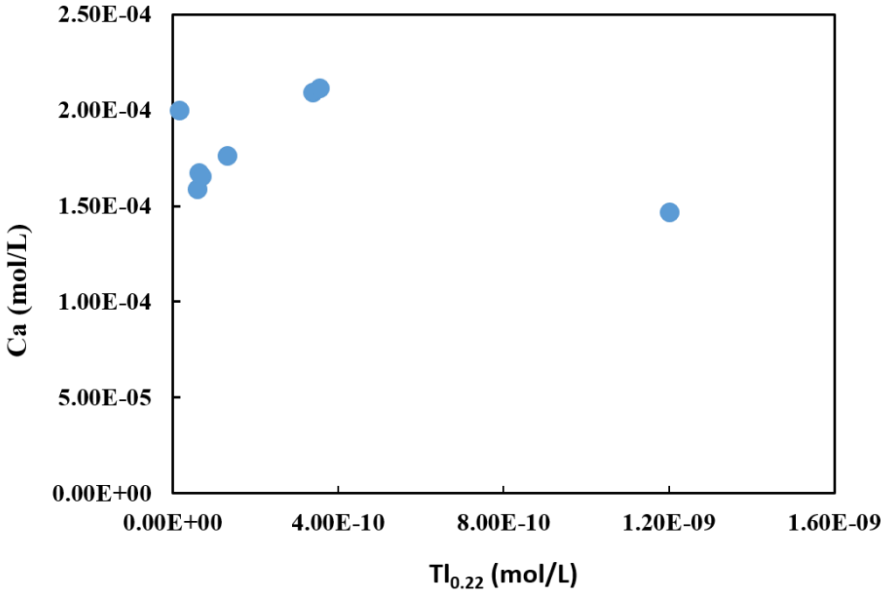

Figure S8: Ca vs. Tl

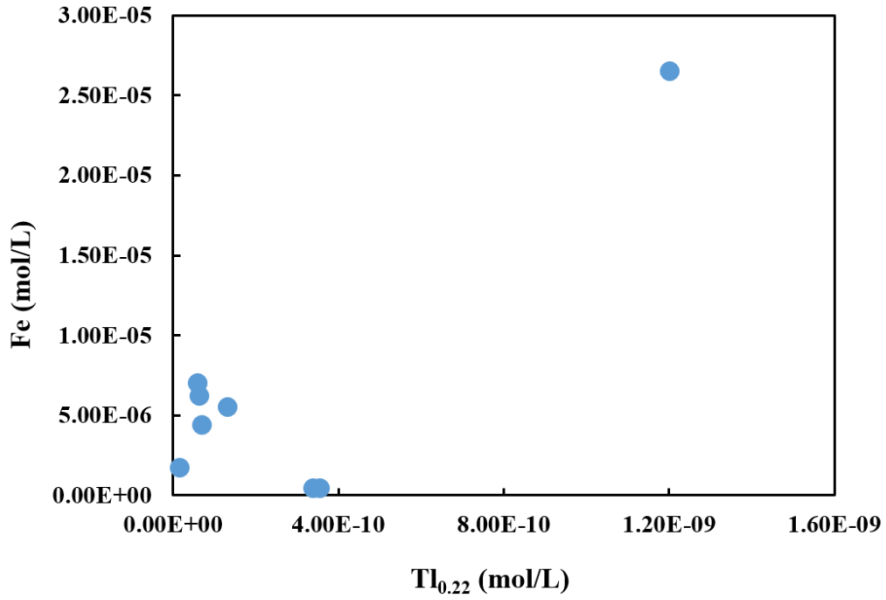

Figure S9: Fe vs. Tl

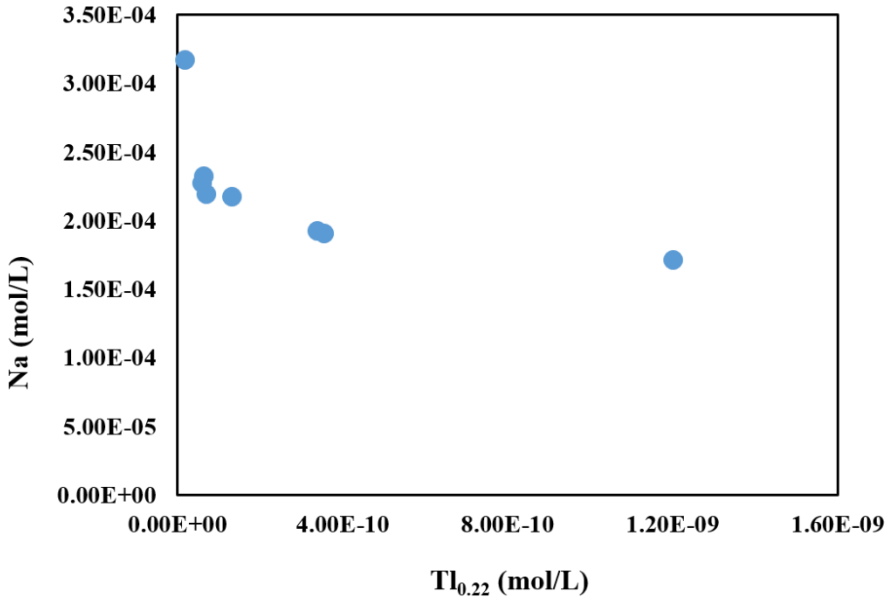

Figure S10: Na vs. Tl

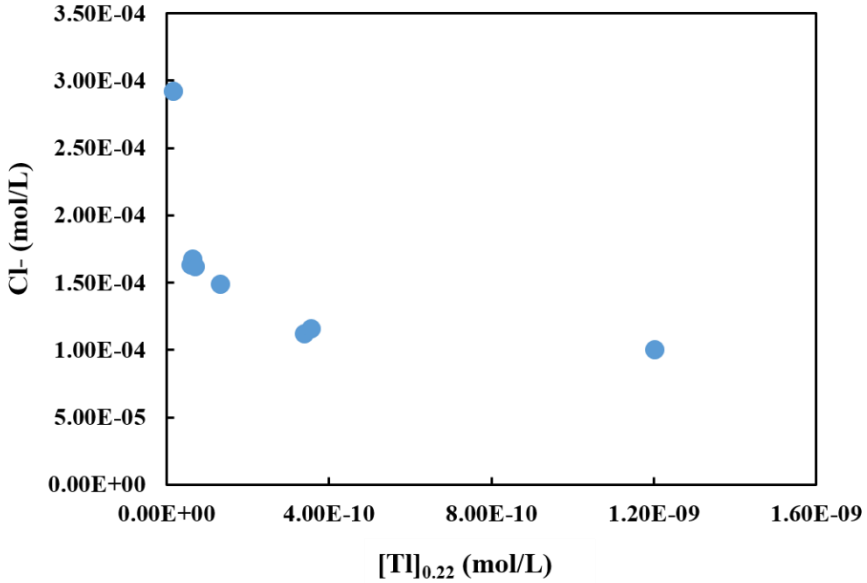

Figure S11: Cl vs. Tl

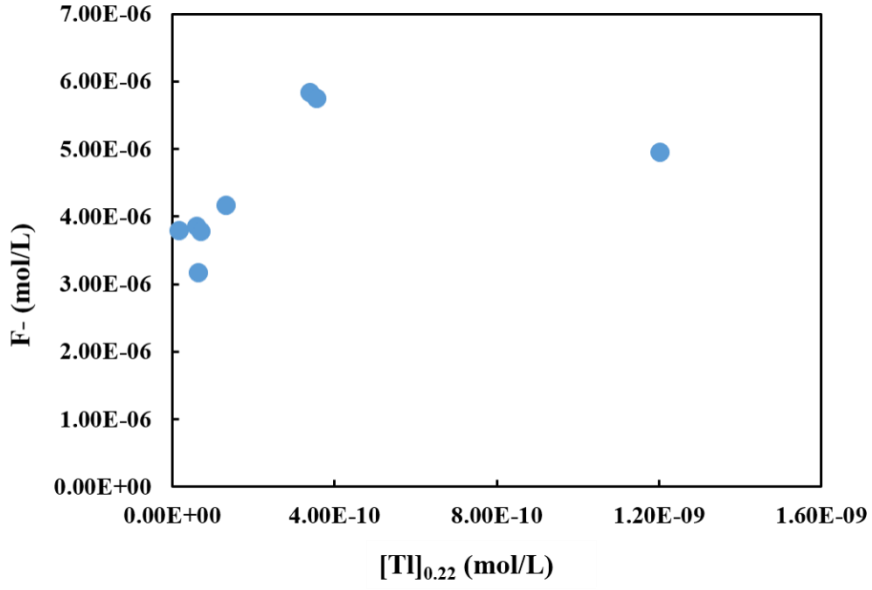

Figure S12: F vs. Tl

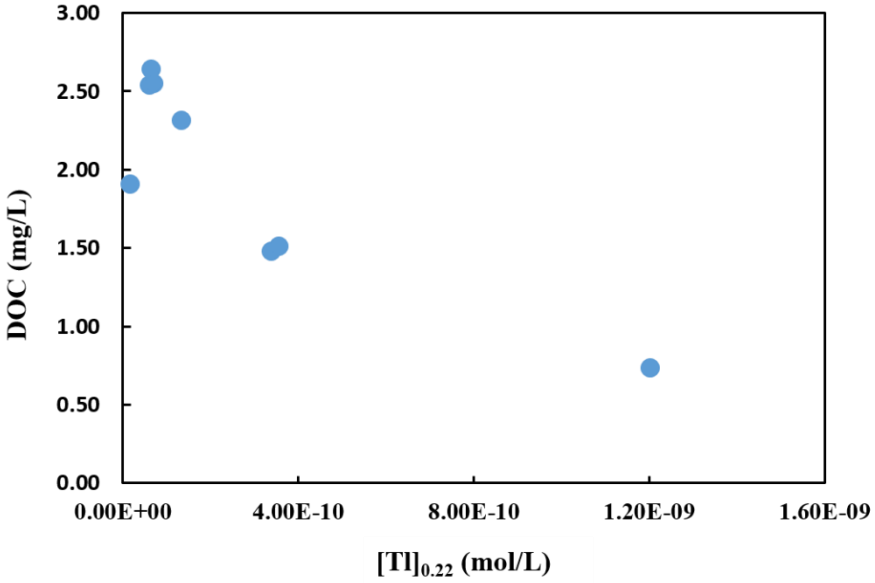

Figure S13: DOC vs. Tl

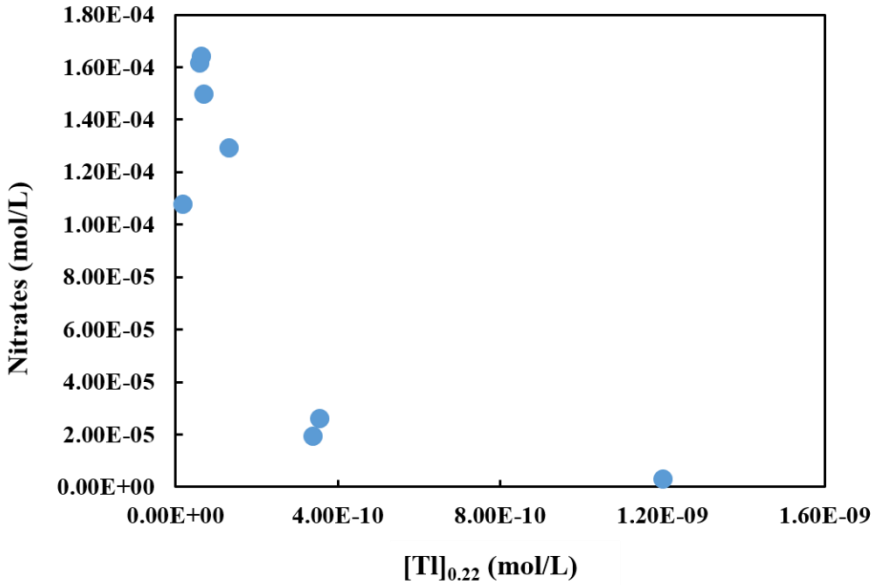

Figure S14: Nitrates vs. Tl

Chapitre VI : Conclusions et perspectives

Ce travail s'inscrit dans le cadre de l'étude du comportement du radium et du thallium dans l'environnement. Le premier objectif était d'étudier les phases porteuses dont les interactions étaient peu décrites pour ces éléments et de discuter leur rôle dans le cycle du radium et du thallium. Après l'analyse bibliographique, le choix s'est d'abord porté sur l'étude de la complexation avec la matière organique naturelle puis sur l'étude de l'adsorption sur les minéraux argileux. Le second objectif de cette étude était de tester un outil permettant de répondre à la question de la mesure du Radium aux interfaces naturelles, et notamment de répondre aux questions des faibles concentrations environnementales de Ra et des faibles volumes disponibles à ces interfaces.

1. BILAN SUR LES INTERACTIONS AVEC LES PHASES PORTEUSES

1.1. La matière organique naturelle

En utilisant la Donnan Membrane Technique et le modèle NICA-Donnan, cette étude a permis dans le chapitre II de décrire la complexation du radium et du thallium dans un système simple cation-acide humique à différents pH et concentrations. Cela a amené aux calculs des paramètres de NICA-Donnan ($\widetilde{K}_{i,1}$, $\widetilde{K}_{i,2}$, $n_{i,1}$ et $n_{i,2}$) jusqu'ici inexistants pour ces deux éléments.

Le thallium(I) a montré peu d'affinité pour cette phase, comparée à un autre cation monovalent, l'argent. Dans les environnements aquatiques, Tl(I) est donc majoritairement présent sous sa forme libre Tl^+. Cependant le thallium est également présent sous l'état d'oxydation +3 et cette forme pose régulièrement question quant à sa stabilité dans les environnements de surface. Les complexes colloïdaux et/ou dissous sont soupçonnés, en complexant Tl(III) de maintenir cette espèce dans l'environnement où Tl(I) est la forme thermodynamiquement stable. Il serait donc intéressant d'étudier les interactions entre Tl(III) et la matière organique naturelle pour voir si ces types de ligands pourraient jouer un rôle dans le cycle de cette forme de thallium.

Le radium a montré une affinité pour la matière organique naturelle (MON) similaire aux autres alcalino-terreux, notamment le strontium plus que le baryum. Des calculs de spéciation du radium sur des solutions de sols ont montré que le complexe AH-Ra était l'espèce dominante de radium. Ces données sont venues confirmer et compléter le rôle potentiellement important de la

matière organique dans la spéciation du radium dans les sols ou les tourbières par exemple. Des études complémentaires sur des sites naturels permettraient d'étayer ces hypothèses.

1.2. Les minéraux argileux

L'étude des interactions entre les minéraux argileux et le thallium(I) a permis de mettre en évidence une adsorption plus importante du thallium sur l'illite que sur la smectite. Ces résultats confirment les hypothèses du rôle important de l'illite par rapport aux autres phases minérales tout en restant limité par rapport aux oxydes de manganèse.

Ces travaux ont également montré que le thallium décrivait des réactions d'échange, réversibles, avec les sites réactifs des minéraux argileux et les effets de compétition avec les cations majeurs sont responsables de variation dans le comportement de sorption du thallium. Plus de thallium sera adsorbé en présence de sodium qu'en présence de calcium. L'utilisation du modèle d'échange d'ions multi-site a également permis de calculer des coefficients de sélectivité pour le thallium par rapport aux protons et par rapport à Na^+ et Ca^{2+}. Ce formalisme a mis en avant la forte affinité du thallium pour les sites réactifs de faible capacité.

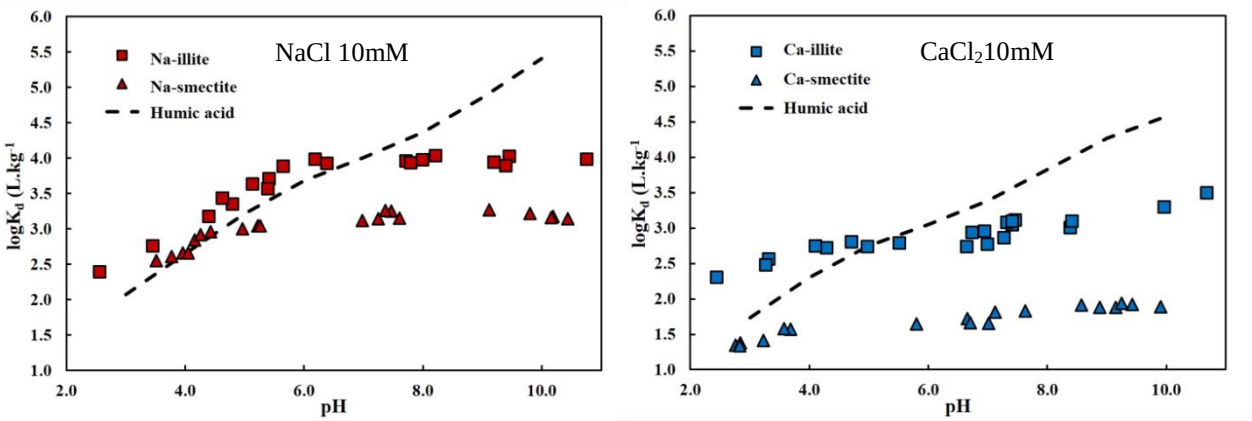

Figure 1 : Comparaison des interactions matière organique thallium et illite/smectite et thallium.

La comparaison des données expérimentales des minéraux argileux avec des données de modélisation du complexe Tl-HA dans des conditions similaires (de concentration et de solution de fond), a montré qu'autant de thallium est piégé sur la matière organique que sur les argiles à pH inférieur à 8 (fig. 1). Cette tendance change à pH alcalins où la matière organique semble alors dominer (fig. 1).

Tableau 2 : Comparaison de la quantité de thallium adsorbé/complexé par rapport à la densité de site des phases porteuses.

Phases porteuses	$mol.eq^{-1}$
Acide humique dans NaCl	$8{,}04 .10^{-7}$
Acide humique dans $CaCl_2$	$1{,}90 .10^{-7}$
Na-illite	$2{,}09 .10^{-7}$
Ca-illite	$2{,}03 .10^{-7}$
Na-smectite	$5{,}65 .10^{-8}$
Ca-smectite	$2{,}60 .10^{-8}$

Ces observations sont confirmées lorsque l'on regarde la quantité de thallium par densité de sites des phases porteuse (tableau 1). Il apparaît que le thallium a autant d'affinité pour la matière organique que pour les argiles. Pourtant, les études sur la spéciation du thallium dans les environnements de surface ont montré que peu de thallium était complexé à la matière organique, tandis que l'illite était l'un des minéraux qui contrôlait le plus la disponibilité du thallium. Cette différence s'explique probablement par la surface réactive des argiles, supérieure à celle de la matière organique. En conséquence il serait intéressant d'étudier les interactions du thallium avec ses phases porteuses dans des systèmes plus complexes, comme par exemple un système acide humique, illite et thallium et d'étudier le comportement de sorption du thallium. De même, ces perspectives ne limitent pas aux argiles et à la matière organique, mais doivent inclure d'autres phases porteuses du thallium comme les oxydes de manganèse et les oxyhydroxydes de fer. Il serait également interessant d'étudier le rôle de la biologie et notamment le rôle des biofilms bactériens dans le cycle géochimique du thallium en s'incrivant dans la continuité des travaux de Smeaton *et al*. (2012).

Comme il l'a déjà été mentionné dans le manuscrit, le rôle des argiles et notament de l'illite semble determinant dans le cycle géochimique du thallium, dans les sols notamment (Jacobson *et al*., 2005; Voegelin *et al*., 2015). Les sédiments de l'ancien site minier étudié au cours ce projet semblent riches en illite et en smectite, il serait donc intéressant d'étudier leurs interactions avec le thallium. La première étape serait alors d'identifier l'origine des minéraux argileux, qu'ils soient d'origine hydrothermale ou que se soit des minéraux secondaires liés à l'érosion/altération des roches et du stérile minier. Ensuite, si du thallium adsorbé est mesuré, il faudrait savoir si ce thallium provient de la circulation des fluides hydrothermaux (thallium déjà présent) ou si ce thallium a été adsorbé après une remise en solution.

2. MESURE DU RADIUM AUX INTERFACES NATURELLES.

Dans cette étude, le choix s'est porté sur l'utilisation de capteurs passifs de type DGT (*Diffusive Grandient in Thin-films*) pour répondre aux contraintes liées à la mesure du radium aux interfaces naturelles. Ces contraintes sont la faible concentration du radium, la difficulté d'accès à ces interfaces, les faibles volumes disponibles ainsi que les conditions changeantes de concentrations et de redox. La littérature recommandait l'utilisation des oxydes de manganèse pour pré-concentrer le radium. Les conditions d'utilisation de ces oxydes ont donc été testées par rapport aux effets de compétition et au changement de redox du milieu. Ces tests ont montré que les oxydes n'étaient pas stables en milieu anoxique et qu'ils n'étaient pas suffisamment sélectifs pour le radium dans les milieux naturels. Ensuite, grâce à la modélisation de la réponse des DGT aux signaux transitoires de concentrations, il a été possible de montrer un fonctionnement classique du capteur. Cependant, la capacité du capteur à enregistrer ces signaux est dépendante du temps de déploiement. Il faudrait mener des tests supplémentaires pour optimiser ce temps de déploiement et ainsi ajuster le fonctionnement du DGT en conséquence. Concernant la mesure du radium avec ce type de capteur, il faudrait tester d'autres agents chélatants, plus spécifiques au radium et moins sensibles au redox.

REFERENCES

Jacobson, A. R., McBride, M. B., Baveye, P., & Steenhuis, T. S. (2005). Environmental factors determining the trace-level sorption of silver and thallium to soils. *Science of The Total Environment*, *345*(1-3), 191–205. http://doi.org/10.1016/j.scitotenv.2004.10.027

Smeaton, C. M., Walshe, G. E., Fryer, B. J., & Weisener, C. G. (2012). Reductive Dissolution of Tl(I) − Jarosite by *Shewanella putrefaciens* : Providing New Insights into Tl Biogeochemistry, *Environmental Science & Technology*, *46*, 11086–11094. dx.doi.org/10.1021/es302292d

Voegelin A., Pfenninger N., Petrikis J., Majzlan J., Plötze M., Senn A.-C. and Göttlicher J. (2015). Thallium speciation and extractability in a thallium- and arsenic-rich soil developed from mineralized carbonate rock. *Environmental Science & Technology* **49**, 5390–5398.

Annexes

ANNEXE A : Propriétés physico-chimique du thallium (d'après Lide, 2009 et Nriagu, 1998)

Tableau A1 : Propriétés physico-chimique de l'élément Tl

Propriété	Valeur
Numéro atomique	81
Configuration électronique	[Xe]$4f^{14}5d^{10}6s^{2}6p^{1}$
Point de fusion (K)	577
Point d'ébullition (K)	1746
Energie d'ionisation (kJ.mol^{-1})	
$M \rightarrow M^{+}$	589,3
$M^{+} \rightarrow M^{2+}$	1971,0
$M^{2+} \rightarrow M^{3+}$	2878
$M^{3+} \rightarrow M^{4+}$	~ 4900
Densité (g.cc^{-1})	11,85
Résistivité électrique (Ωm)	18 .10^{-8}
Conductivité thermique à 300K (W.m^{-1}.K^{-1})	46,1
ΔH_{vap} à 298K (kJ.mol^{-1})	180,9
ΔH_{atom} à 298K (kJ.mol^{-1})	182,2
S à 298K (kJ.mol^{-1})	64,18
Electronégativité	
Echelle de Pauling	1,62 (Tl^{+}) 2,04 (Tl^{3+})
Echelle d'Allred	1,44
Echelle de Scanderson	1,96 (0,99 Tl^{+}; 2,25 Tl^{3+})
Echalle de Pearson	3,2
Rayon atomique (Å)	1,704 (forme α)
Rayon covalent (Å)	1,55
Rayon de van der Waals (Å)	2,00
Rayon ionique en coordination VI (Å)*	
Tl^{+}	1,50
Tl^{3+}	0,885
Potentiel redox standard	
$Tl^{+} + e^{-} \rightarrow Tl(s)$	-0,336
$Tl^{3+} + 3e^{-} \rightarrow Tl(s)$	+0,1741
$Tl^{3+} + 2e^{-} \rightarrow Tl^{+}$	+1,28
**d'après Shannon 1976*	

REFERENCES

Lide, D. R. (2009) CRC Handbook of Chemistry and Physics. CRC Press Inc, 90th ed., 2804 p. ISBN 978-1-420-09084-0

Nriagu, J. O. (1998), Thallium in the Environment. Wiley Series in Advances in Environmental Science and Technology, 29, 284p. John Wiley & Sons, Inc. New York

ANNEXE B : Les espèces de thallium

Tableau B1 : Constantes de stabilité des différents complexes de Tl(I)

Equations	logK (298 K)					
	Kaplan et Mattigod 1998	Lin et Nriagu, 1998	Laforte *et al*., 2005	Xiong, 2007	Xiong, 2009	Brown et Ekberg, 2016
$Tl^+ + OH^- \leftrightarrow TlOH$	0,79	-	0,79	0,69	-	0,63
$Tl^+ + SO_4^{2-} \leftrightarrow TlSO_4^-$	1,8	0,95	1,37	1,38	-	-
$Tl^+ + 2SO_4^{2-} \leftrightarrow Tl(SO_4)_2^{3-}$	-	1,02	-	-	-	-
$Tl^+ + Cl^- \leftrightarrow TlCl(aq)$	0,49	0,52	0,51	0,49	-	-
$Tl^+ + 2Cl^- \leftrightarrow TlCl_2^-$	0,0	-	0,28	0,003	-	-
$Tl^+ + CO_3^{2-} \leftrightarrow TlCO_3^-$	2,25	-	0,51	2,16	-	-
$Tl^+ + 2CO_3^{2-} \leftrightarrow Tl(CO_3)_2^{3-}$	-	2,79	0,11	-	-	-
$Tl^+ + NO_3^- \leftrightarrow TlNO_3(aq)$	0,33	0,45	-	-	-	-
$Tl^+ + HCO_3^- \leftrightarrow TlHCO_3$	1,2	3,42	-	0,9	-	-
$Tl^+ + HPO_4^{2-} \leftrightarrow TlHPO_4^-$	1,2	3,31	-	-	1,27	-
$Tl^+ + PO_4^{3-} \leftrightarrow TlPO_4^{2-}$	3,14	-	-	3,54	-	-
$Tl^+ + H_2PO_4^- \leftrightarrow TlH_2PO_4^-$	0,68	-	-	-	-	-
$Tl^+ + HP_2O_7^{3-} \leftrightarrow TlHP_2O_7^{2-}$	-	-		-	3,17	
$Tl^+ + P_2O_7^{3-} \leftrightarrow TlP_2O_7^{3-}$	-	-	-	-	4,09	
$Tl^+ + HS^- \leftrightarrow TlHS$	-	-	2,27	2,71	-	-
$2Tl^+ + HS^- \leftrightarrow Tl_2HS^+$	-	-	8,04	-	-	-
$2Tl^+ + 2H_2O + 2HS^- \leftrightarrow Tl_2(OH)_2(HS)_2^{2-} + 2H^+$	-	-	-11,068	-	-	-
$2Tl^+ + H_2O + 3HS^- \leftrightarrow Tl_2OH_2(HS)_3^{2-} + H^+$	-	-	1,004	-	-	-
$Tl^+ + F^- \leftrightarrow TlF$	0,10	0,10	-	0,1	-	-
$Tl^+ + Br^- \leftrightarrow TlBr$	-	0,93	-	-	-	-
$Tl^+ + I^- \leftrightarrow TlI$	-	0,72	-	-	-	-
$Tl^+ + Cit^{3-} \leftrightarrow TlCit^{2-}$	-	1,04	-	-	2,00	-
$Tl^+ + Ox^{2-} \leftrightarrow TlOx^-$	-	-	-	-	1,39	-
$Tl^+ + Ac^- \leftrightarrow TlAc^0$	-	0,79	-	-0,11	-	-
$Tl^+ + Suc^{2-} \leftrightarrow TlSuc^-$	-			-	1,61	
$Tl^+ + Mal^{2-} \leftrightarrow TlMal^-$	-	-		-	1,07	
$Tl^+ + EDTA^{4-} \leftrightarrow TlEDTA^{3-}$	-	-		-	7,57	
$Tl^+ + NTA^- \leftrightarrow TlNTA^0$	-	3,44	-	-	-	-
$Tl^+ + Fulv1^- \leftrightarrow TlFulv1^0$	4,83	-	-	-	-	-
$Tl^+ + Fulv2^- \leftrightarrow TlFulv2^0$	3,32	-	-	-	-	-

Tableau B2 : Constantes d'équilibre des solides de Tl(I). Certaines valeurs sont calculées à partir des constantes thermodynamiques provenant de Xiong (2007).

Equations	logK (298 K)	Référence
$Tl^+ + H_2O \leftrightarrow TlOH(s) + H^+$	-12,919	Laforte *et al*., 2005
$2Tl^+ + CO_3^{2-} \leftrightarrow Tl_2CO_3(s)$	3,837	Laforte *et al*., 2005
$2Tl^+ + SO_4^{2-} \leftrightarrow Tl_2SO_4(s)$	3,787	Laforte *et al*., 2005
$2Tl^+ H_2O \leftrightarrow Tl_2O(s) + 2H^+$	-27,091	Laforte *et al*., 2005
$2Tl^+ HS^- \leftrightarrow Tl_2S(s) + H^+$	7,19	Laforte *et al*., 2005
$Tl^+ 2SO_4^{2-} + 3Fe^{3+} + 6H_2O \leftrightarrow TlFe_3(SO_4)_2(OH)_6(s) + 6H^+$	2,245	Casiot *et al*., 2011
$Tl^+ + Al^{3+} + 2SO_4^{2-} + 12H_2O \leftrightarrow TlAl(SO_4)_2{\cdot}12H_2O$ (s)	16,551	Casiot *et al*., 2011
$Tl^+ + H_2AsO_3^- + 2HS^- + 2H^+ \leftrightarrow TlAsS_2$ (s) $+ 3H_2O$	38,256	Casiot *et al*., 2011

Tableau B3: Constantes d'équilibre et de stabilité des différents composés de Tl(III).

Equations	logK (298 K)			
	Lin et Nriagu, 1998	Laforte *et al*., 2005	Brown et Ekberg, 2016	Casiot *et al*., 2011
$Tl^{3+} + 3OH^- \leftrightarrow Tl(OH)_3(aq)$	6,58	-	-	-
$Tl^{3+} + OH^- \leftrightarrow Tl(OH)^{2+}$	11,31	-	13.77	-
$Tl^{3+} + 2OH^- \leftrightarrow Tl(OH)_2^+$	7,64	-	-	-
$Tl^{3+} + 4OH^- \leftrightarrow Tl(OH)_4^-$	5,22	-	-	-
$Tl^{3+} + SO_4^{2-} \leftrightarrow TlSO_4^+$	9,02	-	-	1,929
$Tl^{3+} + 2SO_4^{2-} \leftrightarrow Tl(SO_4)_2^-$	9,28	-	-	3,719
$Tl^{3+} + SO_4^{2-} + H^+ \leftrightarrow TlHSO_4^{2+-}$	-	-	-	3,129
$Tl^{3+} + 2SO_4^{2-} + 2H^+ \leftrightarrow Tl(HSO_4)_2^{2+}$	-	-	-	5,939
$Tl^{3+} + Cl^- \leftrightarrow TlCl^{2+}$	8,14	-	-	7,72
$Tl^{3+} + 2Cl^- \leftrightarrow TlCl_2^+$	13,60	-	-	13,48
$Tl^{3+} + 3Cl^- \leftrightarrow TlCl_3(aq)$	15,78	-	-	16,5
$Tl^{3+} + 4Cl^- \leftrightarrow TlCl_4^-$	18,00	-	-	18,3
$Tl^{3+} + CO_3^{2-} \leftrightarrow TlCO_3^+$	-	-	-	
$Tl^+ + 2CO_3^{2-} \leftrightarrow Tl(CO_3)_2^-$	15,76	-	-	
$Tl^{3+} + NO_3^- \leftrightarrow TlNO_3^{2+}$	7,20	-	-	3,129
$Tl^+ + HCO_3^- \leftrightarrow TlHCO_3^{2+}$	18,07	-	-	5,939
$Tl^+ + HPO_4^{2-} \leftrightarrow TlHPO_4^+$	17,66	-	-	-
$Tl^{3+} + F^- \leftrightarrow TlF^{2+}$	6,44	-	-	-
$Tl^{3+} + Br^- \leftrightarrow TlBr^{2+}$	9,70	-	-	-
$Tl^{3+} + 2Br^- \leftrightarrow TlBr_2^+$	16,60	-	-	-
$Tl^{3+} + 3Br^- \leftrightarrow TlBr_3$	21,20	-	-	-
$Tl^{3+} + 4Br^- \leftrightarrow TlBr_4^-$	23,90	-	-	-
$Tl^{3+} + I^- \leftrightarrow TlI^{2+}$	11,42	-	-	-
$Tl^{3+} + 2I^- \leftrightarrow TlI_2^+$	20,88	-	-	-
$Tl^{3+} + 3I^- \leftrightarrow TlI_3$	27,60	-	-	-
$Tl^{3+} + 4I^- \leftrightarrow TlI_4^-$	31,82	-	-	-
$Tl^{3+} + Cit^{3-} \leftrightarrow TlCit^0$	12,02	-	-	-
$Tl^{3+} + Ac^- \leftrightarrow TlAc^{2+}$	8,42	-	-	-
$Tl^{3+} + EDTA^{4-} \leftrightarrow TlEDTA^-$	22,50	-	-	-
$Tl^{3+} + NTA^- \leftrightarrow TlNTA^{2+}$	16,81	-	-	-
$Tl^+ + 2H^+ + 0.5O_2 \leftrightarrow Tl^{3+} + H_2O$	-	-	-	-0,2751
$Tl^{3+} + 3H_2O \leftrightarrow Tl(OH)_3(aq) +$	-	-	-	-3,291

$3H^+$				
$Tl^{3+} + H_2O \leftrightarrow TlOH^{2+} + H^+$	-	-	-	-0,597
$Tl^{3+} + 2H_2O \leftrightarrow Tl(OH)_2^+ + 2H^+$	-	-	-	-1,394
$Tl^{3+} + 4H_2O \leftrightarrow Tl(OH)_4^- + 4H^+$	-	-	-	-14,988
$Tl^{3+} + Cl^- + H_2O \leftrightarrow TlOHCl^+ + H^+$	-	-	-	7,338
$Tl^{3+} + 3H_2O \leftrightarrow Tl(OH)_3(s) + 3H^+$	-	-	-	2,15
$2Tl(OH)_3(aq) \leftrightarrow Tl_2O_3(s) + 3H_2O$	-	-	-	16,3237
$Tl(OH)_3(aq) + 3H^+ \leftrightarrow Tl^{3+} + 3H_2O$	-	3,291	-	-
$Tl(OH)_3(aq) + 2H^+ \leftrightarrow TlOH^{2+} + 2H_2O$	-	2,694	-	-
$Tl(OH)_3(aq) + H^+ \leftrightarrow Tl(OH)_2^+ + H_2O$	-	1,897	-	-
$Tl(OH)_3(aq) + H_2O \leftrightarrow Tl(OH)_4^- + H^+$	-	-11,697	-	-
$Tl(OH)_3(aq) + 2H^+ + Cl^- \leftrightarrow TlOHCl^+ + 2H_2O$	-	10,629	-	-
$Tl(OH)_3(aq) + 3H^+ + Cl^- \leftrightarrow TlCl^{2+} + 3H_2O$	-	11,011	-	-
$Tl(OH)_3(aq) + 3H^+ + 2Cl^- \leftrightarrow TlCl_2^+ + 3H_2O$	-	16,771	-	-
$Tl(OH)_3(aq) + 3H^+ + 3Cl^- \leftrightarrow TlCl_3 + 3H_2O$	-	19,791	-	-
$Tl(OH)_3(aq) + 3H^+ + 4Cl^- \leftrightarrow TlCl_4^- + 3H_2O$	-	21,591	-	-
$Tl(OH)_3(aq) + 3H^+ + SO_4^{2-} \leftrightarrow TlSO_4^+ + 3H_2O$	-	5,22	-	-
$Tl(OH)_3(aq) + 3H^+ + 2SO_4^{2-} \leftrightarrow Tl(SO_4)_2^- + 3H_2O$	-	7,01	-	-
$Tl(OH)_3(aq) + 4H^+ + SO_4^{2-} \leftrightarrow TlHSO_4^{2+} + 3H_2O$	-	6,42	-	-
$Tl(OH)_3(aq) + 5H^+ + 2SO_4^{2-} \leftrightarrow Tl(HSO_4)_2^+ + 3H_2O$	-	9,23	-	-
$Tl(OH)_3(aq) = Tl(OH)_3(s)$	-	5,441	-	-

Suite tableau B3

RÉFÉRENCES

Brown, P. L., Ekberg, C. (2016). Hydrolysis of Metal Ions. *Wiley VCM*, p217-218 & p825

Casiot, C., Egal, M., Bruneel, O., Verma, N., Parmentier, M. & Elbaz-Poulichet F. (2011). Predominance of Aqueous Tl(I) Species in the River System Downstream from the Abandoned Carnoulès Mine (Southern France). *Environ. Sci. Technol*., *45*, 2056–2064.

Kaplan, D. I., & Mattigod S. V. (1998). Aqueous geochemistry of thallium. In *Thallium in the Environment*, 15–29. Edited by J. O. Nriagu. John Wiley & Sons, Inc. New York

Laforte, L., Tessier, A., Gobeil, C., & Carignan, R. (2005). Thallium diagenesis in lacustrine sediments. *Geochimica et Cosmochimica Acta*, *69*, 5295–5306. http://doi.org/10.1016/j.gca.2005.06.006

Lin, T.-S., & Nriagu, J. (1998). Speciation of thallium in natural waters. In *Thallium in the Environment*, 31–43. Edited by J. O. Nriagu. John Wiley & Sons, Inc. New York

Xiong, Y. (2007). Hydrothermal thallium mineralization up to 300 ° C : A thermodynamic approach, *32*, 291–313. http://doi.org/10.1016/j.oregeorev.2006.10.003

Xiong, Y. (2009). The aqueous geochemistry of thallium : speciation and solubility of thallium in low temperature systems, 441–451. http://doi.org/10.1071/EN08086

ANNEXE C : Le thallium dans le bassin amazonien

Tableau C1 : Concentration en thallium dissous (< 0,45 µm) des grands fleuves amazoniens. Les concentrations en thallium représentent les moyennes de 2 séries de mesures effectuées au premier trimestre 2017 sur HR-ICP-MS Element 2 (Thermo Scientific). Les échnatillons proviennent de différentes missions effectuées par des chercheurs de l'Institut de Physique du Globe de Paris.

Fleuve	Localisation	[Tl] ($mol.L^{-1}$)
Rio Negro	?	$4,82 \pm 0,34 .10^{-11}$ (n = 2)
Rio Amazonas	Óbidos, Pará, Brésil	$3,27 \pm 0,67 .10^{-11}$ (n = 2)
Rio Solimões	Tamshiyacu, Loreto, Pérou	$3,44 \pm 0,26 .10^{-11}$ (n = 2)
Rio Madeira	Foz Madeira ?	$2,04 \pm 2,50 .10^{-11}$ (n = 2)
Rio Beni	Rurrenabaque, Beni, Bolivie	$4,35 \pm 0,38 .10^{-11}$ (n = 4)
Rio Madre de Dios	Riberalta, Beni, Bolivie	$2,52 \pm 0,24 .10^{-11}$ (n = 2)
Rio Mamoré	Guayaramerín, Beni, Bolivie	$3,39 \pm 0,35 .10^{-11}$ (n = 2)
Rio Ucayali	Jenaro Herrera, Loreto, Pérou	$2,18 \pm 0,01 .10^{-11}$ (n = 2)
Rio Marañon	San Regis, Loreto, Pérou	$4,45 \pm 0,57 .10^{-11}$ (n = 2)
Rio Morona	?	$3,50 \pm 0,50 .10^{-11}$ (n = 2)
Rio Tigre	Nueva York, Loreto, Pérou	$8,52 \pm 0,26 .10^{-11}$ (n = 2)

Tableau C2 : Concentrations en Tl dissous (< 0,2 µm) au niveau de la zone de confluence entre le Rio Negro et le Rio Solimões. Les veleurs en thallium représentent les moyennes de duplicats. Les mesures ont été effectuées au premier trimestre 2017 sur HR-ICP-MS Element 2 (Thermo Scientific). Les échnatillons proviennent de l'étude de D. Guinoiseau (Guinoiseau et al., 2016a et Guinoiseau 2016b).

Id	[Tl] ($mol.L^{-1}$)	Profondeur (m)	Fleuve
N2-A	$3,60 \pm 0,09 .10^{-11}$	2,0	Rio Negro
N2-B	$3,95 \pm 0,12 .10^{-11}$	9,0	Rio Negro
N2-C	$4,30 \pm 0,24 .10^{-11}$	19,0	Rio Negro
N2-D	$4,01 \pm 0,43 .10^{-11}$	29,0	Rio Negro
N2-E	$4,18 \pm 0,14 .10^{-11}$	39,5	Rio Negro
N3-A	$3,85 \pm 0,09 .10^{-11}$	2,0	Rio Negro
N3-B	$3,83 \pm 0,28 .10^{-11}$	12,0	Rio Negro
N3-C	$3,68 \pm 0,30 .10^{-11}$	22,5	Rio Negro
N3-D	$3,80 \pm 0,03 .10^{-11}$	32,1	Rio Negro
N3-E	$3,57 \pm 0,22 .10^{-11}$	42,3	Rio Negro
N5-A	$3,35 \pm 0,02 .10^{-11}$	2,0	Rio Negro
N5-B	$3,44 \pm 0,09 .10^{-11}$	11,0	Rio Negro
N5-C	$3,54 \pm 0,07 .10^{-11}$	19,0	Rio Negro
S3-A	$3,38 \pm 0,01 .10^{-11}$	2,0	Rio Solimões
S3-B	$3,19 \pm 0,02 .10^{-11}$	11,2	Rio Solimões
S3-C	$3,16 \pm 0,01 .10^{-11}$	18,0	Rio Solimões
S3-D	$3,35 \pm 0,01 .10^{-11}$	24,0	Rio Solimões
S3-E	$3,37 \pm 0,02 .10^{-11}$	30,0	Rio Solimões
A1-A	$3,93 \pm 0,35 .10^{-11}$	2,0	Rio Amazonas
A1-B	$3,49 \pm 0,30 .10^{-11}$	12,0	Rio Amazonas
A1-C	$3,28 \pm 0,02 .10^{-11}$	24,0	Rio Amazonas
A1-D	$3,62 \pm 0,11 .10^{-11}$	36,0	Rio Amazonas

A1-E	$3,73 \pm 0,09 .10^{-11}$	46,0	Rio Amazonas
A4-A	$3,23 \pm 0,24 .10^{-11}$	2,0	Rio Amazonas
A4-B	$3,38 \pm 0,19 .10^{-11}$	12,0	Rio Amazonas
A4-C	$3,42 \pm 0,01 .10^{-11}$	24,0	Rio Amazonas
A4-D	$3,28 \pm 0,13 .10^{-11}$	36,0	Rio Amazonas
A4-E	$3,64 \pm 0,11 .10^{-11}$	49,0	Rio Amazonas
A5-A	$3,28 \pm 0,04 .10^{-11}$	2,0	Rio Amazonas
A5-B	$3,18 \pm 0,05 .10^{-11}$	11,0	Rio Amazonas
A5-C	$3,38 \pm 0,04 .10^{-11}$	22,0	Rio Amazonas
A5-D	$3,28 \pm 0,09 .10^{-11}$	32,0	Rio Amazonas
A5-E	$3,35 \pm 0,12 .10^{-11}$	41,0	Rio Amazonas

Suite tableau C2

REFERENCE

Guinoiseau, D., Bouchez, J., Gélabert, A., Louvat, P., Filizola, N., & Benedetti, M. F. (2016a). The geochemical filter of large river confluences. *Chemical Geology*, *441*, 191-203.

Guinoiseau, D. (2016b). Impact des processus physico-chimiques eau-roche sur le comportement des isotopes du Zn et du Cu en systèmes contrôlés et naturels: application au bassin amazonien. *Ph. D. thesis*. Sorbonne Paris Cité.